May 2016

Improving the Subgrid-Scale Representation of Hydrometeors and Microphysical Feedback Effects Using a Multivariate Pdf

Brian Martin Griffin
University of Wisconsin-Milwaukee

Improving the Subgrid-Scale Representation of Hydrometeors and Microphysical Feedback Effects Using a Multivariate PDF

by

Brian M. Griffin

A Dissertation Submitted in

Partial Fulfillment of the

Requirements for the Degree of

Doctor of Philosophy

in Mathematics

at

The University of Wisconsin – Milwaukee

May 2016

Abstract

Improving the Subgrid-Scale Representation of Hydrometeors and Microphysical Feedback Effects Using a Multivariate PDF

by

Brian M. Griffin

The University of Wisconsin – Milwaukee, 2016
Under the Supervision of Professor Vincent E. Larson

The subgrid-scale representation of hydrometeor fields is important for calculating microphysical process rates. In order to represent subgrid-scale variability, the Cloud Layers Unified By Binormals (CLUBB) parameterization uses a multivariate Probability Density Function (PDF). In addition to vertical velocity, temperature, and moisture fields, the PDF includes hydrometeor fields. Previously, each hydrometeor field was assumed to follow a multivariate single lognormal distribution. Now, in order to better represent the distribution of hydrometeors, two new multivariate PDFs are formulated and introduced in part one of this two-part project.

The new PDFs represent hydrometeors using either a delta-lognormal or a delta-double-lognormal shape. The two new PDF distributions, plus the previous single lognormal shape, are compared to histograms of data taken from Large-Eddy Simulations (LES) of a precipitating cumulus case, a drizzling stratocumulus case, and a deep convective case. Finally, the warm microphysical process rates produced by the different hydrometeor PDFs are compared to the same process rates produced by the LES.

Microphysics processes have feedback effects on moisture and heat content. Not only do these processes influence mean values, but also variability and fluxes of moisture and heat content. For example, evaporation of rain below cloud base may produce cold pools. This evaporative cooling may increase the variability in temperature in the below-cloud layer.

Likewise, rain production in the moistest part of cloud tends to decrease variability in cloud water. These effects are usually not included in most coarse-resolution weather and climate models, or else are crudely parameterized.

In part two of this two-part project, the microphysical effects on moisture and heat content are parameterized using the PDF method. This approach is based on predictive, horizontally-averaged equations for the variances, covariances, and fluxes of moisture and heat content. These higher-order moment equations contain microphysical source terms. Using a simple warm-rain microphysics scheme, the microphysics terms can be calculated by integrating analytically over the multivariate PDF.

A LES of a precipitating cumulus case indicates that microphysical terms are dominant in some budgets. The analytic integrals for the microphysics terms are implemented in the CLUBB model. Interactive single-column simulations agree qualitatively with the LES.

For Christina and Bree

Table of Contents

List of Figures

List of Tables

List of Symbols

r_t	Total water mixing ratio
r_v	Water vapor mixing ratio
r_c	Cloud water mixing ratio
r_r	Rain water mixing ratio
T	Temperature
T_l	Liquid water temperature
θ	Potential temperature
θ_l	Liquid water potential temperature
w	Vertical velocity
p_a	Air pressure
p_d	Dry air pressure
p_v	Water vapor pressure
p_0	Reference pressure of 10^5 Pa.
ρ_a	Density of air
ρ_l	Density of liquid water
ρ_s	Density of dry air for anelastic base state
N_c	Cloud droplet concentration (per unit mass)
N_r	Rain drop concentration (per unit mass)
N_{cV}	Cloud droplet concentration (per unit volume)
N_{rV}	Rain drop concentration (per unit volume)
R_d	Gas constant for dry air
R_v	Gas constant for water vapor
C_{pd}	Specific heat of dry air (constant pressure)
L_v	Latent heat of vaporization
$e_s(T)$	Saturation vapor pressure
$r_s(T,p)$	Saturation mixing ratio
S	Supersaturation
$H(x)$	Heaviside step function
$D_\nu(x)$	Parabolic cylinder function of order ν
$\Gamma(x)$	Gamma function
$\mathrm{erf}(x)$	Error function
$\mathrm{erfc}(x)$	Complimentary error function

Acknowledgements

First and foremost, I am very appreciative for all the support that I have received from my amazing, beautiful, wonderful wife, Christina, and our sweet, wonderful daughter, Brianna, while I have been pursuing my Doctorate over the past five years. They have been loving, understanding, and supportive at every step along the way. They have shown an incredible amount of patience throughout this entire project. I would not have been able to complete this project without their great support and encouragement. A great family is truly a blessing from God.

I would like to thank Dr. Vincent E. Larson for all the support that he has provided me. I have been very fortunate to benefit from working with him for the past 14 years. He has taught me a wealth of knowledge about numerical modeling and parameterization. He has been very important to the success of my research in these topics.

Chapter 1

A New Subgrid-Scale Representation of Hydrometeor Fields Using a Multivariate PDF

1.1 Introduction

The atmospheric portion of the hydrological cycle depends on the formation and dissipation of precipitation. In a numerical model, precipitation processes are represented by the microphysics process rates. These process rates are highly dependent on the values of hydrometeor fields at any place and time. Hydrometeors (such as rain water mixing ratio) can vary significantly on spatial scales smaller than the size of a numerical model grid box (Boutle et al. 2014; Lebsock et al. 2013). This means that a good representation of subgrid-scale variability is important for the parameterization of microphysical process rates.

Subgrid-scale variability (but not spatial organization) can be accounted for through use of a Probability Density Function (PDF). PDFs have been used in atmospheric modeling to account for subgrid variability in moisture and temperature (e.g., Mellor 1977; Sommeria and Deardorff 1977; Tompkins 2002; Naumann et al. 2013) in order to calculate such fields as cloud fraction and mean (liquid) cloud mixing ratio, and have been extended to vertical velocity in order to calculate fields such as liquid water flux (Lewellen and Yoh 1993; Lappen and Randall 2001; Larson et al. 2002; Bogenschutz et al. 2010; Firl and Randall 2015). PDFs have been used in microphysics to account for subgrid variability in cloud water (Zhang et al. 2002; Morrison and Gettelman 2008) and in warm hydrometeor fields (Larson and Griffin 2006, 2013; Cheng and Xu 2009; Kogan and Mechem 2014, 2015) in order to calculate warm microphysics process rates. They also have been used to represent cloud ice (Kärcher and Burkhardt 2008).

Regarding the PDF's functional form, generality is highly desired. For instance, we would like the PDF to be capable of representing interactions among species, such as accretion (collection) of cloud droplets by rain drops. In addition, the PDF should be able to represent a variety of cloud types, such as cumulus and stratocumulus. Generality in the PDF's functional form is important because it facilitates the formulation of unified cloud parameterizations (e.g., Lappen and Randall 2001; Neggers et al. 2009; Sušelj et al. 2013; Bogenschutz and Krueger 2013; Guo et al. 2015; Cheng and Xu 2015; Thayer-Calder et al. 2015).

Cloud Layers Unified By Binormals (CLUBB) is a single-column model that uses a multivariate PDF to account for the subgrid-scale variability of model fields (Golaz et al. 2002a,b; Larson and Golaz 2005). The original PDF used by CLUBB consisted of only vertical velocity, w, total water mixing ratio (vapor + liquid cloud), r_t, and liquid water potential temperature, θ_l. The PDF is a weighted mixture, or sum, of two multivariate normal functions. Each one of these multivariate normal functions is known as a PDF component. Although a normal distribution is unskewed, the two-component shape makes it possible to include skewness in model fields.

Larson and Griffin (2013) extended CLUBB's PDF to account for subgrid variability in rain water mixing ratio, r_r, and rain drop concentration (per unit mass), N_r. Each of these hydrometeor species was assumed to follow a single lognormal (SL) distribution on the subgrid domain. This treatment worked well for calculating microphysics process rates in a drizzling stratocumulus case (Griffin and Larson 2013). Subsequently, CLUBB's PDF was extended to other hydrometeor species involving ice, snow, and graupel.

However, the single lognormal treatment of hydrometeors is less successful when it is applied to a partly cloudy, precipitating case. The problem is that the single lognormal assumes that a hydrometeor is found (that is, has a value greater than 0) at every point on the subgrid domain. This is not realistic in a partly cloudy regime, such as precipitating shallow cumulus, which has non-zero precipitation over only a small fraction of the domain.

Consider an example in which rain covers 10% of the grid level. Then the in-precipitation mean of r_r is ten times greater than the grid-mean value. This can cause problems when microphysics process rates are calculated using the SL. The accretion rate of r_r is proportional to the value of r_r inside cloud. In this example, the SL, which distributes the lognormal around the grid mean, would underpredict accretion rate because it causes r_r to be too small in cloud. Likewise, evaporation rate is proportional to the value of r_r outside cloud. The SL would overpredict evaporation rate because it spreads r_r throughout the domain, including the clear portion.

The solution to this problem is to account for the non-precipitating region of the subgrid domain. This is done by representing the non-precipitating region of the domain with a delta function at a value of the hydrometeor of 0. The in-precipitation portion of the subgrid domain can still be handled by using a single lognormal distribution to represent subgrid variability in the hydrometeor species. The resulting distribution is called a delta-lognormal (DL). In the above example with 10% rain fraction, the (in-precipitation) lognormal from the DL PDF would be distributed around the in-precipitation mean, as desired, rather than around the grid mean, which is a factor of 10 smaller.

Further improvements in accuracy can be achieved with relatively minor modifications to the PDF. As previously mentioned, CLUBB's PDF contains two components. Each of these components can be easily subdivided into an in-precipitation sub-component and an outside-precipitation sub-component. The result is a delta-lognormal representation of the hydrometeor field *in each PDF component*. Both delta functions are at 0 and represent the region outside of precipitation, but the in-precipitation hydrometeor values are distributed as two lognormals that may have different means and/or variances. When the two lognormals differ in some way, the resulting distribution is called a delta-double-lognormal (DDL). Figure 1.1 illustrates the SL, DL, and DDL hydrometeor PDF shapes.

The main purpose of this paper is to present the formulation of an updated multivariate PDF that extends CLUBB's traditional PDF to include the DL and DDL hydrometeor PDF

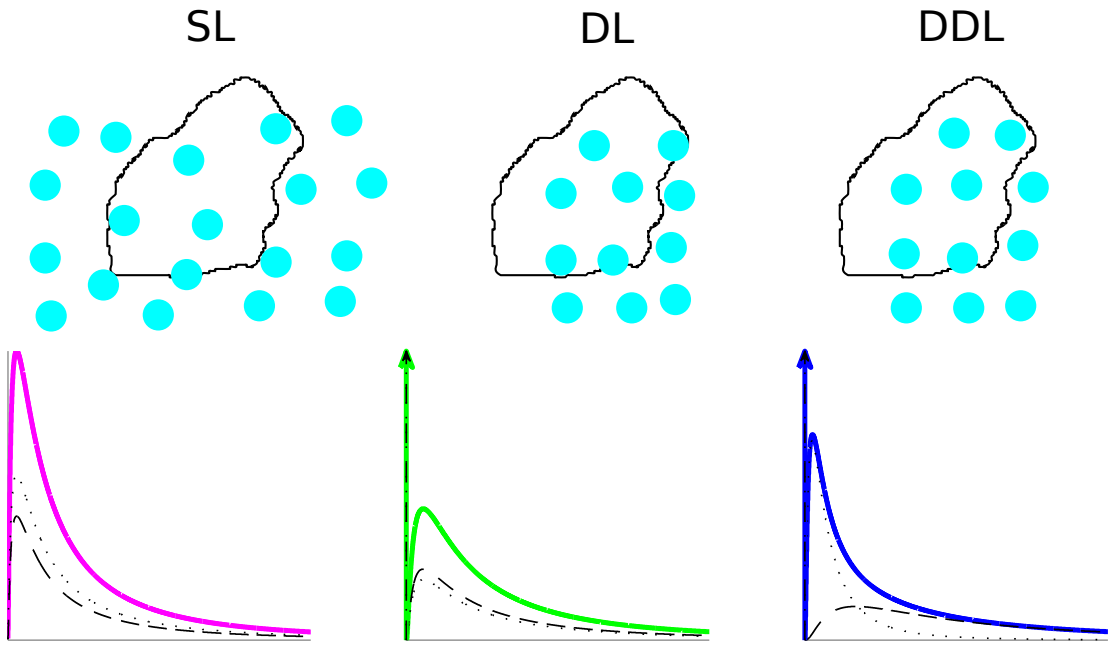

Figure 1.1: A schematic of the single lognormal (SL), delta-lognormal (DL), and delta-double-lognormal (DDL) hydrometeor PDF shapes. The SL PDF shape is precipitating over the entire subgrid domain, whereas the DL and DDL shapes are not. In all three plots of the PDFs (where each PDF is a function of a hydrometeor species, such as r_r), the weighted PDF from each PDF component is shown (black dashes and black dots). The sum of the two are the SL (solid magenta), the DL (solid green), and the DDL (solid blue). The SL does not contain a delta at 0, and the mean and variance of each PDF component are the same. Each component of the DL has a delta at 0 (upward pointing black arrows on the y-axis). The sum of the two component deltas forms the DL's delta at 0 (upward pointing green arrow). The mean and variance of each DL PDF component are the same within precipitation. Each component of the DDL also has a delta at 0 (upward pointing black arrows). The sum of the two component deltas forms the DDL's delta at 0 (upward pointing blue arrow). The mean and/or variance differ between DDL PDF components within precipitation.

shapes. Additionally, a new method is derived to divide the *grid-box* mean and variance of a hydrometeor species into *PDF component* means and standard deviations. A secondary purpose of this paper is to present a preliminary comparison of the new PDF shapes with PDFs output by large-eddy simulations (LESs). The SL, DL, and DDL hydrometeor PDF shapes are compared to histograms of hydrometeor data taken from precipitating LES. Additionally, microphysics process rates are calculated using each of the idealized PDF shapes and compared to microphysics process rates taken from the LES.

The remainder of the paper is organized as follows. Section 1.2 gives a detailed description of the new PDF. Section 1.3 discusses the PDF parameters and includes the derivation of a new method to divide the grid-box mean and variance into PDF component means and standard deviations for a hydrometeor species. Section 1.4 describes the LES setup and the test cases, as well as the driving of CLUBB's PDF for the tests. Section 1.5 presents a comparison of hydrometeors between the LES and the SL, DL, and DDL PDF shapes. The comparison includes plots of PDFs, Kolmogorov-Smirnov and Cramer-von Mises scores, and microphysics process rates. Section 1.6 contains all conclusions.

1.2 Description of the multivariate PDF

We now describe how the multivariate PDF used by CLUBB is modified to improve the representation of hydrometeors. Perhaps the most important modification is the introduction of precipitation fraction, f_p, to the PDF. Precipitation fraction is defined as the fraction of the subgrid domain that contains any kind of precipitation (where any hydrometeor species has a positive value). In order to account for any precipitation-less region in the subgrid domain, the PDF is modified to add a delta function at a value of 0 for all hydrometeor species. Each PDF component contains its own precipitation fraction. Expressed generally for a PDF of n components, the overall precipitation fraction is related to the component

precipitation fractions by

$$f_p = \sum_{i=1}^{n} \xi_{(i)} f_{p(i)}, \tag{1.1}$$

where $f_{p(i)}$ denotes precipitation fraction in the ith PDF component, and where $0 \leq f_{p(i)} \leq 1$ for all $f_{p(i)}$. Additionally

$$\sum_{i=1}^{n} \xi_{(i)} = 1, \tag{1.2}$$

where $\xi_{(i)}$ is the relative weight, or mixture fraction, of the ith PDF component, and where $0 < \xi_{(i)} < 1$ for all $\xi_{(i)}$. A PDF with more than one component requires that each PDF component have a mixture fraction.

Before writing the form of the multi-component PDF, we digress to discuss a special case, the cloud droplet concentration (per unit mass), N_c. In Larson and Griffin (2013), N_c was introduced to the PDF and was assumed to follow a single lognormal distribution. This assumption for N_c means that when any cloud is found at a grid level, $N_c > 0$ at every point on the subgrid domain. This is unphysical in a partly cloudy situation, for cloud droplets would be found at points where cloud water is not found. Additionally, the single lognormal treatment of N_c can cause problems with the microphysics. The grid-level mean of N_c, denoted $\overline{N_c}$ (for the remainder of this paper, an overbar denotes a grid-level mean and a prime denotes a turbulent value), is handed to the PDF by the model, and this mean value includes clear air in a partly cloudy situation. This results in a value of $\overline{N_c}$ that is much smaller than the in-cloud values of N_c. Since the single lognormal in N_c is distributed around $\overline{N_c}$, N_c is much too small in cloud for cases with small cloud fraction, leading to an excessive autoconversion (raindrop formation) rate.

In order to distribute N_c where (and only where) cloud water mixing ratio, r_c, is found on the subgrid domain, it cannot use the same method as the other hydrometeors. Hydrometeors such as r_r can be found outside cloud where r_c is not found, or alternatively hydrometeors might be absent inside cloud where r_c is found. Instead the PDF is modified so that a new variable, N_{cn}, replaces N_c in the PDF. The variable N_{cn} is a mathematical construct that can

be viewed as an extended cloud droplet concentration or even as a simplified, conservative cloud condensation nuclei concentration. It is distributed as a single lognormal over the subgrid domain. At points where cloud water is found, N_c is set equal to N_{cn}. Otherwise, N_c is set to 0 at points where no cloud water is found (see Eq. (1.4) below). The value of $\overline{N_{cn}}$ is approximately the in-cloud mean of N_c, and in special cases, is exactly the in-cloud mean of N_c. Please see Appendix D for a more detailed explanation.

The PDF includes all the hydrometeor species found in the chosen microphysics scheme with the exception of r_c, which is calculated from other variables in the PDF through a saturation adjustment, and N_c, which is described above. In addition to r_r and N_r, a microphysics scheme may include hydrometeor species such as ice mixing ratio, r_i, ice crystal concentration (per unit mass), N_i, snow mixing ratio, r_s, snowflake concentration (per unit mass), N_s, graupel mixing ratio, r_g, and graupel concentration (per unit mass), N_g. The vector containing all the hydrometeor species included in the PDF will be denoted $\vec{\boldsymbol{h}}$. The full PDF can be written as $P\left(w, r_t, \theta_l, N_{cn}, \vec{\boldsymbol{h}}\right)$.

In order to calculate quantities that depend on saturation, such as $\overline{r_c}$ and cloud fraction, a PDF transformation is required. The PDF transformation is a change of coordinates. The multivariate PDF undergoes translation, stretching, and rotation of the axes (Larson et al. 2005; Mellor 1977). Within each PDF component, a separate PDF transformation takes place. The ith component PDF, $P_{(i)}\left(w, r_t, \theta_l, N_{cn}, \vec{\boldsymbol{h}}\right)$, is transformed to $P_{(i)}\left(w, \chi, \eta, N_{cn}, \vec{\boldsymbol{h}}\right)$, where χ is an "extended" liquid water mixing ratio that, when the air is supersaturated, has a positive value and furthermore is equal to r_c. When the air is subsaturated, χ has a negative value. The variable η is orthogonal to χ. The variables r_c and N_c can now be written as

$$r_c = \chi\, H\left(\chi\right) \text{ and} \tag{1.3}$$

$$N_c = N_{cn}\, H\left(\chi\right), \tag{1.4}$$

where $H(x)$ is the Heaviside step function.

The general form of a PDF with n components and D variables (whether D includes all the variables in the PDF or any subset of those variables in a multivariate marginal PDF) can be written as

$$P(x_1, x_2, \ldots, x_D) = \sum_{i=1}^{n} \xi_{(i)} P_{(i)}(x_1, x_2, \ldots, x_D). \tag{1.5}$$

Of the D variables listed, the first J variables are normally distributed in each PDF component (i.e. w, r_t, and θ_l, or w, χ and η), the next K variables are lognormally distributed (i.e. N_{cn}), and the last Ω variables are the hydrometeor species, such that $D = J + K + \Omega$. The ith component of the PDF, $P_{(i)}(x_1, x_2, \ldots, x_D)$, accounts for both the precipitating and precipitation-less regions, and is given by

$$\begin{aligned} P_{(i)}(x_1, x_2, \ldots, x_D) = {} & f_{p(i)} P_{(J,K+\Omega)(i)}(x_1, x_2, \ldots, x_D) \\ & + \left(1 - f_{p(i)}\right) P_{(J,K)(i)}(x_1, x_2, \ldots, x_{J+K}) \left(\prod_{\epsilon=J+K+1}^{D} \delta(x_\epsilon) \right). \end{aligned} \tag{1.6}$$

The subscripts in the ith component, $P_{(J,K)(i)}$ or $P_{(J,K+\Omega)(i)}$, denote the number of normal variates, J, and the number of lognormal variates, K or $K + \Omega$, used in Eq. (1.7).

Each original PDF component is split into precipitating and precipitation-less subcomponents. The component means, variances, and correlations for variables $x_1 \ldots x_{J+K}$ do not differ between the precipitating and precipitation-less parts of Eq. (1.6). This greatly simplifies the procedure for parameterizing the component means and variances, given the grid-level means and variances. Additionally, keeping the component means and variances the same between the in-precipitation and outside-precipitation parts of Eq. (1.6) allows the PDF to be reduced back to prior versions. For instance, the multivariate PDF in Eqs. (1.5) and (1.6) reduces to the version given in Larson and Griffin (2013) when all $f_{p(i)} = 1$ and various PDF parameters are chosen appropriately. Furthermore, when microphysics is not used in a simulation, hydrometeors are not found in the PDF. In this scenario, the PDF reduces to the original version found in Golaz et al. (2002a).

The PDF does not contain a fraction for each hydrometeor species or type, but rather one precipitation fraction. Each PDF component is split into two sub-components (in-precipitation and outside-precipitation). Including a fraction for each hydrometeor type (rain, snow, etc.) would cause the number of sub-components to grow exponentially with the number of fractions. Using n_f hydrometeor fractions increases the number of sub-components to 2^{n_f} in each PDF component. This would make setting the PDF parameters associated with each sub-component increasingly difficult.

The multivariate PDF can be adjusted to account for a situation when a variable has a constant value in a PDF (sub-)component. In that situation, the variable can be reduced to a delta function at the (sub-)component mean value. A good example of this would be setting N_{cn} to a constant value in order to use a constant in-cloud value of cloud droplet concentration. This is also especially useful when dealing with more than one hydrometeor. If one hydrometeor species is found at a grid level, but another hydrometeor species is not found at that level, the hydrometeor that is not found can reduce to a delta function at 0 in the precipitating sub-component of Eq. (1.6).

The general form of the m-variate hybrid normal/lognormal distribution in the ith PDF component, $P_{(j,k)(i)}\left(x_1, x_2, \ldots, x_m\right)$, which is found in each sub-component of Eq. (1.6), consists of j normal variates and k lognormal variates, where $m = j + k$. The first j variables are normally distributed and the remaining k variables are lognormally distributed. The multivariate normal/lognormal PDF is given by (Fletcher and Zupanski 2006)

$$\begin{aligned} P_{(j,k)(i)}\left(x_1, x_2, \ldots, x_m\right) = & \frac{1}{(2\pi)^{\frac{m}{2}} \left|\boldsymbol{\Sigma}_{(i)}\right|^{\frac{1}{2}}} \left(\prod_{\tau=j+1}^{m} \frac{1}{x_\tau} \right) \\ & \times \exp\left\{ -\frac{1}{2} \left(\vec{\boldsymbol{x}} - \vec{\boldsymbol{\mu}}_{(i)} \right)^{\mathrm{T}} \boldsymbol{\Sigma}_{(i)}^{-1} \left(\vec{\boldsymbol{x}} - \vec{\boldsymbol{\mu}}_{(i)} \right) \right\}. \end{aligned} \tag{1.7}$$

Both $\vec{\boldsymbol{x}}$ and $\vec{\boldsymbol{\mu}}_{(i)}$ are $m \times 1$ vectors and are given by

$$\vec{\boldsymbol{x}} = \begin{bmatrix} x_1 \\ \vdots \\ x_j \\ \ln x_{j+1} \\ \vdots \\ \ln x_m \end{bmatrix} \qquad \text{and} \qquad \vec{\boldsymbol{\mu}}_{(i)} = \begin{bmatrix} \mu_{x_1(i)} \\ \vdots \\ \mu_{x_j(i)} \\ \tilde{\mu}_{x_{j+1}(i)} \\ \vdots \\ \tilde{\mu}_{x_m(i)} \end{bmatrix}, \tag{1.8}$$

where $\mu_{x(i)}$ is the ith component mean of x and where $\tilde{\mu}_{x(i)}$, which is relevant for the lognormal variates, is the ith component mean of $\ln x$. This represents the mean of x in normal space. The covariance matrix is denoted $\boldsymbol{\Sigma}_{(i)}$ and its determinant is denoted $\left|\boldsymbol{\Sigma}_{(i)}\right|$. It has dimension $m \times m$ and is given by

$$\boldsymbol{\Sigma}_{(i)} = \begin{bmatrix} \sigma^2_{x_1(i)} & \cdots & \rho_{x_1,x_j(i)}\sigma_{x_1(i)}\sigma_{x_j(i)} & \cdots & \tilde{\rho}_{x_1,x_m(i)}\sigma_{x_1(i)}\tilde{\sigma}_{x_m(i)} \\ \vdots & \ddots & \vdots & & \vdots \\ \rho_{x_1,x_j(i)}\sigma_{x_1(i)}\sigma_{x_j(i)} & \cdots & \sigma^2_{x_j(i)} & \cdots & \tilde{\rho}_{x_j,x_m(i)}\sigma_{x_j(i)}\tilde{\sigma}_{x_m(i)} \\ \vdots & & \vdots & \ddots & \vdots \\ \tilde{\rho}_{x_1,x_m(i)}\sigma_{x_1(i)}\tilde{\sigma}_{x_m(i)} & \cdots & \tilde{\rho}_{x_j,x_m(i)}\sigma_{x_j(i)}\tilde{\sigma}_{x_m(i)} & \cdots & \tilde{\sigma}^2_{x_m(i)} \end{bmatrix}. \tag{1.9}$$

The ith PDF component standard deviation of x is denoted $\sigma_{x(i)}$. For lognormal variates, the ith PDF component standard deviation of $\ln x$ is denoted $\tilde{\sigma}_{x(i)}$. This represents the standard deviation of x in normal space. The correlation of x and y in the ith PDF component, when both x and y are normal variates, is written as $\rho_{x,y(i)}$. The ith PDF component correlation of either x and $\ln y$ (one normal variate and one lognormal variate) or $\ln x$ and $\ln y$ (two lognormal variates) is written as $\tilde{\rho}_{x,y(i)}$. This represents the correlation of x and y in normal space. The advantage of a *single* multivariate PDF, as opposed to a collection of individual marginal PDFs, is that the multivariate PDF accounts for correlations among the variables in the PDF. This is advantageous when calculating such quantities as rain water accretion

rate and rain water evaporation rate.

When variables are integrated out of the full multivariate PDF, the result is a multivariate marginal PDF consisting of fewer variables. When all variables but one are integrated out of the PDF, the result is a univariate marginal or individual marginal PDF. For any hydrometeor species, h, found in the full multivariate PDF in Eq. (1.5), the univariate marginal distribution is

$$P(h) = \sum_{i=1}^{n} \xi_{(i)} \left(f_{p(i)} P_{L(i)}(h) + \left(1 - f_{p(i)}\right) \delta(h) \right), \tag{1.10}$$

where $P_{L(i)}(h)$ is a lognormal distribution in the ith PDF component, which is given by

$$P_{L(i)}(h) = \frac{1}{(2\pi)^{\frac{1}{2}} \, \tilde{\sigma}_{h(i)} \, h} \exp\left\{ \frac{-\left(\ln h - \tilde{\mu}_{h(i)}\right)^2}{2 \, \tilde{\sigma}_{h(i)}^2} \right\}. \tag{1.11}$$

The in-precipitation mean of h in the ith PDF component is $\mu_{h(i)}$. This is the mean of the ith lognormal of h. However, $\tilde{\mu}_{h(i)}$, as in Eq. (1.11), is the normal-space component mean of h. It is the in-precipitation mean of $\ln h$ in the ith PDF component and is given by

$$\tilde{\mu}_{h(i)} = \ln\left(\mu_{h(i)} \left(1 + \frac{\sigma_{h(i)}^2}{\mu_{h(i)}^2} \right)^{-\frac{1}{2}} \right), \tag{1.12}$$

where $\sigma_{h(i)}$ is the in-precipitation standard deviation of h in the ith PDF component. The quantity $\sigma_{h(i)}$ is the standard deviation of the ith lognormal of h. The normal-space component standard deviation of h is $\tilde{\sigma}_{h(i)}$, as found in Eq. (1.11). It is the in-precipitation standard deviation of $\ln h$ in the ith PDF component and is given by

$$\tilde{\sigma}_{h(i)} = \sqrt{\ln\left(1 + \frac{\sigma_{h(i)}^2}{\mu_{h(i)}^2} \right)}. \tag{1.13}$$

The variables that are distributed marginally as binormals use similar notation. For example, $\mu_{w(i)}$ is the mean of w in the ith PDF component, or the mean of the ith normal.

Likewise, $\sigma_{w(i)}$ is the standard deviation of w in the ith PDF component, or the standard deviation of the ith normal.

1.3 PDF parameters

This paper will use the phrase "PDF parameters" to refer to the PDF *component* means, standard deviations, and correlations involving variables in the PDF, as well as the mixture fractions and the PDF component precipitation fractions. The PDF parameters are calculated from various grid-mean input variables. In this paper, the component means, standard deviations, and correlations involving w, r_t, and θ_l, and the mixture fractions, $\xi_{(1)}$ and $\xi_{(2)}$, are calculated according to the Analytic Double Gaussian 2 (ADG2) PDF, as described in Section (e) of the Appendix of Larson et al. (2002). ADG2 requires the following quantities as input: the overall (grid-box) mean, variance, and third-order central moment of w ($\overline{w}$, $\overline{w'^2}$, and $\overline{w'^3}$, respectively), the overall mean and variance of r_t ($\overline{r_t}$ and $\overline{r_t'^2}$, respectively), and the overall mean and variance of θ_l ($\overline{\theta_l}$ and $\overline{\theta_l'^2}$, respectively). ADG2 preserves the values of these input variables, meaning that the PDF parameters can be used to successfully reconstruct the values of the input variables. Additionally, ADG2 requires and preserves the overall covariance of w and r_t ($\overline{w'r_t'}$), the overall covariance of w and θ_l ($\overline{w'\theta_l'}$), and the overall covariance of r_t and θ_l ($\overline{r_t'\theta_l'}$). All of the aforementioned quantities are prognosed or diagnosed in CLUBB and are not the subject of this paper.

The individual marginal distribution for N_{cn} is specified to be a single lognormal over the entire subgrid domain. This requires that both PDF component means equal the overall (grid-box) mean ($\mu_{N_{cn}(1)} = \mu_{N_{cn}(2)} = \overline{N_{cn}}$). Likewise, this requires that both PDF component standard deviations equal the overall standard deviation ($\sigma_{N_{cn}(1)} = \sigma_{N_{cn}(2)} = \overline{N_{cn}'^2}^{1/2}$).

When no hydrometeor species are found at a grid level ($\vec{\boldsymbol{h}} = 0$), $f_p = f_{p(1)} = f_{p(2)} = 0$. Otherwise, if any hydrometeor species in $\vec{\boldsymbol{h}}$ is found at a grid level (has a value greater than 0), $f_p|_{\text{tol}} \leq f_p \leq 1$, where $f_p|_{\text{tol}}$ is the minimum value allowed for precipitation fraction when

hydrometeors are present. We now describe how CLUBB parameterizes $f_{p(1)}$ and $f_{p(2)}$, given f_p. First, we note that

$$f_p = \xi_{(1)} f_{p(1)} + \xi_{(2)} f_{p(2)}. \tag{1.14}$$

A tunable parameter, υ_* (where the $*$ subscript denotes a tunable or adjustable parameter), is introduced and is defined as the ratio of $\xi_{(1)} f_{p(1)}$ to f_p, where $0 \leq \upsilon_* \leq 1$. The precipitation fraction of PDF component 1 is solved by

$$f_{p(1)} = \min\left(\frac{\upsilon_* f_p}{\xi_{(1)}},\, 1\right). \tag{1.15}$$

The PDF component 2 precipitation fraction can now be solved by

$$f_{p(2)} = \min\left(\frac{f_p - \xi_{(1)} f_{p(1)}}{\xi_{(2)}},\, 1\right). \tag{1.16}$$

When $f_{p(1)}$ calculated by Eq. (1.15) is small enough to force $f_{p(2)}$ calculated by Eq. (1.16) to be limited at 1, the value of $f_{p(1)}$ is recalculated (with $f_{p(2)} = 1$) and is increased enough to satisfy Eq. (1.14).

1.3.1 Hydrometeor PDF parameters

A mean-and-variance-preserving method is used to calculate the in-precipitation means of the hydrometeor field in the two PDF components, $\mu_{h(1)}$ and $\mu_{h(2)}$, and the in-precipitation standard deviations of the hydrometeor field in the two PDF components, $\sigma_{h(1)}$ and $\sigma_{h(2)}$. The fields that need to be provided as inputs are the overall (grid-box) mean of the hydrometeor, $\overline{h}$, the overall variance of the hydrometeor, $\overline{h'^2}$, the mixture fraction in each PDF component, $\xi_{(1)}$ and $\xi_{(2)}$, the overall precipitation fraction, f_p, and the precipitation fraction in each PDF component, $f_{p(1)}$ and $f_{p(2)}$. Given these inputs, the in-precipitation mean of the hydrometeor, $\overline{h|_{\rm ip}}$, can be calculated by

$$\overline{h|_{\rm ip}} = \frac{\overline{h}}{f_p}, \tag{1.17}$$

and the in-precipitation variance of the hydrometeor, $\overline{h|_{\text{ip}}'^2}$, can be calculated by

$$\overline{h|_{\text{ip}}'^2} = \frac{\overline{h'^2} + \overline{h}^2 - f_p \overline{h|_{\text{ip}}}^2}{f_p}. \tag{1.18}$$

The grid-level mean value of any function that is written in terms of variables involved in the PDF can be found be integrating over the product of that function and the PDF. For example,

$$\overline{h} = \int_0^\infty h\, P(h)\ \mathrm{d}h \qquad \text{and} \qquad \overline{h'^2} = \int_0^\infty \left(h - \overline{h}\right)^2 P(h)\ \mathrm{d}h. \tag{1.19}$$

After integrating, the equation for $\overline{h}$ expressed in terms of PDF parameters is

$$\overline{h} = \xi_{(1)} f_{p(1)} \mu_{h(1)} + \xi_{(2)} f_{p(2)} \mu_{h(2)}. \tag{1.20}$$

Likewise, the equation for $\overline{h'^2}$ expressed in terms of PDF parameters is

$$\overline{h'^2} = \xi_{(1)} f_{p(1)} \left(\mu_{h(1)}^2 + \sigma_{h(1)}^2\right) + \xi_{(2)} f_{p(2)} \left(\mu_{h(2)}^2 + \sigma_{h(2)}^2\right) - \overline{h}^2. \tag{1.21}$$

When the hydrometeor is not found at a grid level, $\overline{h} = \overline{h'^2} = 0$ and the *component* means and standard deviations of the hydrometeor also have a value of 0. When the hydrometeor is found at a grid level, $\overline{h} > 0$. Precipitation may be found in only PDF component 1, only PDF component 2, or in both PDF components. When precipitation is found in only PDF component 1, $\mu_{h(2)} = \sigma_{h(2)} = 0$ and $\mu_{h(1)}$ and $\sigma_{h(1)}$ can easily be solved by Eq. (1.20) and Eq. (1.21). Likewise, when precipitation is found in only PDF component 2, $\mu_{h(1)} = \sigma_{h(1)} = 0$ and $\mu_{h(2)}$ and $\sigma_{h(2)}$ can easily be solved by the same equation set.

When there is precipitation found in both PDF components, further information is required to solve for the two component means and the two component standard deviations.

The variable R is introduced such that

$$R \equiv \frac{\sigma_{h(2)}^2}{\mu_{h(2)}^2}. \tag{1.22}$$

In order to allow the ratio of $\sigma_{h(1)}^2$ to $\mu_{h(1)}^2$ to vary, the parameter ζ_* is introduced, such that

$$R\,(1+\zeta_*) = \frac{\sigma_{h(1)}^2}{\mu_{h(1)}^2}, \tag{1.23}$$

where $\zeta_* > -1$. When $\zeta_* > 0$, then $\sigma_{h(1)}^2/\mu_{h(1)}^2$ increases at the expense of $\sigma_{h(2)}^2/\mu_{h(2)}^2$, which decreases in this variance-preserving equation set. When $\zeta_* = 0$, then $\sigma_{h(1)}^2/\mu_{h(1)}^2 = \sigma_{h(2)}^2/\mu_{h(2)}^2$. When $-1 < \zeta_* < 0$, then $\sigma_{h(2)}^2/\mu_{h(2)}^2$ increases at the expense of $\sigma_{h(1)}^2/\mu_{h(1)}^2$, which decreases. Combining Eq. (1.21), Eq. (1.22), and Eq. (1.23), the equation for $\overline{h'^2}$ can be rewritten as

$$\overline{h'^2} = \xi_{(1)} f_{p(1)} \left(1 + R\,(1+\zeta_*)\right) \mu_{h(1)}^2 + \xi_{(2)} f_{p(2)} \left(1 + R\right) \mu_{h(2)}^2 - \overline{h}^{\,2}. \tag{1.24}$$

Both the variance of each PDF component and the spread between the means of each PDF component contribute to the in-precipitation variance of the hydrometeor ($\overline{h|_{\text{ip}}'^2}$). At one extreme, the standard deviation of each component could be set to 0 and the in-precipitation variance could be accounted for by spreading the PDF component (in-precipitation) means far apart. The value of R in this scenario would be its minimum possible value, which is 0. At the other extreme, the means of each component could be set equal to each other and the in-precipitation variance could be accounted for entirely by the PDF component (in-precipitation) standard deviations. The value of R in this scenario would be its maximum possible value, which is $R_{\max}$.

In order to calculate the value of $R_{\max}$, set $\mu_{h(1)} = \mu_{h(2)} = \overline{h|_{\text{ip}}}$ and $R = R_{\max}$. Eq. (1.24)

becomes

$$\overline{h'^2} + \overline{h}^2 = \overline{h|_{\text{ip}}}^2 \left(\xi_{(1)} f_{p(1)} \left(1 + R_{\max} \left(1 + \zeta_* \right) \right) + \xi_{(2)} f_{p(2)} \left(1 + R_{\max} \right) \right). \tag{1.25}$$

When Eq. (1.18) is substituted into Eq. (1.25), $R_{\max}$ is solved for and the equation is

$$R_{\max} = \left(\frac{f_p}{\xi_{(1)} f_{p(1)} \left(1 + \zeta_* \right) + \xi_{(2)} f_{p(2)}} \right) \frac{\overline{h|_{\text{ip}}'^2}}{\overline{h|_{\text{ip}}}^2}. \tag{1.26}$$

In the scenario that $\zeta_* = 0$ the equation for $R_{\max}$ reduces to the ratio of $\overline{h|_{\text{ip}}'^2}$ to $\overline{h|_{\text{ip}}}^2$.

In order to calculate the value of R, a parameter is used to prescribe the ratio of R to its maximum value, $R_{\max}$. The prescribed parameter is denoted o_*, where

$$R = o_* R_{\max}, \tag{1.27}$$

and where $0 \leq o_* \leq 1$. Both R and $R_{\max}$ are known functions of the inputs and tunable parameters. When $o_* = 0$, the standard deviation of each PDF component is 0, and $\mu_{h(1)}$ is spread far from $\mu_{h(2)}$. When $o_* = 1$, then $\mu_{h(1)} = \mu_{h(2)}$, and the standard deviations of the PDF components account for all of the in-precipitation variance. At intermediate values of o_*, the means of each PDF component are somewhat spread apart and each PDF component has some width. The new equation for hydrometeor variance becomes

$$\overline{h'^2} = \xi_{(1)} f_{p(1)} \left(1 + o_* R_{\max} \left(1 + \zeta_* \right) \right) \mu_{h(1)}^2 + \xi_{(2)} f_{p(2)} \left(1 + o_* R_{\max} \right) \mu_{h(2)}^2 - \overline{h}^2. \tag{1.28}$$

The two remaining unknowns, $\mu_{h(1)}$ and $\mu_{h(2)}$, can be solved by a set of two equations, Eq. (1.20) for $\overline{h}$ and Eq. (1.28) for $\overline{h'^2}$. All other quantities in the equation set are known quantities. To find the solution, Eq. (1.20) is rewritten to isolate $\mu_{h(2)}$ such that

$$\mu_{h(2)} = \frac{\overline{h} - \xi_{(1)} f_{p(1)} \mu_{h(1)}}{\xi_{(2)} f_{p(2)}}. \tag{1.29}$$

The above equation is substituted into Eq. (1.28). The resulting equation is rewritten in the form

$$Q_a \mu_{h(1)}^2 + Q_b \mu_{h(1)} + Q_c = 0, \tag{1.30}$$

so the solution to the quadratic equation for $\mu_{h(1)}$ is

$$\mu_{h(1)} = \frac{-Q_b \pm \sqrt{Q_b^2 - 4Q_a Q_c}}{2Q_a}, \tag{1.31}$$

where:

$$\begin{aligned} Q_a &= \xi_{(1)} f_{p(1)} \left(1 + o_* R_{\max} \left(1 + \zeta_*\right)\right) + \frac{\xi_{(1)}^2 f_{p(1)}^2}{\xi_{(2)} f_{p(2)}} \left(1 + o_* R_{\max}\right), \\ Q_b &= -2 \frac{\xi_{(1)} f_{p(1)}}{\xi_{(2)} f_{p(2)}} \left(1 + o_* R_{\max}\right) \overline{h}, \text{ and} \\ Q_c &= -\left(\overline{h'^2} + \left(1 - \frac{1 + o_* R_{\max}}{\xi_{(2)} f_{p(2)}}\right) \overline{h}^2\right). \end{aligned} \tag{1.32}$$

The value of Q_a is always positive and the value of Q_b is always negative. The value of Q_c can be positive, negative, or zero. Since $\left(1 - \left(1 + o_* R_{\max}\right) / \left(\xi_{(2)} f_{p(2)}\right)\right) \overline{h}^2$ is always negative and $\overline{h'^2}$ is always positive, the sign of Q_c depends on which term is greater in magnitude.

When $\overline{h'^2}$ is greater, the sign of Q_c is negative. This means that $-4Q_a Q_c$ is positive, which in turn means that $\sqrt{Q_b^2 - 4Q_a Q_c}$ is greater in magnitude than $-Q_b$. If the subtraction option of the $\pm$ were to be chosen, the value of $\mu_{h(1)}$ would be negative in this scenario. At first glance, it might appear natural to always choose the addition option. However, this set of equations was derived with the condition that $\mu_{h(1)}$ equals $\mu_{h(2)}$ when $o_* = 1$. When $\zeta_* \geq 0$, this happens when the addition option is chosen, but not when the subtraction option is chosen. However, when $\zeta_* < 0$, this happens when the subtraction option is chosen, but

not when the addition option is chosen. So, the equation for $\mu_{h(1)}$ becomes

$$\mu_{h(1)} = \begin{cases} \dfrac{-Q_b + \sqrt{Q_b^2 - 4Q_aQ_c}}{2Q_a}, & \text{when } \zeta_* \geq 0; \text{ and} \\ \\ \dfrac{-Q_b - \sqrt{Q_b^2 - 4Q_aQ_c}}{2Q_a}, & \text{when } \zeta_* < 0. \end{cases} \tag{1.33}$$

The value of $\mu_{h(2)}$ can now be found using Eq. (1.29). After $\mu_{h(1)}$ and $\mu_{h(2)}$ have been solved, $\sigma_{h(1)}$ and $\sigma_{h(2)}$ can be solved by plugging Eq. (1.27) back into Eq. (1.23) and Eq. (1.22), respectively.

As the value of $\overline{h|_{\text{ip}}'^2}/\overline{h|_{\text{ip}}}^2$ increases and as the value of o_* decreases (narrowing the in-precipitation standard deviations and increasing the spread between the in-precipitation means), one of the component means may become negative. This happens because there is a limit to the amount of in-precipitation variance that can be represented by this kind of distribution. In order to prevent out-of-bounds values of $\mu_{h(1)}$ or $\mu_{h(2)}$, a lower limit is declared, called $\mu_h|_{\text{min}}$, where $\mu_h|_{\text{min}}$ is a small, positive value that is typically set to be two orders of magnitude smaller than $\overline{h|_{\text{ip}}}$. The value of $\mu_{h(1)}$ or $\mu_{h(2)}$ will be limited from becoming any smaller (or negative) at this value. From there, the value of the other hydrometeor in-precipitation component mean is easy to calculate. Then, both values will be entered into the calculation of hydrometeor variance in Eq. (1.24), which will be rewritten to solve for R. Then, both the hydrometeor mean and hydrometeor variance will be preserved with a valid distribution.

When the value of $\zeta_* \geq 0$, the value of $\mu_{h(1)}$ tends to be larger than the value of $\mu_{h(2)}$. Likewise when the value of $\zeta_* < 0$, the value of $\mu_{h(2)}$ tends to be larger than the value of $\mu_{h(1)}$. Since most cloud water and cloud fraction tends to be found in PDF component 1, it is appropriate and advantageous to have the larger in-precipitation component mean of the hydrometeor also found in PDF component 1. The recommended value of ζ_* is a value greater than or equal to 0.

This method of closing the hydrometeor PDF parameter equation set produces a DDL hydrometeor PDF shape when $0 < o_* < 1$ or when $\zeta_* \neq 0$. The DL hydrometeor PDF shape is produced simply by setting $o_* = 1$ and $\zeta_* = 0$. These settings force $\mu_{h(1)} = \mu_{h(2)}$ and $\sigma_{h(1)} = \sigma_{h(2)}$, which result in a single lognormal within the precipitating portion of the subgrid domain. Furthermore, if, in addition to setting $o_* = 1$ and $\zeta_* = 0$, one simply sets $f_{p(1)} = f_{p(2)} = 1$, then precipitation is found everywhere within the subgrid domain, producing the SL hydrometeor PDF shape. Hence it is very easy to change between DDL, DL, and SL hydrometeor PDF shapes. Additionally, it should be noted that there is only one o_* and only one ζ_* applied to all the hydrometeor species in $\vec{\boldsymbol{h}}$.

In limited testing, the value of the tunable parameter ζ_* did not affect the results much for CLUBB's DDL PDF shape. The value of ζ_* has been left at 0, effectively eliminating a tunable or adjustable parameter from the scheme. When $\zeta_* = 0$, the DDL shape approaches the DL shape as o_* approaches 1. As o_* approaches 0, the DDL shape approaches a double-delta in precipitation (in addition to the delta at 0). Additionally, when $0 < o_* < 1$, the in-precipitation skewness of the hydrometeor field is influenced by υ_*. As υ_* approaches 0, the in-precipitation distribution becomes more highly (positively) skewed. In Gaussian space (see Section 1.5), the in-precipitation distribution is positively skewed. As υ_* approaches 1, the in-precipitation distribution is less (positively) skewed. In Gaussian space, the in-precipitation distribution is negatively skewed. For the results presented in this paper for the DDL hydrometeor PDF shape, the remaining two tunable parameters have been set to the values $o_* = 0.5$ and $\upsilon_* = 0.55$.

1.4 Model setup and testing

There is insufficient data from observations to calculate all the fields that need to be input into CLUBB's PDF. However, this data can be supplied easily and plentifully by a LES. In this paper, LES output of precipitating cases is simulated by the System for At-

mospheric Modeling (SAM) (Khairoutdinov and Randall 2003). SAM uses an anelastic equation set that predicts liquid water static energy, total water mixing ratio, vertical velocity, and both the south-north and west-east components of horizontal velocity. Additionally, it predicts hydrometeor fields as directed by the chosen microphysics scheme. A predictive 1.5-order subgrid-scale turbulent kinetic energy closure is used to compute the subgrid-scale fluxes (Deardorff 1980). SAM uses a fixed, Cartesian spatial grid and a third-order Adams-Bashforth time-stepping scheme to advance the predictive equations of motion. It uses periodic boundary conditions and a rigid lid at the top of the domain. The second-order MPDATA (multidimensional positive definite advection transport algorithm) scheme is used to advect the predictive variables (Smolarkiewicz and Grabowski 1990).

In order to assess the generality of the different hydrometeor PDF shapes for different cloud regimes, SAM was used to run three idealized test cases — a precipitating shallow cumulus case, a drizzling stratocumulus case, and a deep convective case. The use of cases from differing cloud regimes help avoid overfitting the parameterizations of PDF shape. The setup for the precipitating shallow cumulus test case was based on the Rain in Cumulus over the Ocean (RICO) LES intercomparison (van Zanten et al. 2011). The horizontal resolution was 100 m, and 256 grid boxes were used in each horizontal direction. The vertical resolution was a constant 40 m and 100 grid boxes were used in the vertical. The model top was located at 4000 m in altitude. The model time step was 1 s and the duration of the simulation was 72 hours. A vertical profile of level-averaged statistics was output every minute and a three-dimensional snapshot of hydrometeor fields was output every hour.

The RICO simulation was run with SAM's implementation of the Khairoutdinov and Kogan (2000, hereafter KK) warm microphysics scheme. KK microphysics predicts both r_r and N_r. SAM's implementation of KK microphysics uses a saturation adjustment to diagnose r_c, and cloud droplet concentration is set to a constant value (which is 70 cm^{-3} for RICO).

The setup for the drizzling stratocumulus test case was taken from the LES intercom-

parison based on research flight two (RF02) of the second Dynamics and Chemistry of Marine Stratocumulus (DYCOMS-II) field experiment (Ackerman et al. 2009). The horizontal resolution was 50 m and 128 grid boxes were used in each horizontal direction. An unevenly-spaced vertical grid was used containing 96 grid boxes and covering a domain of depth 1459.3 m. The model time step was 0.5 s and the duration of the simulation was six hours. A vertical profile of level-averaged statistics was output every minute and a three-dimensional snapshot of hydrometeor fields was output every 30 minutes. The DYCOMS-II RF02 simulation was also run with SAM's implementation of KK microphysics and used a constant cloud droplet concentration of 55 cm^{-3}.

The setup for the deep convective test case was taken from the LES intercomparison based on the Large-Scale Biosphere-Atmosphere (LBA) experiment (Grabowski et al. 2006). The horizontal resolution was 1000 m, and 128 grid boxes were used in each horizontal direction. An unevenly-spaced vertical grid was used, containing 128 grid boxes and covering a domain of depth 27500 m. The model time step was 6 s and the duration of the simulation was six hours. A vertical profile of level-averaged statistics was output every minute and a three-dimensional snapshot of hydrometeor fields was output every 15 minutes for the final 3.5 hours of the simulation.

The LBA case requires a microphysics scheme that can account for ice-phase hydrometeor species. The LBA simulation was run with Morrison et al. (2005) microphysics, which predicts the mixing ratio and number concentration (per unit mass) of rain, cloud ice, snow, and graupel. SAM's implementation of Morrison microphysics diagnoses r_c using a saturation adjustment right before the microphysics is called and then allows microphysics to update the value of r_c, which in turn is used to update the value r_t. Cloud droplet concentration was set to a constant value of 100 cm^{-3}.

CLUBB's hydrometeor PDF shapes will be compared to histograms of hydrometeors produced by SAM LES data. Our goal is to isolate errors in the PDF shape itself. In order to eliminate sources of error outside of the PDF shape and provide an "apples-to-apples"

comparison of CLUBB's PDF shapes to SAM data, we drive CLUBB's PDF using SAM LES fields, rather than perform interactive CLUBB simulations. The following fields are taken from SAM's statistical profiles and are used as inputs to CLUBB's PDF: $\overline{r_t}$, $\overline{\theta_l}$, $\overline{w'^2}$, $\overline{r_t'^2}$, $\overline{\theta_l'^2}$, $\overline{w'r_t'}$, $\overline{w'\theta_l'}$, $\overline{r_t'\theta_l'}$, $\overline{w'^3}$, f_p, $\overline{r_r}$, $\overline{r_r'^2}$, $\overline{N_r}$, and $\overline{N_r'^2}$. For the LBA case, we add $\overline{r_i}$, $\overline{r_i'^2}$, $\overline{N_i}$, $\overline{N_i'^2}$, $\overline{r_s}$, $\overline{r_s'^2}$, $\overline{N_s}$, $\overline{N_s'^2}$, $\overline{r_g}$, $\overline{r_g'^2}$, $\overline{N_g}$, and $\overline{N_g'^2}$. Another input to CLUBB's PDF is $\overline{w}$. The value of $\overline{w}$ from large-scale forcing is set according to case specifications in both SAM and CLUBB. CLUBB's PDF is generated at every SAM vertical level and at every output time of SAM level-averaged statistical profiles.

Additionally, covariances that involve at least one hydrometeor are added to the above list and are used to calculate the PDF component correlations of the same two variables. These covariances are $\overline{r_t'r_r'}$, $\overline{\theta_l'r_r'}$, $\overline{r_t'N_r'}$, $\overline{\theta_l'N_r'}$, and $\overline{r_r'N_r'}$. Please see Appendix B for more details on the calculation of PDF component correlations. The values of the component correlations do not affect the individual marginal PDFs of the hydrometeors. They are included for the calculation of microphysics process rates (see Section 1.5.2).

Owing to differences between the KK and Morrison microphysics schemes in SAM, f_p used by CLUBB's PDF is computed slightly differently depending on which microphysics scheme is used by SAM. The differences are due to the number of hydrometeor species involved in the microphysics, the thresholding found internally in the microphysics codes, and the variables that are output to statistics by SAM. KK microphysics contains only rain, and SAM's implementation of KK microphysics clips any value of r_r (and with it N_r) below a threshold value in clear air. Therefore, it is simple to set f_p to the fraction of the domain occupied by non-zero values of r_r and N_r. Morrison microphysics predicts rain, ice, snow, and graupel. For each of these species, SAM outputs a fraction. To provide an apples-to-apples comparison with CLUBB, f_p is approximated as the greatest of these four fractions at any particular grid level.

Although f_p is provided by the LES for this study, it can be diagnosed based on the cloud fraction using a method such as that of Morrison and Gettelman (2008). If the cloud

fraction, in turn, is diagnosed based on the omnipresent prediction of means, variances, and other moments — as in higher-order moment parameterizations such as CLUBB — then the onset of partial cloudiness is well defined and indeterminacy about the time of cloud initiation is avoided. In contrast, parameterizations that diagnose cloud fraction based on, e.g., cloud water mixing ratio, lack crucial information in cloudless grid boxes, as discussed in Tompkins (2002). The well-defined onset of CLUBB's cloud fraction is inherited by the precipitation fraction.

1.5 Results

We first evaluate the shape of the idealized PDFs directly against LES. Histograms of SAM LES data are generated from the three-dimensional snapshots of hydrometeor fields. One histogram is generated at every vertical level for each hydrometeor field. A histogram of a SAM hydrometeor field is compared to the CLUBB marginal PDF of that hydrometeor field at the same vertical level and output time. The comparison is done with each of the SL, DL, and DDL PDF shapes.

Figure 1.2 compares marginal PDFs involving r_r and N_r for the RICO case at an altitude of 380 m and a time of 4200 min. For the plot of the PDF of r_r in Fig. 1.2a, the delta function at $r_r = 0$ has been omitted. The SAM data is divided into 100 bins, equally-sized in r_r, that range from the largest value of r_r to the smallest positive value of r_r. (In what follows, all histograms use 100 equal-size bins, arranged from smallest to largest value.) The SL hydrometeor PDF shape significantly overpredicts the PDF at small values of r_r and significantly underpredicts it at large values of r_r. These errors are an expected consequence of the single lognormal's attempt to fit the precipitation-less area. The DL and DDL PDF shapes provide a much closer match qualitatively to the SAM data. A quantitative assessment of the quality of the fit will follow in Section 1.5.1.

Each of the CLUBB hydrometeor PDF shapes has a lognormal distribution within precip-

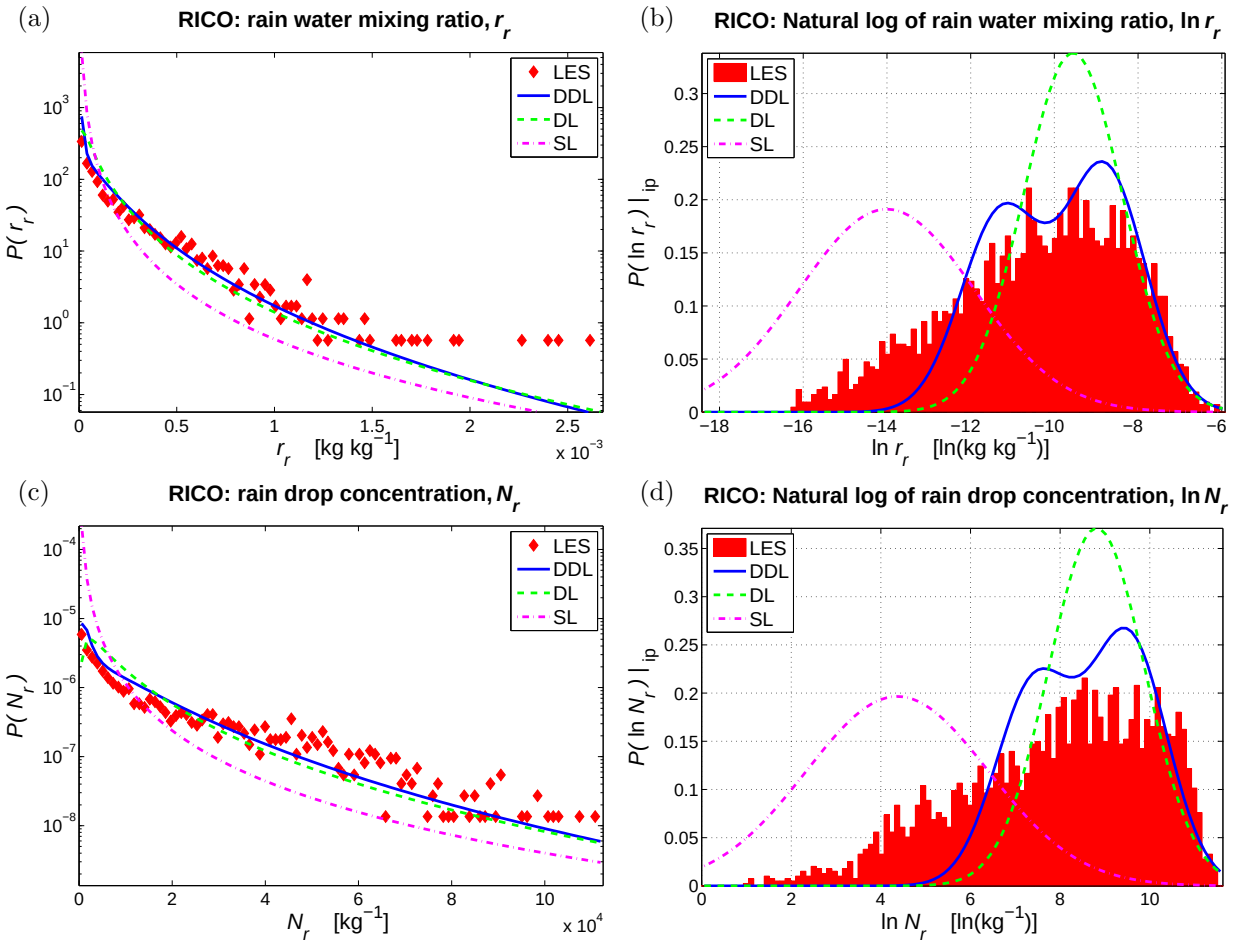

Figure 1.2: PDFs of rain in the RICO precipitating shallow cumulus case at an altitude of 380 m and a time of 4200 min. The SAM LES results are in red, the DDL results are blue solid lines, the DL results are green dashed lines, and the SL results are magenta dashed-dotted lines. (a) The marginal distribution of r_r with the delta at $r_r = 0$ omitted. (b) The marginal distribution of $\ln r_r$ using the "in-precipitation PDF." This is the in-precipitation marginal PDF in Gaussian space. (c) The marginal distribution of N_r with the delta at $N_r = 0$ omitted. (d) The marginal distribution of $\ln N_r$ using the "in-precipitation PDF." Again, this is the in-precipitation marginal PDF in Gaussian space. The DDL provides a better fit to SAM LES than the DL, which in turn provides a better fit than the SL.

itation in each PDF component. Taking the natural logarithm of every point of a lognormal distribution produces a normal distribution, and so the plot of the PDF of $\ln r_r$ in Fig. 1.2b is a normal distribution in each PDF component for each of the DDL, DL, and SL PDF shapes. The plot of the PDF of $\ln r_r$ (hereafter referred to as the PDF of r_r in Gaussian space) complements the aforementioned plot of the PDF of r_r (Fig. 1.2a). The plot of the PDF of r_r is log-scaled on the y-axis, accentuating the small values of $P(r_r)$ that are found at large values of r_r. The plot of the PDF of $\ln r_r$ accentuates the PDF at small values of r_r.

The plot of the PDF of $\ln r_r$ is a plot of only the in-precipitation portion of the distribution, omitting all zero-values. The in-precipitation portion of the PDF is divided by f_p, which allows the area under the curve to integrate to 1. The PDF shown in Fig. 1.2b is the Gaussianized form of Eq. (1.34).

Figure 1.2b shows that the SL hydrometeor PDF shape significantly misses the mark, for its peak is located too far to the left of the bulk of the SAM LES data. This shift of the peak to excessively small values is to be expected of a continuous PDF shape that tries to include a delta function at zero. The DL PDF shape is far too peaked in comparison to the SAM LES data, which is spread out broadly in Gaussian space. The DDL PDF shape is able to achieve a spread-out shape because it has two different means within precipitation. This allows it to better fit the more platykurtic shape of the SAM LES data in Gaussian space.

The plot of the PDF of RICO N_r is found in Fig. 1.2c and the Gaussian-space plot of N_r is found in Fig. 1.2d. Similar to r_r, the SL shape overpredicts the PDF at small values of N_r and underpredicts it at large values of N_r. In Gaussian space, it is easy to see that SL's peak is located too far to the left. The DDL shape provides a better fit than the DL shape to SAM LES data in Fig. 1.2c. Again, the DL shape is too peaked in Fig. 1.2d, whereas the bimodal DDL is able to spread out, which provides a better match to SAM LES data.

Figure 1.3 contains scatterplots that show the bivariate PDF of r_r and N_r for both SAM LES and CLUBB's PDF in RICO at the same altitude and time as Fig. 1.2. The CLUBB PDF scatterpoints were generated by sampling the DDL PDF using an unweighted Monte

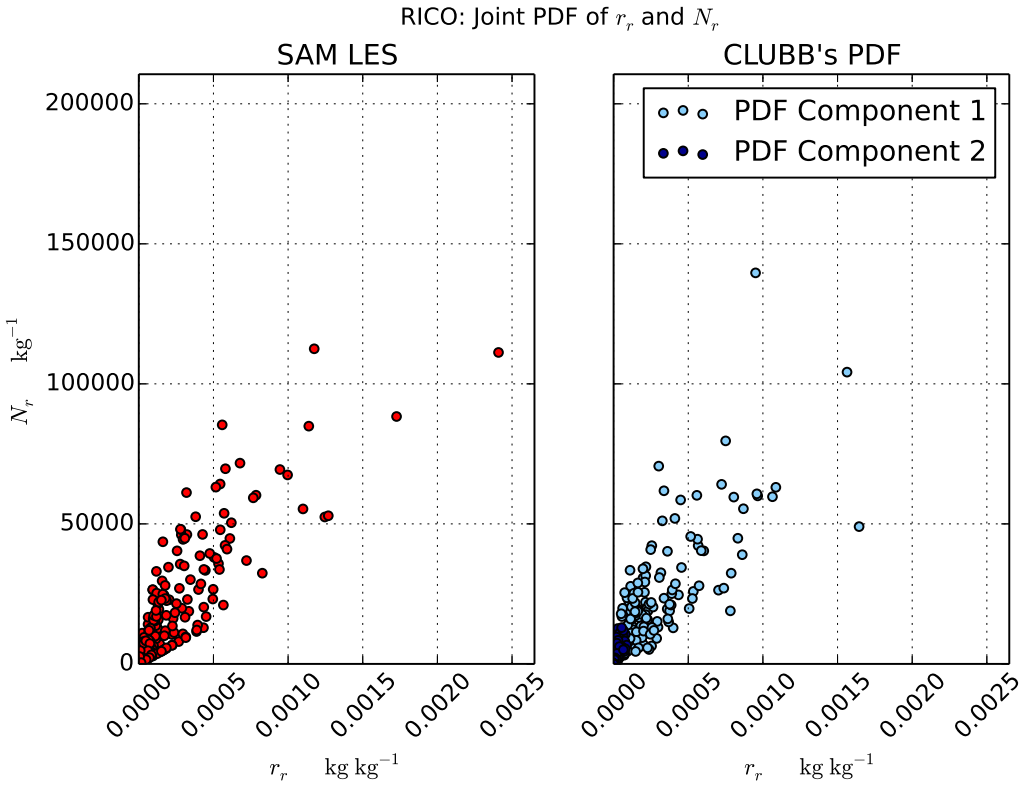

Figure 1.3: Joint PDF of r_r and N_r in the RICO precipitating shallow cumulus case at an altitude of 380 m and a time of 4200 min. SAM LES results are the red scatterpoints. CLUBB PDF scatterpoints were generated by sampling the DDL PDF using an unweighted Monte Carlo scheme. The SAM LES domain is 256×256 grid points, so to provide for the best comparison of LES points to CLUBB PDF sample points, 65536 CLUBB PDF sample points were used. The light blue scatterpoints are from PDF component 1 and the dark blue scatterpoints are from PDF component 2. Every 10th point was plotted from both SAM LES and CLUBB's PDF. The joint nature of the PDF allows r_r and N_r to correlate the same way in CLUBB as they do in SAM.

Carlo sampling scheme. This demonstrates the advantages of the multivariate nature of CLUBB's PDF. The hydrometeor fields are correlated the same way in CLUBB's PDF as they are in SAM LES.

Figure 1.4 compares marginal PDFs involving r_r and N_r for the DYCOMS-II RF02 case at an altitude of 400 m and a time of 330 min. All three hydrometeor PDF shapes provide a decent match to the SAM LES data. In Fig. 1.4a and Fig. 1.4c, the SL and DL PDF shapes dip a little below the SAM LES line in the middle of the data range for r_r and N_r, respectively. The DDL PDF shape stays closer to the SAM LES line in this region. Additionally, the SL PDF shape overestimates the SAM LES line close to the y-axis. In Fig. 1.4b and Fig. 1.4d, the Gaussian-space plots show that the two components of the DDL shape superimpose more than they did for the RICO case, owing to the reduced in-precipitation variance in the drizzling stratocumulus case.

In order to assess how well the PDF shapes are able to capture ice PDFs as well as liquid PDFs, we turn to the LBA case. In LBA, liquid and ice appear at different altitudes and times. Figure 1.5 compares marginal PDFs involving r_r and N_r for the LBA case at an altitude of 2424 m and a time of 330 min. Compared to SAM's PDF, the DDL hydrometeor PDF shape is too bimodal, but it still provides the best visual match of the three hydrometeor PDF shapes to SAM data. The fit will be quantified in Section 1.5.1.

To indicate whether the three PDF shapes work for ice-phase hydrometeors, we compare marginal PDFs involving r_i and N_i for the LBA case at an altitude of 10500 m and a time of 360 min (Figure 1.6). Similar to the r_r and N_r plots for RICO and LBA, Fig. 1.6a and Fig. 1.6c show that the SL PDF shape overpredicts the PDF at small values of r_i and N_i and underpredicts it at large values of r_i and N_i. The DL shape provides a better fit than the SL, and the DDL has a slightly better fit than the DL. The Gaussian-space plots in Fig. 1.6b and Fig. 1.6d show that the SAM LES distribution of $\ln r_i$ and $\ln N_i$ is again platykurtic. The SL PDF shape has a peak that is shifted to the left. The DDL hydrometeor PDF shape is able to spread out the most to cover the platykurtic shape of the LES in Gaussian space.

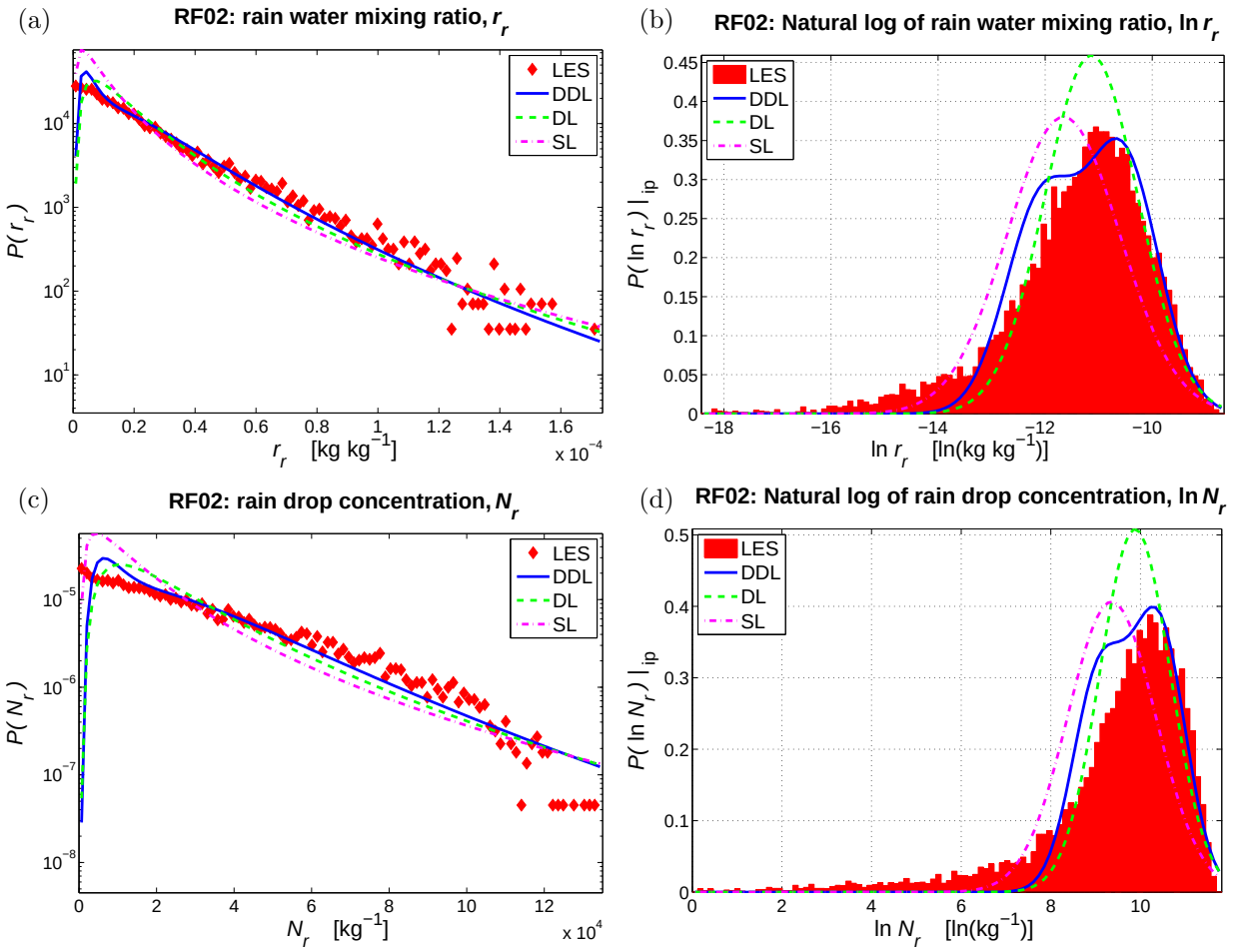

Figure 1.4: PDFs of rain in the DYCOMS-II RF02 drizzling stratocumulus case at an altitude of 400 m and a time of 330 min. The SAM LES results are in red, the DDL results are blue solid lines, the DL results are green dashed lines, and the SL results are magenta dashed-dotted lines. (a) The marginal distribution of r_r with the delta at $r_r = 0$ omitted. (b) The marginal distribution of $\ln r_r$ using the "in-precipitation PDF." This is the in-precipitation marginal PDF in Gaussian space. (c) The marginal distribution of N_r with the delta at $N_r = 0$ omitted. (d) The marginal distribution of $\ln N_r$ using the "in-precipitation PDF", which is the in-precipitation marginal PDF in Gaussian space. Owing to relatively low within-precipitating variance, the three hydrometeor PDF shapes are all a close match to SAM LES.

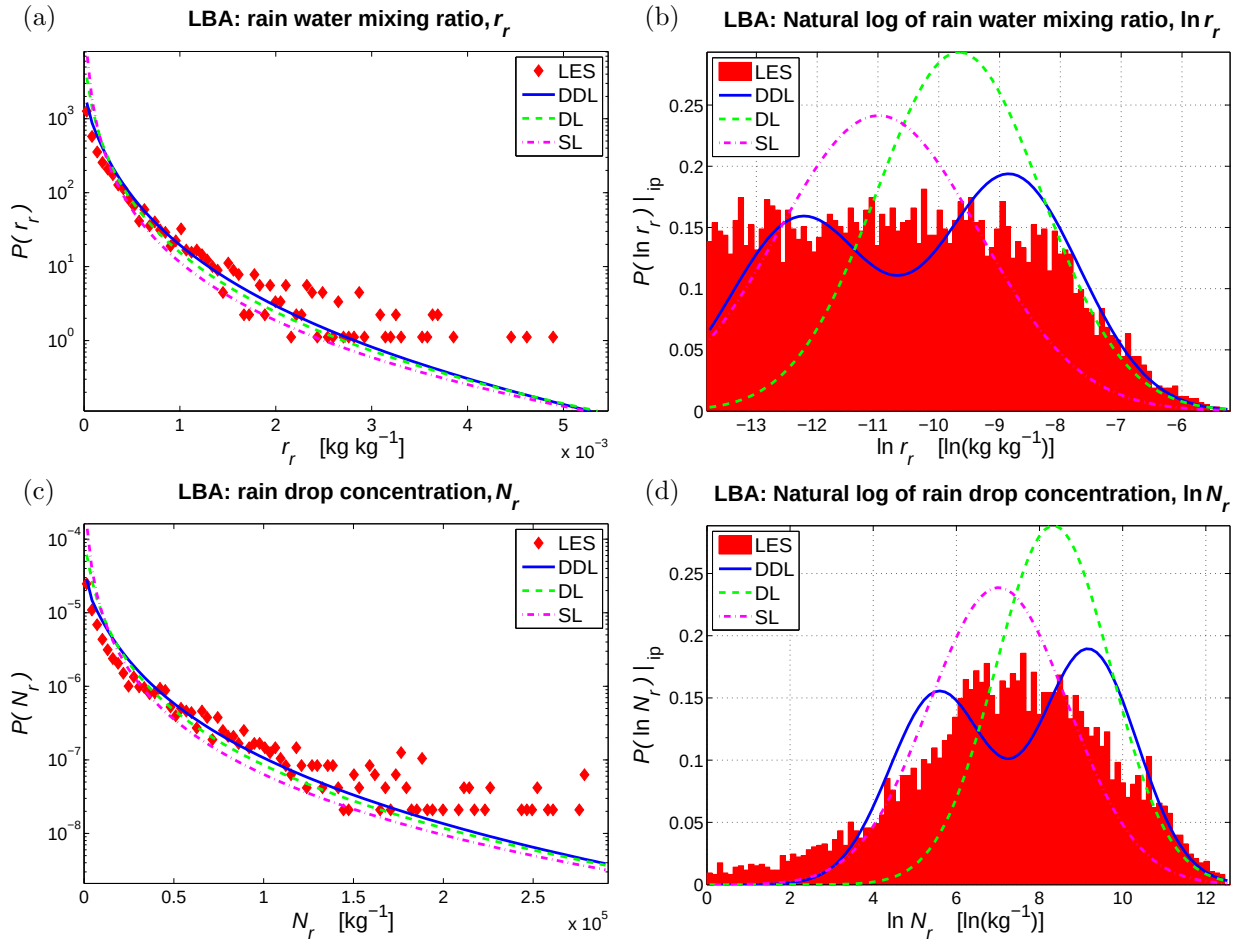

Figure 1.5: PDFs of rain in the LBA deep convective case at an altitude of 2424 m and a time of 330 min. The SAM LES results are in red, the DDL results are blue solid lines, the DL results are green dashed lines, and the SL results are magenta dashed-dotted lines. (a) The marginal distribution of r_r with the delta at $r_r = 0$ omitted. (b) The marginal distribution of $\ln r_r$ using the "in-precipitation PDF." This is the in-precipitation marginal PDF in Gaussian space. (c) The marginal distribution of N_r with the delta at $N_r = 0$ omitted. (d) The marginal distribution of $\ln N_r$ using the "in-precipitation PDF", which is the in-precipitation marginal PDF in Gaussian space. Again, the DDL provides the best fit to SAM LES.

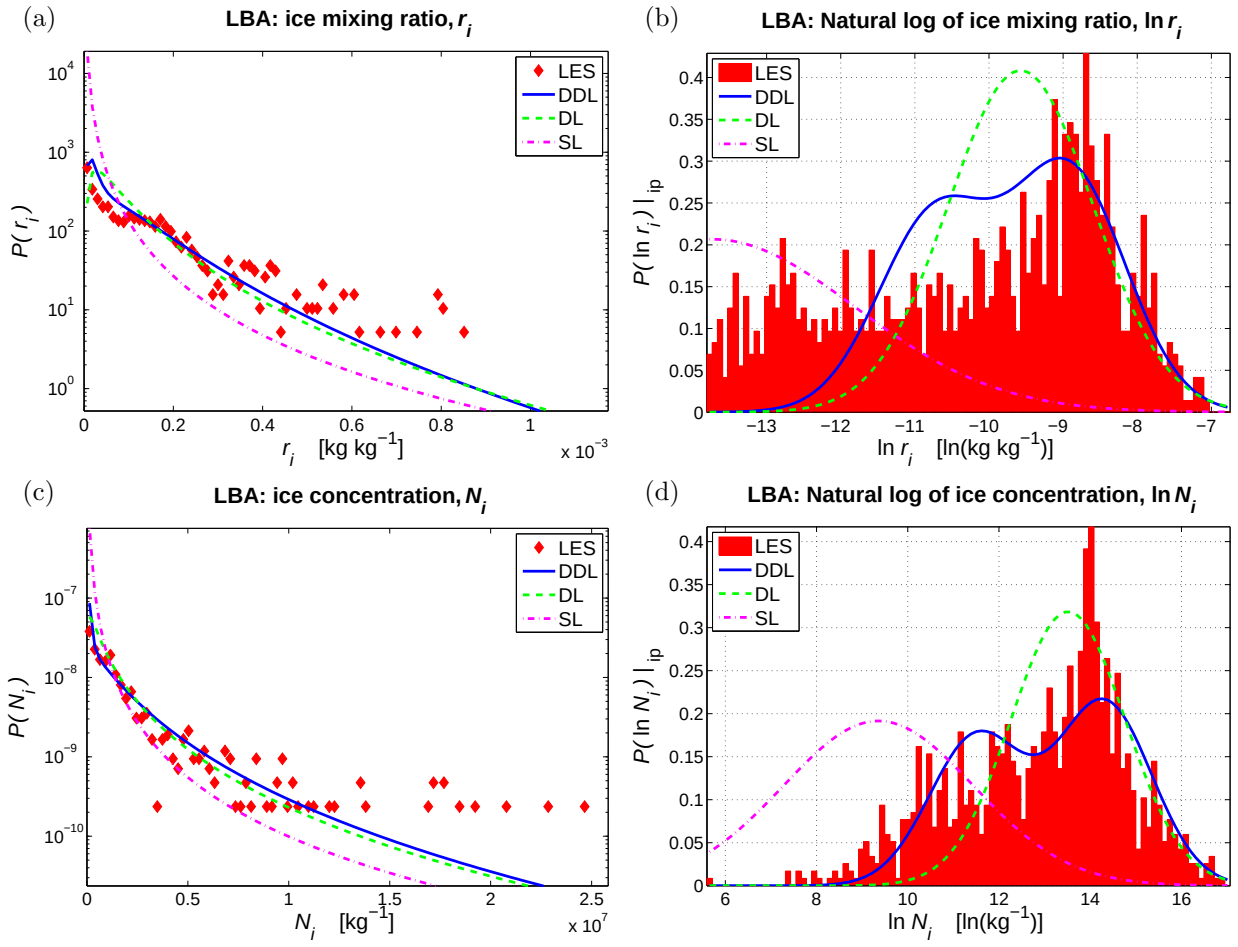

Figure 1.6: PDFs of ice in the LBA deep convective case at an altitude of 10500 m and a time of 360 min. The SAM LES results are in red, the DDL results are blue solid lines, the DL results are green dashed lines, and the SL results are magenta dashed-dotted lines. (a) The marginal distribution of r_i with the delta at $r_i = 0$ omitted. (b) The marginal distribution of $\ln r_i$ using the "in-precipitation PDF." This is the in-precipitation marginal PDF in Gaussian space. (c) The marginal distribution of N_i with the delta at $N_i = 0$ omitted. (d) The marginal distribution of $\ln N_i$ using the "in-precipitation PDF." Again, this is the in-precipitation marginal PDF in Gaussian space. The method works for frozen hydrometeor species as well, as the DDL provides a better fit to SAM LES than the DL, which in turn provides a better fit than the SL.

Why does the DDL PDF shape match LES output better than the DL shape in the aforementioned figures? The PDFs (in Gaussian space) for the LES of RICO and LBA show a broad, flat distribution of hydrometeor values from the LES. The DL shape is too peaked in comparison to the LES data. The DDL PDF is able to spread out the component means and thereby represent the platykurtic shape more accurately. However, even the DDL PDF fails to capture the far left-hand tail of the LES PDF. In the RICO, DYCOMS-II RF02, and LBA cases, between about 5% and 20% of the LES PDF is found to the left of the DDL PDF (see Figures 1.2b, 1.4b, 1.5b, and 1.6b). However, these values of hydrometeor mixing ratios are small. They are roughly a factor of 20 or more smaller than the median value. By combining these factors, we see that the percentage contribution of hydrometeor mixing ratios that are omitted on the left-hand tail is only about 1%.

Why does SAM LES data have a platykurtic shape in Gaussian space in these cases? One possible cause is the partly cloudy (and partly rainy) nature of these cases. In these partly rainy cases, a relatively high percentage of the precipitation occurs in "edge regions" near the non-precipitating region. These regions usually correspond to the edge of cloud or outside of cloud. Evaporation (or less accretion) occurs in these regions, increasing the area occupied by smaller amounts of rain. Yet, there is also an area of more intense precipitation near the center of the precipitating region, which produces larger amounts of rain. Collectively, the areas of small and large rain amount produce the large spread in the hydrometeor spectrum.

The DYCOMS-II RF02 PDFs from the LES tend not to share the platykurtic shape seen in the other cases. The RF02 case is overcast, so there are not as many "edge" regions of precipitation as found in partly rainy cases. There is much less in-precipitation variance in the RF02 case. The simpler PDF shape is easier to fit by all the PDF shapes (SL, DL, and DDL). To further illuminate the physics underlying the PDF shapes produced by LES, further study would be needed.

1.5.1 Quality of fit: general scores

While a lot can be learned by looking at plots of the hydrometeor PDFs, they are anecdotal and cannot tell us how well the idealized PDF shapes work generally. To obtain an *overall* quantification of the quality of the fit, we calculate the Kolmogorov-Smirnov (K-S) and the Cramer-von Mises (C-vM) scores.

Both the K-S and C-vM tests compare the cumulative distribution function (CDF) of the idealized distribution to the CDF of the empirical data (in this case, SAM LES data). Both tests require that the CDFs be continuous. Therefore, the scores are calculated using only the in-precipitation portion of the hydrometeor PDF in Eq. (1.10). The DDL, DL, and SAM LES data all have the same precipitation fraction. The in-precipitation portion of the PDF is normalized by dividing by precipitation fraction so that it integrates to 1. The equation for the in-precipitation portion of the marginal PDF, $P(h)|_{\text{ip}}$, is

$$P(h)|_{\text{ip}} = \xi_{(1)} \frac{f_{p(1)}}{f_p} P_{L(1)}(h) + \xi_{(2)} \frac{f_{p(2)}}{f_p} P_{L(2)}(h), \tag{1.34}$$

where $P_{L(i)}$ is given by Eq. (1.11).

The K-S score is the greatest difference between the empirical in-precipitation CDF, $C_e(h)|_{\text{ip}}$, and the idealized in-precipitation CDF, $C(h)|_{\text{ip}}$, at any point in $h > 0$. In order to run the tests, the SAM LES data from the requested level and time was sorted in the order of increasing value. This was done only for points where the requested hydrometeor was found. The K-S score is given by (Stephens 1970)

$$\begin{aligned} &\text{KS} = \max_h \left| C_e(h)|_{\text{ip}} - C(h)|_{\text{ip}} \right| = \max\left(\text{KS}^+, \text{KS}^-\right), \quad \text{where} \\ &\text{KS}^+ = \max_{1 \le \kappa \le n_p} \left(\frac{\kappa}{n_p} - C(h_\kappa)|_{\text{ip}} \right) \quad \text{and} \quad \text{KS}^- = \max_{1 \le \kappa \le n_p} \left(C(h_\kappa)|_{\text{ip}} - \frac{\kappa - 1}{n_p} \right). \end{aligned} \tag{1.35}$$

The number of data points in SAM LES where the hydrometeor is found is denoted n_p, and h_κ is the value of the hydrometeor at SAM LES ordered data point κ.

Unlike the K-S test, which only considers the greatest difference between the CDFs, the C-vM test is based on an integral that includes the differences between the CDFs over the entire distribution. The integral is (Anderson 1962)

$$\omega^2 = \int \left(C_e\left(h\right)\big|_{\text{ip}} - C\left(h\right)\big|_{\text{ip}} \right)^2 \mathrm{d}\, C\left(h\right)\big|_{\text{ip}} \,. \tag{1.36}$$

The C-vM score is calculated by (Anderson 1962; Stephens 1970)

$$\text{CVM} = \omega^2 n_p = \frac{1}{12 n_p} + \sum_{\kappa=1}^{n_p} \left(\frac{2\kappa - 1}{2 n_p} - C\left(h_\kappa\right)\big|_{\text{ip}} \right)^2 . \tag{1.37}$$

The K-S and C-vM test scores are produced at every LES vertical level and three-dimensional statistical output time for every hydrometeor species. This results in a large number of scores. We desire that each hydrometeor species have a single K-S score and a single C-vM score in order to more easily compare the DDL, DL, and SL hydrometeor shapes. We calculate this score by averaging the individual level scores over multiple levels and multiple output times. For K-S this is simple, and the result is $\langle \text{KS} \rangle$ (where angle brackets denote an average over multiple levels and times). The C-vM test score in Eq. (1.37) is dependent on the number of precipitating grid points. This number changes between vertical levels and output times, so the C-vM scores cannot simply be averaged. Rather, they are normalized first by dividing CVM by n_p to produce ω^2 at every level and time. Those results are averaged to calculate $\langle \omega^2 \rangle$.

After inspecting profiles of SAM LES results for mean mixing ratios in height and time, regions were identified in height and time where the mean mixing ratio of a species was always at least 5.0×10^{-6} kg kg^{-1}. Averaging of the scores was restricted to these regions in order to eliminate from consideration levels that do not contain the hydrometeor or contain only small amounts of the hydrometeor with a small number of samples. RICO test scores for r_r and N_r were averaged from the surface through 2780 m and from 4200 min through 4320 min. DYCOMS-II RF02 test scores for r_r and N_r were averaged from 277 m through

808 m and from 300 min to 360 min.

The LBA case contains both liquid and frozen-phase hydrometeor species that evolve as the cloud system transitions from shallow to deep convection. The various hydrometeor species develop and maximize at different altitudes and times, so different periods and altitude ranges are chosen for averaging test scores for each species. LBA test scores for r_r and N_r were averaged from the surface through 6000 m and from 285 min through 360 min. The test scores for r_g and N_g were averaged from 4132 m through 9750 m and from 315 min through 360 min. The test scores for r_s and N_s were averaged from 5026 m through 9000 m and from 345 min through 360 min. Finally, the test scores for r_i and N_i were averaged from 10250 m through 11750 m at 360 min. For the LBA case, the value of f_p used by CLUBB's PDF was based on the greatest value of SAM output variables for rain fraction, ice fraction, snow fraction, and graupel fraction. Each of these statistics is the fraction of the SAM domain occupied by values of the relevant mixing ratio of at least 1.0×10^{-6} kg kg^{-1}. In order to keep the comparison of the PDF shapes to SAM data consistent, values lower than this threshold were omitted from the calculations of the individual level-and-time scores for K-S and C-vM.

The results of $\langle \text{KS} \rangle$ are listed in Table 1.1 for every hydrometeor species in every case. The DDL PDF shape has the lowest average score for every case and hydrometeor species except for one. The DL PDF shape edges out the DDL in the DYCOMS-II RF02 N_r comparison. The SL PDF shape has the highest average score for every case and hydrometeor species, except for the LBA r_r comparison, where it has the second-lowest score and the DL has the highest score. The results of $\langle \omega^2 \rangle$ are listed in Table 1.2. The DDL PDF shape has the lowest average score for every case and hydrometeor species, the DL shape has the second-lowest average score, and the SL shape has the highest average score.

We note the important caveat that, as compared to DL, DDL has more adjustable parameters. A parameterization with more free parameters would be expected to provide a better fit to a training data set. Therefore, although DDL matches the LES output more

Average Kolmogorov-Smirnov Statistic			
Case-Species	$\langle \text{KS} \rangle$ DDL	$\langle \text{KS} \rangle$ DL	$\langle \text{KS} \rangle$ SL
RICO r_r	**0.223**	0.373	0.496
RICO N_r	**0.182**	0.263	0.634
RF02 r_r	**0.131**	0.133	0.148
RF02 N_r	0.152	**0.150**	0.170
LBA r_r	**0.152**	0.240	0.201
LBA N_r	**0.142**	0.187	0.295
LBA r_g	**0.197**	0.307	0.429
LBA N_g	**0.165**	0.222	0.566
LBA r_s	**0.177**	0.267	0.432
LBA N_s	**0.173**	0.238	0.492
LBA r_i	**0.212**	0.282	0.614
LBA N_i	**0.122**	0.210	0.647

Table 1.1: Kolmogorov-Smirnov statistic averaged over multiple grid levels and statistical output timesteps comparing each of DDL, DL, and SL hydrometeor PDF shapes to SAM LES results. The best (lowest) average score for each case and hydrometeor species is listed in bold. The DDL has the lowest average score most often, and the DL has the second-lowest average score most often.

Average Normalized Cramer-von Mises Statistic			
Case-Species	$\langle \omega^2 \rangle$ DDL	$\langle \omega^2 \rangle$ DL	$\langle \omega^2 \rangle$ SL
RICO r_r	**0.0187**	0.0508	0.1255
RICO N_r	**0.0100**	0.0238	0.1872
RF02 r_r	**0.0041**	0.0049	0.0094
RF02 N_r	**0.0064**	0.0070	0.0136
LBA r_r	**0.0078**	0.0231	0.0282
LBA N_r	**0.0081**	0.0145	0.0537
LBA r_g	**0.0159**	0.0351	0.1092
LBA N_g	**0.0129**	0.0194	0.1576
LBA r_s	**0.0107**	0.0240	0.1072
LBA N_s	**0.0089**	0.0174	0.1261
LBA r_i	**0.0126**	0.0246	0.1968
LBA N_i	**0.0046**	0.0134	0.2046

Table 1.2: Normalized Cramer-von Mises statistic averaged over multiple grid levels and statistical output timesteps comparing each of DDL, DL, and SL hydrometeor PDF shapes to SAM LES results. The best (lowest) average score for each case and hydrometeor species is listed in bold. The DDL has the lowest average score every time, and the DL has the second-lowest average score every time.

closely than does DL, we cannot be certain, based on the analysis presented here, that DDL will outperform DL on a different validation dataset. For a deeper analysis, one could use a model selection method that penalizes parameterizations with more parameters. We leave such an analysis for future work.

1.5.2 Microphysical process rates

A primary reason to improve the accuracy of hydrometeor PDFs is to improve the accuracy of the calculation of microphysical process rates. In this section, we compare the accuracy of calculations of microphysical process rates based on the SL, DL, and DDL PDF shapes.

In the simulations of RICO and DYCOMS-II RF02, both SAM LES and CLUBB use KK microphysics. The process rates output are the mean evaporation rate of r_r, the mean accretion rate of r_r, and the mean autoconversion rate of r_r. Also recorded is rain drop mean volume radius, which is important for sedimentation velocity of rain. In order to account for subgrid variability in the microphysics, the KK microphysics process rate equations have been upscaled (to grid-box scale) using analytic integration over the PDF (Larson and Griffin 2013; Griffin and Larson 2013). The updates to the multivariate PDF (see Section 1.2) require updates to the upscaled process rate equations. The updated forms of these equations are listed in Appendix C.

Figure 1.7 shows profiles of RICO mean microphysics process rates. The mean evaporation rate profile in Fig. 1.7a shows that all three shapes over-evaporate at higher altitudes, but that SL and DL over-evaporate more than DDL. It should be noted that the reason for the over-evaporation at higher altitudes in the RICO case is the marginal PDF of χ produced by ADG2. While it provides a good match between CLUBB and SAM LES in the fields of cloud fraction and $\overline{r_c}$, the value of $\sigma_{\chi(1)}$ is far too large. When χ and r_r (or N_r) are distributed jointly, this results in too many large values of r_r (or N_r) being placed in air that is far too dry. RICO mean evaporation rate could benefit from an improved ADG2 in order to produce a better marginal distribution of χ, but that is beyond the scope of this paper.

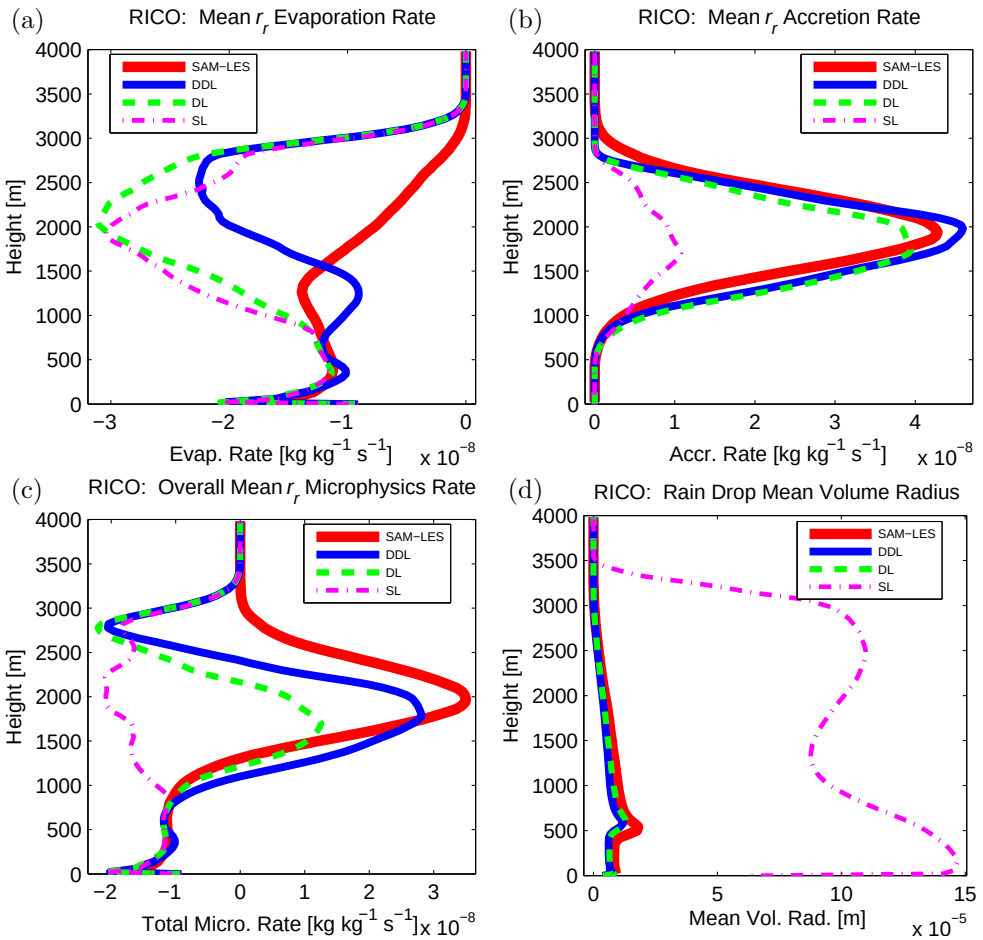

Figure 1.7: Profiles of mean microphysics process rates in the RICO precipitating shallow cumulus case time-averaged over the last two hours of the simulation (minutes 4200 through 4320). The SAM LES results are red solid lines, the DDL results are blue solid lines, the DL results are green dashed lines, and the SL results are magenta dashed-dotted lines. (a) The mean evaporation rate of r_r. (b) The mean accretion rate of r_r. (c) The overall mean microphysics tendency for r_r. (d) The mean volume radius of rain drops. Overall, the DDL provides a better fit to SAM LES than the DL, which in turn provides a better fit than the SL.

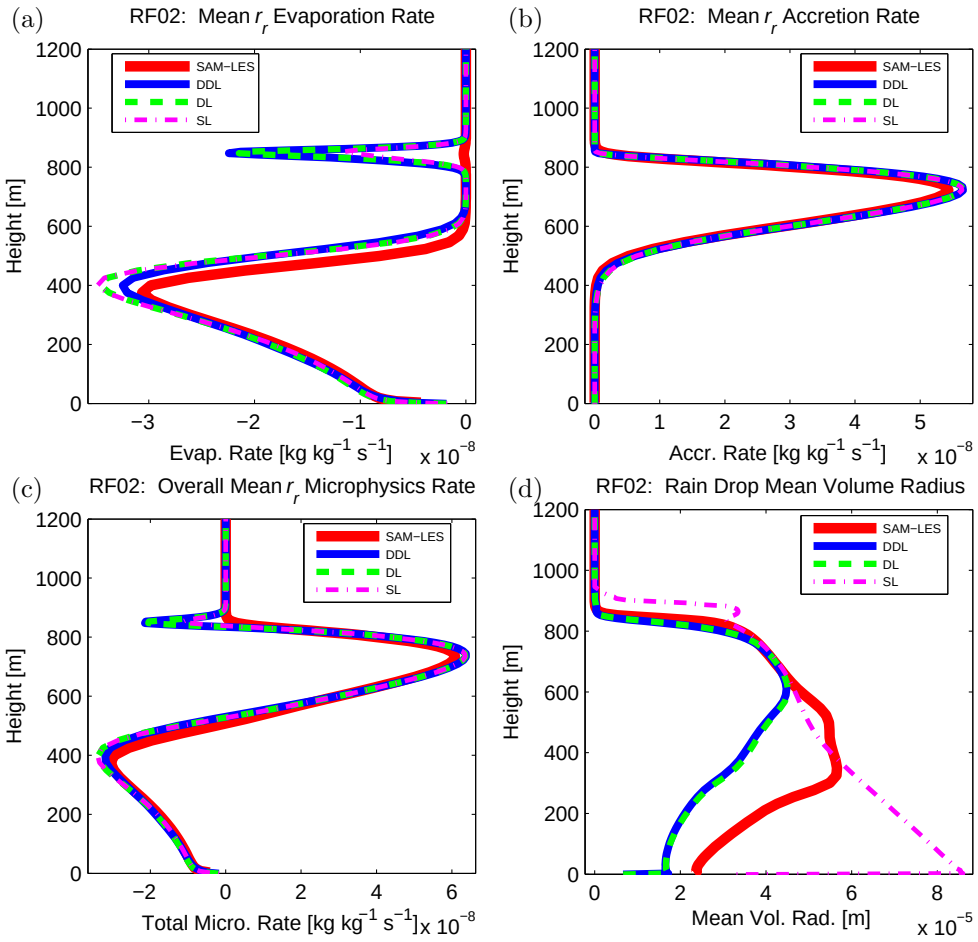

Figure 1.8: Profiles of mean microphysics process rates in the DYCOMS-II RF02 drizzling stratocumulus case time-averaged over the last hour of the simulation (minutes 300 through 360). The SAM LES results are red solid lines, the DDL results are blue solid lines, the DL results are green dashed lines, and the SL results are magenta dashed-dotted lines. (a) The mean evaporation rate of r_r. (b) The mean accretion rate of r_r. (c) The overall mean microphysics tendency for r_r. (d) The mean volume radius of rain drops. All hydrometeor PDF shapes provide a good fit to SAM LES.

Figure 1.7b shows that both the DL and DDL PDF shapes match the LES mean accretion rate profile much better than does the SL shape. The mean autoconversion rate depends on χ and N_{cn} but not hydrometeor variables, and so the autoconversion rate is the same for all three PDF shapes (not shown). The overall mean microphysics rate — i.e., the sum of the evaporation, accretion, and autoconversion rates — is fit best by the DDL shape and worst by the SL shape. Both DDL and DL are a much better match to the SAM profile of rain drop mean volume radius than SL (Fig. 1.7d).

Figure 1.8 shows that all three hydrometeor PDF shapes provide a good match to SAM

LES for DYCOMS-II RF02. In Fig. 1.8d, the SL PDF shape deviates more strongly from SAM LES than does DL or DDL near the bottom of the profile of rain drop mean volume radius.

In the simulation of LBA, Morrison microphysics was used in both the SAM LES and CLUBB. In order to account for subgrid variability in the microphysics, sample points from the PDF are produced at every grid level using the Subgrid Importance Latin Hypercube Sampler (SILHS) (Raut and Larson 2016; Larson and Schanen 2013; Larson et al. 2005). For the LBA case, 128 sample points were drawn. Morrison microphysics is then called using each set of sample points, and the results are averaged to calculate the mean microphysics process rates.

Figure 1.9 shows the same mean microphysics process rates as in previous figures, but here for LBA. The profile of mean evaporation rate in Fig. 1.9a shows that DDL is the best match to SAM LES. The profile of mean accretion rate in Fig. 1.9b shows that DDL is the best match to SAM, followed by DL and then SL. The overall (autoconversion + accretion + evaporation) warm microphysics process rate profile is best matched by the DDL hydrometeor PDF shape, followed by the DL shape, which in turn is followed by the SL shape (Fig. 1.9c).

1.6 Conclusion

The multivariate PDF used by CLUBB has been updated to improve the subgrid representation of hydrometeor species. The most important update is the introduction of precipitation fraction to the PDF. The precipitating fraction contains any non-zero values of any hydrometeor species included in the microphysics scheme. The remainder of the subgrid domain is precipitation-less and is represented by a delta function where every hydrometeor species has a value of zero. When a hydrometeor is found at a grid level, its representation in the precipitating portion of the subgrid domain is a lognormal or double lognormal distribution.

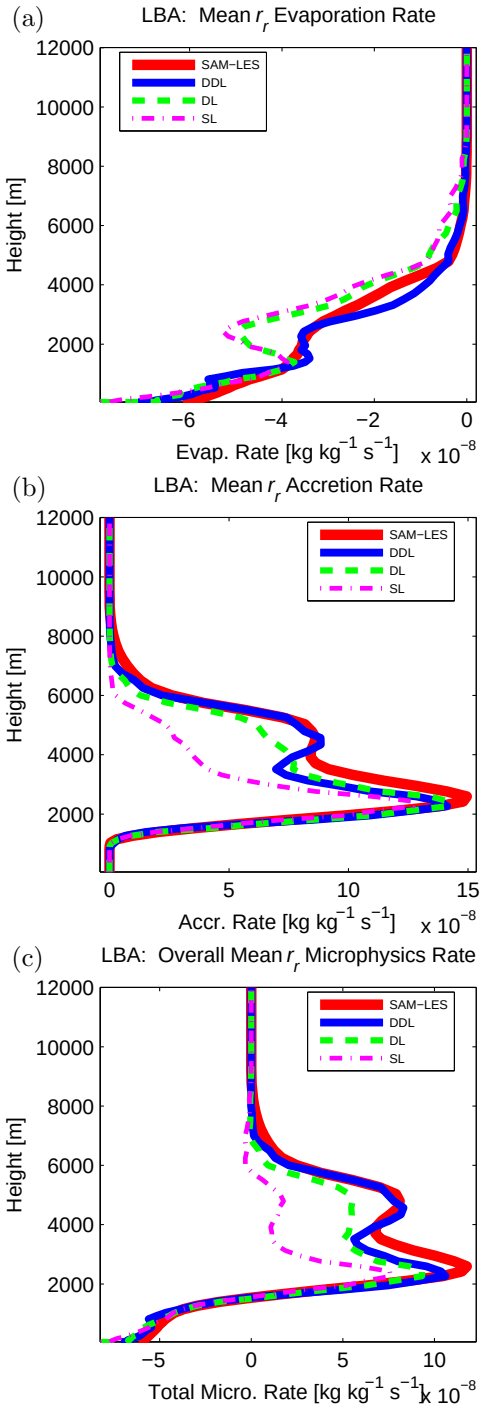

Figure 1.9: Profiles of mean warm microphysics process rates in the LBA deep convective case time-averaged over the last hour of the simulation (minutes 300 through 360). The SAM LES results are red solid lines, the DDL results are blue solid lines, the DL results are green dashed lines, and the SL results are magenta dashed-dotted lines. (a) The mean evaporation rate of r_r. (b) The mean accretion rate of r_r. (c) The overall mean microphysics tendency for r_r. Again, the DDL provides a better fit to SAM LES than the DL, which in turn provides a better fit than the SL.

The introduction of precipitation fraction increases accretion and decreases evaporation in cumulus cases, allowing more precipitation to reach the ground.

Additionally, a new method has been developed to calculate the in-precipitation mean and standard deviation of a hydrometeor species in each component of CLUBB's two-component PDF. This method preserves the grid-box mean and variance of the hydrometeor species. By simply changing the values of tunable parameters, CLUBB's marginal PDF for a hydrometeor can be changed from a delta-double-lognormal (DDL) to a delta-lognormal (DL) or to a single-lognormal (SL) shape.

In order to compare the effectiveness of the three hydrometeor PDF shapes, three simulations – a precipitating shallow cumulus case (RICO), a drizzling stratocumulus case (DYCOMS-II RF02), and a deep convective case (LBA) – were run using SAM LES. Statistical output values from the LES for the grid-level mean and turbulent fields were used to drive the PDF for each hydrometeor PDF shape. The idealized PDF shapes were compared to the SAM LES results. The DDL PDF shape produced the lowest average K-S and average normalized C-vM scores when compared to SAM LES results, followed by the DL PDF shape. Both produced lower scores than the original SL PDF shape. However, for DYCOMS-II RF02, all three PDF shapes were in almost equal agreement with SAM LES results.

The DL and DDL PDFs possess three important properties: 1) they are multivariate, and hence can represent interactions among multiple hydrometeor species; 2) they admit a precipitation-less region, which is necessary to permit realistic process rates in cumulus cloud layers; and 3) they have realistic tails, as evidenced by the comparisons with LES shown here. Because of these three properties, the DL and DDL PDFs may be general enough and accurate enough to adequately represent hydrometeor variability over a range of important cloud types, including shallow cumulus, deep cumulus, and stratocumulus clouds. This generality, in turn, may help enable parameterization of these clouds types in a more unified way. Indeed, an early version of the DDL PDF has already been used to represent

hydrometeor subgrid variability in some interactive simulations with a unified cloud parameterization. Namely, the DDL PDF was used in the interactive single-column simulations of these cloud types by Storer et al. (2015) and in the global simulations by Thayer-Calder et al. (2015). Further testing would be required, however, to better understand the limits of the DL and DDL PDFs. Better understanding is particularly desirable in, for instance, mixed-phase and glaciated clouds. This has been left for future work.

Chapter 2

Parameterizing Microphysical Effects on Variances and Covariances of Moisture and Heat Content Using a Multivariate PDF

2.1 Introduction

The structure, development, and dissipation of precipitating cumulus clouds are influenced by interactions between microphysical, thermodynamic, and turbulent processes. For example, consider the diurnal cycle of precipitation over land in the tropics. Over tropical land masses, there is a gradual transition from shallow convection in the morning to deep convection several hours later (e.g., Grabowski et al. 2006). Early clouds remain shallow because they entrain dry environmental air (Derbyshire et al. 2004). Successive clouds moisten the environment. The transition to deep convection is aided by a positive feedback involving rain, evaporative cooling, the formation of cold pools, and the triggering of fresh convection and rain. Namely, when precipitation initiates, rain falls and evaporates below cloud base, generating cold pools in the boundary layer. The cold pools, in turn, can lift boundary layer air upwards and thereby trigger new convection (e.g., Kuang and Bretherton 2006; Khairoutdinov and Randall 2006; Mapes and Neale 2011; Böing et al. 2012; Gentine et al. 2016). There may also occur a negative feedback between thermodynamic variability in clouds and precipitation. Namely, updrafts and turbulent mixing may generate variability in cloud water mixing ratio. Then rain forms preferentially in the moistest part of the cloud, reducing peak cloud water contents, and thereby diminishing variability in cloud water (Khairoutdinov and Randall 2002). Although these effects may be most pronounced in deep

cumuli, which precipitate strongly, they are also present in precipitating shallow cumulus. Relatedly, some shallow cumulus layers produce cold pools (e.g., Zuidema et al. 2012) and/or exhibit mesoscale organization (e.g., Rauber et al. 2007; Xue et al. 2008).

Some effects of microphysics influence the spatial arrangement of cloud parcels. For instance, precipitation may lead to an increase in cloud diameter or to the development of mesoscale cloud organization (e.g., Kuang and Bretherton 2006; Khairoutdinov and Randall 2006; Schlemmer and Hohenegger 2014). Such effects of microphysics on cloud *structure* will not be discussed here. Instead, the focus will be on the effects of microphysics on the *variances and covariances* of cloud-related fields. Microphysics affects more than just horizontal averages; it also affects variability. For instance, rain production in the moistest parts of a cloud tends to diminish variability in cloud water. Also, evaporative cooling of rain in cold downdrafts below cloud base may increase the variability in temperature in the subcloud layer. Even though the effects of microphysics on cloud *structure* may be difficult to quantify, the effects of microphysics on *variances and covariances* are simpler to define and calculate. Those effects appear as well-defined covariance terms on the right-hand side of spatially-filtered equations for the scalar variances and turbulent fluxes. These filtered moment equations can be derived rigorously from the governing equations, and the microphysical terms emerge naturally from the derivation. However, most coarse-resolution climate or weather models either treat such effects crudely or else ignore them entirely.

The microphysical terms in the predictive variance and covariance equations can be parameterized by integrating microphysical formulas over the Probability Density Function (PDF) representing subgrid variability. A primary purpose of this paper is to perform those integrals analytically and to implement the resulting formulas in a particular PDF parameterization, the Cloud Layers Unified By Binormals (CLUBB) model. The integrals can be performed analytically because the microphysical formulas that are integrated are simple power laws (Khairoutdinov and Kogan 2000), and because it is assumed that the variables involved are distributed according to a multivariate PDF based on normal and

lognormal functions (see Chapter 1). The implementation of the integrals may serve as a benchmark calculation that is based on idealized (Khairoutdinov-Kogan) microphysics. The benchmark calculation can be used to assess the accuracy and convergence of more general integration methods, as in Larson and Schanen (2013). Alternatively, the integrals may serve directly as a parameterization. Full evaluation of the use of the integrals as a parameterization is deferred to future work, but for illustrative purposes, a single-column CLUBB simulation of one shallow convective case, Rain in Cumulus over the Ocean (RICO) (van Zanten et al. 2011), is presented. In addition, budgets from a large-eddy simulation (LES) of RICO are also presented. The LES indicates which variances and covariances are most influenced by microphysical processes.

The remainder of the paper is organized as follows. Section 2.2 overviews the origin of the microphysical terms from the predictive equations, summarizes the microphysics scheme involved in the development of this parameterization, and summarizes the multivariate PDF used by CLUBB. Section 2.3 describes the test case simulation, the LES used for comparison, and the setup of the CLUBB model. Section 2.4 compares the budget terms for relevant variances and covariances between the LES and CLUBB. Section 2.5 contains concluding remarks.

2.2 Mathematical and physical overview

CLUBB is a single-column model (SCM) that predicts variances and covariances involving vertical velocity, moisture, and temperature fields using spatially-filtered moment equations (Golaz et al. 2002a; Larson and Golaz 2005; Larson and Griffin 2013; Griffin and Larson 2013). CLUBB uses a multivariate Probability Density Function (PDF) to represent subgrid variability in vertical velocity, moisture, temperature, and hydrometeor fields. The subgrid PDF is used to close the higher-order moment terms found in the predictive moment equations and also to provide information on cloud water and cloud fraction.

CLUBB's PDF and corresponding predictive equation set are based on vertical velocity, w, total water mixing ratio, r_t, and liquid water potential temperature, θ_l. Total water mixing ratio is defined such that $r_t = r_v + r_c$, where r_v is water vapor mixing ratio and r_c is (liquid) cloud water mixing ratio. Liquid water potential temperature is defined by the equation

$$\theta_l = T_l \left(\frac{p}{p_0} \right)^{-\frac{R_d}{C_{pd}}}, \tag{2.1}$$

where p is pressure, p_0 is a reference pressure of 1.0×10^5 Pa, R_d is the gas constant for dry air, and C_{pd} is the specific heat of dry air at a constant pressure. Liquid water temperature, T_l, is defined as

$$T_l = T - \frac{L_v}{C_{pd}} r_c, \tag{2.2}$$

where T is temperature and L_v is the latent heat of vaporization. In subsaturated air, r_t reduces to r_v and θ_l reduces to potential temperature, θ.

The CLUBB model uses r_t and θ_l because those variables are conserved with regard to adiabatic processes and phase changes between water vapor and liquid cloud water. However, r_t and θ_l are not conserved with respect to transfers between precipitation and water vapor or cloud water. As a result, the time-tendency equations for each of r_t and θ_l include a microphysics tendency term. Omitting all other terms, such as advection, these equations can be written as

$$\frac{\partial r_t}{\partial t} = \ldots + \left. \frac{\partial r_t}{\partial t} \right|_{\text{mc}}, \quad \text{and} \tag{2.3}$$

$$\frac{\partial \theta_l}{\partial t} = \ldots + \left. \frac{\partial \theta_l}{\partial t} \right|_{\text{mc}}; \tag{2.4}$$

where t is time, and where $\left. \frac{\partial r_t}{\partial t} \right|_{\text{mc}}$ and $\left. \frac{\partial \theta_l}{\partial t} \right|_{\text{mc}}$ are the microphysics tendency terms for r_t and θ_l, respectively. They are the source or sink of r_t and θ_l due to microphysics process rates.

The time-tendency equations are split into mean and turbulent components. For the

remainder of this paper, an overbar will denote a mean value, while the prime symbol ($'$) will donate a deviation from the mean value (turbulent value). The Reynolds-averaged predictive equations for grid-box mean fields $\overline{r_t}$ and $\overline{\theta_l}$ include the terms

$$\frac{\partial \overline{r_t}}{\partial t} = \ldots + \overline{\left.\frac{\partial r_t}{\partial t}\right|_{\text{mc}}}, \quad \text{and} \tag{2.5}$$

$$\frac{\partial \overline{\theta_l}}{\partial t} = \ldots + \overline{\left.\frac{\partial \theta_l}{\partial t}\right|_{\text{mc}}}. \tag{2.6}$$

The omitted terms in the predictive equations for $\overline{r_t}$ and $\overline{\theta_l}$ are listed in Golaz et al. (2002a), with the only change being that the CLUBB equation set is now written in anelastic form.

In order to obtain the fields necessary to generate the PDF, CLUBB also contains predictive equations for the subgrid variances and covariances involving w, r_t, and θ_l. The fields that contain a microphysics term are $\overline{w'r_t'}$, $\overline{w'\theta_l'}$, $\overline{r_t'^2}$, $\overline{\theta_l'^2}$, and $\overline{r_t'\theta_l'}$. The Reynolds-averaged predictive equations for these subgrid variances and covariances include the terms:

$$\frac{\partial \overline{w'r_t'}}{\partial t} = \ldots + \overline{w' \left.\frac{\partial r_t}{\partial t}\right|_{\text{mc}}'}, \tag{2.7}$$

$$\frac{\partial \overline{w'\theta_l'}}{\partial t} = \ldots + \overline{w' \left.\frac{\partial \theta_l}{\partial t}\right|_{\text{mc}}'}, \tag{2.8}$$

$$\frac{\partial \overline{r_t'^2}}{\partial t} = \ldots + 2\,\overline{r_t' \left.\frac{\partial r_t}{\partial t}\right|_{\text{mc}}'}, \tag{2.9}$$

$$\frac{\partial \overline{\theta_l'^2}}{\partial t} = \ldots + 2\,\overline{\theta_l' \left.\frac{\partial \theta_l}{\partial t}\right|_{\text{mc}}'}, \quad \text{and} \tag{2.10}$$

$$\frac{\partial \overline{r_t'\theta_l'}}{\partial t} = \ldots + \overline{r_t' \left.\frac{\partial \theta_l}{\partial t}\right|_{\text{mc}}'} + \overline{\theta_l' \left.\frac{\partial r_t}{\partial t}\right|_{\text{mc}}'}. \tag{2.11}$$

The full forms, including all omitted terms, of the predictive equations for $\overline{w'r_t'}$, $\overline{w'\theta_l'}$, $\overline{r_t'^2}$, $\overline{\theta_l'^2}$, and $\overline{r_t'\theta_l'}$ are given by Eq. (2.26), Eq. (2.27), Eq. (2.28), Eq. (2.29), and Eq. (2.30), respectively, in Section 2.4.

If r_t and θ_l were extended to include precipitation, the extended variables would be conserved with respect to transfers between hydrometeors and water vapor or cloud wa-

ter (microphysics process rates). However, this extension would cause the microphysical effects to appear in sedimentation terms. The sedimentation terms contain vertical derivatives, whereas the process rates do not. Some turbulent components of the sedimentation term contain a vertical derivative within a horizontal average. To illustrate, consider a hydrometeor-inclusive total water mixing ratio, denoted r_T, such that $r_T = r_v + r_c + r_r$, where r_r is rain water mixing ratio. For simplicity, r_r will be the only hydrometeor considered in the microphysics. The microphysics term on the right-hand side of the Reynolds-averaged $\overline{r_T'^2}$ predictive equation would have the form

$$2\,\overline{r_T'\left(-\frac{1}{\rho_s}\frac{\partial \rho_s\, V_{r_r}\, r_r}{\partial z}\right)'} = -\frac{2}{\rho_s}\overline{r_T'\frac{\partial \rho_s\,\overline{V_{r_r}}\, r_r'}{\partial z}} - \frac{2}{\rho_s}\overline{r_T'\frac{\partial \rho_s\, V_{r_r}'\,\overline{r_r}}{\partial z}} - \frac{2}{\rho_s}\overline{r_T'\frac{\partial \rho_s\, V_{r_r}'\, r_r'}{\partial z}},$$

where V_{r_r} is the sedimentation velocity of r_r, ρ_s is the dry, base-state air density, and z is height. Every predictive moisture or temperature (co)variance equation would contain terms analogous to the above sedimentation terms. Since these terms contain vertical derivatives ($\partial/\partial z$) embedded within integrals over the horizontal, they are difficult to treat analytically and cannot be described solely by a multivariate subgrid PDF at a single vertical grid level. For this reason, CLUBB's calculations of the microphysics terms use r_t and θ_l defined in terms of cloud water, not precipitation.

2.2.1 KK microphysics

The source terms for the model predictive equations require microphysical process rates from a microphysics scheme. The scheme used here is the warm microphysics scheme described in Khairoutdinov and Kogan (2000, hereafter KK). KK is a two-moment scheme that predicts r_r and rain drop concentration (per unit mass), N_r. It was developed by using the least squares method to find a "best-fit" curve through microphysical rate data that was generated by simulating a drizzling stratocumulus case using an explicit (or "bin") microphysics scheme.

The KK scheme was chosen because of its simplicity. It expresses microphysical rates

as power laws of two or three variables, which means that the product of a microphysical rate and the corresponding PDF is always integrable. More recently, the coefficients and exponents in the KK scheme have been tailored to cumulus clouds (Kogan 2013). The Kogan scheme is covered by the analytic integrals presented in this paper because they are generalized for arbitrary coefficients and exponents. However, this paper uses the original KK coefficients and exponents because the KK scheme has been widely used for a variety of cloud types and is adequate for the idealized purposes of this paper.

The KK warm microphysics scheme produces r_r through the processes of autoconversion (collision) and accretion (collection). These processes produce rain water, deplete cloud water, and leave water vapor unchanged. As a result, these processes increase the value of θ_l, as shown by Eq. (2.1) and Eq. (2.2), and decrease the value of r_t. Evaporation reduces r_r as rain falls through subsaturated air. Condensational growth does not apply to rain water in CLUBB. Instead, all supersaturation is automatically applied to cloud water. When rain water evaporates, cloud water remains unchanged, and r_t increases due to the increase in water vapor. Meanwhile, evaporative cooling decreases θ_l due to the decrease in temperature.

The relationship of all three KK microphysics tendencies to the r_t microphysics tendency can be written as

$$\left.\frac{\partial r_t}{\partial t}\right|_{\text{mc}} = -\left.\frac{\partial r_r}{\partial t}\right|_{\text{auto}} - \left.\frac{\partial r_r}{\partial t}\right|_{\text{accr}} - \left.\frac{\partial r_r}{\partial t}\right|_{\text{evap}}, \tag{2.12}$$

where $\left.\frac{\partial r_r}{\partial t}\right|_{\text{auto}}$ is the rate of change of r_r due to the process of autoconversion, $\left.\frac{\partial r_r}{\partial t}\right|_{\text{accr}}$ is the rate of change of r_r due to the process of accretion, and $\left.\frac{\partial r_r}{\partial t}\right|_{\text{evap}}$ is the rate of change of r_r due to the process of evaporation. Note that when evaporation occurs, $\left.\frac{\partial r_r}{\partial t}\right|_{\text{evap}} < 0$. The relationship of all three tendencies to θ_l microphysics tendency can be written as

$$\left.\frac{\partial \theta_l}{\partial t}\right|_{\text{mc}} = \frac{L_v}{C_{pd}}\left(\frac{p}{p_0}\right)^{-\frac{R_d}{C_{pd}}}\left(\left.\frac{\partial r_r}{\partial t}\right|_{\text{auto}} + \left.\frac{\partial r_r}{\partial t}\right|_{\text{accr}} + \left.\frac{\partial r_r}{\partial t}\right|_{\text{evap}}\right). \tag{2.13}$$

The decrease in temperature from the evaporation of a unit of rain water is the same as the

decrease in temperature from the evaporation of the same amount of cloud water.

The Reynolds-averaged microphysics term in the predictive equation for $\overline{w' r_t'}$, as found in Eq. (2.7), is rewritten as

$$\overline{w' \left.\frac{\partial r_t}{\partial t}\right|_{\text{mc}}'} = - \overline{w' \left.\frac{\partial r_r}{\partial t}\right|_{\text{auto}}'} - \overline{w' \left.\frac{\partial r_r}{\partial t}\right|_{\text{accr}}'} - \overline{w' \left.\frac{\partial r_r}{\partial t}\right|_{\text{evap}}'} . \tag{2.14}$$

Likewise, the Reynolds-averaged microphysics term in the predictive equation for $\overline{w' \theta_l'}$, as found in Eq. (2.8), is rewritten as

$$\overline{w' \left.\frac{\partial \theta_l}{\partial t}\right|_{\text{mc}}'} = \frac{L_v}{C_{pd}} \left(\frac{\overline{p}}{p_0}\right)^{-\frac{R_d}{C_{pd}}} \left(\overline{w' \left.\frac{\partial r_r}{\partial t}\right|_{\text{auto}}'} + \overline{w' \left.\frac{\partial r_r}{\partial t}\right|_{\text{accr}}'} + \overline{w' \left.\frac{\partial r_r}{\partial t}\right|_{\text{evap}}'} \right) . \tag{2.15}$$

Any variability of p within the grid box is ignored for simplicity. Additionally, the $-R_d/C_{pd}$ exponent would greatly limit the effects of variability of p on the solution. As a result, $\overline{p}$ is used in the equation. In the predictive equation for $\overline{r_t'^2}$, Eq. (2.9), the microphysics term becomes

$$\overline{r_t' \left.\frac{\partial r_t}{\partial t}\right|_{\text{mc}}'} = - \overline{r_t' \left.\frac{\partial r_r}{\partial t}\right|_{\text{auto}}'} - \overline{r_t' \left.\frac{\partial r_r}{\partial t}\right|_{\text{accr}}'} - \overline{r_t' \left.\frac{\partial r_r}{\partial t}\right|_{\text{evap}}'} . \tag{2.16}$$

In the predictive equation for $\overline{\theta_l'^2}$, Eq. (2.10), the microphysics term becomes

$$\overline{\theta_l' \left.\frac{\partial \theta_l}{\partial t}\right|_{\text{mc}}'} = \frac{L_v}{C_{pd}} \left(\frac{\overline{p}}{p_0}\right)^{-\frac{R_d}{C_{pd}}} \left(\overline{\theta_l' \left.\frac{\partial r_r}{\partial t}\right|_{\text{auto}}'} + \overline{\theta_l' \left.\frac{\partial r_r}{\partial t}\right|_{\text{accr}}'} + \overline{\theta_l' \left.\frac{\partial r_r}{\partial t}\right|_{\text{evap}}'} \right) . \tag{2.17}$$

The Reynolds-averaged microphysics terms in the predictive equation for $\overline{r_t' \theta_l'}$, as found in Eq. (2.11), are rewritten as

$$\overline{\theta_l' \left.\frac{\partial r_t}{\partial t}\right|_{\text{mc}}'} = - \overline{\theta_l' \left.\frac{\partial r_r}{\partial t}\right|_{\text{auto}}'} - \overline{\theta_l' \left.\frac{\partial r_r}{\partial t}\right|_{\text{accr}}'} - \overline{\theta_l' \left.\frac{\partial r_r}{\partial t}\right|_{\text{evap}}'} , \text{ and} \tag{2.18}$$

$$\overline{r_t' \left.\frac{\partial \theta_l}{\partial t}\right|_{\text{mc}}'} = \frac{L_v}{C_{pd}} \left(\frac{\overline{p}}{p_0}\right)^{-\frac{R_d}{C_{pd}}} \left(\overline{r_t' \left.\frac{\partial r_r}{\partial t}\right|_{\text{auto}}'} + \overline{r_t' \left.\frac{\partial r_r}{\partial t}\right|_{\text{accr}}'} + \overline{r_t' \left.\frac{\partial r_r}{\partial t}\right|_{\text{evap}}'} \right) . \tag{2.19}$$

The above equation set contains nine individual microphysical covariance terms, each involving one of w, r_t, or θ_l with one of autoconversion, accretion, or evaporation rate. These terms can be parameterized through use of the PDF method.

2.2.2 PDF method

The multivariate PDF used by CLUBB consists of w, r_t, θ_l, all hydrometeor species used by the selected microphysics scheme (in the case of KK microphysics, r_r and N_r), and an extended cloud droplet concentration, N_{cn}, which is equal to cloud droplet concentration, N_c, within cloud, but has a positive value outside of cloud (see Section 1.2). CLUBB's PDF is a weighted mixture, or sum, of two multivariate normal/lognormal functions. Each multivariate function is known as a PDF component.

When variables are integrated out of the multivariate PDF, a marginal PDF consisting of fewer variables remains. When all variables but one are integrated out of the PDF, the result is a univariate marginal or individual marginal. The individual marginal for each of w, r_t, and θ_l is a two-component normal (also known as a binormal) distribution. The two-component shape allows skewness to be included in model fields. The individual marginal for N_{cn} is assumed to be a (single) lognormal distribution.

The individual marginal for each of r_r and N_r is delta-lognormal *within each PDF component* (see Section 1.2). Each PDF component can contain precipitating and precipitationless regions. The fraction of each PDF component that contains any hydrometeor species (other than cloud liquid water) is known as the component's precipitation fraction. The precipitation-less region is represented by a delta at 0 for all hydrometeor species. Within precipitation, a lognormal distribution is used to represent a hydrometeor species. The lognormal distributions can differ between the two components, so that when the components are summed to form the overall distribution, a delta double lognormal (DDL) distribution results.

The PDF method for parameterizing the nine microphysics covariance terms requires

analytic integration over the multivariate PDF. As listed in Section 1.2, the general form of a multivariate PDF of n components and D variables, where D can be all the variables involved in the PDF or any subset of those, is given by

$$P\left(x_1, x_2, \ldots, x_D\right) = \sum_{i=1}^{n} \xi_{(i)} P_{(i)}\left(x_1, x_2, \ldots, x_D\right), \tag{2.20}$$

where $\xi_{(i)}$ is the mixture fraction, or relative weight of the ith PDF component. The sum of the mixture fractions is equal to 1.

The D variables listed are categorized, and the first J variables are normally distributed in each PDF component (w, r_t, and θ_l), the next K variables are lognormally distributed (N_{cn}), and the last Ω variables are the hydrometeor species that are distributed delta-lognormally in each PDF component (r_r and/or N_r). The equation for the ith PDF component is

$$\begin{aligned} P_{(i)}\left(x_1, x_2, \ldots, x_D\right) = {} & f_{p(i)} P_{(J,K+\Omega)(i)}\left(x_1, x_2, \ldots, x_D\right) \\ & + \left(1 - f_{p(i)}\right) P_{(J,K)(i)}\left(x_1, x_2, \ldots, x_{J+K}\right) \left(\prod_{\epsilon=J+K+1}^{D} \delta\left(x_\epsilon\right) \right), \end{aligned} \tag{2.21}$$

where $f_{p(i)}$ is the precipitation fraction in the ith PDF component. The subscripts in the ith component, $P_{(J,K)(i)}$ or $P_{(J,K+\Omega)(i)}$, denote the number of normal variates, J, and the number of lognormal variates, K or $K + \Omega$, used in Eq. (2.22).

Both the precipitating and precipitation-less portions (sub-components) of Eq. (2.21) contain a hybrid normal/lognormal distribution of m variables, where the first j variables are normally distributed and the remaining k variables are lognormally distributed. The general form of this multivariate normal/lognormal PDF is given by (Fletcher and Zupanski 2006)

$$\begin{aligned} P_{(j,k)(i)}\left(x_1, x_2, \ldots, x_m\right) = {} & \frac{1}{(2\pi)^{\frac{m}{2}} \left|\boldsymbol{\Sigma}_{(i)}\right|^{\frac{1}{2}}} \left(\prod_{\tau=j+1}^{m} \frac{1}{x_\tau} \right) \\ & \times \exp\left\{ -\frac{1}{2} \left(\vec{\boldsymbol{x}} - \vec{\boldsymbol{\mu}}_{(i)}\right)^{\mathrm{T}} \boldsymbol{\Sigma}_{(i)}^{-1} \left(\vec{\boldsymbol{x}} - \vec{\boldsymbol{\mu}}_{(i)}\right) \right\}, \end{aligned} \tag{2.22}$$

where $\vec{\boldsymbol{x}}$ is a $m \times 1$ vector of the variables (in normal-space) in the PDF and $\vec{\boldsymbol{\mu}}_{(i)}$ is a $m \times 1$ vector of the (normal-space) PDF sub-component means. The transpose of the vector is denoted T. The $m \times m$ (normal-space) covariance matrix is denoted $\boldsymbol{\Sigma}_{(i)}$ and its determinant is denoted $\left|\boldsymbol{\Sigma}_{(i)}\right|$ (Fletcher and Zupanski 2006).

Using a two-component PDF requires a method to divide one *overall* (grid-box) mean value of a variable into two PDF *component* mean values of that variable. Likewise, one overall variance needs to be split into two PDF component standard deviations. The multivariate PDF also requires information on the correlations between variables.

The PDF component means, standard deviations, and correlations involving w, r_t, and θ_l, as well as the mixture fractions, are calculated according to the Analytic Double Gaussian 1 (ADG1) PDF presented in Section (d) of the Appendix of Larson et al. (2002). The overall (grid-box) precipitation fraction is set to the maximum cloud fraction found at or above that grid level (Morrison and Gettelman 2008). The calculation of the component precipitation fractions $f_{p(i)}$ from the overall precipitation fraction are outlined in Section 1.3. Also described there is the calculation of the PDF component means and standard deviations involving N_{cn}, r_r, and N_r. Interactive CLUBB runs prescribe a constant ratio of the in-precipitation variance to the square of the in-precipitation mean for r_r and N_r. Additionally, all remaining correlations between variables are prescribed constants.

The covariance of PDF variables x_1 and x_2 can be calculated by

$$\overline{x_1' x_2'} = \int \int \left(x_1 - \overline{x_1}\right) \left(x_2 - \overline{x_2}\right) P\left(x_1, x_2\right) \mathrm{d}x_2 \, \mathrm{d}x_1. \tag{2.23}$$

The covariance of a PDF variable and a microphysics function (written in terms of PDF variables) can be calculated in the same manner. For example, the covariance of θ_l and KK evaporation rate found in Eq. (2.17) and Eq. (2.18) can be rewritten as

$$\overline{\theta_l' \left.\frac{\partial r_r}{\partial t}\right|_{\text{evap}}'} = \overline{\left(\theta_l - \overline{\theta_l}\right) \left(\left.\frac{\partial r_r}{\partial t}\right|_{\text{evap}} - \overline{\left.\frac{\partial r_r}{\partial t}\right|_{\text{evap}}} \right)}, \tag{2.24}$$

where mean evaporation rate, $\overline{\left.\frac{\partial r_r}{\partial t}\right|_{\text{evap}}}$, is also calculated by integrating over the PDF (see Appendix C). The KK evaporation rate can be written as a function of θ_l, r_t, r_r, and N_r, so here it will be referred to as $\text{EV}\left(\theta_l, r_t, r_r, N_r\right)$. The covariance of θ_l and KK evaporation rate is calculated by

$$\begin{aligned}\overline{\theta_l' \left.\frac{\partial r_r}{\partial t}\right|_{\text{evap}}'} = \int\int\int\int \left(\theta_l - \overline{\theta_l}\right) \left(\text{EV}\left(\theta_l, r_t, r_r, N_r\right) - \overline{\text{EV}\left(\theta_l, r_t, r_r, N_r\right)}\right) \\ \times P\left(\theta_l, r_t, r_r, N_r\right) \mathrm{d}N_r \, \mathrm{d}r_r \, \mathrm{d}r_t \, \mathrm{d}\theta_l.\end{aligned} \tag{2.25}$$

The remaining eight covariances involving microphysical functions are calculated in the same manner. Further and more detailed description of this method can be found in Appendix E.

2.3 Test case and model setups

To perform an initial test of the parameterization, we choose the Rain in Cumulus over the Ocean (RICO) model intercomparison case of a precipitating shallow cumulus layer (van Zanten et al. 2011). The intercomparison model configuration is based on a field study conducted off the coast of Antigua and Barbuda (Rauber et al. 2007). RICO uses prescribed radiative and large-scale forcings for temperature and moisture, as well as prescribed large-scale subsidence. These quantities vary with altitude but are constant over time. The surface fluxes are calculated using bulk aerodynamic equations. The simulation was run for a period of 72 hours.

RICO was chosen as a test case for two main reasons. First, ice microphysics is not necessary for a shallow trade-wind cumulus case; hence, a warm microphysics scheme is sufficient. Secondly, RICO is a partly cloudy case that precipitates over a small portion of the horizontal domain and contains significant variance of r_r within the precipitating region. These factors lead to significant microphysical effects on the subgrid variances and covariances. In contrast, the effects of microphysics on the same subgrid variances and covariances are neg-

ligible (not shown) in the drizzling stratocumulus case based on research flight two (RF02) of the second Dynamics and Chemistry of Marine Stratocumulus (DYCOMS-II) field study (Ackerman et al. 2009; Wyant et al. 2007). DYCOMS-II RF02 is entirely overcast and the in-precipitation variance of r_r is much smaller than found in RICO.

In order to provide a benchmark for comparison, a large-eddy simulation (LES) of RICO was run using the System for Atmospheric Modeling (SAM) (Khairoutdinov and Randall 2003). SAM uses an anelastic equation set that predicts all three components of velocity, total water mixing ratio, liquid water static energy, and hydrometeor fields (based on the selected microphysics scheme). A third-order Adams-Bashforth time-stepping scheme is used to advance the predictive equations of motion. The predictive fields are advected by the second-order MPDATA (multidimensional positive definite advection transport algorithm) scheme (Smolarkiewicz and Grabowski 1990). The subgrid-scale fluxes are computed by a 1.5-order subgrid-scale turbulence kinetic energy closure.

The SAM LES of RICO was run using KK microphysics. SAM's implementation of KK microphysics predicts both r_r and N_r. Cloud water mixing ratio, r_c, is calculated using a simple saturation adjustment scheme. Cloud droplet concentration, N_c, is set to a constant value of 70 cm^{-3} within cloud. SAM uses a fixed, Cartesian grid. For the RICO case, a 256×256 horizontal grid is used with a grid spacing of 100 m in each direction. The vertical grid contains 100 levels with 40 m grid spacing, spanning a domain of depth 4000 m. The model time step is 1 s, and horizontally averaged statistical profiles are sampled and output every 60 s. SAM uses periodic boundary conditions at the lateral boundaries and a rigid lid at the top of the domain.

The single-column CLUBB simulation of RICO was run using the analytically upscaled version of KK microphysics, including the microphysical effects on the predictive variances and covariances as described in Section 2.2. In addition to $\overline{r_t}$, $\overline{\theta_l}$, $\overline{w'r_t'}$, $\overline{w'\theta_l'}$, $\overline{r_t'^2}$, $\overline{\theta_l'^2}$, and $\overline{r_t'\theta_l'}$, CLUBB also predicts the variance and third-order central moment of vertical velocity ($\overline{w'^2}$ and $\overline{w'^3}$, respectively), the mean and variance of the horizontal west-east wind component ($\overline{u}$

and $\overline{u'^2}$, respectively), the mean and variance of the horizontal south-north wind component ($\overline{v}$ and $\overline{v'^2}$, respectively), and the mean of each hydrometeor field involved in the microphysics ($\overline{r_r}$ and $\overline{N_r}$ for KK microphysics). The anelastic approximation is used in all predictive equations. CLUBB calculates $\overline{r_c}$ by using a simple saturation adjustment and integration over the subgrid PDF. Just as in SAM LES, cloud droplet concentration is set to a constant value in cloud for the RICO case. CLUBB uses a vertically stretched grid containing 37 levels covering a domain of depth 4904 m. The model time step is 180 s, and statistical profiles are sampled and output at every model time step.

In the following analysis, profiles of the SAM LES and CLUBB SCM budget terms for the $\overline{w'r_t'}$, $\overline{w'\theta_l'}$, $\overline{r_t'^2}$, $\overline{\theta_l'^2}$, and $\overline{r_t'\theta_l'}$ fields are time-averaged over the last two hours of the RICO simulation (minutes 4200 through 4320). The RICO fields are in an approximately steady state during this time period.

2.4 Results

In order to assess which physical processes are most important, the LES budget terms for turbulent fields are analyzed. Additionally, the LES budgets and CLUBB's budgets are compared in order to assess the accuracy of CLUBB's PDF shape and its closures.

Unlike the LES, the CLUBB budget terms for turbulent fields are taken directly from the predictive equation set. The anelastic predictive equations for the turbulent fluxes $\overline{w'r_t'}$ and $\overline{w'\theta_l'}$ are given by

$$\begin{aligned}\frac{\partial \overline{w'r_t'}}{\partial t} = & \underbrace{-\frac{1}{\rho_s}\frac{\partial \rho_s \overline{w}\,\overline{w'r_t'}}{\partial z} - \frac{1}{\rho_s}\frac{\partial \rho_s \overline{w'^2 r_t'}}{\partial z}}_{\text{advection}} \underbrace{-\overline{w'^2}\,\frac{\partial \overline{r_t}}{\partial z} - \overline{w'r_t'}\,\frac{\partial \overline{w}}{\partial z}}_{\text{production}} \underbrace{-\frac{1}{\rho_s}\overline{r_t'\frac{\partial p'}{\partial z}}}_{\text{pressure}} \\ & \underbrace{+\frac{g}{\theta_{vs}}\overline{r_t'\theta_v'}}_{\text{buoyancy}} \underbrace{+\varepsilon_{w\,r_t}}_{\text{diffusion}} \underbrace{+\overline{w'\left.\frac{\partial r_t}{\partial t}\right|_{\text{mc}}'}}_{\text{microphysics}}, \qquad \text{and}\end{aligned} \tag{2.26}$$

$$\frac{\partial \overline{w'\theta_l'}}{\partial t} = \underbrace{-\frac{1}{\rho_s}\frac{\partial \rho_s \, \overline{w} \, \overline{w'\theta_l'}}{\partial z} - \frac{1}{\rho_s}\frac{\partial \rho_s \, \overline{w'^2\theta_l'}}{\partial z}}_{\text{advection}} \underbrace{-\overline{w'^2}\,\frac{\partial \overline{\theta_l}}{\partial z} - \overline{w'\theta_l'}\,\frac{\partial \overline{w}}{\partial z}}_{\text{production}} \underbrace{-\frac{1}{\rho_s}\overline{\theta_l'\frac{\partial p'}{\partial z}}}_{\text{pressure}}$$
$$\underbrace{+\frac{g}{\theta_{vs}}\overline{\theta_l'\theta_v'}}_{\text{buoyancy}} \underbrace{+\varepsilon_{w\,\theta_l}}_{\text{diffusion}} \underbrace{+\overline{w'\left.\frac{\partial \theta_l}{\partial t}\right|_{\text{mc}}'}}_{\text{microphysics}}, \tag{2.27}$$

where g is gravity and θ_v is virtual potential temperature. The dry, anelastic base-state values of air density, ρ_s, and θ_v, denoted θ_{vs}, vary only with altitude. The higher-order turbulent advection terms, $\overline{w'^2 r_t'}$ and $\overline{w'^2\theta_l'}$, are closed using the PDF (Larson and Golaz 2005). The pressure terms are parameterized following André et al. (1978) (see also Golaz et al. (2002a)). The slow (return-to-isotropy) term is approximated by Newtonian dampling. The buoyancy terms are closed by linearizing and then integrating over the PDF (Larson et al. 2002). The terms denoted $\varepsilon_{w\,r_t}$ and $\varepsilon_{w\,\theta_l}$ are background numerical vertical diffusion terms (Golaz et al. 2002a).

As in CLUBB, the SAM LES budgets for the horizontally averaged turbulent fluxes contain advective transport terms and turbulent (gradient) production terms, which both ultimately arise from the 3D advection of w, r_t, and θ_l. The turbulent production terms generate variability when the vertical derivative of the mean field is non-zero. SAM also records the effects of pressure, buoyancy, and microphysics on the turbulent fluxes. SAM's budget term for diffusion of $\overline{w'r_t'}$ and $\overline{w'\theta_l'}$ records the effects of diffusion associated with the subgrid TKE scheme. In Fig. 2.1 and Fig. 2.2, following Khairoutdinov and Randall (2002), the SAM LES budget terms for buoyancy and pressure are combined because they are both large compared to other terms, yet are in close equilibrium because of the quasi-hydrostatic balance of perturbation buoyancy and perturbation pressure gradient. The CLUBB buoyancy and pressure terms have been combined in an analogous manner.

The SAM LES turbulent flux budgets show that the largest terms are pressure+buoyancy, which usually acts as a net sink of turbulent flux, and turbulent production, which acts as a source of turbulent flux (see Fig. 2.1(a) and Fig. 2.2(a)). Another major term in the budget is the (turbulent) advection term. It has a mass-weighted vertical integral of zero. That is,

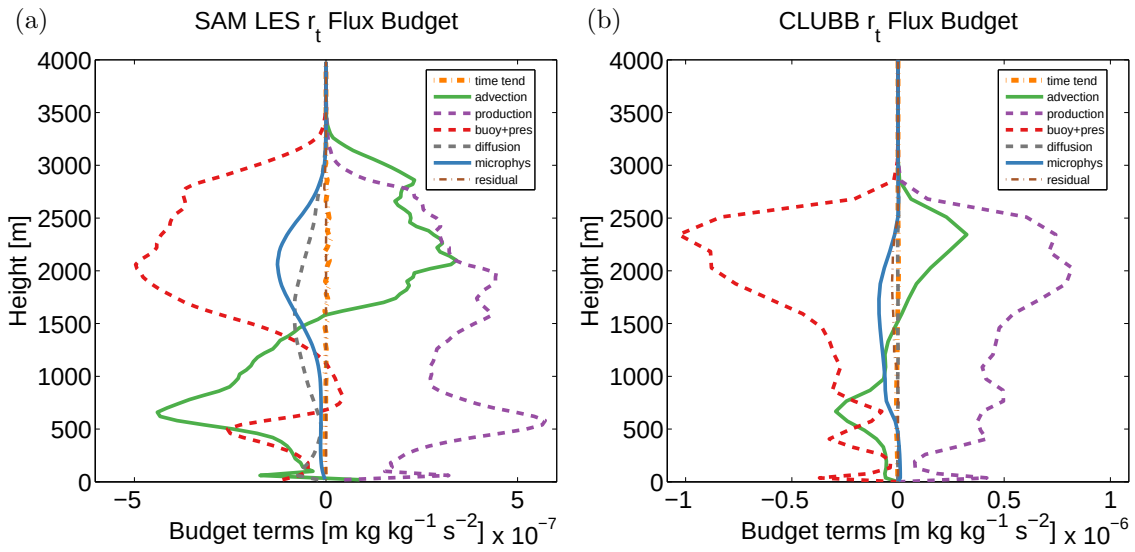

Figure 2.1: Profiles of $\overline{w'r_t'}$ budget terms for the RICO precipitating shallow cumulus case, time-averaged over the last two hours of the simulation (minutes 4200 through 4320), for (a) SAM LES and (b) CLUBB SCM. The profiles of overall time tendency are orange dashed-dotted lines, the advection terms are green solid lines, and the production terms are purple dashed lines. The sum of the buoyancy and pressure terms are the red dashed lines. The diffusion terms are gray dashed lines, the microphysics (precipitation) terms are blue solid lines, and the residuals are brown dashed-dotted lines. SAM LES shows that the microphysics term is modest, but not negligible. The CLUBB microphysics term has the same sign and approximate magnitude as the SAM LES microphysics term.

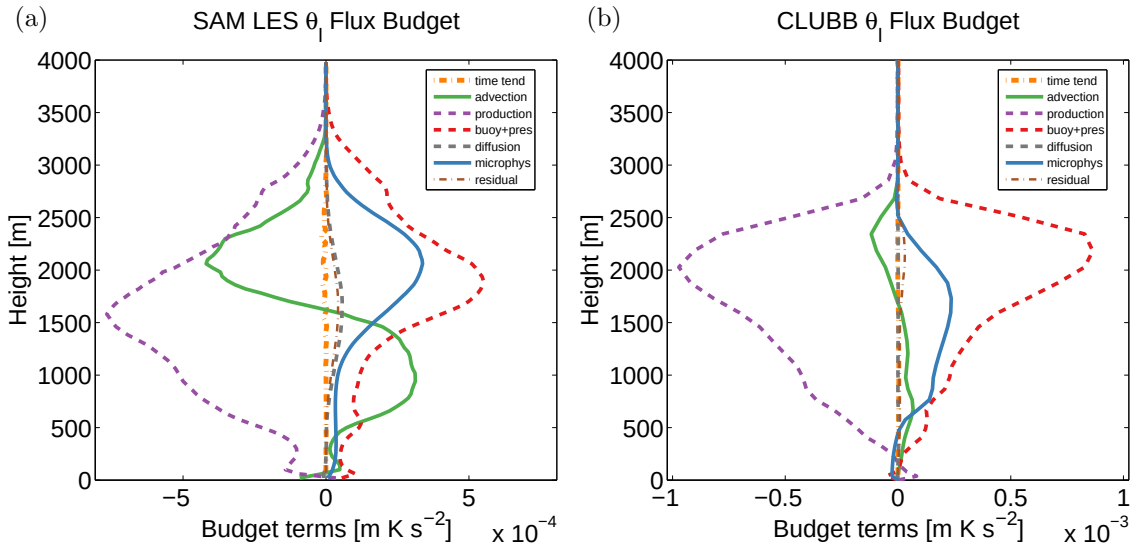

Figure 2.2: Profiles of $\overline{w'\theta_l'}$ budget terms for the RICO precipitating shallow cumulus case, time-averaged over the last two hours of the simulation (minutes 4200 through 4320), for (a) SAM LES and (b) CLUBB SCM. The profiles of overall time tendency are orange dashed-dotted lines, the advection terms are green solid lines, and the production terms are purple dashed lines. The sum of the buoyancy and pressure terms are the red dashed lines. The diffusion terms are gray dashed lines, the microphysics (precipitation) terms are blue solid lines, and the residuals are brown dashed-dotted lines. SAM LES shows that the microphysics term is more significant for $\overline{w'\theta_l'}$ than it was for $\overline{w'r_t'}$. The CLUBB microphysics term has the same sign and approximate magnitude at peak as the SAM LES microphysics term.

averaged in the vertical, it is neither a net source nor a net sink. Instead, it takes the excess variability at some altitudes and transports it to regions with a deficit of variability. The microphysics term is a sink of turbulent flux in the cloudy layer, a layer which spans the altitude range from 500 m to 3000 m. The microphysics term is more significant for $\overline{w'\theta_l'}$ than for $\overline{w'r_t'}$, but even for $\overline{w'r_t'}$, it is non-negligible.

CLUBB's turbulent flux budgets usually agree qualitatively with those from LES (Fig. 2.1(b) and Fig. 2.2(b)). The microphysics terms in both the $\overline{w'r_t'}$ and $\overline{w'\theta_l'}$ budgets have the same signs and close to the same peak magnitudes as their counterparts in the LES. In CLUBB, the range of altitudes where the microphysics budget terms have significant values is shifted lower than in SAM LES. This occurs because $\overline{r_r}$ peaks at a lower altitude in CLUBB than in SAM LES. CLUBB's advection terms have approximately the correct shape, although they are usually too small in magnitude. In CLUBB, the buoyancy+pressure and turbulent production terms are dominant, as in SAM LES, but in CLUBB's RICO simulation their magnitudes are larger than in SAM LES.

The CLUBB anelastic predictive equations for the scalar variances $\overline{r_t'^2}$ and $\overline{\theta_l'^2}$, and the covariance $\overline{r_t'\theta_l'}$, are given by

$$\frac{\partial \overline{r_t'^2}}{\partial t} = \underbrace{-\frac{1}{\rho_s}\frac{\partial \rho_s \, \overline{w}\, \overline{r_t'^2}}{\partial z} - \frac{1}{\rho_s}\frac{\partial \rho_s \, \overline{w' r_t'^2}}{\partial z}}_{\text{advection}} \underbrace{-2\,\overline{w'r_t'}\,\frac{\partial \overline{r_t}}{\partial z}}_{\text{production}} \underbrace{+\varepsilon_{r_t\, r_t}}_{\text{diss+diff}} \underbrace{+2\,\overline{r_t'\left.\frac{\partial r_t}{\partial t}\right|_{\text{mc}}'}}_{\text{microphysics}}, \tag{2.28}$$

$$\frac{\partial \overline{\theta_l'^2}}{\partial t} = \underbrace{-\frac{1}{\rho_s}\frac{\partial \rho_s \, \overline{w}\, \overline{\theta_l'^2}}{\partial z} - \frac{1}{\rho_s}\frac{\partial \rho_s \, \overline{w' \theta_l'^2}}{\partial z}}_{\text{advection}} \underbrace{-2\,\overline{w'\theta_l'}\,\frac{\partial \overline{\theta_l}}{\partial z}}_{\text{production}} \underbrace{+\varepsilon_{\theta_l\, \theta_l}}_{\text{diss+diff}} \underbrace{+2\,\overline{\theta_l'\left.\frac{\partial \theta_l}{\partial t}\right|_{\text{mc}}'}}_{\text{microphysics}}, \text{ and} \tag{2.29}$$

$$\begin{aligned}\frac{\partial \overline{r_t'\theta_l'}}{\partial t} = &\underbrace{-\frac{1}{\rho_s}\frac{\partial \rho_s \, \overline{w}\, \overline{r_t'\theta_l'}}{\partial z} - \frac{1}{\rho_s}\frac{\partial \rho_s \, \overline{w' r_t'\theta_l'}}{\partial z}}_{\text{advection}} \underbrace{-\overline{w'r_t'}\,\frac{\partial \overline{\theta_l}}{\partial z} - \overline{w'\theta_l'}\,\frac{\partial \overline{r_t}}{\partial z}}_{\text{production}} \underbrace{+\varepsilon_{r_t\, \theta_l}}_{\text{diss+diff}} \\ &\underbrace{+\overline{r_t'\left.\frac{\partial \theta_l}{\partial t}\right|_{\text{mc}}'} + \overline{\theta_l'\left.\frac{\partial r_t}{\partial t}\right|_{\text{mc}}'}}_{\text{microphysics}}.\end{aligned} \tag{2.30}$$

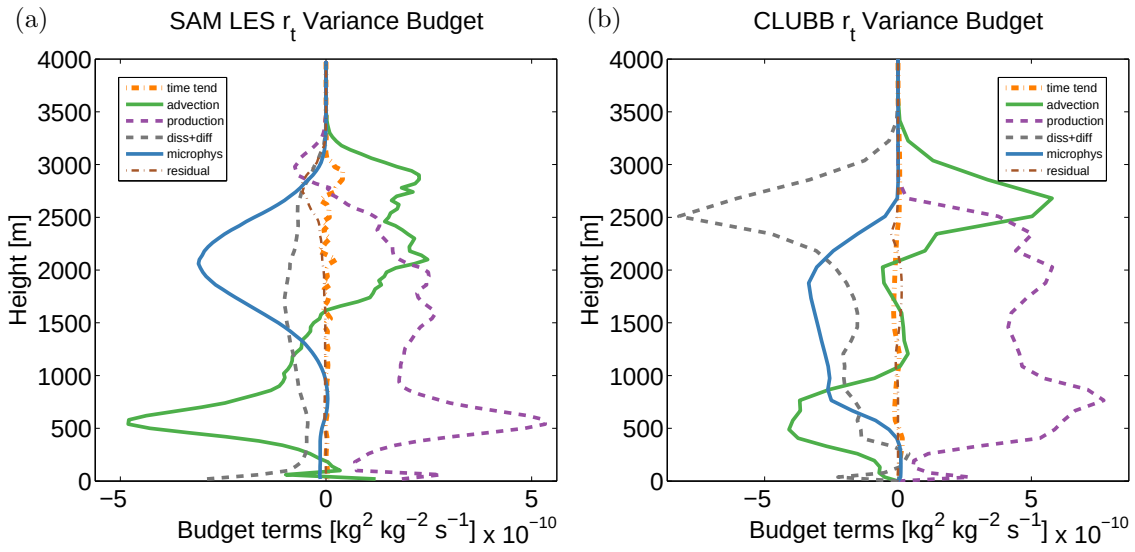

Figure 2.3: Profiles of $\overline{r_t'^2}$ budget terms for the RICO precipitating shallow cumulus case, time-averaged over the last two hours of the simulation (minutes 4200 through 4320), for (a) SAM LES and (b) CLUBB SCM. The profiles of overall time tendency are orange dashed-dotted lines, the advection terms are green solid lines, and the production terms are purple dashed lines. The sum of the dissipation and diffusion terms are gray dashed lines. The microphysics (precipitation) terms are blue solid lines, and the residuals are brown dashed-dotted lines. SAM LES shows that the microphysics term is significant. The CLUBB microphysics term is also significant, and has the same sign and approximate magnitude as the SAM LES microphysics term.

As in the predictive equations for the fluxes, the higher-order turbulent advection terms, $\overline{w' r_t'^2}$, $\overline{w' \theta_l'^2}$, and $\overline{w' r_t' \theta_l'}$, are closed using the PDF (Larson and Golaz 2005). The terms denoted $\varepsilon_{r_t r_t}$, $\varepsilon_{\theta_l \theta_l}$, and $\varepsilon_{r_t \theta_l}$ each contain a dissipation term (parameterized in CLUBB as Newtonian damping) that reduces the magnitude of the turbulent field, as well as a background numerical vertical diffusion term (Golaz et al. 2002a; André et al. 1978).

The SAM LES budgets for the horizontally averaged turbulent (co)variances contain advective transport terms and turbulent (gradient) production terms, as well as microphysics terms. In Fig. 2.3, Fig. 2.4, and Fig. 2.5, the diffusion and dissipation terms are combined for both SAM and CLUBB. Both SAM and CLUBB contain vertical diffusion, with SAM's associated with TKE. However, SAM's subgrid TKE is also used to diffuse fields horizontally. Horizontal diffusion smooths out a model field across the grid level, reducing the variances and covariances of model fields. In CLUBB, this effect is parameterized by the dissipation (Newtonian damping) term.

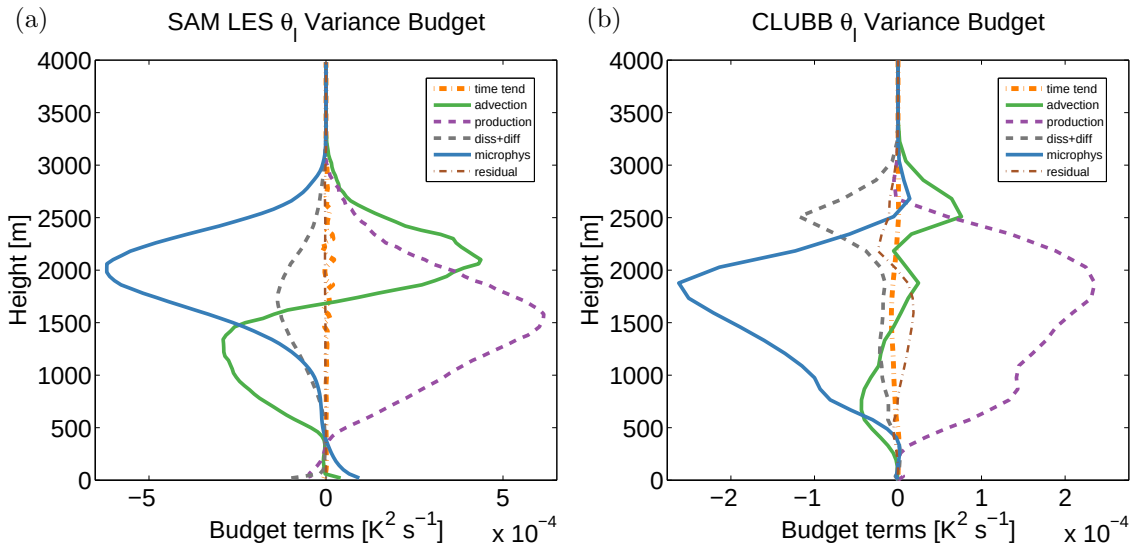

Figure 2.4: Profiles of $\overline{\theta_l'^2}$ budget terms for the RICO precipitating shallow cumulus case, time-averaged over the last two hours of the simulation (minutes 4200 through 4320), for (a) SAM LES and (b) CLUBB SCM. The profiles of overall time tendency are orange dashed-dotted lines, the advection terms are green solid lines, and the production terms are purple dashed lines. The sum of the dissipation and diffusion terms are gray dashed lines. The microphysics (precipitation) terms are blue solid lines, and the residuals are brown dashed-dotted lines. SAM LES shows that the microphysics term is a dominant term in the budget. The CLUBB microphysics term is also a dominant term, balancing the production term.

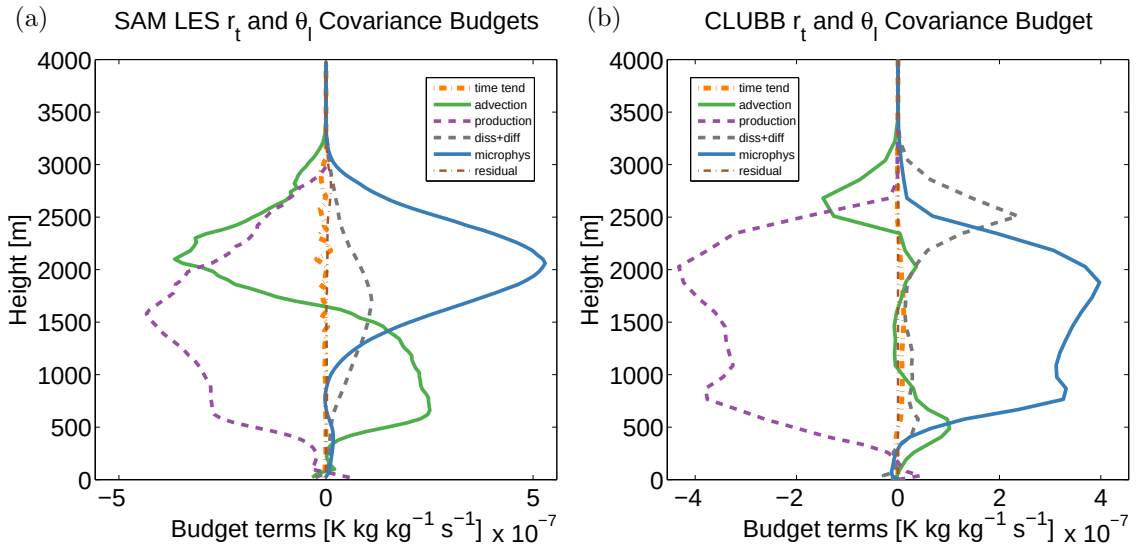

Figure 2.5: Profiles of $\overline{r_t'\theta_l'}$ budget terms for the RICO precipitating shallow cumulus case, time-averaged over the last two hours of the simulation (minutes 4200 through 4320), for (a) SAM LES and (b) CLUBB SCM. The profiles of overall time tendency are orange dashed-dotted lines, the advection terms are green solid lines, and the production terms are purple dashed lines. The sum of the dissipation and diffusion terms are gray dashed lines. The microphysics (precipitation) terms are blue solid lines, and the residuals are brown dashed-dotted lines. Again, SAM LES shows that the microphysics term is dominant. The CLUBB microphysics term is also dominant, and balances the production term in the budget.

The SAM LES budgets for $\overline{r_t'^2}$, $\overline{\theta_l'^2}$, and $\overline{r_t'\theta_l'}$ show that microphysics is a dominant term in the upper half of the cloud layer. At those levels, microphysics is balanced by turbulent production and turbulent advection (at higher altitudes) (Figs. 2.3(a), 2.4(a), and 2.5(a)). Near cloud base, the budget is predominantly a balance of advection and production. The dissipation/diffusion terms are smaller, but not negligible.

The time-averaged CLUBB SCM budgets found in Fig. 2.3(b), Fig. 2.4(b), and Fig. 2.5(b) show that the CLUBB scalar (co)variance budgets are qualitatively similar to the LES budgets. The microphysics term in the $\overline{r_t'^2}$ budget has the correct sign and approximate peak magnitude, and the shape of the profile of the advection and production terms qualitatively resemble the LES. CLUBB's dissipation term is too large, but the microphysics terms in the $\overline{\theta_l'^2}$ and $\overline{r_t'\theta_l'}$ budgets are dominant terms in the cloudy layer, just as in the LES. The production terms largely balance the microphysics terms. The advection terms are too small in magnitude relative to the other terms, but have approximately the right shape.

The figures show that the microphysics terms are sink terms in the cloudy layer, reducing the variances and the magnitudes of the covariances, for all five of these turbulent fields. Physically, this happens because cumulus clouds arise in the regions of the horizontal domain that are moister than average. Additionally, cloudy regions are usually associated with updrafts (where vertical velocity is greater than average) in a cumulus regime. Within cloud, the moistest regions contain the greatest amount of cloud (liquid) water. The microphysics processes of autoconversion and accretion occur only in cloud and at greater rates in regions with a greater amount of cloud water. When autoconversion and accretion occur, rain water is produced at the expense of cloud water. The local value of r_c decreases, which decreases r_t and increases θ_l preferentially in the moistest portions of domain. As a result, scalar variances $\overline{r_t'^2}$ and $\overline{\theta_l'^2}$ are reduced, and the (negative) covariance $\overline{r_t'\theta_l'}$ is reduced in magnitude. Similarly, since moister regions of cloud are associated with stronger updrafts, the covariance $\overline{w'r_t'}$ is reduced by microphysics and the (negative) covariance $\overline{w'\theta_l'}$ is reduced in magnitude by microphysics.

In the region below cloud, a different microphysical process occurs: rain falls into clear air below cloud and evaporates. Evaporation increases water vapor at the expense of rain water and also cools the air. Hence, where evaporation occurs, r_t is increased and θ_l is decreased. If rain preferentially falls through regions of air that have already been cooled by evaporation, then cool air is further cooled. In a partly rainy case such as RICO, rain cools the rainshafts but not other portions of the domain, increasing variability in θ_l. In the SAM LES of RICO, the increase of subcloud $\overline{\theta_l'^2}$ by microphysics is significant, as shown in Fig. 2.4(a).

Unfortunately, in the present simulation, CLUBB severely underestimates the positive, subcloud microphysical source of $\overline{\theta_l'^2}$ found in SAM LES. The underestimate is not caused by inaccuracy in the form of the integral, but rather by inaccurate inputs to the integral. The CLUBB results below cloud may be improved by a better method to divide the grid-box means and variances of r_t and θ_l into the PDF component means and standard deviations of r_t and θ_l. The development of this method is beyond the scope of this paper. It should be noted that changing the way the PDF component means, standard deviations, correlations, and/or relevant fractions are calculated does *not* change the general form of the integral equations. A change would only be required if the distribution type, i.e. normal/lognormal, were abandoned.

2.5 Conclusion

Microphysical sources of (co)variances of total water and liquid water potential temperature are significant. A LES of the RICO shallow cumulus case shows that, in this cloud case, microphysical sources are major terms in the budgets of variances and turbulent fluxes. In particular, microphysical processes have three main effects. First, precipitation formation and growth is the major sink of $\overline{r_t'^2}$, $\overline{\theta_l'^2}$, and the magnitude of $\overline{r_t'\theta_l'}$ in the upper half of the cloud layer (see Figs. 2.3, 2.4, and 2.5). In particular, microphysical damping is greater than tur-

bulent dissipation. The damping of scalar variances occurs because rain formation depletes cloud water preferentially in the moistest part of the cloud. This depletion preferentially reduces the largest values of (liquid) cloud water, thereby reducing the horizontally-averaged variance. Second, microphysics also damps the turbulent flux of scalars, $\overline{w'r_t'}$ and $\overline{w'\theta_l'}$ (see Figs. 2.1 and 2.2). The mechanism is the same: precipitation reduces cloud water in the moistest part of the cloud, which also contains stronger updrafts. Although the effects of microphysics on fluxes are smaller than those on variances, microphysics is still a major term in the $\overline{w'\theta_l'}$ budget and ought not to be ignored. Third, evaporation of rain below cloud acts as a source of $\overline{\theta_l'^2}$. The positive sign arises because evaporation of rain cools the cooler part of the subcloud layer. This evaporation-induced generation of $\overline{\theta_l'^2}$ is a key aspect of cold pool formation. It leads to buoyant generation of $\overline{w'\theta_l'}$ below cloud base, which in turn leads to new convection.

This paper demonstrates that all these microphysical sources and sinks can be calculated analytically, given a sufficiently simple warm-rain microphysics scheme and a sufficiently simple multivariate PDF. These analytic expressions have been implemented in the predictive equations for variances and covariances involving r_t and θ_l in the CLUBB parameterization. When applied in an interactive, single-column simulation of the RICO case by CLUBB, the microphysical terms agree qualitatively with LES in sign and in relative magnitude, except for the underestimate of the microphysical source of $\overline{\theta_l'^2}$ below cloud.

In the future, if the parameterized subcloud source of $\overline{\theta_l'^2}$ can be increased, then analytic integration of microphysical sources of scalar (co)variances may provide a useful step for the parameterization of cold pools and cloud organization. It does not parameterize cold pools and cloud organization directly, because it does not account for spatial arrangement of cloud parcels. Furthermore, it does not even parameterize all *effects* of cold pools and cloud organization. However, it does parameterize effects that are directly related to scalar variability, and it parameterizes these effects in a mathematically rigorous way. Namely, it defines the microphysical sources with precise, mathematical expressions, and it provides

explicit formulas for the case of idealized, warm-rain microphysics.

In addition, analytic integration assists in the development of more general integration methods, such as Monte Carlo integration (Larson and Schanen 2013). For instance, analytic integration allows a researcher to rapidly explore behaviors in idealized settings while avoiding the contamination of sampling noise or other integration errors. More importantly, analytic integration provides an alternative solution that can be used to test whether a Monte Carlo integration code converges to the correct solution (Larson and Schanen 2013). In past experience, we have found such testing to be crucial. Bugs are surprisingly easy to introduce, and without comparison against an independent solution, results produced by a Monte Carlo integrator will be subject to lingering doubts. On the other hand, once a Monte Carlo integrator has been tested against an analytic solution, it can be used more confidently with a comprehensive microphysics scheme that includes ice in order to simulate a variety of shallow and deep cloud cases. In fact, this has already been done in Storer et al. (2015). In this way, analytic integration of the microphysical effects on scalar variances and fluxes is an enabling technology: it enables the verification of general subgrid integration methods.

Bibliography

Ackerman, A. S., M. C. van Zanten, B. Stevens, V. Savic-Jovcic, C. S. Bretherton, A. Chlond, J.-C. Golaz, H. Jiang, M. Khairoutdinov, S. K. Krueger, D. C. Lewellen, A. Lock, C.-H. Moeng, K. Nakamura, M. D. Petters, J. R. Snider, S. Weinbrecht, and M. Zulauf, 2009: Large-eddy simulations of a drizzling, stratocumulus-topped marine boundary layer. *Mon. Wea. Rev.*, **137**, 1083–1110. doi: 10.1175/2008MWR2582.1.

Anderson, T. W., 1962: On the distribution of the two-sample Cramer-von Mises criterion. *Ann. Math. Statist.*, **33**, 1148–1159.

André, J. C., G. de Moor, P. Lacarrère, and R. du Vachat, 1978: Modeling the 24-hour evolution of the mean and turbulent structures of the planetary boundary layer. *J. Atmos. Sci.*, **35**, 1861–1883.

Bogenschutz, P. A. and S. K. Krueger, 2013: A simplified PDF parameterization of subgrid-scale clouds and turbulence for cloud-resolving models. *J. Adv. Model. Earth Syst.*, **5**, doi:10.1002/jame.20018.

Bogenschutz, P. A., S. K. Krueger, and M. Khairoutdinov, 2010: Assumed probability density functions for shallow and deep convection. *J. Adv. Model. Earth Syst.*, **2**, doi:10.3894/JAMES.2010.2.10.

Böing, S. J., H. J. Jonker, A. P. Siebesma, and W. W. Grabowski, 2012: Influence of the subcloud layer on the development of a deep convective ensemble. *J. Atmos. Sci.*, **69**, 2682–2698.

Boutle, I., S. Abel, P. Hill, and C. Morcrette, 2014: Spatial variability of liquid cloud and rain: Observations and microphysical effects. *Quarterly Journal of the Royal Meteorological Society*, **140**, 583–594.

Cheng, A. and K.-M. Xu, 2009: A pdf-based microphysics parameterization for simulation of drizzling boundary layer clouds. *J. Atmos. Sci.*, **66**, 2317–2334.

Cheng, A. and K.-M. Xu, 2015: Improved low-cloud simulation from the Community Atmosphere Model with an advanced third-order turbulence closure. *Journal of Climate*, **28**. doi:http://dx.doi.org/10.1175/JCLI-D-14-00776.1.

Deardorff, J. W., 1980: Stratocumulus-capped mixed layers derived from a three-dimensional model. *Bound.-Layer Meteor.*, **18**, 495–527.

Derbyshire, S. H., I. Beau, P. Bechtold, J. Y. Grandpeix, J. M. Piriou, J. L. Redelsperger, and P. M. M. Soares, 2004: Sensitivity of moist convection to environmental humidity. *Quart. J. Roy. Meteor. Soc.*, **130**, 3055–3079.

Firl, G. J. and D. A. Randall, 2015: Fitting and analyzing LES using multiple trivariate gaussians. *J. Atmos. Sci.*, **72**, 1094–1116.

Fletcher, S. J. and M. Zupanski, 2006: A hybrid multivariate normal and lognormal distribution for data assimilation. *Atmos. Sci. Lett.*, **7**, 43–46. doi:10.1002/asl.128.

Gentine, P., A. Garelli, S.-B. Park, J. Nie, G. Torri, and Z. Kuang, 2016: Role of surface heat fluxes underneath cold pools. *Geophys. Res. Lett.*, **43**, 874–883. 2015GL067262.

Golaz, J.-C., V. E. Larson, and W. R. Cotton, 2002a: A PDF-based model for boundary layer clouds. Part I: Method and model description. *J. Atmos. Sci.*, **59**, 3540–3551.

Golaz, J.-C., V. E. Larson, and W. R. Cotton, 2002b: A PDF-based model for boundary layer clouds. Part II: Model results. *J. Atmos. Sci.*, **59**, 3552–3571.

Grabowski, W. W., P. Bechtold, A. Cheng, R. Forbes, C. Halliwell, M. Khairoutdinov, S. Lang, T. Nasuno, J. Petch, W. K. Tao, R. Wong, X. Wu, and K. M. Xu, 2006: Daytime convective development over land: A model intercomparison based on LBA observations. *Quart. J. Roy. Meteor. Soc.*, **132**, 317–344.

Griffin, B. M. and V. E. Larson, 2013: Analytic upscaling of local microphysics parameterizations, Part II: Simulations. *Quart. J. Royal Met. Soc.*, **139**, 58–69.

Guo, H., J.-C. Golaz, L. Donner, B. Wyman, M. Zhao, and P. Ginoux, 2015: CLUBB as a unified cloud parameterization: opportunities and challenges. *Geophys. Res. Lett.*, **42**, 4540–4547. doi:10.1002/2015GL063672.

Kärcher, B. and U. Burkhardt, 2008: A cirrus cloud scheme for general circulation models. *Quart. J. Royal Met. Soc.*, **134**, 1439–1461.

Khairoutdinov, M. and Y. Kogan, 2000: A new cloud physics parameterization in a large-eddy simulation model of marine stratocumulus. *Mon. Wea. Rev.*, **128**, 229–243.

Khairoutdinov, M. and D. A. Randall, 2002: Similarity of deep continental cumulus convection as revealed by a three-dimensional cloud-resolving model. *J. Atmos. Sci.*, **59**, 2550–2566.

Khairoutdinov, M. and D. A. Randall, 2003: Cloud resolving modeling of the ARM Summer 1997 IOP: Model formulation, results, uncertainties, and sensitivities. *J. Atmos. Sci.*, **60**, 607–624.

Khairoutdinov, M. and D. A. Randall, 2006: High-resolution simulation of shallow-to-deep convection transition over land. *J. Atmos. Sci.*, **63**, 3421–3436.

Kogan, Y., 2013: A cumulus cloud microphysics parameterization for cloud-resolving models. *J. Atmos. Sci.*, **70**, 1423–1436.

Kogan, Y. L. and D. B. Mechem, 2014: A PDF-based microphysics parameterization for shallow cumulus clouds. *J. Atmos. Sci.*, **71**, 1070–1089.

Kogan, Y. L. and D. B. Mechem, 2015: A PDF-based formulation of microphysical variability in cumulus congestus clouds. *J. Atmos. Sci.*.

Kuang, Z. and C. S. Bretherton, 2006: A mass-flux scheme view of a high-resolution simulation of a transition from shallow to deep cumulus convection. *J. Atmos. Sci.*, **63**, 1895–1909.

Lappen, C.-L. and D. A. Randall, 2001: Towards a unified parameterization of the boundary layer and moist convection. Part I: A new type of mass-flux model. *J. Atmos. Sci.*, **58**, 2021–2036.

Larson, V. E. and J.-C. Golaz, 2005: Using probability density functions to derive consistent closure relationships among higher-order moments. *Mon. Wea. Rev.*, **133**, 1023–1042.

Larson, V. E. and B. M. Griffin, 2006: Coupling microphysics parameterizations to cloud parameterizations. Preprints*, 12th Conference on Cloud Physics*, Madison, WI, American Meteorological Society.

Larson, V. E. and B. M. Griffin, 2013: Analytic upscaling of local microphysics parameterizations, Part I: Derivation. *Quart. J. Royal Met. Soc.*, **139**, 46–57.

Larson, V. E. and D. P. Schanen, 2013: The Subgrid Importance Latin Hypercube Sampler (SILHS): a multivariate subcolumn generator. *Geosci. Model Dev.*, **6**, 1813–1829. doi:10.5194/gmdd-6-1813-2013.

Larson, V. E., R. Wood, P. R. Field, J.-C. Golaz, T. H. Vonder Haar, and W. R. Cotton, 2001: Systematic biases in the microphysics and thermodynamics of numerical models that ignore subgrid-scale variability. *J. Atmos. Sci.*, **58**, 1117–1128.

Larson, V. E., J.-C. Golaz, and W. R. Cotton, 2002: Small-scale and mesoscale variability in cloudy boundary layers: Joint probability density functions. *J. Atmos. Sci.*, **59**, 3519–3539.

Larson, V. E., J.-C. Golaz, H. Jiang, and W. R. Cotton, 2005: Supplying local microphysics parameterizations with information about subgrid variability: Latin hypercube sampling. *J. Atmos. Sci.*, **62**, 4010–4026.

Lebsock, M., H. Morrison, and A. Gettelman, 2013: Microphysical implications of cloud-precipitation covariance derived from satellite remote sensing. *Journal of Geophysical Research: Atmospheres*, **118**, 6521–6533.

Lewellen, W. S. and S. Yoh, 1993: Binormal model of ensemble partial cloudiness. *J. Atmos. Sci.*, **50**, 1228–1237.

Mapes, B. and R. Neale, 2011: Parameterizing convective organization to escape the entrainment dilemma. *J. Adv. Model. Earth Syst.*, **3**, doi:10.1029/2011MS000042.

Mellor, G. L., 1977: The Gaussian cloud model relations. *J. Atmos. Sci.*, **34**, 356–358.

Morrison, H. and A. Gettelman, 2008: A new two-moment bulk stratiform cloud microphysics scheme in the Community Atmosphere Model, Version 3 (CAM3). Part I: Description and numerical tests. *J. Climate.*, **21**, 3642–3659.

Morrison, H., J. A. Curry, and V. I. Khvorostyanov, 2005: A new double-moment microphysics parameterization for application in cloud and climate models. Part I: Description. *J. Atmos. Sci.*, **62**, 1665–1677.

Naumann, A. K., A. Seifert, and J. P. Mellado, 2013: A refined statistical cloud closure using double-Gaussian probability density functions. *Geosci. Model Dev.*, **6**, 1641–1657.

Neggers, R. A. J., M. Köhler, and A. C. M. Beljaars, 2009: A dual mass flux framework for boundary layer convection. Part I: Transport. *J. Atmos. Sci.*, **66**, 1465–1488.

Rauber, R. M., B. Stevens, H. T. Ochs, C. Knight, B. A. Albrecht, A. M. Blyth, C. W. Fairall, J. B. Jensen, S. G. Lasher-Trapp, O. L. Mayol-Bracero, G. Vali, J. R. Anderson, B. A. Baker, A. R. Bandy, E. Burnet, J.-L. Brenguier, W. A. Brewer, P. R. A. Brown, P. Chuang, W. R. Cotton, L. D. Girolamo, B. Geerts, H. Gerber, S. Göke, L. Gomes, B. G. Heikes, J. G. Hudson, P. Kollias, R. P. Lawson, S. K. Krueger, D. H. Lenschow, L. Nuijens, D. W. O'Sullivan, R. A. Rilling, D. C. Rogers, A. P. Siebesma, E. Snodgrass, J. L. Stith, D. C. Thornton, S. Tucker, C. H. Twohy, , P. Zuidema, K. R. Sperber, and D. E. Waliser, 2007: Rain in shallow cumulus over the ocean: The RICO campaign. *Bull. Amer. Meteor. Soc.*, **88**, 1912 – 1928.

Raut, E. K. and V. E. Larson, 2016: A flexible importance sampling method for integrating subgrid processes. *Geosci. Model Dev.*, **9**, 413–429.

Rogers, R. R. and M. K. Yau, 1989: *A short course in cloud physics*. 3rd edition, Butterworth-Heinemann, 290 pp.

Schlemmer, L. and C. Hohenegger, 2014: The formation of wider and deeper clouds as a result of cold-pool dynamics. *J. Atmos. Sci.*, **71**, 2842–2858.

Smolarkiewicz, P. K. and W. W. Grabowski, 1990: The multidimensional positive definite advection transport algorithm: nonoscillatory option. *J. Comput. Phys.*, **86**, 355–375.

Sommeria, G. and J. W. Deardorff, 1977: Subgrid-scale condensation in models of nonprecipitating clouds. *J. Atmos. Sci.*, **34**, 344–355.

Stephens, M. A., 1970: Use of the Kolmogorov-Smirnov, Cramer-von Mises and related statistics without extensive tables. *J. Roy. Statist. Soc. Ser. B*, **32**, 115–122.

Storer, R. L., B. M. Griffin, J. Höft, J. K. Weber, E. Raut, V. E. Larson, M. Wang, and P. J. Rasch, 2015: Parameterizing deep convection using the assumed probability density function method. *Geosci. Model Dev.*, **8**, 1–19. doi:10.5194/gmd-8-1-2015.

Sušelj, K., J. Teixeira, and D. Chung, 2013: A unified model for moist convective boundary layers based on a stochastic eddy-diffusivity/mass-flux parameterization. *J. Atmos. Sci.*, **70**, 1929–1953.

Thayer-Calder, K., A. Gettelman, C. Craig, S. Goldhaber, P. A. Bogenschutz, C.-C. Chen, H. Morrison, J. Höft, E. Raut, B. M. Griffin, J. K. Weber, V. E. Larson, M. C. Wyant, M. Wang, Z. Guo, and S. J. Ghan, 2015: A unified parameterization of clouds and turbulence using CLUBB and subcolumns in the Community Atmosphere Model. *Geosci. Model Dev.*, **8**, 3801–3821.

Tompkins, A. M., 2002: A prognostic parameterization for the subgrid-scale variability of water vapor and clouds in large-scale models and its use to diagnose cloud cover. *J. Atmos. Sci.*, **59**, 1917–1942.

van Zanten, M., B. Stevens, L. Nuijens, A. Siebesma, A. Ackerman, F. Burnet, A. Cheng, F. Couvreux, H. Jiang, M. Khairoutdinov, Y. Kogan, D. Lewellen, D. Mechem, K. Nakamura, A. Noda, B. Shipway, J. Slawinska, S. Wang, and A. Wyszogrodzki, 2011: Controls on precipitation and cloudiness in simulations of trade-wind cumulus as observed during RICO. *J. Adv. Model. Earth Syst.*, **3**, M06001.

Wyant, M. C., C. S. Bretherton, A. Chlond, B. M. Griffin, H. Kitagawa, C.-L. Lappen, V. E. Larson, A. Lock, S. Park, S. R. de Roode, J. Uchida, M. Zhao, and A. S. Ackerman, 2007: A single-column-model intercomparison of a heavily drizzling stratocumulus topped boundary layer. *J. Geophys. Res.*, **112**, D24204. doi:10.1029/2007JD008536.

Xue, H., G. Feingold, and B. Stevens, 2008: Aerosol effects on clouds, precipitation, and the organization of shallow cumulus convection. *J. Atmos. Sci.*, **65**, 392–406.

Zhang, J., U. Lohmann, and B. Lin, 2002: A new statistically based autoconversion rate parameterization for use in large-scale models. *J. Geophys. Res.*, **107**, Article No. 4750. doi:10.1029/2001JD001484.

Zuidema, P., Z. Li, R. J. Hill, L. Bariteau, B. Rilling, C. Fairall, W. A. Brewer, B. Albrecht, and J. Hare, 2012: On trade wind cumulus cold pools. *J. Atmos. Sci.*, **69**, 258–280.

Appendix A: Saturation and the PDF

A.1 Expressing cloud water mixing ratio in terms of the PDF

The CLUBB model predicts both mean values and subgrid moments (variances and covariances) of relevant model fields, including total water mixing ratio, r_t, and liquid water potential temperature, θ_l. The CLUBB model uses an assumed joint PDF to account for subgrid variability in the relevant model fields. The PDF method requires that the model produce information on the aforementioned variances and covariances. In turn, one of the uses of the PDF is to provide information on subgrid saturation, including the amount of cloud water and cloud fraction. In other words, the PDF reveals the subgrid character, including how much of the air in the subgrid domain is saturated and how much is unsaturated.

The CLUBB model uses a simple saturation adjustment when determining cloudiness. The saturated portion of the subgrid domain is considered to be cloudy, while the unsaturated portion of the subgrid domain is considered to be clear air. In detail, the CLUBB model considers any amount of r_t in excess of the saturation mixing ratio with respect to liquid water, $r_{sw}(T,p)$, to be cloud water. Cloud water mixing ratio, r_c, is given by the equation:

$$r_c = (r_t - r_{sw}(T,p))\, H(r_t - r_{sw}(T,p))\,; \tag{A1}$$

where T is temperature, p is pressure, and $H(x)$ is the Heaviside step function on the form

$$H(x) = \begin{cases} 0 & \text{where } x < 0 \\ 1 & \text{where } x > 0. \end{cases}$$

This saturation adjustment is a good approximation to nature because cloud droplets form

in saturated air or evaporate in subsaturated air very quickly.

Many quantities are found by integrating (over the domain of PDF) the product of a function and the functional form of the PDF. Some of these quantities include mean cloud water mixing ratio, cloud fraction, and microphysical process rates. In order to integrate over the PDF when a variable that is not part of the PDF is found in the integrand, that variable must be expressed in terms of variables that are part of the PDF. This is the case when the integral involves cloud water mixing ratio. Cloud water mixing ratio must be expressed in terms of variables that are part of the joint PDF. From Eq. (A1), cloud water mixing ratio is dependent on r_t and $r_{sw}(T,p)$. Since the temperature variable found in CLUBB's PDF and predictive equation set is θ_l, the appropriate variables to use to express r_c are r_t and θ_l.

As an example of integrating over r_c, the mean of r_c^{α} is found by evaluating the integral:

$$\begin{aligned}\overline{r_c^{\alpha}} &= \int_{-\infty}^{\infty}\int_{-\infty}^{\infty} r_c^{\alpha} P(r_t,\theta_l)\,\mathrm{d}\theta_l\,\mathrm{d}r_t \\ &= \sum_{i=1}^{n} \xi_{(i)} \int_{-\infty}^{\infty}\int_{-\infty}^{\infty} r_c^{\alpha} P_{NN(i)}(r_t,\theta_l)\,\mathrm{d}\theta_l\,\mathrm{d}r_t;\end{aligned} \tag{A2}$$

where $P(r_t,\theta_l)$ is the overall PDF of r_t and θ_l, $\xi_{(i)}$ is the mixture fraction (relative weight) of the ith PDF component, n is the number of PDF components (for CLUBB, $n=2$), and $P_{NN(i)}(r_t,\theta_l)$ is the ith component PDF of r_t and θ_l, which is a bivariate normal distribution. In order to evaluate the above integral, r_c must be written in terms of r_t and θ_l.

The first step in deriving an expression for r_c in terms of r_t and θ_l is to evaluate $r_{sw}(T,p)$ through a Taylor expansion around $T = T_l$ in a manner similar to Sommeria and Deardorff (1977), Lewellen and Yoh (1993), and Larson et al. (2001, 2005). Liquid water temperature, T_l, is defined as

$$T_l = T - \frac{L_v}{C_{pd}} r_c; \tag{A3}$$

where L_v is the latent heat of vaporization and C_{pd} is the specific heat of dry air at a constant

pressure. T_l is related to θ_l according to

$$\theta_l = T_l \left(\frac{p}{p_0} \right)^{-\frac{R_d}{C_{pd}}}; \tag{A4}$$

where p_0 is a reference pressure of 1.0 x 10^5 Pa. and R_d is the gas constant for dry air. Since CLUBB considers pressure to be constant (in the horizontal) at any given vertical level, $r_{sw}(T,p)$ varies only according to temperature, and the Taylor expansion is written as

$$r_{sw}(T,p) = r_{sw}(T_l,p) + \left.\frac{\partial r_{sw}}{\partial T}\right|_{T_l,p} (T - T_l) + \frac{1}{2} \left.\frac{\partial^2 r_{sw}}{\partial T^2}\right|_{T_l,p} (T - T_l)^2 + \ldots \tag{A5}$$

Substituting Eq. (A3) into Eq. (A5) and truncating the Taylor series after the first-order term, the equation becomes

$$r_{sw}(T,p) = r_{sw}(T_l,p) + \left.\frac{\partial r_{sw}}{\partial T}\right|_{T_l,p} \left(\frac{L_v}{C_{pd}} r_c \right). \tag{A6}$$

The value of $\frac{\partial r_{sw}}{\partial T}$ is derived through use of $\frac{\mathrm{d}e_{sw}}{\mathrm{d}T}$, which is given by the Clausius-Clapeyron equation, and where $e_{sw}(T)$ is the saturation vapor pressure with respect to liquid water. The rate of change of $r_{sw}(T,p)$ with respect to temperature is

$$\frac{\partial r_{sw}}{\partial T} = \frac{\partial r_{sw}}{\partial e_{sw}} \frac{\mathrm{d}e_{sw}}{\mathrm{d}T} = \frac{R_d}{R_v} \frac{L_v r_{sw}(T,p)}{R_d\, T^2} \left(1 + \frac{R_v}{R_d} r_{sw}(T,p) \right); \tag{A7}$$

where R_v is the gas constant for water vapor. Since $\frac{R_v}{R_d} r_{sw}(T,p) << 1$, the equation is approximated as

$$\left.\frac{\partial r_{sw}}{\partial T}\right|_{T_l,p} \approx \frac{R_d}{R_v} \frac{L_v r_{sw}(T_l,p)}{R_d\, T_l^2}. \tag{A8}$$

Substituting Eq. (A8) and Eq. (A1) into Eq. (A6) results in the equation

$$\begin{aligned} r_{sw}(T,p) &= r_{sw}(T_l,p) + \frac{R_d}{R_v}\frac{L_v r_{sw}(T_l,p)}{R_d\, T_l^2}\frac{L_v}{C_{pd}}\left(r_t - r_{sw}(T,p)\right) H\left(r_t - r_{sw}(T,p)\right) \\ &= r_{sw}(T_l,p) + \Lambda(T_l)\, r_{sw}(T_l,p)\left(r_t - r_{sw}(T,p)\right) H\left(r_t - r_{sw}(T,p)\right); \end{aligned} \tag{A9}$$

where

$$\Lambda(T_l) = \frac{R_d}{R_v}\left(\frac{L_v}{R_d T_l}\right)\left(\frac{L_v}{C_{pd} T_l}\right). \tag{A10}$$

The next step in deriving an appropriate equation for r_c in terms of r_t and θ_l is to subtract $r_{sw}(T,p)$ from r_t. The new equation becomes

$$\begin{aligned} &r_t - r_{sw}(T,p) \\ &\quad = r_t - r_{sw}(T_l,p) - \Lambda(T_l)\, r_{sw}(T_l,p)\left(r_t - r_{sw}(T,p)\right) H\left(r_t - r_{sw}(T,p)\right), \end{aligned} \tag{A11}$$

which can be rewritten as

$$r_t - r_{sw}(T,p) = \frac{r_t - r_{sw}(T_l,p)}{1 + \Lambda(T_l)\, r_{sw}(T_l,p)\, H\left(r_t - r_{sw}(T,p)\right)}. \tag{A12}$$

In a scenario where there is cloud water, $r_t > r_{sw}(T,p)$, and Eq. (A12) can be written as

$$r_t - r_{sw}(T,p) = \frac{r_t - r_{sw}(T_l,p)}{1 + \Lambda(T_l)\, r_{sw}(T_l,p)}. \tag{A13}$$

For simplicity, the form of the equation found in Eq. (A13) will be used to represent $r_t - r_{sw}(T,p)$ whether the air is saturated or subsaturated. In the scenario whether the air is subsaturated, Eq. (A13) is a close approximation to Eq. (A12). Eq. (A13) is used in conjunction with Eq. (A1) and substituted into the integral in Eq. (A2) to form

$$\begin{aligned} \overline{r_c^{\alpha}} = \sum_{i=1}^{n} \xi_{(i)} \int_{-\infty}^{\infty}\int_{-\infty}^{\infty} &\left(\frac{r_t - r_{sw}(T_l,p)}{1 + \Lambda(T_l)\, r_{sw}(T_l,p)}\, H\left(\frac{r_t - r_{sw}(T_l,p)}{1 + \Lambda(T_l)\, r_{sw}(T_l,p)}\right)\right)^{\alpha} \\ &\times P_{NN(i)}(r_t,\theta_l)\, \mathrm{d}\theta_l\, \mathrm{d}r_t. \end{aligned} \tag{A14}$$

The representation of r_c in Eq. (A14) still does not properly represent r_c in terms of r_t and θ_l. In order to do, a multivariate Taylor Series expansion around the mean of r_t in the ith PDF component, $\mu_{r_t(i)}$, and around the mean of T_l in the ith PDF component, $\mu_{T_l(i)}$, is utilized for Eq. (A13). This is written as

$$\begin{aligned} r_t - r_{sw}\left(T,p\right) = & \frac{\mu_{r_t(i)} - r_{sw}\left(\mu_{T_l(i)},p\right)}{1+\Lambda\left(\mu_{T_l(i)}\right) r_{sw}\left(\mu_{T_l(i)},p\right)} \\ & + \frac{\partial}{\partial r_t}\left(\frac{r_t - r_{sw}\left(T_l,p\right)}{1+\Lambda\left(T_l\right) r_{sw}\left(T_l,p\right)}\right)\Bigg|_{\mu_{T_l(i)},\mu_{r_t(i)}} \left(r_t - \mu_{r_t(i)}\right) \\ & + \frac{\partial}{\partial T_l}\left(\frac{r_t - r_{sw}\left(T_l,p\right)}{1+\Lambda\left(T_l\right) r_{sw}\left(T_l,p\right)}\right)\Bigg|_{\mu_{T_l(i)},\mu_{r_t(i)}} \left(T_l - \mu_{T_l(i)}\right) \\ & + \text{higher order terms}\ldots \end{aligned} \tag{A15}$$

The Taylor Series in Eq. (A15) is truncated after the first-order terms. The equation can finally be written in terms of θ_l through the use of Eq. (A4). The equation is now linear in terms of r_t and θ_l, and can be written more simply as

$$\begin{aligned} r_t - r_{sw}\left(T,p\right) = & \frac{\mu_{r_t(i)} - r_{sw}\left(\mu_{T_l(i)},p\right)}{1+\Lambda\left(\mu_{T_l(i)}\right) r_{sw}\left(\mu_{T_l(i)},p\right)} \\ & + c_{r_t(i)}\left(r_t - \mu_{r_t(i)}\right) - c_{\theta_l(i)}\left(\theta_l - \mu_{\theta_l(i)}\right); \end{aligned} \tag{A16}$$

where the constant coefficient with respect to r_t is written as

$$c_{r_t(i)} = \frac{1}{1+\Lambda\left(\mu_{T_l(i)}\right) r_{sw}\left(\mu_{T_l(i)},p\right)}; \tag{A17}$$

and since

$$\left(\frac{2\ L_v}{\mu_{T_l(i)} C_{pd}}\right) \frac{\left|\mu_{r_t(i)} - r_{sw}\left(\mu_{T_l(i)},p\right)\right|}{1+\Lambda\left(\mu_{T_l(i)}\right)\mu_{r_t(i)}} << 1,$$

the constant coefficient with respect to the θ_l is written as

$$c_{\theta_l(i)} = \frac{\left(1+\Lambda\left(\mu_{T_l(i)}\right)\mu_{r_t(i)}\right)\Lambda\left(\mu_{T_l(i)}\right) r_{sw}\left(\mu_{T_l(i)},p\right)}{\left(1+\Lambda\left(\mu_{T_l(i)}\right) r_{sw}\left(\mu_{T_l(i)},p\right)\right)^2} \frac{C_{pd}}{L_v}\left(\frac{p}{p_0}\right)^{R_d/C_{pd}}, \tag{A18}$$

as found in Larson et al. (2005). Eq. (A16) is used in conjunction with Eq. (A1) and is substituted into Eq. (A2), which replaces the integral found in Eq. (A14). The new equation is

$$\begin{aligned}\overline{r_c^{\alpha}} = \sum_{i=1}^{n} \xi_{(i)} \int_{-\infty}^{\infty} \int_{-\infty}^{\infty} \Bigg(& \frac{\mu_{r_t(i)} - r_{sw}\left(\mu_{T_l(i)}, p\right)}{1 + \Lambda\left(\mu_{T_l(i)}\right) r_{sw}\left(\mu_{T_l(i)}, p\right)} \\ & + c_{r_t(i)}\left(r_t - \mu_{r_t(i)}\right) - c_{\theta_l(i)}\left(\theta_l - \mu_{\theta_l(i)}\right) \Bigg)^{\alpha} \\ & \times \Bigg(H\Bigg(\frac{\mu_{r_t(i)} - r_{sw}\left(\mu_{T_l(i)}, p\right)}{1 + \Lambda\left(\mu_{T_l(i)}\right) r_{sw}\left(\mu_{T_l(i)}, p\right)} \\ & + c_{r_t(i)}\left(r_t - \mu_{r_t(i)}\right) - c_{\theta_l(i)}\left(\theta_l - \mu_{\theta_l(i)}\right) \Bigg) \Bigg)^{\alpha} \\ & \times P_{NN(i)}\left(r_t, \theta_l\right) \mathrm{d}\theta_l \; \mathrm{d}r_t. \end{aligned} \tag{A19}$$

Cloud water mixing ratio is now represented in terms of r_t and θ_l, and Eq. (A19) is now based entirely on variables found in the PDF.

A.2 PDF Transformation

It is advantageous to solve integrals involving r_c by using a change of coordinates. The multi-variate PDF for the ith component, which was originally written in terms of r_t and θ_l, undergoes translation, stretching, and rotation of the axes. The multiple integral in Eq. (A19) is transformed linearly from r_t and θ_l coordinates to new coordinates χ and η (Mellor 1977).

The linear transformation is accomplished by setting the linear forms of r_t and θ_l in Eq. (A19) equivalent to a combination of linear forms of χ and η, such that

$$c_{r_t(i)}\left(r_t - \mu_{r_t(i)}\right) = \frac{(\eta - \eta_0) + (\chi - \chi_0)}{2}, \text{ and} \tag{A20}$$

$$c_{\theta_l(i)}\left(\theta_l - \mu_{\theta_l(i)}\right) = \frac{(\eta - \eta_0) - (\chi - \chi_0)}{2}. \tag{A21}$$

Adding Eq. (A20) and Eq. (A21) results in

$$\eta - \eta_0 = c_{r_t(i)}\left(r_t - \mu_{r_t(i)}\right) + c_{\theta_l(i)}\left(\theta_l - \mu_{\theta_l(i)}\right),$$

while subtracting Eq. (A21) from Eq. (A20) produces

$$\chi - \chi_0 = c_{r_t(i)}\left(r_t - \mu_{r_t(i)}\right) - c_{\theta_l(i)}\left(\theta_l - \mu_{\theta_l(i)}\right).$$

A substitution can be made into Eq. (A19) by setting

$$\chi_0 = \frac{\mu_{r_t(i)} - r_{sw}\left(\mu_{T_l(i)}, p\right)}{1 + \Lambda\left(\mu_{T_l(i)}\right) r_{sw}\left(\mu_{T_l(i)}, p\right)},$$

and defining *extended liquid water mixing ratio*, χ, which has units of kg kg^{-1}, as

$$\begin{aligned}\chi \equiv & \frac{\mu_{r_t(i)} - r_{sw}\left(\mu_{T_l(i)}, p\right)}{1 + \Lambda\left(\mu_{T_l(i)}\right) r_{sw}\left(\mu_{T_l(i)}, p\right)} \\ & + c_{r_t(i)}\left(r_t - \mu_{r_t(i)}\right) - c_{\theta_l(i)}\left(\theta_l - \mu_{\theta_l(i)}\right).\end{aligned} \tag{A22}$$

Extended liquid water mixing ratio is a variable that is approximately equal to r_c when $\chi > 0$, but is allowed to be negative by a factor. The ith component mean value of χ can be found be integrating the product of Eq. (A22) and $P_{(i)}\left(r_t, \theta_l\right)$ over r_t and θ_l, resulting in

$$\mu_{\chi(i)} = \chi_0 = \frac{\mu_{r_t(i)} - r_{sw}\left(\mu_{T_l(i)}, p\right)}{1 + \Lambda\left(\mu_{T_l(i)}\right) r_{sw}\left(\mu_{T_l(i)}, p\right)}. \tag{A23}$$

The variable η is orthogonal to χ. The ith component mean value of η can be found in the same manner as the ith component mean value of χ, and simply has the value $\mu_{\eta(i)} = \eta_0$. As it turns out, this value is trivial, since it does not factor in any of the model equations.

The value is simply set to

$$\mu_{\eta(i)} = 0.$$

The linear transformations listed in Eq. (A20) and Eq. (A21) can now be restated in terms of PDF parameters, such that

$$c_{r_t(i)}\left(r_t - \mu_{r_t(i)}\right) = \frac{\left(\eta - \mu_{\eta(i)}\right) + \left(\chi - \mu_{\chi(i)}\right)}{2}, \text{ and} \tag{A24}$$

$$c_{\theta_l(i)}\left(\theta_l - \mu_{\theta_l(i)}\right) = \frac{\left(\eta - \mu_{\eta(i)}\right) - \left(\chi - \mu_{\chi(i)}\right)}{2}. \tag{A25}$$

The relationships in Eq. (A24) and Eq. (A25) allow the calculation of more PDF parameters by integrating over the product of a function and the PDF. The ith component variance of χ is denoted $\sigma^2_{\chi(i)}$, where

$$\sigma^2_{\chi(i)} = c^2_{r_t(i)}\sigma^2_{r_t(i)} - 2\rho_{r_t,\theta_l(i)}c_{r_t(i)}\sigma_{r_t(i)}c_{\theta_l(i)}\sigma_{\theta_l(i)} + c^2_{\theta_l(i)}\sigma^2_{\theta_l(i)}, \tag{A26}$$

and the ith component variance of η is denoted $\sigma^2_{\eta(i)}$, where

$$\sigma^2_{\eta(i)} = c^2_{r_t(i)}\sigma^2_{r_t(i)} + 2\rho_{r_t,\theta_l(i)}c_{r_t(i)}\sigma_{r_t(i)}c_{\theta_l(i)}\sigma_{\theta_l(i)} + c^2_{\theta_l(i)}\sigma^2_{\theta_l(i)}. \tag{A27}$$

The correlations between χ, η, and other variables are found in the same manner. The ith component correlation between χ and η is denoted $\rho_{\chi,\eta(i)}$, and is given by the equation

$$\begin{aligned}\rho_{\chi,\eta(i)} &= \frac{c^2_{r_t(i)}\sigma^2_{r_t(i)} - c^2_{\theta_l(i)}\sigma^2_{\theta_l(i)}}{\sigma_{\chi(i)}\sigma_{\eta(i)}} \\ &= \frac{c^2_{r_t(i)}\sigma^2_{r_t(i)} - c^2_{\theta_l(i)}\sigma^2_{\theta_l(i)}}{\sqrt{\left(c^2_{r_t(i)}\sigma^2_{r_t(i)} + c^2_{\theta_l(i)}\sigma^2_{\theta_l(i)}\right)^2 - 4\rho^2_{r_t,\theta_l(i)}c^2_{r_t(i)}\sigma^2_{r_t(i)}c^2_{\theta_l(i)}\sigma^2_{\theta_l(i)}}}.\end{aligned} \tag{A28}$$

The ith component correlation between χ and a PDF-variable x is denoted $\rho_{\chi,x(i)}$ and given

by the equation

$$\begin{aligned}\rho_{\chi,x(i)} &= \frac{\rho_{r_t,x(i)}c_{r_t(i)}\sigma_{r_t(i)} - \rho_{\theta_l,x(i)}c_{\theta_l(i)}\sigma_{\theta_l(i)}}{\sigma_{\chi(i)}} \\ &= \frac{\rho_{r_t,x(i)}c_{r_t(i)}\sigma_{r_t(i)} - \rho_{\theta_l,x(i)}c_{\theta_l(i)}\sigma_{\theta_l(i)}}{\sqrt{c^2_{r_t(i)}\sigma^2_{r_t(i)} - 2\rho_{r_t,\theta_l(i)}c_{r_t(i)}\sigma_{r_t(i)}c_{\theta_l(i)}\sigma_{\theta_l(i)} + c^2_{\theta_l(i)}\sigma^2_{\theta_l(i)}}}.\end{aligned} \tag{A29}$$

Likewise, the ith component correlation between η and PDF-variable x is denoted $\rho_{\eta,x(i)}$ and is given by the equation

$$\begin{aligned}\rho_{\eta,x(i)} &= \frac{\rho_{r_t,x(i)}c_{r_t(i)}\sigma_{r_t(i)} + \rho_{\theta_l,x(i)}c_{\theta_l(i)}\sigma_{\theta_l(i)}}{\sigma_{\eta(i)}} \\ &= \frac{\rho_{r_t,x(i)}c_{r_t(i)}\sigma_{r_t(i)} + \rho_{\theta_l,x(i)}c_{\theta_l(i)}\sigma_{\theta_l(i)}}{\sqrt{c^2_{r_t(i)}\sigma^2_{r_t(i)} + 2\rho_{r_t,\theta_l(i)}c_{r_t(i)}\sigma_{r_t(i)}c_{\theta_l(i)}\sigma_{\theta_l(i)} + c^2_{\theta_l(i)}\sigma^2_{\theta_l(i)}}}.\end{aligned} \tag{A30}$$

The equations for the correlation between χ or η and x, given by Eq. (A29) and Eq. (A30) respectively, are the same whether the individual marginal of x is distributed normally or lognormally. Additionally, in the scenarios where x is distributed lognormally, the correlation between χ and $\ln x$, denoted $\tilde{\rho}_{\chi,x(i)}$, and the correlation between η and $\ln x$, denoted $\tilde{\rho}_{\eta,x(i)}$, can be found by using the above equations and replacing $\rho_{r_t,x(i)}$ and $\rho_{\theta_l,x(i)}$ with $\tilde{\rho}_{r_t,x(i)}$ and $\tilde{\rho}_{\theta_l,x(i)}$, respectively.

The multivariate PDF can now be rewritten to use χ and η instead of r_t and θ_l by substituting Eq. (A23) through Eq. (A30) into the multivariate PDF involving r_t and θ_l. The result for a PDF of m variables is

$$P_{(i)}\left(r_t, \theta_l, \ldots, x_m\right) = 2c_{r_t(i)}c_{\theta_l(i)}P_{(i)}\left(\chi, \eta, \ldots, x_m\right). \tag{A31}$$

Besides the transformation for r_t and θ_l to χ and η, all other variables in the PDF remain the same. The individual marginal for χ and η is a normal distribution for the ith PDF component.

The change of coordinates from r_t and θ_l to χ and η requires re-evaluation of the limits

of integration and the integrand. The limits of integration were $-\infty$ to ∞ for both r_t and θ_l, and they remain that way for both χ and η. Due to the change of variables, the integrand needs to be multiplied by the absolute value of the Jacobian, $|J(\chi, \eta, \ldots, x_m)|$, which is given by

$$|J(\chi, \eta, \ldots, x_m)| = \frac{1}{2c_{r_t(i)}c_{\theta_l(i)}}. \tag{A32}$$

The new form of Eq. (A19) is found by substitution using χ as found in Eq. (A22), and by transforming the PDF and variables of integration according to Eq. (A31) and Eq. (A32). This results in the equation

$$\overline{r_c^{\alpha}} = \sum_{i=1}^{n} \xi_{(i)} \int_{-\infty}^{\infty} \int_{-\infty}^{\infty} \chi^{\alpha} \left(H(\chi)\right)^{\alpha} P_{NN(i)}(\chi, \eta)\, \mathrm{d}\eta\, \mathrm{d}\chi. \tag{A33}$$

Integrating over η reduces the PDF and the integral to univariate form, while the Heaviside step function has the effect of changing the lower limit of integration for χ, such that

$$\overline{r_c^{\alpha}} = \sum_{i=1}^{n} \xi_{(i)} \int_{0}^{\infty} \chi^{\alpha} P_{N(i)}(\chi)\, \mathrm{d}\chi; \tag{A34}$$

where $P_{N(i)}(\chi)$ is the ith component PDF of χ, which is a normal distribution. The integral is evaluated, resulting in the equation for $\overline{r_c^{\alpha}}$:

$$\overline{r_c^{\alpha}} = \sum_{i=1}^{n} \xi_{(i)} \frac{1}{\sqrt{2\pi}} \sigma_{\chi(i)}^{\alpha} \exp\left\{-\frac{1}{4}\frac{\mu_{\chi(i)}^2}{\sigma_{\chi(i)}^2}\right\} \Gamma(\alpha+1)\, \mathrm{D}_{-(\alpha+1)}\left(-\frac{\mu_{\chi(i)}}{\sigma_{\chi(i)}}\right); \tag{A35}$$

where $\Gamma(x)$ is the gamma function and $\mathrm{D}_{\nu}(x)$ is the parabolic cylinder function of order ν. When $\alpha = 1$, the equation for mean cloud water mixing ratio, $\overline{r_c}$, is produced:

$$\overline{r_c} = \sum_{i=1}^{n} \xi_{(i)} \left(\frac{1}{\sqrt{2\pi}} \sigma_{\chi(i)} \exp\left\{-\frac{1}{2}\frac{\mu_{\chi(i)}^2}{\sigma_{\chi(i)}^2}\right\} + \frac{1}{2}\mu_{\chi(i)} \mathrm{erfc}\left(-\frac{\mu_{\chi(i)}}{\sqrt{2}\,\sigma_{\chi(i)}}\right)\right); \tag{A36}$$

where $\mathrm{erfc}(x)$ is the complimentary error function, which is given by $\mathrm{erfc}(x) = 1 - \mathrm{erf}(x)$,

where erf (x) is the error function.

A.3 Expressing supersaturation in terms of the PDF

Another variable that can be handled in a manner similar to r_c is saturation ratio. Some microphysical process equations, such as an equation for evaporation rate, involve supersaturation, S. Evaporation occurs where the air is subsaturated on the subgrid domain. In order to integrate over an equation involving supersaturation, it must be expressed in terms of variables that are part of the joint PDF, just like integrals involving cloud water mixing ratio. Supersaturation needs to be written as a function of r_t and θ_l. Supersaturation is defined as a function of e and $e_{sw}(T)$ such that

$$S \equiv \frac{e}{e_{sw}(T)} - 1. \tag{A37}$$

Where the value of S is positive, the air is supersaturated, and where the value of S is negative, the air is subsaturated. Water vapor mixing ratio, r_v, can be written in terms of e by

$$r_v = \frac{R_d}{R_v}\left(\frac{e}{p-e}\right). \tag{A38}$$

The equivalent equation for $r_{sw}(T,p)$ is

$$r_{sw}(T,p) = \frac{R_d}{R_v}\left(\frac{e_{sw}(T)}{p-e_{sw}(T)}\right). \tag{A39}$$

This can be rewritten in terms of water vapor mixing ratio, r_v, and saturation mixing ratio with respect to liquid, such that

$$S = \left(\frac{\frac{R_d}{R_v}}{\frac{R_d}{R_v}+r_v}\right)\left(\frac{r_v - r_{sw}(T,p)}{r_{sw}(T,p)}\right). \tag{A40}$$

Since $r_v << R_d/R_v$, S can be approximated as

$$S = \frac{r_v - r_{sw}\left(T, p\right)}{r_{sw}\left(T, p\right)}. \tag{A41}$$

Evaporation only occurs when $S < 0$, and the air is subsaturated. In this scenario $r_v = r_t$, $T = T_l$, and $\theta = \theta_l$. The equation for S can be rewritten as

$$S = \frac{r_t - r_{sw}\left(T_l, p\right)}{r_{sw}\left(T_l, p\right)}. \tag{A42}$$

Multiplying both the numerator and the denominator by a factor results in the equation

$$S = \left(\frac{1 + \Lambda\left(T_l\right) r_{sw}\left(T_l, p\right)}{r_{sw}\left(T_l, p\right)}\right)\left(\frac{r_t - r_{sw}\left(T_l, p\right)}{1 + \Lambda\left(T_l\right) r_{sw}\left(T_l, p\right)}\right). \tag{A43}$$

The equation for S in now terms of $\left(r_t - r_{sw}\left(T_l, p\right)\right) / \left(1 + \Lambda\left(T_l\right) r_{sw}\left(T_l, p\right)\right)$. This is used to rewrite S in terms of χ within an integral. For example, the mean value of $S^\alpha \left(H\left(-S\right)\right)^\alpha$ is calculated by

$$\overline{S^\alpha \left(H\left(-S\right)\right)^\alpha} = \int_{-\infty}^{\infty}\int_{-\infty}^{\infty} S^\alpha \left(H\left(-S\right)\right)^\alpha P\left(r_t, \theta_l\right) \mathrm{d}r_t \, \mathrm{d}\theta_l. \tag{A44}$$

Supersaturation is approximated as

$$S \approx \left(\frac{1 + \Lambda\left(\overline{T_l}\right) r_{sw}\left(\overline{T_l}, p\right)}{r_{sw}\left(\overline{T_l}, p\right)}\right)\left(\frac{r_t - r_{sw}\left(T_l, p\right)}{1 + \Lambda\left(T_l\right) r_{sw}\left(T_l, p\right)}\right). \tag{A45}$$

Substituting Eq. (A45) into the integral results in

$$\begin{aligned}
&\overline{S^{\alpha}\left(H\left(-S\right)\right)^{\alpha}} \\
&= \left(\frac{1+\Lambda\left(\overline{T_l}\right) r_{sw}\left(\overline{T_l},p\right)}{r_{sw}\left(\overline{T_l},p\right)}\right)^{\alpha} \\
&\quad \times \int_{-\infty}^{\infty}\int_{-\infty}^{\infty} \left(\frac{r_t - r_{sw}\left(T_l,p\right)}{1+\Lambda\left(T_l\right) r_{sw}\left(T_l,p\right)}\right)^{\alpha} \\
&\qquad \times \left(H\left(-\left(\frac{1+\Lambda\left(\overline{T_l}\right) r_{sw}\left(\overline{T_l},p\right)}{r_{sw}\left(\overline{T_l},p\right)}\right)\left(\frac{r_t - r_{sw}\left(T_l,p\right)}{1+\Lambda\left(T_l\right) r_{sw}\left(T_l,p\right)}\right)\right)\right)^{\alpha} \\
&\qquad \times P\left(r_t,\theta_l\right) \mathrm{d}r_t \, \mathrm{d}\theta_l.
\end{aligned} \tag{A46}$$

The integral in Eq. (A46) is very similar to the integral found in Eq. (A14). Ultimately, the PDF is split into components and the PDF transformation changes coordinates from r_t and θ_l to χ and η. The relationship between S and χ within each PDF component is given by

$$S = \left(\frac{1+\Lambda\left(\overline{T_l}\right) r_{sw}\left(\overline{T_l},p\right)}{r_{sw}\left(\overline{T_l},p\right)}\right)\chi. \tag{A47}$$

The resulting integral, after η is integrated out of the PDF, is reduced to

$$\overline{S^{\alpha}\left(H\left(-S\right)\right)^{\alpha}} = \left(\frac{1+\Lambda\left(\overline{T_l}\right) r_{sw}\left(\overline{T_l},p\right)}{r_{sw}\left(\overline{T_l},p\right)}\right)^{\alpha} \sum_{i=1}^{n} \xi_{(i)} \int_{-\infty}^{\infty} \chi^{\alpha}\left(H\left(-\chi\right)\right)^{\alpha} P_{N(i)}\left(\chi\right) \mathrm{d}\chi, \tag{A48}$$

and the solution is

$$\begin{aligned}
\overline{S^{\alpha}\left(H\left(-S\right)\right)^{\alpha}} &= \left(\frac{1+\Lambda\left(\overline{T_l}\right) r_{sw}\left(\overline{T_l},p\right)}{r_{sw}\left(\overline{T_l},p\right)}\right)^{\alpha} \\
&\quad \times \sum_{i=1}^{n} \xi_{(i)} \frac{1}{\sqrt{2\pi}} \left(-\sigma_{\chi(i)}\right)^{\alpha} \exp\left\{-\frac{1}{4}\frac{\mu_{\chi(i)}^2}{\sigma_{\chi(i)}^2}\right\} \Gamma\left(\alpha+1\right) \mathrm{D}_{-(\alpha+1)}\left(\frac{\mu_{\chi(i)}}{\sigma_{\chi(i)}}\right),
\end{aligned} \tag{A49}$$

where $(-1)^{\alpha}$ must not be a complex number.

Appendix B: Back-Solving PDF Component Correlations

In Section 1.5, mean microphysics process rates were calculated either by using the analytical integration of a local microphysics scheme or by using SILHS to sample the PDF in order to drive a local microphysics scheme. Both methods require information on the PDF component correlations. These correlations can be back-solved when given the overall (grid-box) covariance of the necessary variables.

B.1 PDF component correlation of a binormal variate and a hydrometeor

The PDF *component* correlation of a binormal variate (using r_t as an example) and a hydrometeor can be back-solved when their covariance, $\overline{r_t' h'}$, is provided. Their covariance can be written in terms of PDF parameters by integrating over the PDF, such that

$$\overline{r_t' h'} = \int_{-\infty}^{\infty} \int_{0}^{\infty} \left(r_t - \overline{r_t}\right) \left(h - \overline{h}\right) P\left(r_t, h\right) \mathrm{d}h \, \mathrm{d}r_t, \tag{B1}$$

where $P\left(r_t, h\right)$ is the bivariate marginal PDF of r_t and h. This equation can be rewritten as

$$\begin{aligned} \overline{r_t' h'} = \sum_{i=1}^{n} \xi_{(i)} \int_{-\infty}^{\infty} \int_{0}^{\infty} \left(r_t - \overline{r_t}\right) \left(h - \overline{h}\right) \Big(& f_{p(i)} P_{NL(i)}\left(r_t, h\right) \\ & + \left(1 - f_{p(i)}\right) P_{N(i)}\left(r_t\right) \delta\left(h\right) \Big) \mathrm{d}h \, \mathrm{d}r_t, \end{aligned} \tag{B2}$$

where $P_{NL(i)}\left(r_t, h\right)$ is the ith component bivariate PDF involving one normal variate and one lognormal variate, and where $P_{N(i)}\left(r_t\right)$ is a normal distribution in the ith component.

This equation is integrated and reduced, resulting in

$$\overline{r_t' h'} = \sum_{i=1}^{n} \xi_{(i)} f_{p(i)} \left(\mu_{r_t(i)} - \overline{r_t} + \tilde{\rho}_{r_t,h(i)} \sigma_{r_t(i)} \tilde{\sigma}_{h(i)} \right) \mu_{h(i)}, \tag{B3}$$

where $\mu_{r_t(i)}$ and $\sigma_{r_t(i)}$ are the mean and standard deviation, respectively, of r_t in the ith PDF component.

The variable that needs to be solved for is $\tilde{\rho}_{r_t,h(i)}$, which is the in-precipitation correlation of r_t and $\ln h$ in the ith PDF component. This is the normal-space correlation that is required for use in the microphysics. It is related to the ith component in-precipitation correlation of r_t and h, $\rho_{r_t,h(i)}$, by

$$\rho_{r_t,h(i)} = \tilde{\rho}_{r_t,h(i)} \tilde{\sigma}_{h(i)} \frac{\mu_{h(i)}}{\sigma_{h(i)}}. \tag{B4}$$

The covariance $\overline{r_t' h'}$ given by Eq. (B3) can be written in terms of CLUBB's two-component PDF ($n = 2$) as

$$\begin{aligned} \overline{r_t' h'} = & \xi_{(1)} f_{p(1)} \left(\mu_{r_t(1)} - \overline{r_t} + \tilde{\rho}_{r_t,h(1)} \sigma_{r_t(1)} \tilde{\sigma}_{h(1)} \right) \mu_{h(1)} \\ & + \xi_{(2)} f_{p(2)} \left(\mu_{r_t(2)} - \overline{r_t} + \tilde{\rho}_{r_t,h(2)} \sigma_{r_t(2)} \tilde{\sigma}_{h(2)} \right) \mu_{h(2)}. \end{aligned} \tag{B5}$$

The overall covariance is provided, so the component correlation can be back-solved by setting $\tilde{\rho}_{r_t,h(1)} = \tilde{\rho}_{r_t,h(2)} \, (= \tilde{\rho}_{r_t,h})$. The result is

$$\tilde{\rho}_{r_t,h} = \frac{\overline{r_t' h'} - \xi_{(1)} f_{p(1)} \left(\mu_{r_t(1)} - \overline{r_t} \right) \mu_{h(1)} - \xi_{(2)} f_{p(2)} \left(\mu_{r_t(2)} - \overline{r_t} \right) \mu_{h(2)}}{\xi_{(1)} f_{p(1)} \sigma_{r_t(1)} \tilde{\sigma}_{h(1)} \mu_{h(1)} + \xi_{(2)} f_{p(2)} \sigma_{r_t(2)} \tilde{\sigma}_{h(2)} \mu_{h(2)}}, \tag{B6}$$

where $-1 \leq \tilde{\rho}_{r_t,h} \leq 1$.

The equation for $\overline{r_t' h'}$ given in Eq. (B5) is for a fully-varying PDF in both components ($\sigma_{r_t(i)} > 0$ and $\sigma_{h(i)} > 0$). A variable may have a constant value in a PDF sub-component. When this happens, the PDF of the constant variable is a delta function at the ith sub-component mean. When $\sigma_{r_t(i)} > 0$ and $\sigma_{h(i)} = 0$, r_t varies in ith component but h is constant within precipitation. The PDF $P_{NL(i)}(r_t, h)$ becomes $P_{N(i)}(r_t) \, \delta\left(h - \mu_{h(i)}\right)$. There

also may be situations where $\sigma_{r_t(i)} = 0$ but $\sigma_{h(i)} > 0$, or even where $\sigma_{r_t(i)} = 0$ and $\sigma_{h(i)} = 0$.

When $\sigma_{r_t(1)}\sigma_{h(1)} > 0$ but $\sigma_{r_t(2)}\sigma_{h(2)} = 0$, the equation for $\overline{r_t' h'}$ is written as

$$\overline{r_t' h'} = \xi_{(1)} f_{p(1)} \left(\mu_{r_t(1)} - \overline{r_t} + \tilde{\rho}_{r_t,h(1)} \sigma_{r_t(1)} \tilde{\sigma}_{h(1)} \right) \mu_{h(1)} + \xi_{(2)} f_{p(2)} \left(\mu_{r_t(2)} - \overline{r_t} \right) \mu_{h(2)}. \tag{B7}$$

The above equation can be rewritten to solve for $\tilde{\rho}_{r_t,h(1)}$, such that

$$\tilde{\rho}_{r_t,h(1)} = \frac{\overline{r_t' h'} - \xi_{(1)} f_{p(1)} \left(\mu_{r_t(1)} - \overline{r_t} \right) \mu_{h(1)} - \xi_{(2)} f_{p(2)} \left(\mu_{r_t(2)} - \overline{r_t} \right) \mu_{h(2)}}{\xi_{(1)} f_{p(1)} \sigma_{r_t(1)} \tilde{\sigma}_{h(1)} \mu_{h(1)}}, \tag{B8}$$

while $\tilde{\rho}_{r_t,h(2)}$ is undefined and irrelevant to the microphysics. When $\sigma_{r_t(1)}\sigma_{h(1)} = 0$ but $\sigma_{r_t(2)}\sigma_{h(2)} > 0$, the equation for $\overline{r_t' h'}$ is analogous to Eq. (B7). An equation analogous to Eq. (B8) solves for $\tilde{\rho}_{r_t,h(2)}$, while $\tilde{\rho}_{r_t,h(1)}$ is undefined. In a scenario where $\sigma_{r_t(1)}\sigma_{h(1)} = 0$ and $\sigma_{r_t(2)}\sigma_{h(2)} = 0$, the equation for $\overline{r_t' h'}$ is

$$\overline{r_t' h'} = \xi_{(1)} f_{p(1)} \left(\mu_{r_t(1)} - \overline{r_t} \right) \mu_{h(1)} + \xi_{(2)} f_{p(2)} \left(\mu_{r_t(2)} - \overline{r_t} \right) \mu_{h(2)}. \tag{B9}$$

When this is the case, both $\tilde{\rho}_{r_t,h(1)}$ and $\tilde{\rho}_{r_t,h(2)}$ are undefined.

This method of back-solving for the component correlations was used to calculate the PDF component correlations of r_t and r_r, r_t and N_r, θ_l and r_r, and θ_l and N_r. These were the only correlations of this type that were necessary to produce the microphysics process rates used in the comparison.

B.2 PDF component correlation of two hydrometeors

The PDF *component* correlation of two hydrometeors, h_x and h_y, can be back-solved when their covariance, $\overline{h_x' h_y'}$, is provided. Their covariance can be written in terms of PDF param-

eters by integrating over the PDF, such that

$$\overline{h'_x h'_y} = \int_0^\infty \int_0^\infty \left(h_x - \overline{h_x}\right)\left(h_y - \overline{h_y}\right) P\left(h_x, h_y\right) \mathrm{d}h_y \, \mathrm{d}h_x, \tag{B10}$$

where $P\left(h_x, h_y\right)$ is the bivariate marginal PDF of h_x and h_y. This equation can be rewritten as

$$\begin{aligned}\overline{h'_x h'_y} = \sum_{i=1}^{n} \xi_{(i)} \int_0^\infty \int_0^\infty \left(h_x - \overline{h_x}\right)\left(h_x - \overline{h_y}\right)\Big(f_{p(i)} P_{LL(i)}\left(h_x, h_y\right) \\ + \left(1 - f_{p(i)}\right)\, \delta\left(h_x\right)\, \delta\left(h_y\right)\Big) \mathrm{d}h_y \, \mathrm{d}h_x,\end{aligned} \tag{B11}$$

where $P_{LL(i)}\left(h_x, h_y\right)$ is the ith component bivariate PDF involving two lognormal variates.

This equation is integrated and reduced, resulting in

$$\overline{h'_x h'_y} = -\overline{h_x}\ \overline{h_y} + \sum_{i=1}^{n} \xi_{(i)} f_{p(i)} \left(\mu_{h_x(i)} \mu_{h_y(i)} + \rho_{h_x, h_y(i)} \sigma_{h_x(i)} \sigma_{h_y(i)}\right), \tag{B12}$$

where $\rho_{h_x, h_y(i)}$ is the in-precipitation correlation of h_x and h_y in the ith PDF component. When the PDF is fully-varying in both components ($\sigma_{h_x(i)} > 0$ and $\sigma_{h_y(i)} > 0$), the covariance $\overline{h'_x h'_y}$ given by Eq. (B12) can be written in terms of CLUBB's two-component PDF as

$$\begin{aligned}\overline{h'_x h'_y} = &\xi_{(1)} f_{p(1)} \left(\mu_{h_x(1)} \mu_{h_y(1)} + \rho_{h_x, h_y(1)} \sigma_{h_x(1)} \sigma_{h_y(1)}\right) \\ &+ \xi_{(2)} f_{p(2)} \left(\mu_{h_x(2)} \mu_{h_y(2)} + \rho_{h_x, h_y(2)} \sigma_{h_x(2)} \sigma_{h_y(2)}\right) - \overline{h_x}\ \overline{h_y}.\end{aligned} \tag{B13}$$

The overall covariance is provided, so the component correlation is solved by setting $\rho_{h_x, h_y(1)} = \rho_{h_x, h_y(2)} \left(= \rho_{h_x, h_y}\right)$. The result is

$$\rho_{h_x, h_y} = \frac{\overline{h'_x h'_y} + \overline{h_x}\ \overline{h_y} - \xi_{(1)} f_{p(1)} \mu_{h_x(1)} \mu_{h_y(1)} - \xi_{(2)} f_{p(2)} \mu_{h_x(2)} \mu_{h_y(2)}}{\xi_{(1)} f_{p(1)} \sigma_{h_x(1)} \sigma_{h_y(1)} + \xi_{(2)} f_{p(2)} \sigma_{h_x(2)} \sigma_{h_y(2)}}. \tag{B14}$$

When $\sigma_{h_x(1)}\sigma_{h_y(1)} > 0$ but $\sigma_{h_x(2)}\sigma_{h_y(2)} = 0$, the equation for $\overline{h'_x h'_y}$ is written as

$$\overline{h'_x h'_y} = \xi_{(1)} f_{p(1)} \left(\mu_{h_x(1)} \mu_{h_y(1)} + \rho_{h_x,h_y(1)} \sigma_{h_x(1)} \sigma_{h_y(1)} \right) + \xi_{(2)} f_{p(2)} \mu_{h_x(2)} \mu_{h_y(2)} - \overline{h_x}\ \overline{h_y}. \quad \text{(B15)}$$

The above equation can be rewritten to solve for $\rho_{h_x,h_y(1)}$, such that

$$\rho_{h_x,h_y(1)} = \frac{\overline{h'_x h'_y} + \overline{h_x}\ \overline{h_y} - \xi_{(1)} f_{p(1)} \mu_{h_x(1)} \mu_{h_y(1)} - \xi_{(2)} f_{p(2)} \mu_{h_x(2)} \mu_{h_y(2)}}{\xi_{(1)} f_{p(1)} \sigma_{h_x(1)} \sigma_{h_y(1)}}, \quad \text{(B16)}$$

while $\rho_{h_x,h_y(2)}$ is undefined and irrelevant to the microphysics. When $\sigma_{h_x(1)}\sigma_{h_y(1)} = 0$ but $\sigma_{h_x(2)}\sigma_{h_y(2)} > 0$, the equation for $\overline{h'_x h'_y}$ is analogous to Eq. (B15). An equation analogous to Eq. (B16) solves for $\rho_{h_x,h_y(2)}$, while $\rho_{h_x,h_y(1)}$ is undefined. In a scenario where $\sigma_{h_x(1)}\sigma_{h_y(1)} = 0$ and $\sigma_{h_x(2)}\sigma_{h_y(2)} = 0$, the equation for $\overline{h'_x h'_y}$ is

$$\overline{h'_x h'_y} = \xi_{(1)} f_{p(1)} \mu_{h_x(1)} \mu_{h_y(1)} + \xi_{(2)} f_{p(2)} \mu_{h_x(2)} \mu_{h_y(2)} - \overline{h_x}\ \overline{h_y}. \quad \text{(B17)}$$

When this is the case, both $\rho_{h_x,h_y(1)}$ and $\rho_{h_x,h_y(2)}$ are undefined.

The variable that needs to be solved for is $\tilde{\rho}_{h_x,h_y(i)}$, which is the in-precipitation correlation of $\ln h_x$ and $\ln h_y$ in the ith PDF component. This is the normal-space correlation that is required for use in the microphysics, and it is given by

$$\tilde{\rho}_{h_x,h_y(i)} = \frac{\ln\left(1 + \rho_{h_x,h_y(i)} \dfrac{\sigma_{h_x(i)} \sigma_{h_y(i)}}{\mu_{h_x(i)} \mu_{h_y(i)}}\right)}{\tilde{\sigma}_{h_x(i)} \tilde{\sigma}_{h_y(i)}}, \quad \text{(B18)}$$

where $-1 \leq \tilde{\rho}_{h_x,h_y(i)} \leq 1$.

This method of back-solving for the component correlations was used to calculate the PDF component correlation of r_r and N_r. This was the only correlation of this type that was necessary to produce the microphysics process rates used in the comparison.

Appendix C: Modified Analytically Upscaled Microphysics Equations

The analytically upscaled (to grid-box size) form of the Khairoutdinov and Kogan (2000, hereafter KK) microphysics equations were first derived in Larson and Griffin (2013). KK is a warm scheme that predicts r_r and N_r. It contains equations for the warm process rates of accretion, autoconversion, and evaporation, as well rain drop mean volume radius, that are written as power laws of two-or-three variables. The modifications to the PDF in Section 1.2 require modifications to the analytically upscaled microphysics equations. The upscaled microphysics calculates the grid-box mean values of microphysics process rates by integrating over the product of the microphysics function and the PDF.

C.1 Accretion rate

The KK accretion rate of r_r is of the form

$$\left.\frac{\partial r_r}{\partial t}\right|_{\text{accr}} = C_{\text{accr}}\, r_c^{\alpha}\, r_r^{\beta}, \tag{C1}$$

where $C_{\text{accr}} = 67$, $\alpha = 1.15$, and $\beta = 1.15$. Upscaling is accomplished by integrating over Eq. (C1), and in the process, using Eq. (1.3) as a substitution. This produces the following equation for mean accretion rate

$$\begin{aligned}\overline{\left.\frac{\partial r_r}{\partial t}\right|_{\text{accr}}} &= C_{\text{accr}} \sum_{i=1}^{n} \xi_{(i)} \text{ACCR}_{(i)} \\ &= C_{\text{accr}} \sum_{i=1}^{n} \xi_{(i)} \int_{-\infty}^{\infty} \int_{0}^{\infty} \chi^{\alpha} \left(H\left(\chi\right)\right)^{\alpha} r_r^{\beta} P_{(i)}\left(\chi, r_r\right) \mathrm{d}r_r \, \mathrm{d}\chi,\end{aligned} \tag{C2}$$

where $P_{(i)}\left(\chi, r_r\right)$ is the bivariate marginal PDF of χ and r_r in the ith PDF component.

Since $\alpha > 0$, $\mathrm{ACCR}_{(i)}$ can be rewritten

$$\mathrm{ACCR}_{(i)} = \int_0^\infty \int_0^\infty \chi^\alpha r_r^\beta \left(f_{p(i)} P_{NL(i)}\left(\chi, r_r\right) + \left(1 - f_{p(i)}\right) P_{N(i)}\left(\chi\right) \delta\left(r_r\right)\right) \mathrm{d}r_r \, \mathrm{d}\chi, \tag{C3}$$

where $P_{NL(i)}\left(\chi, r_r\right)$ is the ith component bivariate PDF involving one normal variate and one lognormal variate, and where $P_{N(i)}\left(\chi\right)$ is a normal distribution in the ith PDF component. This equation is integrated, solving for $\mathrm{ACCR}_{(i)}$,

$$\mathrm{ACCR}_{(i)} = f_{p(i)} \frac{1}{\sqrt{2\pi}} \sigma_{\chi(i)}^\alpha \exp\left\{ \tilde{\mu}_{r_r(i)}\beta + \frac{1}{2}\tilde{\sigma}_{r_r(i)}^2 \beta^2 - \frac{1}{4}\varsigma^2 \right\} \Gamma\left(\alpha + 1\right) D_{-(\alpha+1)}\left(-\varsigma\right), \tag{C4}$$

where $D_\nu\left(x\right)$ is the parabolic cylinder function of order ν, and where ς is given by

$$\varsigma = \frac{\mu_{\chi(i)}}{\sigma_{\chi(i)}} + \tilde{\rho}_{\chi, r_r(i)} \tilde{\sigma}_{r_r(i)} \beta.$$

The in-precipitation mean of $\ln r_r$ in the ith PDF component is $\tilde{\mu}_{r_r(i)}$, and it is given by

$$\tilde{\mu}_{r_r(i)} = \ln\left(\mu_{r_r(i)} \left(1 + \frac{\sigma_{r_r(i)}^2}{\mu_{r_r(i)}^2} \right)^{-\frac{1}{2}} \right), \tag{C5}$$

where $\mu_{r_r(i)}$ and $\sigma_{r_r(i)}$ are the in-precipitation mean and in-precipitation standard deviation, respectively, of r_r in the ith PDF component. The in-precipitation standard deviation of $\ln r_r$ in the ith PDF component is $\tilde{\sigma}_{r_r(i)}$, and it is given by

$$\tilde{\sigma}_{r_r(i)} = \sqrt{\ln\left(1 + \frac{\sigma_{r_r(i)}^2}{\mu_{r_r(i)}^2} \right)}. \tag{C6}$$

The in-precipitation correlation of χ and $\ln r_r$ in the ith PDF component is $\tilde{\rho}_{\chi, r_r(i)}$, and it is given by

$$\tilde{\rho}_{\chi, r_r(i)} = \frac{\rho_{\chi, r_r(i)}}{\tilde{\sigma}_{r_r(i)}} \frac{\sigma_{r_r(i)}}{\mu_{r_r(i)}}, \tag{C7}$$

where $\rho_{\chi,r_r(i)}$ is the in-precipitation correlation of χ and r_r in the ith PDF component.

The evaluated integral for $\mathrm{ACCR}_{(i)}$ given in Eq. (C4) is for a fully-varying PDF in the ith component ($\sigma_{\chi(i)} > 0$ and $\sigma_{r_r(i)} > 0$). There are times when a variable may have a constant value in a PDF sub-component. When this happens, the PDF of the constant variable is a delta function at the ith PDF sub-component mean. When $\sigma_{\chi(i)} > 0$ and $\sigma_{r_r(i)} = 0$, χ varies in ith component but r_r is constant within precipitation. The PDF $P_{NL(i)}(\chi, r_r)$ becomes $P_{N(i)}(\chi)\ \delta\left(r_r - \mu_{r_r(i)}\right)$. The integral is solved and the equation for $\mathrm{ACCR}_{(i)}$ becomes

$$\mathrm{ACCR}_{(i)} = f_{p(i)} \frac{1}{\sqrt{2\pi}} \sigma_{\chi(i)}^{\alpha} \mu_{r_r(i)}^{\beta} \exp\left\{ -\frac{1}{4} \frac{\mu_{\chi(i)}^2}{\sigma_{\chi(i)}^2} \right\} \Gamma(\alpha + 1)\, D_{-(\alpha+1)}\left(-\frac{\mu_{\chi(i)}}{\sigma_{\chi(i)}} \right). \tag{C8}$$

For the remaining forms of $\mathrm{ACCR}_{(i)}$, $\sigma_{\chi(i)} = 0$. When $\mu_{\chi(i)} \geq 0$, the air is entirely saturated and accretion occurs. In this scenario, when $\sigma_{r_r(i)} > 0$,

$$\mathrm{ACCR}_{(i)} = f_{p(i)} \mu_{\chi(i)}^{\alpha} \exp\left\{ \tilde{\mu}_{r_r(i)} \beta + \frac{1}{2} \tilde{\sigma}_{r_r(i)}^2 \beta^2 \right\}, \tag{C9}$$

and when $\sigma_{r_r(i)} = 0$,

$$\mathrm{ACCR}_{(i)} = f_{p(i)} \mu_{\chi(i)}^{\alpha} \mu_{r_r(i)}^{\beta}. \tag{C10}$$

Otherwise, when $\sigma_{\chi(i)} = 0$ and $\mu_{\chi(i)} < 0$, the air is entirely subsaturated, accretion does not occur, and $\mathrm{ACCR}_{(i)} = 0$.

C.2 Autoconversion rate

The KK autoconversion rate of r_r is of the form

$$\left. \frac{\partial r_r}{\partial t} \right|_{\text{auto}} = C_{\text{auto}}\, r_c^{\alpha}\, N_c^{\beta}, \tag{C11}$$

where constant $C_{\text{auto}} = 1350 \left(10^{-6} \rho_d\right)^{\beta}$, and where ρ_d is the density of dry air. Additionally, $\alpha = 2.47$ and $\beta = -1.79$. In the manner similar to accretion rate, upscaling is accom-

plished by integrating over Eq. (C11), and in the process, using Eq. (1.3) and Eq. (1.4) as substitutions. This produces the following equation for mean autoconversion rate

$$\begin{aligned}\overline{\left.\frac{\partial r_r}{\partial t}\right|_{\text{auto}}} &= C_{\text{auto}} \sum_{i=1}^{n} \xi_{(i)} \text{AUTO}_{(i)} \\ &= C_{\text{auto}} \sum_{i=1}^{n} \xi_{(i)} \int_{-\infty}^{\infty} \int_{0}^{\infty} \chi^{\alpha} N_{cn}^{\beta} \left(H\left(\chi\right)\right)^{\alpha+\beta} P_{(i)}\left(\chi, N_{cn}\right) \mathrm{d}N_{cn}\, \mathrm{d}\chi.\end{aligned} \tag{C12}$$

Since $\alpha + \beta > 0$, $\text{AUTO}_{(i)}$ can be rewritten

$$\text{AUTO}_{(i)} = \int_{0}^{\infty} \int_{0}^{\infty} \chi^{\alpha} N_{cn}^{\beta} P_{NL(i)}\left(\chi, N_{cn}\right) \mathrm{d}N_{cn}\, \mathrm{d}\chi. \tag{C13}$$

This equation is integrated, solving for $\text{AUTO}_{(i)}$ in the scenario of a fully-varying PDF ($\sigma_{\chi(i)} > 0$ and $\sigma_{N_{cn}(i)} > 0$),

$$\text{AUTO}_{(i)} = \frac{1}{\sqrt{2\pi}} \sigma_{\chi(i)}^{\alpha} \exp\left\{\tilde{\mu}_{N_{cn}(i)}\beta + \frac{1}{2}\tilde{\sigma}_{N_{cn}(i)}^{2}\beta^{2} - \frac{1}{4}\varsigma^{2}\right\} \Gamma\left(\alpha+1\right) D_{-(\alpha+1)}\left(-\varsigma\right), \tag{C14}$$

where ς is given by

$$\varsigma = \frac{\mu_{\chi(i)}}{\sigma_{\chi(i)}} + \tilde{\rho}_{\chi, N_{cn}(i)} \tilde{\sigma}_{N_{cn}(i)} \beta.$$

The values of $\tilde{\mu}_{N_{cn}(i)}$, $\tilde{\sigma}_{N_{cn}(i)}$, and $\tilde{\rho}_{\chi, N_{cn}(i)}$ are calculated analogously to the same variables for r_r in Eq. (C5), Eq. (C6), and Eq. (C7), respectively.

There are many case specifications that require a constant cloud droplet concentration within cloud, $N_{c\,0}$. The RICO, DYCOMS-II RF02, and LBA cases described in Section 1.4 all use a constant cloud droplet concentration within cloud. In CLUBB's PDF, this is easily accomplished by setting $\overline{N_{cn}'^{2}} = 0$, which causes $\sigma_{N_{cn}(1)} = 0$ and $\sigma_{N_{cn}(2)} = 0$. Additionally, $\mu_{N_{cn}(1)} = \mu_{N_{cn}(2)} = \overline{N_{cn}} = N_{c\,0}$ (where $N_{c\,0}$ has units of kg^{-1}) in this scenario.

When $\sigma_{\chi(i)} > 0$ and $\sigma_{N_{cn}(i)} = 0$, χ varies in ith component but N_{cn} is constant. The

integral is solved and the equation for $\mathrm{AUTO}_{(i)}$ becomes

$$\mathrm{AUTO}_{(i)} = \frac{1}{\sqrt{2\pi}}\,\sigma_{\chi(i)}^{\alpha}\mu_{N_{cn}(i)}^{\beta}\exp\left\{-\frac{1}{4}\frac{\mu_{\chi(i)}^{2}}{\sigma_{\chi(i)}^{2}}\right\}\Gamma\left(\alpha+1\right)D_{-(\alpha+1)}\left(-\frac{\mu_{\chi(i)}}{\sigma_{\chi(i)}}\right). \tag{C15}$$

For the remaining forms of $\mathrm{AUTO}_{(i)}$, $\sigma_{\chi(i)} = 0$. When $\mu_{\chi(i)} \geq 0$, the air is entirely saturated and autoconversion occurs. In this scenario, when $\sigma_{N_{cn}(i)} > 0$,

$$\mathrm{AUTO}_{(i)} = \mu_{\chi(i)}^{\alpha}\exp\left\{\tilde{\mu}_{N_{cn}(i)}\beta + \frac{1}{2}\tilde{\sigma}_{N_{cn}(i)}^{2}\beta^{2}\right\}, \tag{C16}$$

and when $\sigma_{N_{cn}(i)} = 0$,

$$\mathrm{AUTO}_{(i)} = \mu_{\chi(i)}^{\alpha}\mu_{N_{cn}(i)}^{\beta}. \tag{C17}$$

Otherwise, when $\sigma_{\chi(i)} = 0$ and $\mu_{\chi(i)} < 0$, the air is entirely subsaturated, autoconversion does not occur, and $\mathrm{AUTO}_{(i)} = 0$.

The mean KK autoconversion rate of N_r is found by dividing the mean KK autoconversion rate of r_r by a constant. The constant is $(4\pi\rho_l/3)\,r_0^3$, where r_0 is the assumed initial size of rain drops and is set to its recommended value of 25×10^{-6} m.

C.3 Evaporation rate

The KK equation set contains an equation for condensation or evaporation of r_r. CLUBB treats all liquid water in excess of saturation as cloud water and does not allow rain water to increase by condensational growth. The KK equation for evaporation of r_r is of the form

$$\left.\frac{\partial r_r}{\partial t}\right|_{\mathrm{evap}} = 3\,c_{\mathrm{evap}*}G\left(T,p\right)\left(\frac{4}{3}\pi\rho_l\right)^{\gamma}\left(S\,H\left(-S\right)\right)^{\alpha}r_r^{\beta}N_r^{\gamma}, \tag{C18}$$

where $\alpha = 1$, $\beta = 1/3$, and $\gamma = 1 - \beta = 2/3$, and where T is temperature, p is pressure, ρ_l is the density of liquid water, and the function $G\left(T,p\right)$ is the coefficient in the drop radius growth equation (Rogers and Yau 1989, Eq. 7.17). The constant $c_{\mathrm{evap}*}$ is the ratio

of raindrop mean geometric radius to raindrop mean volume radius, and is set by KK to a value of 0.86. Supersaturation, S, is positive when the air is saturated and negative when the air is subsaturated, and $S+1$ is the ratio of water vapor pressure to saturation vapor pressure with respect to liquid water.

Upscaling is accomplished by integrating over Eq. (C18). This requires a substitution that relates S to χ (see Eq. (A47)). Additionally, $G\left(T,p\right)$ is approximated as $G\left(\overline{T_l},p\right)$, where T_l is liquid water temperature and is given by

$$T_l = \theta_l \left(\frac{p}{p_0}\right)^{\frac{R_d}{C_{pd}}}, \tag{C19}$$

and where R_d is the gas constant for dry air, C_{pd} is the specific heat of dry air at constant pressure, and p_0 is a reference pressure of 1×10^5 Pa. This is a good approximation because $T = T_l$ when the air is subsaturated and $G\left(T,p\right)$ is slowly-varying with regards to temperature. The resulting $G\left(\overline{T_l},p\right)$ is a constant and can be pulled outside the integral.

This produces the following equation for mean evaporation rate

$$\begin{aligned}\overline{\left.\frac{\partial r_r}{\partial t}\right|_{\text{evap}}} &= C_{\text{evap}} \sum_{i=1}^{n} \xi_{(i)} \text{EVAP}_{(i)} \\ &= C_{\text{evap}} \sum_{i=1}^{n} \xi_{(i)} \int_{-\infty}^{\infty} \int_{0}^{\infty} \int_{0}^{\infty} \chi^{\alpha} \left(H\left(-\chi\right)\right)^{\alpha} r_r^{\beta} N_r^{\gamma} P_{(i)}\left(\chi, r_r, N_r\right) \mathrm{d}N_r \, \mathrm{d}r_r \, \mathrm{d}\chi,\end{aligned} \tag{C20}$$

where $P_{(i)}\left(\chi, r_r, N_r\right)$ is the trivariate marginal PDF of χ, r_r, N_r in the ith PDF component. The constant C_{evap} is given by

$$C_{\text{evap}} = 3\, c_{\text{evap}*} G\left(\overline{T_l},p\right) \left(\frac{4}{3}\pi\rho_l\right)^{\gamma} \left(\frac{1+\Lambda\left(\overline{T_l}\right) r_{sw}\left(\overline{T_l},p\right)}{r_{sw}\left(\overline{T_l},p\right)}\right)^{\alpha}, \tag{C21}$$

where $r_{sw}\left(\overline{T_l},p\right)$ is the saturation mixing ratio with respect to liquid water. Additionally,

$$\Lambda\left(\overline{T_l}\right) = \frac{R_d}{R_v}\left(\frac{L_v}{R_d\overline{T_l}}\right)\left(\frac{L_v}{C_{pd}\overline{T_l}}\right), \tag{C22}$$

where R_v is the gas constant for water vapor and L_v is the latent heat of vaporization.

Since $\alpha > 0$, $\text{EVAP}_{(i)}$ can be rewritten

$$\begin{aligned}\text{EVAP}_{(i)} = \int_{-\infty}^{0} \int_{0}^{\infty} \int_{0}^{\infty} \chi^{\alpha} r_r^{\beta} N_r^{\gamma} \Big(& f_{p(i)} P_{NLL(i)} \left(\chi, r_r, N_r\right) \\ & + \left(1 - f_{p(i)}\right) P_{N(i)} \left(\chi\right) \delta \left(r_r\right) \delta \left(N_r\right) \Big) \, \mathrm{d}N_r \, \mathrm{d}r_r \, \mathrm{d}\chi,\end{aligned} \tag{C23}$$

where $P_{NLL(i)} \left(\chi, r_r, N_r\right)$ is the ith component trivariate PDF involving one normal variate and two lognormal variates. When the PDF is fully-varying in the ith PDF component ($\sigma_{\chi(i)} > 0$, $\sigma_{r_r(i)} > 0$, and $\sigma_{N_r(i)} > 0$), the integrated equation for $\text{EVAP}_{(i)}$ is

$$\begin{aligned}\text{EVAP}_{(i)} = & f_{p(i)} \frac{1}{\sqrt{2\pi}} \left(-\sigma_{\chi(i)}\right)^{\alpha} \exp\left\{\tilde{\mu}_{r_r(i)} \beta + \tilde{\mu}_{N_r(i)} \gamma\right\} \\ & \times \exp\left\{ \frac{1}{2} \left(1 - \tilde{\rho}_{\chi, r_r(i)}^2\right) \tilde{\sigma}_{r_r(i)}^2 \beta^2 + \frac{1}{2} \left(1 - \tilde{\rho}_{\chi, N_r(i)}^2\right) \tilde{\sigma}_{N_r(i)}^2 \gamma^2 \right. \\ & \qquad \left. + \left(\tilde{\rho}_{r_r, N_r(i)} - \tilde{\rho}_{\chi, r_r(i)} \tilde{\rho}_{\chi, N_r(i)}\right) \tilde{\sigma}_{r_r(i)} \beta \tilde{\sigma}_{N_r(i)} \gamma \right\} \\ & \times \exp\left\{ \frac{1}{4} \varsigma^2 - \frac{\mu_{\chi(i)}}{\sigma_{\chi(i)}} \varsigma + \frac{1}{2} \frac{\mu_{\chi(i)}^2}{\sigma_{\chi(i)}^2} \right\} \Gamma\left(\alpha + 1\right) D_{-(\alpha+1)} \left(\varsigma\right),\end{aligned} \tag{C24}$$

where

$$\varsigma = \frac{\mu_{\chi(i)}}{\sigma_{\chi(i)}} + \tilde{\rho}_{\chi, r_r(i)} \tilde{\sigma}_{r_r(i)} \beta + \tilde{\rho}_{\chi, N_r(i)} \tilde{\sigma}_{N_r(i)} \gamma.$$

The values of $\tilde{\mu}_{N_r(i)}$, $\tilde{\sigma}_{N_r(i)}$, and $\tilde{\rho}_{\chi, N_r(i)}$ are calculated analogously to the same variables for r_r in Eq. (C5), Eq. (C6), and Eq. (C7), respectively. Additionally, the in-precipitation correlation of $\ln r_r$ and $\ln N_r$ in the ith PDF component is $\tilde{\rho}_{r_r, N_r(i)}$, and it is given by

$$\tilde{\rho}_{r_r, N_r(i)} = \frac{\ln\left(1 + \rho_{r_r, N_r(i)} \dfrac{\sigma_{r_r(i)} \sigma_{N_r(i)}}{\mu_{r_r(i)} \mu_{N_r(i)}}\right)}{\tilde{\sigma}_{r_r(i)} \tilde{\sigma}_{N_r(i)}}, \tag{C25}$$

where $\rho_{r_r, N_r(i)}$ is the correlation of r_r and N_r in the ith PDF component.

Just as with accretion and autoconversion, when one of the variables is constant in the

ith PDF sub-component, the equation simplifies. In the scenario when $\sigma_{\chi(i)} > 0$, $\sigma_{r_r(i)} = 0$, and $\sigma_{N_r(i)} > 0$,

$$\begin{aligned} \mathrm{EVAP}_{(i)} = & f_{p(i)} \frac{1}{\sqrt{2\pi}} \left(-\sigma_{\chi(i)}\right)^{\alpha} \mu_{r_r(i)}^{\beta} \\ & \times \exp\left\{\tilde{\mu}_{N_r(i)}\gamma + \frac{1}{2}\tilde{\sigma}_{N_r(i)}^2\gamma^2 - \frac{1}{4}\varsigma^2\right\} \Gamma\left(\alpha+1\right) D_{-(\alpha+1)}\left(\varsigma\right), \end{aligned} \tag{C26}$$

where

$$\varsigma = \frac{\mu_{\chi(i)}}{\sigma_{\chi(i)}} + \tilde{\rho}_{\chi,N_r(i)}\tilde{\sigma}_{N_r(i)}\gamma;$$

when $\sigma_{\chi(i)} > 0$, $\sigma_{r_r(i)} > 0$, and $\sigma_{N_r(i)} = 0$,

$$\begin{aligned} \mathrm{EVAP}_{(i)} = & f_{p(i)} \frac{1}{\sqrt{2\pi}} \left(-\sigma_{\chi(i)}\right)^{\alpha} \mu_{N_r(i)}^{\gamma} \\ & \times \exp\left\{\tilde{\mu}_{r_r(i)}\beta + \frac{1}{2}\tilde{\sigma}_{r_r(i)}^2\beta^2 - \frac{1}{4}\varsigma^2\right\} \Gamma\left(\alpha+1\right) D_{-(\alpha+1)}\left(\varsigma\right), \end{aligned} \tag{C27}$$

where

$$\varsigma = \frac{\mu_{\chi(i)}}{\sigma_{\chi(i)}} + \tilde{\rho}_{\chi,r_r(i)}\tilde{\sigma}_{r_r(i)}\beta;$$

and when $\sigma_{\chi(i)} > 0$, $\sigma_{r_r(i)} = 0$, and $\sigma_{N_r(i)} = 0$,

$$\begin{aligned} \mathrm{EVAP}_{(i)} = & f_{p(i)} \frac{1}{\sqrt{2\pi}} \left(-\sigma_{\chi(i)}\right)^{\alpha} \mu_{r_r(i)}^{\beta}\mu_{N_r(i)}^{\gamma} \\ & \times \exp\left\{-\frac{1}{4}\frac{\mu_{\chi(i)}^2}{\sigma_{\chi(i)}^2}\right\} \Gamma\left(\alpha+1\right) D_{-(\alpha+1)}\left(\frac{\mu_{\chi(i)}}{\sigma_{\chi(i)}}\right). \end{aligned} \tag{C28}$$

For the remaining forms of $\mathrm{EVAP}_{(i)}$, $\sigma_{\chi(i)} = 0$. When $\mu_{\chi(i)} \leq 0$, the air is entirely subsaturated and evaporation occurs. In this scenario, when $\sigma_{r_r(i)} > 0$ and $\sigma_{N_r(i)} > 0$,

$$\begin{aligned} \mathrm{EVAP}_{(i)} = f_{p(i)}\mu_{\chi(i)}^{\alpha} \exp\Bigg\{ & \tilde{\mu}_{r_r(i)}\beta + \tilde{\mu}_{N_r(i)}\gamma + \frac{1}{2}\tilde{\sigma}_{r_r(i)}^2\beta^2 \\ & + \frac{1}{2}\tilde{\sigma}_{N_r(i)}^2\gamma^2 + \tilde{\rho}_{r_r,N_r(i)}\tilde{\sigma}_{r_r(i)}\beta\tilde{\sigma}_{N_r(i)}\gamma\Bigg\}; \end{aligned} \tag{C29}$$

when $\sigma_{r_r(i)} = 0$ and $\sigma_{N_r(i)} > 0$,

$$\text{EVAP}_{(i)} = f_{p(i)} \mu_{\chi(i)}^{\alpha} \mu_{r_r(i)}^{\beta} \exp\left\{ \tilde{\mu}_{N_r(i)} \gamma + \frac{1}{2} \tilde{\sigma}_{N_r(i)}^2 \gamma^2 \right\}; \tag{C30}$$

when $\sigma_{r_r(i)} > 0$ and $\sigma_{N_r(i)} = 0$,

$$\text{EVAP}_{(i)} = f_{p(i)} \mu_{\chi(i)}^{\alpha} \mu_{N_r(i)}^{\gamma} \exp\left\{ \tilde{\mu}_{r_r(i)} \beta + \frac{1}{2} \tilde{\sigma}_{r_r(i)}^2 \beta^2 \right\}; \tag{C31}$$

and when $\sigma_{r_r(i)} = 0$ and $\sigma_{N_r(i)} = 0$,

$$\text{EVAP}_{(i)} = f_{p(i)} \mu_{\chi(i)}^{\alpha} \mu_{r_r(i)}^{\beta} \mu_{N_r(i)}^{\gamma}. \tag{C32}$$

Otherwise, when $\sigma_{\chi(i)} = 0$ and $\mu_{\chi(i)} > 0$, the air is entirely saturated, evaporation does not occur, and $\text{EVAP}_{(i)} = 0$.

The KK evaporation rate of N_r is related to the evaporation rate of r_r by

$$\frac{\Delta N_r|_{\text{evap}}}{N_r} = \left(\frac{\Delta r_r|_{\text{evap}}}{r_r} \right)^{\nu_*}, \tag{C33}$$

where $\Delta N_r|_{\text{evap}}$ is the change in N_r due to evaporation, $\Delta r_r|_{\text{evap}}$ is the change in r_r due to evaporation, and ν_* is a tunable parameter in KK that is set to its recommended value of 1. CLUBB does not handle microphysics process rates in a sequential manner, but rather in a parallel manner. However, the microphysics process rates are explicit terms in the predictive equation set, so the change in a hydrometeor due to a microphysics process is related to the rate of change by

$$\Delta r_r|_{\text{evap}} = \left. \frac{\partial r_r}{\partial t} \right|_{\text{evap}} \Delta t \qquad \text{and} \qquad \Delta N_r|_{\text{evap}} = \left. \frac{\partial N_r}{\partial t} \right|_{\text{evap}} \Delta t, \tag{C34}$$

where Δt is the duration of one model timestep. Substituting Eq. (C34) into Eq. (C33) and

solving for the rate of change of N_r due to evaporation results in

$$\left.\frac{\partial N_r}{\partial t}\right|_{\text{evap}} = (\Delta t)^{\nu_*-1}\,\frac{N_r}{{r_r}^{\nu_*}}\left(\left.\frac{\partial r_r}{\partial t}\right|_{\text{evap}}\right)^{\nu_*}. \tag{C35}$$

The mean N_r evaporation rate is calculated in the same way as the mean r_r evaporation rate with α replaced by $\alpha\nu_*$, β replaced by $(\beta-1)\,\nu_*$, and γ replaced by $\gamma\nu_*+1$. Additionally, the constant C_{evap} is taken to the ν_* power and the result is multiplied by $(\Delta t)^{\nu_*-1}$. When ν_* is set to its recommended value of 1, the mean N_r evaporation rate is more simply solved the same way as the mean r_r evaporation rate with β replaced by $\beta-1$ and γ replaced by $\gamma+1$.

C.4 Mean volume radius of rain drops

The KK mean volume radius of rain drops (in meters), R_{vr}, is of the form

$$R_{vr} = C_{\text{mvrr}}\,r_r^{\alpha}\,N_r^{\beta}, \tag{C36}$$

where $C_{\text{mvrr}} = (4\pi\rho_l/3)^{\beta}$, $\alpha = 1/3$, and $\beta = -\alpha = -1/3$. Upscaling is accomplished by integrating over Eq. (C36), producing the following equation for mean volume radius

$$\begin{aligned}\overline{R_{vr}} &= C_{\text{mvrr}}\sum_{i=1}^{n}\xi_{(i)}\text{MVRR}_{(i)} \\ &= C_{\text{mvrr}}\sum_{i=1}^{n}\xi_{(i)}\int_0^{\infty}\int_0^{\infty} r_r^{\alpha}N_r^{\beta}P_{(i)}\left(r_r,N_r\right)\mathrm{d}N_r\,\mathrm{d}r_r,\end{aligned} \tag{C37}$$

where $P_{(i)}\left(r_r,N_r\right)$ is the bivariate marginal PDF of r_r and N_r in the ith PDF component.

Additionally, $\text{MVRR}_{(i)}$ can be rewritten

$$\text{MVRR}_{(i)} = \int_0^{\infty}\int_0^{\infty} r_r^{\alpha}N_r^{\beta}\left(f_{p(i)}P_{LL(i)}\left(r_r,N_r\right) + \left(1-f_{p(i)}\right)\,\delta\left(r_r\right)\,\delta\left(N_r\right)\right)\mathrm{d}N_r\,\mathrm{d}r_r, \tag{C38}$$

where $P_{LL(i)}(r_r, N_r)$ is the ith component bivariate PDF involving two lognormal variates. When the PDF is fully-varying in the ith PDF component ($\sigma_{r_r(i)} > 0$ and $\sigma_{N_r(i)} > 0$), the integrated equation for $\text{MVRR}_{(i)}$ is

$$\begin{aligned}\text{MVRR}_{(i)} =& f_{p(i)} \exp\left\{ \tilde{\mu}_{r_r(i)}\alpha + \tilde{\mu}_{N_r(i)}\beta + \frac{1}{2}\tilde{\sigma}^2_{r_r(i)}\alpha^2 \right. \\ & \left. + \frac{1}{2}\tilde{\sigma}^2_{N_r(i)}\beta^2 + \tilde{\rho}_{r_r,N_r(i)}\tilde{\sigma}_{r_r(i)}\alpha\tilde{\sigma}_{N_r(i)}\beta \right\}.\end{aligned} \tag{C39}$$

In the scenario when $\sigma_{r_r(i)} = 0$ and $\sigma_{N_r(i)} > 0$,

$$\text{MVRR}_{(i)} = f_{p(i)}\mu^{\alpha}_{r_r(i)} \exp\left\{ \tilde{\mu}_{N_r(i)}\beta + \frac{1}{2}\tilde{\sigma}^2_{N_r(i)}\beta^2 \right\}, \tag{C40}$$

when $\sigma_{r_r(i)} > 0$ and $\sigma_{N_r(i)} = 0$,

$$\text{MVRR}_{(i)} = f_{p(i)}\mu^{\beta}_{N_r(i)} \exp\left\{ \tilde{\mu}_{r_r(i)}\alpha + \frac{1}{2}\tilde{\sigma}^2_{r_r(i)}\alpha^2 \right\}, \tag{C41}$$

and when $\sigma_{r_r(i)} = 0$ and $\sigma_{N_r(i)} = 0$,

$$\text{MVRR}_{(i)} = f_{p(i)}\mu^{\alpha}_{r_r(i)}\mu^{\beta}_{N_r(i)}. \tag{C42}$$

The upscaled mean volume radius is used to calculate mean sedimentation velocity of r_r and N_r. The mean sedimentation velocity of r_r is $\overline{V_{r_r}} = \min\left(-0.012\left(10^6\,\overline{R_{vr}}\right) + 0.2, 0\right)$, and the mean sedimentation velocity of N_r is $\overline{V_{N_r}} = \min\left(-0.007\left(10^6\,\overline{R_{vr}}\right) + 0.1, 0\right)$.

Appendix D: The Relationship Between $\overline{N_c}$ and $\overline{N_{cn}}$

The relationship between N_c and N_{cn} is given in Eq. (1.4) and described in Section 1.2. The overall (grid-box) mean value of cloud droplet concentration, $\overline{N_c}$, is calculated by integrating over the product of Eq. (1.4) and the PDF of χ and N_{cn}, such that

$$\overline{N_c} = \int_{-\infty}^{\infty} \int_{0}^{\infty} N_{cn}\, H\left(\chi\right) \sum_{i=1}^{n} \xi_{(i)} P_{(i)}\left(\chi, N_{cn}\right) \mathrm{d}N_{cn}\, \mathrm{d}\chi, \tag{D1}$$

where $P_{(i)}\left(\chi, N_{cn}\right)$ is the bivariate marginal PDF of χ and N_{cn} in the ith PDF component. This equation can be rewritten as

$$\begin{aligned} \overline{N_c} &= \sum_{i=1}^{n} \xi_{(i)} \int_{0}^{\infty} \int_{0}^{\infty} N_{cn} P_{NL(i)}\left(\chi, N_{cn}\right) \mathrm{d}N_{cn}\, \mathrm{d}\chi \\ &= \sum_{i=1}^{n} \xi_{(i)}\, \mathrm{NC}_{(i)}, \end{aligned} \tag{D2}$$

where $P_{NL(i)}\left(\chi, N_{cn}\right)$ is the ith component bivariate PDF involving one normal variate and one lognormal variate. This equation is integrated and reduced, resulting in

$$\mathrm{NC}_{(i)} = \frac{1}{2}\, \mu_{N_{cn}(i)}\, \mathrm{erfc}\left(-\frac{1}{\sqrt{2}} \left(\frac{\mu_{\chi(i)}}{\sigma_{\chi(i)}} + \tilde{\rho}_{\chi, N_{cn}(i)} \tilde{\sigma}_{N_{cn}(i)} \right) \right), \tag{D3}$$

where $\mathrm{erfc}\left(x\right)$ is the complimentary error function, and where $\mu_{\chi(i)}$ and $\sigma_{\chi(i)}$ are the mean and standard deviation, respectively, of χ in the ith PDF component. Additionally, $\tilde{\sigma}_{N_{cn}(i)}$ is the standard deviation of $\ln N_{cn}$ in the ith PDF component and $\tilde{\rho}_{\chi, N_{cn}(i)}$ is the correlation of χ and $\ln N_{cn}$ in the ith PDF component.

The evaluated integral for $\mathrm{NC}_{(i)}$ given in Eq. (D3) is for a fully-varying PDF in the ith component ($\sigma_{\chi(i)} > 0$ and $\sigma_{N_{cn}(i)} > 0$). There are times when a variable may have a constant value in a PDF component. When this happens, the PDF of the constant variable is a delta

function at the ith PDF component mean. When $\sigma_{\chi(i)} > 0$ and $\sigma_{N_{cn}(i)} = 0$, χ varies in ith component but N_{cn} is constant. The PDF $P_{NL(i)}(\chi, r_r)$ becomes $P_{N(i)}(\chi)\ \delta\left(N_{cn} - \mu_{N_{cn}(i)}\right)$. The integral is solved and the equation for $\mathrm{NC}_{(i)}$ becomes

$$\mathrm{NC}_{(i)} = \mu_{N_{cn}(i)} \frac{1}{2} \operatorname{erfc}\left(-\frac{\mu_{\chi(i)}}{\sqrt{2}\,\sigma_{\chi(i)}}\right). \tag{D4}$$

Likewise, when $\sigma_{\chi(i)} = 0$ and $\sigma_{N_{cn}(i)} > 0$, χ varies in ith component but N_{cn} is constant, and when both $\sigma_{\chi(i)} = 0$ and $\sigma_{N_{cn}(i)} = 0$, both χ and N_{cn} are constant in the ith PDF component. In either scenario, the equation becomes

$$\mathrm{NC}_{(i)} = \begin{cases} \mu_{N_{cn}(i)}, & \text{when } \mu_{\chi(i)} > 0; \text{ and} \\ 0, & \text{when } \mu_{\chi(i)} \leq 0. \end{cases} \tag{D5}$$

It is important to be able to back-solve $\overline{N_{cn}}$ from $\overline{N_c}$ because numerical models and microphysics schemes usually either predict $\overline{N_c}$, predict the mean in-cloud value of cloud droplet concentration, $\overline{N_c|_{\mathrm{ic}}}$, or specify the in-cloud value of cloud droplet concentration. The value of $\overline{N_{cn}}$ needs to be calculated from this information for use in the PDF. The relationship between grid-box mean N_c and the mean in-cloud value of cloud droplet concentration is $\overline{N_c|_{\mathrm{ic}}} = \overline{N_c}/f_c$, where f_c is cloud fraction. CLUBB calculates cloud fraction by integrating over the PDF of χ, such that

$$f_c = \int_{-\infty}^{\infty} H(\chi) \sum_{i=1}^{n} \xi_{(i)} P_{(i)}(\chi)\, \mathrm{d}\chi = \sum_{i=1}^{n} \xi_{(i)} f_{c(i)}, \tag{D6}$$

where $f_{c(i)}$ is the cloud fraction in the ith PDF component, which is calculated by

$$f_{c(i)} = \begin{cases} \dfrac{1}{2} \operatorname{erfc}\left(-\dfrac{\mu_{\chi(i)}}{\sqrt{2}\,\sigma_{\chi(i)}}\right), & \text{when } \sigma_{\chi(i)} > 0; \\ 1, & \text{when } \sigma_{\chi(i)} = 0 \text{ and } \mu_{\chi(i)} > 0; \text{ and} \\ 0, & \text{when } \sigma_{\chi(i)} = 0 \text{ and } \mu_{\chi(i)} \leq 0. \end{cases} \tag{D7}$$

The value of $\overline{N_{cn}}$ from can be back-solved $\overline{N_c}$. As described in Section 1.3, $\mu_{N_{cn}(i)} = \overline{N_{cn}}$ and $\sigma_{N_{cn}(i)} = \sqrt{\overline{N_{cn}'^2}}$. Additionally, $\tilde{\rho}_{\chi,N_{cn}(i)}$ is related to $\rho_{\chi,N_{cn}(i)}$ in the manner described by Eq. (B4). These substitutions are made into Eq. (D3), Eq. (D4), and Eq. (D5). However, further simplification is necessary to solve for $\overline{N_{cn}}$. The value of $\overline{N_{cn}'^2} \,/\, \overline{N_{cn}}^2$ is set to a prescribed constant value, denoted $C_{N_{cn}*}$. Additionally, the correlation $\rho_{\chi,N_{cn}(i)}$ is also set to a prescribed value, $\rho_{\chi,N_{cn}*}$. The value of N_{cn} can now be solved by

$$\overline{N_{cn}} = \frac{\overline{N_c}}{\sum_{i=1}^{n} \xi_{(i)} \, \mathrm{FCTR}_{(i)}}, \tag{D8}$$

where $\mathrm{FCTR}_{(i)}$ is the factor given by

$$\mathrm{FCTR}_{(i)} = \begin{cases} \dfrac{1}{2} \operatorname{erfc}\left(-\dfrac{1}{\sqrt{2}} \left(\dfrac{\mu_{\chi(i)}}{\sigma_{\chi(i)}} + \rho_{\chi,N_{cn}*} \sqrt{C_{N_{cn}*}} \right) \right), \\ \qquad\qquad \text{when } \sigma_{\chi(i)} > 0 \text{ and } C_{N_{cn}*} > 0; \\ \dfrac{1}{2} \operatorname{erfc}\left(-\dfrac{\mu_{\chi(i)}}{\sqrt{2}\,\sigma_{\chi(i)}} \right), \quad \text{when } \sigma_{\chi(i)} > 0 \text{ and } C_{N_{cn}*} = 0; \\ 1, \qquad \text{when } \sigma_{\chi(i)} = 0 \text{ and } \mu_{\chi(i)} > 0; \text{ and} \\ 0, \qquad \text{when } \sigma_{\chi(i)} = 0 \text{ and } \mu_{\chi(i)} \leq 0. \end{cases} \tag{D9}$$

When the last scenario is found in all components, the denominator of Eq. (D8) is 0. However, cloud fraction is 0, meaning $\overline{N_c}$ is also 0, leaving $\overline{N_{cn}}$ undefined. For numerical purposes, $\overline{N_{cn}}$ can be set to a reasonable value in this scenario.

The relationship between $\overline{N_{cn}}$ and $\overline{N_c|_{\mathrm{ic}}}$ is found by comparing Eq. (D8) and Eq. (D9) with Eq. (D6) and Eq. (D7). Three scenarios emerge in the comparison. When N_{cn} is constant (used for prescribing a constant value of in-cloud N_c, as was done for the RICO, DYCOMS-II RF02, and LBA cases in this paper), $\overline{N_{cn}} = \overline{N_c|_{\mathrm{ic}}}$. When N_{cn} varies, but the correlation of χ and N_{cn} is 0 (or undefined when χ is constant), it still holds that $\overline{N_{cn}} = \overline{N_c|_{\mathrm{ic}}}$. However, when N_{cn} varies and the correlation of χ and N_{cn} is a value other than 0, $\overline{N_{cn}}$ differs

from $\overline{N_c|_{\text{ic}}}$.

In a situation where CLUBB is using SILHS with a microphysics scheme that predicts $\overline{N_c}$, a model time step works as follows. The time step begins with the most recent value of $\overline{N_c}$. The value of $\overline{N_{cn}}$ is calculated for use in the PDF. Then, the PDF parameters are calculated, including those involving N_{cn}. SILHS uses the PDF parameters to generate sample points of all variables involved in the PDF, including χ and N_{cn}. The value of N_c at these sample points is calculated according to Eq. (1.4). The sample points of N_c are then fed to the microphysics scheme, which requires N_c as input. The microphysics tendency of N_c is output from SILHS, and is used to advance the predictive equation for $\overline{N_c}$ for the next model time step.

Appendix E: Covariances Involving Microphysics Process Rates

The nine microphysical covariances involving each of w, r_t, and θ_l with each of KK autoconversion rate, accretion rate, and evaporation rate are calculated by integrating over the PDF. The KK microphysics process rates are calculated, in part, based on variables that involve saturation, such as r_c. In order to calculate quantities that involve saturation, a PDF transformation, which is a change of coordinates, is required. The multivariate PDF undergoes stretching, translation, and rotation of the axes (Larson et al. 2005; Mellor 1977). An independent PDF transformation takes place in each PDF component. Ultimately, r_t and θ_l are replaced in the PDF by χ and η, where χ is an "extended" liquid water mixing ratio that has a positive value when air is supersaturated. In this scenario, χ is also equal to r_c. When air is subsaturated, χ has a negative value. The variable η is orthogonal to χ. The transformations that relate r_t and θ_l to χ and η are given by Eq. (A24) and Eq. (A25).

E.1 Covariances involving autoconversion rate

The general form of the KK equation for autoconversion rate is the product of a coefficient and $r_c^\alpha N_c^\beta$ (where for KK, $\alpha = 2.47$ and $\beta = -1.79$). The integral equation for the covariance of w and autoconversion rate involves the PDF-variables w, r_t, θ_l, and N_{cn}. The equation is

$$\overline{w' \left.\frac{\partial r_r}{\partial t}\right|'_{\text{auto}}} = \int_{-\infty}^{\infty}\int_{-\infty}^{\infty}\int_{-\infty}^{\infty}\int_{0}^{\infty}\left(w - \overline{w}\right)\left(\left.\frac{\partial r_r}{\partial t}\right|_{\text{auto}} - \overline{\left.\frac{\partial r_r}{\partial t}\right|_{\text{auto}}}\right) \times P\left(w, r_t, \theta_l, N_{cn}\right) \mathrm{d}N_{cn}\, \mathrm{d}\theta_l\, \mathrm{d}r_t\, \mathrm{d}w. \tag{E1}$$

The PDF is transformed (in each component) from r_t and θ_l coordinates to χ and η coordinates. Additionally, $r_c = \chi\, H\left(\chi\right)$ and $N_c = N_{cn}\, H\left(\chi\right)$, where $H\left(\chi\right)$ is the Heaviside step

function (see Section 1.2). The equation becomes

$$\overline{w' \left.\frac{\partial r_r}{\partial t}\right|'_{\text{auto}}} = \sum_{i=1}^{n} \xi_{(i)} \int_{-\infty}^{\infty} \int_{-\infty}^{\infty} \int_{-\infty}^{\infty} \int_{0}^{\infty} \left(w - \overline{w}\right) \left(C_{\text{auto}}\, \chi^{\alpha} N_{cn}^{\beta} \left(H\left(\chi\right)\right)^{\alpha+\beta} - \overline{\left.\frac{\partial r_r}{\partial t}\right|_{\text{auto}}} \right) \times P_{(i)}\left(w, \chi, \eta, N_{cn}\right) \mathrm{d}N_{cn}\, \mathrm{d}\eta\, \mathrm{d}\chi\, \mathrm{d}w, \tag{E2}$$

where the coefficient $C_{\text{auto}} = 1350\left(10^{-6}\rho_d\right)^{\beta}$, and where ρ_d is the density of dry air. The variable η can be integrated out of the PDF. The equation for the covariance of w and autoconversion rate is

$$\begin{aligned} &\overline{w' \left.\frac{\partial r_r}{\partial t}\right|'_{\text{auto}}} \\ &= C_{\text{auto}} \sum_{i=1}^{n} \xi_{(i)} \int_{-\infty}^{\infty} \int_{-\infty}^{\infty} \int_{0}^{\infty} \left(w - \overline{w}\right) \left(\chi^{\alpha} N_{cn}^{\beta} \left(H\left(\chi\right)\right)^{\alpha+\beta} - \frac{1}{C_{\text{auto}}} \overline{\left.\frac{\partial r_r}{\partial t}\right|_{\text{auto}}} \right) \\ &\qquad \times P_{NNL(i)}\left(w, \chi, N_{cn}\right) \mathrm{d}N_{cn}\, \mathrm{d}\chi\, \mathrm{d}w, \end{aligned} \tag{E3}$$

where $P_{NNL(i)}\left(w, \chi, N_{cn}\right)$ is the ith component trivariate PDF involving two normal variates and one lognormal variate.

The integral equation for the covariance of r_t and autoconversion rate involves the PDF-variables r_t, θ_l, and N_{cn}. The equation is

$$\overline{r'_t \left.\frac{\partial r_r}{\partial t}\right|'_{\text{auto}}} = \int_{-\infty}^{\infty} \int_{-\infty}^{\infty} \int_{0}^{\infty} \left(r_t - \overline{r_t}\right) \left(\left.\frac{\partial r_r}{\partial t}\right|_{\text{auto}} - \overline{\left.\frac{\partial r_r}{\partial t}\right|_{\text{auto}}} \right) P\left(r_t, \theta_l, N_{cn}\right) \mathrm{d}N_{cn}\, \mathrm{d}\theta_l\, \mathrm{d}r_t. \tag{E4}$$

During the PDF transformation, Eq. (A24) is used to substitute for r_t. The equation becomes

$$\begin{aligned} \overline{r'_t \left.\frac{\partial r_r}{\partial t}\right|'_{\text{auto}}} = \sum_{i=1}^{n} \xi_{(i)} \int_{-\infty}^{\infty} \int_{-\infty}^{\infty} \int_{0}^{\infty} &\left(\mu_{r_t(i)} - \overline{r_t} + \frac{\left(\eta - \mu_{\eta(i)}\right) + \left(\chi - \mu_{\chi(i)}\right)}{2 c_{r_t(i)}} \right) \\ &\times \left(C_{\text{auto}}\, \chi^{\alpha} N_{cn}^{\beta} \left(H\left(\chi\right)\right)^{\alpha+\beta} - \overline{\left.\frac{\partial r_r}{\partial t}\right|_{\text{auto}}} \right) \\ &\times P_{(i)}\left(\eta, \chi, N_{cn}\right) \mathrm{d}N_{cn}\, \mathrm{d}\chi\, \mathrm{d}\eta, \end{aligned} \tag{E5}$$

where $\mu_{r_{t(i)}}$ is the mean of r_t in the ith PDF component. The mean of χ in the ith PDF component, $\mu_{\chi(i)}$, is given by Eq. (A23). The mean of η in the ith PDF component, $\mu_{\eta(i)}$, ultimately does not factor into the solution to the integral equations. Its value is irrelevant and can be set to an arbitrary value, such as 0, for simplicity. However, it should be noted that the PDF component standard deviations of η and PDF component correlations involving η still factor into the solution. The PDF transformation coefficient $c_{r_t(i)}$ is given by Eq. (A17). After splitting and simplifying, Eq. (E5) becomes

$$\begin{aligned}
&\overline{r_t' \left.\frac{\partial r_r}{\partial t}\right|_{\text{auto}}'} \\
&= C_{\text{auto}} \sum_{i=1}^{n} \xi_{(i)} \\
&\quad \times \left(\frac{1}{2c_{r_t(i)}} \int_{-\infty}^{\infty} \int_{-\infty}^{\infty} \int_{0}^{\infty} \left(\eta - \mu_{\eta(i)}\right) \left(\chi^{\alpha} N_{cn}^{\beta} \left(H\left(\chi\right)\right)^{\alpha+\beta} - \frac{1}{C_{\text{auto}}} \overline{\left.\frac{\partial r_r}{\partial t}\right|_{\text{auto}}} \right) \right. \\
&\qquad \left. \times P_{NNL(i)}\left(\eta, \chi, N_{cn}\right) \mathrm{d}N_{cn}\, \mathrm{d}\chi\, \mathrm{d}\eta \right. \\
&\quad + \frac{1}{2c_{r_t(i)}} \int_{0}^{\infty} \int_{0}^{\infty} \chi^{\alpha+1} N_{cn}^{\beta} P_{NL(i)}\left(\chi, N_{cn}\right) \mathrm{d}N_{cn}\, \mathrm{d}\chi \\
&\quad \left. + \left(\mu_{r_t(i)} - \overline{r_t} - \frac{\mu_{\chi(i)}}{2c_{r_t(i)}} \right) \int_{0}^{\infty} \int_{0}^{\infty} \chi^{\alpha} N_{cn}^{\beta} P_{NL(i)}\left(\chi, N_{cn}\right) \mathrm{d}N_{cn}\, \mathrm{d}\chi \right),
\end{aligned} \tag{E6}$$

where $P_{NL(i)}\left(\chi, N_{cn}\right)$ is the ith component bivariate PDF involving one normal variate and one lognormal variate.

The integral equation for the covariance of θ_l and autoconversion rate involves the PDF-variables r_t, θ_l, and N_{cn}. The equation is

$$\overline{\theta_l' \left.\frac{\partial r_r}{\partial t}\right|_{\text{auto}}'} = \int_{-\infty}^{\infty} \int_{-\infty}^{\infty} \int_{0}^{\infty} \left(\theta_l - \overline{\theta_l}\right) \left(\left.\frac{\partial r_r}{\partial t}\right|_{\text{auto}} - \overline{\left.\frac{\partial r_r}{\partial t}\right|_{\text{auto}}} \right) P\left(r_t, \theta_l, N_{cn}\right) \mathrm{d}N_{cn}\, \mathrm{d}\theta_l\, \mathrm{d}r_t. \tag{E7}$$

During the PDF transformation, Eq. (A25) is used to substitute for θ_l. The equation becomes

$$\begin{aligned}\overline{\theta_l' \left.\frac{\partial r_r}{\partial t}\right|_{\text{auto}}'} = \sum_{i=1}^{n} \xi_{(i)} \int_{-\infty}^{\infty}\int_{-\infty}^{\infty}\int_{0}^{\infty} \Bigg(\mu_{\theta_l(i)} - \overline{\theta_l} + \frac{\left(\eta - \mu_{\eta(i)}\right) - \left(\chi - \mu_{\chi(i)}\right)}{2c_{\theta_l(i)}} \Bigg) \\ \times \left(C_{\text{auto}}\, \chi^{\alpha} N_{cn}^{\beta} \left(H\left(\chi\right)\right)^{\alpha+\beta} - \overline{\left.\frac{\partial r_r}{\partial t}\right|_{\text{auto}}} \right) \\ \times P_{(i)}\left(\eta, \chi, N_{cn}\right) \mathrm{d}N_{cn}\, \mathrm{d}\chi\, \mathrm{d}\eta,\end{aligned} \tag{E8}$$

where $\mu_{\theta_{l(i)}}$ is the mean of θ_l in the ith PDF component. The PDF transformation coefficient $c_{\theta_l(i)}$ is given by Eq. (A18). After splitting and simplifying, Eq. (E8) becomes

$$\begin{aligned}&\overline{\theta_l' \left.\frac{\partial r_r}{\partial t}\right|_{\text{auto}}'} \\ &= C_{\text{auto}} \sum_{i=1}^{n} \xi_{(i)} \\ &\quad \times \left(\frac{1}{2c_{\theta_l(i)}} \int_{-\infty}^{\infty}\int_{-\infty}^{\infty}\int_{0}^{\infty} \left(\eta - \mu_{\eta(i)}\right) \left(\chi^{\alpha} N_{cn}^{\beta} \left(H\left(\chi\right)\right)^{\alpha+\beta} - \frac{1}{C_{\text{auto}}} \overline{\left.\frac{\partial r_r}{\partial t}\right|_{\text{auto}}} \right) \right. \\ &\qquad\qquad \left. \times P_{NNL(i)}\left(\eta, \chi, N_{cn}\right) \mathrm{d}N_{cn}\, \mathrm{d}\chi\, \mathrm{d}\eta \right. \\ &\quad - \frac{1}{2c_{\theta_l(i)}} \int_{0}^{\infty}\int_{0}^{\infty} \chi^{\alpha+1} N_{cn}^{\beta} P_{NL(i)}\left(\chi, N_{cn}\right) \mathrm{d}N_{cn}\, \mathrm{d}\chi \\ &\quad + \left(\mu_{\theta_l(i)} - \overline{\theta_l} + \frac{\mu_{\chi(i)}}{2c_{\theta_l(i)}} \right) \int_{0}^{\infty}\int_{0}^{\infty} \chi^{\alpha} N_{cn}^{\beta} P_{NL(i)}\left(\chi, N_{cn}\right) \mathrm{d}N_{cn}\, \mathrm{d}\chi \Bigg).\end{aligned} \tag{E9}$$

E.2 Covariances involving accretion rate

The general form of the KK equation for accretion rate is the product of a coefficient and $r_c^{\alpha} r_r^{\beta}$ (where for KK, $\alpha = 1.15$ and $\beta = 1.15$). The integral equation for the covariance of w

and accretion rate involves the PDF-variables w, r_t, θ_l, and r_r. The equation is

$$\overline{w' \left.\frac{\partial r_r}{\partial t}\right|'_{\text{accr}}} = \int_{-\infty}^{\infty}\int_{-\infty}^{\infty}\int_{-\infty}^{\infty}\int_{0}^{\infty}\left(w - \overline{w}\right)\left(\left.\frac{\partial r_r}{\partial t}\right|_{\text{accr}} - \overline{\left.\frac{\partial r_r}{\partial t}\right|_{\text{accr}}}\right) \times P\left(w, r_t, \theta_l, r_r\right) \mathrm{d}r_r \, \mathrm{d}\theta_l \, \mathrm{d}r_t \, \mathrm{d}w. \tag{E10}$$

The PDF is transformed and the substitution $r_c = \chi\, H\left(\chi\right)$ is made. The equation becomes

$$\overline{w' \left.\frac{\partial r_r}{\partial t}\right|'_{\text{accr}}} = \sum_{i=1}^{n} \xi_{(i)} \int_{-\infty}^{\infty}\int_{-\infty}^{\infty}\int_{-\infty}^{\infty}\int_{0}^{\infty}\left(w - \overline{w}\right)\left(C_{\text{accr}}\, \chi^{\alpha}\left(H\left(\chi\right)\right)^{\alpha} r_r^{\beta} - \overline{\left.\frac{\partial r_r}{\partial t}\right|_{\text{accr}}}\right) \times P_{(i)}\left(w, \chi, \eta, r_r\right) \mathrm{d}r_r \, \mathrm{d}\eta \, \mathrm{d}\chi \, \mathrm{d}w, \tag{E11}$$

where the coefficient $C_{\text{accr}} = 67$. The variable η is integrated out of the PDF, and the equation for the covariance of w and accretion rate is

$$\begin{aligned}\overline{w' \left.\frac{\partial r_r}{\partial t}\right|'_{\text{accr}}} = C_{\text{accr}} \sum_{i=1}^{n} \xi_{(i)} & \\ \times \Bigg(f_{p(i)} \int_{-\infty}^{\infty}\int_{-\infty}^{\infty}\int_{0}^{\infty}\left(w - \overline{w}\right)\left(\chi^{\alpha}\left(H\left(\chi\right)\right)^{\alpha} r_r^{\beta} - \frac{1}{C_{\text{accr}}}\overline{\left.\frac{\partial r_r}{\partial t}\right|_{\text{accr}}}\right) & \\ \times P_{NNL(i)}\left(w, \chi, r_r\right) \mathrm{d}r_r \, \mathrm{d}\chi \, \mathrm{d}w & \\ - \left(1 - f_{p(i)}\right)\left(\mu_{w(i)} - \overline{w}\right)\frac{1}{C_{\text{accr}}}\overline{\left.\frac{\partial r_r}{\partial t}\right|_{\text{accr}}} \Bigg), & \end{aligned} \tag{E12}$$

where $\mu_{w(i)}$ is the mean of w in the ith PDF component.

The integral equation for the covariance of r_t and accretion rate involves the PDF-variables r_t, θ_l, and r_r. The equation is

$$\overline{r_t' \left.\frac{\partial r_r}{\partial t}\right|'_{\text{accr}}} = \int_{-\infty}^{\infty}\int_{-\infty}^{\infty}\int_{0}^{\infty}\left(r_t - \overline{r_t}\right)\left(\left.\frac{\partial r_r}{\partial t}\right|_{\text{accr}} - \overline{\left.\frac{\partial r_r}{\partial t}\right|_{\text{accr}}}\right) P\left(r_t, \theta_l, r_r\right) \mathrm{d}r_r \, \mathrm{d}\theta_l \, \mathrm{d}r_t. \tag{E13}$$

The PDF is transformed (in each component) from r_t and θ_l coordinates to χ and η coordi-

nates. The equation becomes

$$\overline{r_t' \left.\frac{\partial r_r}{\partial t}\right|_{\text{accr}}'} = \sum_{i=1}^{n} \xi_{(i)} \int_{-\infty}^{\infty}\int_{-\infty}^{\infty}\int_{0}^{\infty} \left(\mu_{r_t(i)} - \overline{r_t} + \frac{\left(\eta - \mu_{\eta(i)}\right) + \left(\chi - \mu_{\chi(i)}\right)}{2c_{r_t(i)}} \right) \times \left(C_{\text{accr}}\, \chi^{\alpha} \left(H\left(\chi\right)\right)^{\alpha} r_r^{\beta} - \overline{\left.\frac{\partial r_r}{\partial t}\right|_{\text{accr}}} \right) \times P_{(i)}\left(\eta, \chi, r_r\right) \mathrm{d}r_r \, \mathrm{d}\chi \, \mathrm{d}\eta. \tag{E14}$$

The equation for the covariance of r_t and accretion rate can ultimately be written as

$$\begin{aligned} \overline{r_t' \left.\frac{\partial r_r}{\partial t}\right|_{\text{accr}}'} = {} & C_{\text{accr}} \sum_{i=1}^{n} \xi_{(i)} f_{p(i)} \\ & \times \left(\frac{1}{2c_{r_t(i)}} \int_{-\infty}^{\infty}\int_{-\infty}^{\infty}\int_{0}^{\infty} \left(\eta - \mu_{\eta(i)}\right) \left(\chi^{\alpha} \left(H\left(\chi\right)\right)^{\alpha} r_r^{\beta} - \frac{1}{C_{\text{accr}}} \overline{\left.\frac{\partial r_r}{\partial t}\right|_{\text{accr}}} \right) \right. \\ & \qquad \left. \times P_{NNL(i)}\left(\eta, \chi, r_r\right) \mathrm{d}r_r \, \mathrm{d}\chi \, \mathrm{d}\eta \right. \\ & + \frac{1}{2c_{r_t(i)}} \int_{0}^{\infty}\int_{0}^{\infty} \chi^{\alpha+1} r_r^{\beta} P_{NL(i)}\left(\chi, r_r\right) \mathrm{d}r_r \, \mathrm{d}\chi \\ & + \left. \left(\mu_{r_t(i)} - \overline{r_t} - \frac{\mu_{\chi(i)}}{2c_{r_t(i)}} \right) \int_{0}^{\infty}\int_{0}^{\infty} \chi^{\alpha} r_r^{\beta} P_{NL(i)}\left(\chi, r_r\right) \mathrm{d}r_r \, \mathrm{d}\chi \right). \end{aligned} \tag{E15}$$

The integral equation for the covariance of θ_l and accretion rate involves the PDF-variables r_t, θ_l, and r_r. The equation is

$$\overline{\theta_l' \left.\frac{\partial r_r}{\partial t}\right|_{\text{accr}}'} = \int_{-\infty}^{\infty}\int_{-\infty}^{\infty}\int_{0}^{\infty} \left(\theta_l - \overline{\theta_l}\right) \left(\left.\frac{\partial r_r}{\partial t}\right|_{\text{accr}} - \overline{\left.\frac{\partial r_r}{\partial t}\right|_{\text{accr}}} \right) P\left(r_t, \theta_l, r_r\right) \mathrm{d}r_r \, \mathrm{d}\theta_l \, \mathrm{d}r_t. \tag{E16}$$

A PDF transformation takes place in each component, changing coordinates from r_t and θ_l

to χ and η. The equation becomes

$$\overline{\theta_l' \left.\frac{\partial r_r}{\partial t}\right|'_{\text{accr}}} = \sum_{i=1}^{n} \xi_{(i)} \int_{-\infty}^{\infty}\int_{-\infty}^{\infty}\int_{0}^{\infty} \left(\mu_{\theta_l(i)} - \overline{\theta_l} + \frac{\left(\eta - \mu_{\eta(i)}\right) - \left(\chi - \mu_{\chi(i)}\right)}{2c_{\theta_l(i)}} \right) \times \left(C_{\text{accr}}\, \chi^{\alpha} \left(H\left(\chi\right)\right)^{\alpha} r_r^{\beta} - \overline{\left.\frac{\partial r_r}{\partial t}\right|_{\text{accr}}} \right) \times P_{(i)}\left(\eta, \chi, r_r\right) \mathrm{d}r_r \, \mathrm{d}\chi \, \mathrm{d}\eta. \tag{E17}$$

The equation for the covariance of θ_l and accretion rate can ultimately be written as

$$\begin{aligned}\overline{\theta_l' \left.\frac{\partial r_r}{\partial t}\right|'_{\text{accr}}} = {} & C_{\text{accr}} \sum_{i=1}^{n} \xi_{(i)} f_{p(i)} \\ & \times \left(\frac{1}{2c_{\theta_l(i)}} \int_{-\infty}^{\infty}\int_{-\infty}^{\infty}\int_{0}^{\infty} \left(\eta - \mu_{\eta(i)}\right) \left(\chi^{\alpha} \left(H\left(\chi\right)\right)^{\alpha} r_r^{\beta} - \frac{1}{C_{\text{accr}}} \overline{\left.\frac{\partial r_r}{\partial t}\right|_{\text{accr}}} \right) \right. \\ & \qquad \left. \times P_{NNL(i)}\left(\eta, \chi, r_r\right) \mathrm{d}r_r \, \mathrm{d}\chi \, \mathrm{d}\eta \right. \\ & - \frac{1}{2c_{\theta_l(i)}} \int_{0}^{\infty}\int_{0}^{\infty} \chi^{\alpha+1} r_r^{\beta} P_{NL(i)}\left(\chi, r_r\right) \mathrm{d}r_r \, \mathrm{d}\chi \\ & \left. + \left(\mu_{\theta_l(i)} - \overline{\theta_l} + \frac{\mu_{\chi(i)}}{2c_{\theta_l(i)}} \right) \int_{0}^{\infty}\int_{0}^{\infty} \chi^{\alpha} r_r^{\beta} P_{NL(i)}\left(\chi, r_r\right) \mathrm{d}r_r \, \mathrm{d}\chi \right). \end{aligned} \tag{E18}$$

E.3 Covariances involving evaporation rate

The general form of the KK equation for evaporation rate is the product of a coefficient and $S^{\alpha}\left(H\left(-S\right)\right)^{\alpha} r_r^{\beta} N_r^{\gamma}$ (where for KK, $\alpha = 1$, $\beta = 1/3$, and $\gamma = 2/3$). Supersaturation, S, is the ratio of water vapor pressure over saturation vapor pressure (with respect to liquid water), minus 1, so that S is positive when air is supersaturated and negative when air is subsaturated. The Heaviside step function has been added to allow for only evaporation of rain, not condensational growth. The integral equation for the covariance of w and

evaporation rate involves the PDF-variables w, r_t, θ_l, r_r, and N_r. The equation is

$$\overline{w' \left.\frac{\partial r_r}{\partial t}\right|'_{\text{evap}}} = \int_{-\infty}^{\infty}\int_{-\infty}^{\infty}\int_{-\infty}^{\infty}\int_{0}^{\infty}\int_{0}^{\infty}\left(w - \overline{w}\right)\left(\left.\frac{\partial r_r}{\partial t}\right|_{\text{evap}} - \overline{\left.\frac{\partial r_r}{\partial t}\right|_{\text{evap}}}\right) \times P\left(w, r_t, \theta_l, r_r, N_r\right) \mathrm{d}N_r \, \mathrm{d}r_r \, \mathrm{d}\theta_l \, \mathrm{d}r_t \, \mathrm{d}w. \tag{E19}$$

The PDF is transformed and a substitution is made that relates S to χ, as given by Eq. (A47). The equation becomes

$$\overline{w' \left.\frac{\partial r_r}{\partial t}\right|'_{\text{evap}}} = \sum_{i=1}^{n} \xi_{(i)} \int_{-\infty}^{\infty}\int_{-\infty}^{\infty}\int_{-\infty}^{\infty}\int_{0}^{\infty}\int_{0}^{\infty}\left(w - \overline{w}\right)\left(C_{\text{evap}} \, \chi^{\alpha} \left(H\left(-\chi\right)\right)^{\alpha} r_r^{\beta} N_r^{\gamma} - \overline{\left.\frac{\partial r_r}{\partial t}\right|_{\text{evap}}}\right) \times P_{(i)}\left(w, \chi, \eta, r_r, N_r\right) \mathrm{d}N_r \, \mathrm{d}r_r \, \mathrm{d}\eta \, \mathrm{d}\chi \, \mathrm{d}w. \tag{E20}$$

The coefficient C_{evap} is given by Eq. (C21). The variable η is integrated out of the PDF, and the integral equation for the covariance of w and evaporation rate is

$$\begin{aligned}\overline{w' \left.\frac{\partial r_r}{\partial t}\right|'_{\text{evap}}} &= C_{\text{evap}} \sum_{i=1}^{n} \xi_{(i)} \\ &\times \left(f_{p(i)} \int_{-\infty}^{\infty}\int_{-\infty}^{\infty}\int_{0}^{\infty}\int_{0}^{\infty}\left(w - \overline{w}\right)\left(\chi^{\alpha}\left(H\left(-\chi\right)\right)^{\alpha} r_r^{\beta} N_r^{\gamma} - \frac{1}{C_{\text{evap}}}\overline{\left.\frac{\partial r_r}{\partial t}\right|_{\text{evap}}}\right) \times P_{NNLL(i)}\left(w, \chi, r_r, N_r\right) \mathrm{d}N_r \, \mathrm{d}r_r \, \mathrm{d}\chi \, \mathrm{d}w \right. \\ &\left. - \left(1 - f_{p(i)}\right)\left(\mu_{w(i)} - \overline{w}\right)\frac{1}{C_{\text{evap}}}\overline{\left.\frac{\partial r_r}{\partial t}\right|_{\text{evap}}} \right),\end{aligned} \tag{E21}$$

where $P_{NNLL(i)}\left(w, \chi, r_r, N_r\right)$ is the ith component quadrivariate PDF involving two normal variates and two lognormal variates.

The integral equation for the covariance of r_t and evaporation rate involves the PDF-

variables r_t, θ_l, r_r, and N_r. The equation is

$$\overline{r_t' \left.\frac{\partial r_r}{\partial t}\right|_{\text{evap}}'} = \int_{-\infty}^{\infty}\int_{-\infty}^{\infty}\int_{0}^{\infty}\int_{0}^{\infty}\left(r_t - \overline{r_t}\right)\left(\left.\frac{\partial r_r}{\partial t}\right|_{\text{evap}} - \overline{\left.\frac{\partial r_r}{\partial t}\right|_{\text{evap}}}\right) \times P\left(r_t, \theta_l, r_r, N_r\right) \mathrm{d}N_r \, \mathrm{d}r_r \, \mathrm{d}\theta_l \, \mathrm{d}r_t. \tag{E22}$$

The PDF is transformed, and Eq. (A24) is used to substitute for r_t. The equation becomes

$$\overline{r_t' \left.\frac{\partial r_r}{\partial t}\right|_{\text{evap}}'} = \sum_{i=1}^{n} \xi_{(i)} \int_{-\infty}^{\infty}\int_{-\infty}^{\infty}\int_{0}^{\infty}\int_{0}^{\infty}\left(\mu_{r_t(i)} - \overline{r_t} + \frac{\left(\eta - \mu_{\eta(i)}\right) + \left(\chi - \mu_{\chi(i)}\right)}{2c_{r_t(i)}}\right) \times \left(C_{\text{evap}} \, \chi^{\alpha} \left(H\left(-\chi\right)\right)^{\alpha} r_r^{\beta} N_r^{\gamma} - \overline{\left.\frac{\partial r_r}{\partial t}\right|_{\text{evap}}}\right) \times P_{(i)}\left(\eta, \chi, r_r, N_r\right) \mathrm{d}N_r \, \mathrm{d}r_r \, \mathrm{d}\chi \, \mathrm{d}\eta. \tag{E23}$$

The covariance equation for r_t and evaporation rate is split and simplified, resulting in

$$\begin{aligned}
&\overline{r_t' \left.\frac{\partial r_r}{\partial t}\right|_{\text{evap}}'} \\
&= C_{\text{evap}} \sum_{i=1}^{n} \xi_{(i)} f_{p(i)} \\
&\quad \times \left(\frac{1}{2c_{r_t(i)}} \int_{-\infty}^{\infty}\int_{-\infty}^{\infty}\int_{0}^{\infty}\int_{0}^{\infty} \left(\eta - \mu_{\eta(i)}\right) \left(\chi^{\alpha} \left(H\left(-\chi\right)\right)^{\alpha} r_r^{\beta} N_r^{\gamma} - \frac{1}{C_{\text{evap}}} \overline{\left.\frac{\partial r_r}{\partial t}\right|_{\text{evap}}}\right) \right. \\
&\qquad\qquad \times P_{NNLL(i)}\left(\eta, \chi, r_r, N_r\right) \mathrm{d}N_r \, \mathrm{d}r_r \, \mathrm{d}\chi \, \mathrm{d}\eta \\
&\qquad + \frac{1}{2c_{r_t(i)}} \int_{-\infty}^{0}\int_{0}^{\infty}\int_{0}^{\infty} \chi^{\alpha+1} r_r^{\beta} N_r^{\gamma} P_{NLL(i)}\left(\chi, r_r, N_r\right) \mathrm{d}N_r \, \mathrm{d}r_r \, \mathrm{d}\chi \\
&\qquad \left. + \left(\mu_{r_t(i)} - \overline{r_t} - \frac{\mu_{\chi(i)}}{2c_{r_t(i)}}\right) \int_{-\infty}^{0}\int_{0}^{\infty}\int_{0}^{\infty} \chi^{\alpha} r_r^{\beta} N_r^{\gamma} P_{NLL(i)}\left(\chi, r_r, N_r\right) \mathrm{d}N_r \, \mathrm{d}r_r \, \mathrm{d}\chi \right),
\end{aligned} \tag{E24}$$

where $P_{NLL(i)}\left(\chi, r_r, N_r\right)$ is the ith component trivariate PDF involving one normal variate and two lognormal variates.

The integral equation for the covariance of θ_l and evaporation rate involves the PDF-

variables r_t, θ_l, r_r, and N_r. The equation is

$$\overline{\theta_l' \left.\frac{\partial r_r}{\partial t}\right|_{\text{evap}}'} = \int_{-\infty}^{\infty}\int_{-\infty}^{\infty}\int_{0}^{\infty}\int_{0}^{\infty}\left(\theta_l - \overline{\theta_l}\right)\left(\left.\frac{\partial r_r}{\partial t}\right|_{\text{evap}} - \overline{\left.\frac{\partial r_r}{\partial t}\right|_{\text{evap}}}\right) \times P\left(r_t, \theta_l, r_r, N_r\right) \mathrm{d}N_r \, \mathrm{d}r_r \, \mathrm{d}\theta_l \, \mathrm{d}r_t. \tag{E25}$$

The PDF is transformed, and Eq. (A25) is used to substitute for θ_l. The equation becomes

$$\begin{aligned}\overline{\theta_l' \left.\frac{\partial r_r}{\partial t}\right|_{\text{evap}}'} = \sum_{i=1}^{n} \xi_{(i)} \int_{-\infty}^{\infty}\int_{-\infty}^{\infty}\int_{0}^{\infty}\int_{0}^{\infty}&\left(\mu_{\theta_l(i)} - \overline{\theta_l} + \frac{\left(\eta - \mu_{\eta(i)}\right) - \left(\chi - \mu_{\chi(i)}\right)}{2c_{\theta_l(i)}}\right) \\ &\times \left(C_{\text{evap}} \, \chi^{\alpha} \left(H\left(-\chi\right)\right)^{\alpha} r_r^{\beta} N_r^{\gamma} - \overline{\left.\frac{\partial r_r}{\partial t}\right|_{\text{evap}}}\right) \\ &\times P_{(i)}\left(\eta, \chi, r_r, N_r\right) \mathrm{d}N_r \, \mathrm{d}r_r \, \mathrm{d}\chi \, \mathrm{d}\eta.\end{aligned} \tag{E26}$$

The covariance equation for θ_l and evaporation rate is split and simplified, resulting in

$$\begin{aligned}&\overline{\theta_l' \left.\frac{\partial r_r}{\partial t}\right|_{\text{evap}}'} \\ &= C_{\text{evap}} \sum_{i=1}^{n} \xi_{(i)} f_{p(i)} \\ &\quad \times \left(\frac{1}{2c_{\theta_l(i)}} \int_{-\infty}^{\infty}\int_{-\infty}^{\infty}\int_{0}^{\infty}\int_{0}^{\infty}\left(\eta - \mu_{\eta(i)}\right)\left(\chi^{\alpha}\left(H\left(-\chi\right)\right)^{\alpha} r_r^{\beta} N_r^{\gamma} - \frac{1}{C_{\text{evap}}}\overline{\left.\frac{\partial r_r}{\partial t}\right|_{\text{evap}}}\right)\right. \\ &\qquad\qquad \left. \times P_{NNLL(i)}\left(\eta, \chi, r_r, N_r\right) \mathrm{d}N_r \, \mathrm{d}r_r \, \mathrm{d}\chi \, \mathrm{d}\eta\right. \\ &\quad - \frac{1}{2c_{\theta_l(i)}} \int_{-\infty}^{0}\int_{0}^{\infty}\int_{0}^{\infty} \chi^{\alpha+1} r_r^{\beta} N_r^{\gamma} P_{NLL(i)}\left(\chi, r_r, N_r\right) \mathrm{d}N_r \, \mathrm{d}r_r \, \mathrm{d}\chi \\ &\quad + \left(\mu_{\theta_l(i)} - \overline{\theta_l} + \frac{\mu_{\chi(i)}}{2c_{\theta_l(i)}}\right) \int_{-\infty}^{0}\int_{0}^{\infty}\int_{0}^{\infty} \chi^{\alpha} r_r^{\beta} N_r^{\gamma} P_{NLL(i)}\left(\chi, r_r, N_r\right) \mathrm{d}N_r \, \mathrm{d}r_r \, \mathrm{d}\chi\Bigg).\end{aligned} \tag{E27}$$

The set of covariance equations involving microphysics process rates still contain integrals of four general forms. The solutions to these integrals, including all special cases, are listed in Appendix J, and the functional forms of the PDFs are listed in Appendix F.

Appendix F: Functional Forms of PDFs

F.1 Functional Form of a Quadrivariate PDF

There is one type of quadrivariate PDF used in the equation set. It is quadrivariate normal-normal-lognormal-lognormal distribution, meaning that the individual marginal of x_1 is a normal distribution, the individual marginal of x_2 is a normal distribution, the individual marginal of x_3 is a lognormal distribution, and the individual marginal of x_4 is a lognormal distribution. The functional form of this type of PDF is given by:

$$P_{NNLL(i)}\left(x_1, x_2, x_3, x_4\right) = \frac{\exp\left\{-\frac{1}{2}\lambda_{NNLL}\right\}}{\left(2\pi\right)^2 \sigma_{x_1(i)}\sigma_{x_2(i)}\tilde{\sigma}_{x_3(i)}\tilde{\sigma}_{x_4(i)}C_{Q1}x_3x_4}; \tag{F1}$$

where:

$$\begin{aligned}\lambda_{NNLL} = \frac{1}{C_{Q1}^2}\Big[&C_{Q2}\left(x_1-\mu_{x_1(i)}\right)^2 + C_{Q3}\left(x_2-\mu_{x_2(i)}\right)^2 + C_{Q4}\left(\ln x_3-\tilde{\mu}_{x_3(i)}\right)^2 \\ &+ C_{Q5}\left(\ln x_4-\tilde{\mu}_{x_4(i)}\right)^2 + C_{Q6}\left(x_1-\mu_{x_1(i)}\right)\left(x_2-\mu_{x_2(i)}\right) \\ &+ C_{Q7}\left(x_1-\mu_{x_1(i)}\right)\left(\ln x_3-\tilde{\mu}_{x_3(i)}\right) + C_{Q8}\left(x_1-\mu_{x_1(i)}\right)\left(\ln x_4-\tilde{\mu}_{x_4(i)}\right) \\ &+ C_{Q9}\left(x_2-\mu_{x_2(i)}\right)\left(\ln x_3-\tilde{\mu}_{x_3(i)}\right) + C_{Q10}\left(x_2-\mu_{x_2(i)}\right)\left(\ln x_4-\tilde{\mu}_{x_4(i)}\right) \\ &+ C_{Q11}\left(\ln x_3-\tilde{\mu}_{x_3(i)}\right)\left(\ln x_4-\tilde{\mu}_{x_4(i)}\right)\Big];\end{aligned}$$

and where:

$$\begin{aligned}C_{Q1} = \Big[&1-\left(\rho_{x_1,x_2(i)}^2+\tilde{\rho}_{x_1,x_3(i)}^2+\tilde{\rho}_{x_1,x_4(i)}^2+\tilde{\rho}_{x_2,x_3(i)}^2+\tilde{\rho}_{x_2,x_4(i)}^2+\tilde{\rho}_{x_3,x_4(i)}^2\right) \\ &+ 2\rho_{x_1,x_2(i)}\tilde{\rho}_{x_1,x_3(i)}\tilde{\rho}_{x_2,x_3(i)} + 2\rho_{x_1,x_2(i)}\tilde{\rho}_{x_1,x_4(i)}\tilde{\rho}_{x_2,x_4(i)} \\ &+ 2\tilde{\rho}_{x_1,x_3(i)}\tilde{\rho}_{x_1,x_4(i)}\tilde{\rho}_{x_3,x_4(i)} + 2\tilde{\rho}_{x_2,x_3(i)}\tilde{\rho}_{x_2,x_4(i)}\tilde{\rho}_{x_3,x_4(i)} + \rho_{x_1,x_2(i)}^2\tilde{\rho}_{x_3,x_4(i)}^2 \\ &+ \tilde{\rho}_{x_1,x_3(i)}^2\tilde{\rho}_{x_2,x_4(i)}^2 + \tilde{\rho}_{x_1,x_4(i)}^2\tilde{\rho}_{x_2,x_3(i)}^2 - 2\rho_{x_1,x_2(i)}\tilde{\rho}_{x_1,x_3(i)}\tilde{\rho}_{x_2,x_4(i)}\tilde{\rho}_{x_3,x_4(i)} \\ &- 2\rho_{x_1,x_2(i)}\tilde{\rho}_{x_1,x_4(i)}\tilde{\rho}_{x_2,x_3(i)}\tilde{\rho}_{x_3,x_4(i)} - 2\tilde{\rho}_{x_1,x_3(i)}\tilde{\rho}_{x_1,x_4(i)}\tilde{\rho}_{x_2,x_3(i)}\tilde{\rho}_{x_2,x_4(i)}\Big]^{\frac{1}{2}};\end{aligned}$$

$$C_{Q2} = \frac{1}{\sigma^2_{x_1(i)}}\Big[1 - \big(\tilde{\rho}^2_{x_2,x_3(i)} + \tilde{\rho}^2_{x_2,x_4(i)} + \tilde{\rho}^2_{x_3,x_4(i)}\big) + 2\tilde{\rho}_{x_2,x_3(i)}\tilde{\rho}_{x_2,x_4(i)}\tilde{\rho}_{x_3,x_4(i)}\Big];$$

$$C_{Q3} = \frac{1}{\sigma^2_{x_2(i)}}\Big[1 - \big(\tilde{\rho}^2_{x_1,x_3(i)} + \tilde{\rho}^2_{x_1,x_4(i)} + \tilde{\rho}^2_{x_3,x_4(i)}\big) + 2\tilde{\rho}_{x_1,x_3(i)}\tilde{\rho}_{x_1,x_4(i)}\tilde{\rho}_{x_3,x_4(i)}\Big];$$

$$C_{Q4} = \frac{1}{\tilde{\sigma}^2_{x_3(i)}}\Big[1 - \big(\rho^2_{x_1,x_2(i)} + \tilde{\rho}^2_{x_1,x_4(i)} + \tilde{\rho}^2_{x_2,x_4(i)}\big) + 2\rho_{x_1,x_2(i)}\tilde{\rho}_{x_1,x_4(i)}\tilde{\rho}_{x_2,x_4(i)}\Big];$$

$$C_{Q5} = \frac{1}{\tilde{\sigma}^2_{x_4(i)}}\Big[1 - \big(\rho^2_{x_1,x_2(i)} + \tilde{\rho}^2_{x_1,x_3(i)} + \tilde{\rho}^2_{x_2,x_3(i)}\big) + 2\rho_{x_1,x_2(i)}\tilde{\rho}_{x_1,x_3(i)}\tilde{\rho}_{x_2,x_3(i)}\Big];$$

$$\begin{aligned} C_{Q6} = \frac{2}{\sigma_{x_1(i)}\sigma_{x_2(i)}}\Big(&\rho_{x_1,x_2(i)}\tilde{\rho}^2_{x_3,x_4(i)} - \tilde{\rho}_{x_1,x_4(i)}\tilde{\rho}_{x_2,x_3(i)}\tilde{\rho}_{x_3,x_4(i)} \\ &- \tilde{\rho}_{x_1,x_3(i)}\tilde{\rho}_{x_2,x_4(i)}\tilde{\rho}_{x_3,x_4(i)} + \tilde{\rho}_{x_1,x_3(i)}\tilde{\rho}_{x_2,x_3(i)} + \tilde{\rho}_{x_1,x_4(i)}\tilde{\rho}_{x_2,x_4(i)} \\ &- \rho_{x_1,x_2(i)}\Big); \end{aligned}$$

$$\begin{aligned} C_{Q7} = \frac{2}{\sigma_{x_1(i)}\tilde{\sigma}_{x_3(i)}}\Big(&\tilde{\rho}_{x_1,x_3(i)}\tilde{\rho}^2_{x_2,x_4(i)} - \rho_{x_1,x_2(i)}\tilde{\rho}_{x_2,x_4(i)}\tilde{\rho}_{x_3,x_4(i)} \\ &- \tilde{\rho}_{x_1,x_4(i)}\tilde{\rho}_{x_2,x_3(i)}\tilde{\rho}_{x_2,x_4(i)} + \rho_{x_1,x_2(i)}\tilde{\rho}_{x_2,x_3(i)} + \tilde{\rho}_{x_1,x_4(i)}\tilde{\rho}_{x_3,x_4(i)} \\ &- \tilde{\rho}_{x_1,x_3(i)}\Big); \end{aligned}$$

$$\begin{aligned} C_{Q8} = \frac{2}{\sigma_{x_1(i)}\tilde{\sigma}_{x_4(i)}}\Big(&\tilde{\rho}_{x_1,x_4(i)}\tilde{\rho}^2_{x_2,x_3(i)} - \rho_{x_1,x_2(i)}\tilde{\rho}_{x_2,x_3(i)}\tilde{\rho}_{x_3,x_4(i)} \\ &- \tilde{\rho}_{x_1,x_3(i)}\tilde{\rho}_{x_2,x_3(i)}\tilde{\rho}_{x_2,x_4(i)} + \rho_{x_1,x_2(i)}\tilde{\rho}_{x_2,x_4(i)} + \tilde{\rho}_{x_1,x_3(i)}\tilde{\rho}_{x_3,x_4(i)} \\ &- \tilde{\rho}_{x_1,x_4(i)}\Big); \end{aligned}$$

$$\begin{aligned} C_{Q9} = \frac{2}{\sigma_{x_2(i)}\tilde{\sigma}_{x_3(i)}}\Big(&\tilde{\rho}^2_{x_1,x_4(i)}\tilde{\rho}_{x_2,x_3(i)} - \rho_{x_1,x_2(i)}\tilde{\rho}_{x_1,x_4(i)}\tilde{\rho}_{x_3,x_4(i)} \\ &- \tilde{\rho}_{x_1,x_3(i)}\tilde{\rho}_{x_1,x_4(i)}\tilde{\rho}_{x_2,x_4(i)} + \tilde{\rho}_{x_2,x_4(i)}\tilde{\rho}_{x_3,x_4(i)} + \rho_{x_1,x_2(i)}\tilde{\rho}_{x_1,x_3(i)} \\ &- \tilde{\rho}_{x_2,x_3(i)}\Big); \end{aligned}$$

$$\begin{aligned} C_{Q10} = \frac{2}{\sigma_{x_2(i)}\tilde{\sigma}_{x_4(i)}}\Big(&\tilde{\rho}^2_{x_1,x_3(i)}\tilde{\rho}_{x_2,x_4(i)} - \rho_{x_1,x_2(i)}\tilde{\rho}_{x_1,x_3(i)}\tilde{\rho}_{x_3,x_4(i)} \\ &- \tilde{\rho}_{x_1,x_3(i)}\tilde{\rho}_{x_1,x_4(i)}\tilde{\rho}_{x_2,x_3(i)} + \tilde{\rho}_{x_2,x_3(i)}\tilde{\rho}_{x_3,x_4(i)} + \rho_{x_1,x_2(i)}\tilde{\rho}_{x_1,x_4(i)} \\ &- \tilde{\rho}_{x_2,x_4(i)}\Big); \end{aligned}$$

$$C_{Q11} = \frac{2}{\tilde{\sigma}_{x_3(i)}\tilde{\sigma}_{x_4(i)}}\Big(\rho^2_{x_1,x_2(i)}\tilde{\rho}_{x_3,x_4(i)} - \rho_{x_1,x_2(i)}\tilde{\rho}_{x_1,x_4(i)}\tilde{\rho}_{x_2,x_3(i)} - \rho_{x_1,x_2(i)}\tilde{\rho}_{x_1,x_3(i)}\tilde{\rho}_{x_2,x_4(i)} + \tilde{\rho}_{x_2,x_3(i)}\tilde{\rho}_{x_2,x_4(i)} + \tilde{\rho}_{x_1,x_3(i)}\tilde{\rho}_{x_1,x_4(i)} - \tilde{\rho}_{x_3,x_4(i)}\Big).$$

In Eq. (F1), $\mu_{x_1(i)}$ is the mean of x_1 in the ith component, $\mu_{x_2(i)}$ is the mean of x_2 in the ith component, $\tilde{\mu}_{x_3(i)}$ is the mean of $\ln x_3$ in the ith component, and $\tilde{\mu}_{x_4(i)}$ is the mean of $\ln x_4$ in the ith component. The ith component standard deviation of x_1 is $\sigma_{x_1(i)}$, the ith component standard deviation of x_2 is $\sigma_{x_2(i)}$, the ith component standard deviation of $\ln x_3$ is $\tilde{\sigma}_{x_3(i)}$, and the ith component standard deviation of $\ln x_4$ is $\tilde{\sigma}_{x_4(i)}$. The ith component correlation of x_1 and x_2 is $\rho_{x_1,x_2(i)}$, the ith component correlation of x_1 and $\ln x_3$ is $\tilde{\rho}_{x_1,x_3(i)}$, the ith component correlation of x_1 and $\ln x_4$ is $\tilde{\rho}_{x_1,x_4(i)}$, the ith component correlation of x_2 and $\ln x_3$ is $\tilde{\rho}_{x_2,x_3(i)}$, the ith component correlation of x_2 and $\ln x_4$ is $\tilde{\rho}_{x_2,x_4(i)}$, and the ith component correlation of $\ln x_3$ and $\ln x_4$ is $\tilde{\rho}_{x_3,x_4(i)}$.

F.2 Functional Form of Trivariate PDFs

There are two types of trivariate PDFs used in the equation set. The first one is a trivariate normal-normal-lognormal distribution, meaning that the individual marginal of x_1 is a normal distribution, the individual marginal of x_2 is a normal distribution, and the individual marginal of x_3 is a lognormal distribution. The functional form of this type of PDF is given by:

$$P_{NNL(i)}(x_1, x_2, x_3) = \frac{\exp\left\{-\frac{1}{2}\lambda_{NNL}\right\}}{(2\pi)^{\frac{3}{2}}\sigma_{x_1(i)}\sigma_{x_2(i)}\tilde{\sigma}_{x_3(i)}C_{T1}x_3}; \tag{F2}$$

where:

$$\lambda_{NNL} = \frac{1}{C_{T1}^2}\Big[C_{T2}\left(x_1 - \mu_{x_1(i)}\right)^2 + C_{T3}\left(x_2 - \mu_{x_2(i)}\right)^2 + C_{T4}\left(\ln x_3 - \tilde{\mu}_{x_3(i)}\right)^2 + C_{T5}\left(x_1 - \mu_{x_1(i)}\right)\left(x_2 - \mu_{x_2(i)}\right) + C_{T6}\left(x_1 - \mu_{x_1(i)}\right)\left(\ln x_3 - \tilde{\mu}_{x_3(i)}\right) + C_{T7}\left(x_2 - \mu_{x_2(i)}\right)\left(\ln x_3 - \tilde{\mu}_{x_3(i)}\right)\Big];$$

and where:

$$C_{T1} = \left[1 - \left(\rho_{x_1,x_2(i)}^2 + \tilde{\rho}_{x_1,x_3(i)}^2 + \tilde{\rho}_{x_2,x_3(i)}^2\right) + 2\rho_{x_1,x_2(i)}\tilde{\rho}_{x_1,x_3(i)}\tilde{\rho}_{x_2,x_3(i)}\right]^{\frac{1}{2}};$$

$$C_{T2} = \frac{1 - \tilde{\rho}_{x_2,x_3(i)}^2}{\sigma_{x_1(i)}^2}; \qquad C_{T3} = \frac{1 - \tilde{\rho}_{x_1,x_3(i)}^2}{\sigma_{x_2(i)}^2}; \qquad C_{T4} = \frac{1 - \rho_{x_1,x_2(i)}^2}{\tilde{\sigma}_{x_3(i)}^2};$$

$$C_{T5} = \frac{2\left(\tilde{\rho}_{x_1,x_3(i)}\tilde{\rho}_{x_2,x_3(i)} - \rho_{x_1,x_2(i)}\right)}{\sigma_{x_{1(i)}}\sigma_{x_{2(i)}}}; \quad C_{T6} = \frac{2\left(\rho_{x_1,x_2(i)}\tilde{\rho}_{x_2,x_3(i)} - \tilde{\rho}_{x_1,x_3(i)}\right)}{\sigma_{x_{1(i)}}\tilde{\sigma}_{x_{3(i)}}};$$

$$\text{and} \qquad C_{T7} = \frac{2\left(\rho_{x_1,x_2(i)}\tilde{\rho}_{x_1,x_3(i)} - \tilde{\rho}_{x_2,x_3(i)}\right)}{\sigma_{x_{2(i)}}\tilde{\sigma}_{x_{3(i)}}}.$$

In Eq. (F2), $\mu_{x_1(i)}$ is the mean of x_1 in the ith component, $\mu_{x_2(i)}$ is the mean of x_2 in the ith component, and $\tilde{\mu}_{x_3(i)}$ is the mean of $\ln x_3$ in the ith component. The ith component standard deviation of x_1 is $\sigma_{x_1(i)}$, the ith component standard deviation of x_2 is $\sigma_{x_2(i)}$, and the ith component standard deviation of $\ln x_3$ is $\tilde{\sigma}_{x_3(i)}$. The ith component correlation of x_1 and x_2 is $\rho_{x_1,x_2(i)}$, the ith component correlation of x_1 and $\ln x_3$ is $\tilde{\rho}_{x_1,x_3(i)}$, and the ith component correlation of x_2 and $\ln x_3$ is $\tilde{\rho}_{x_2,x_3(i)}$.

The second type of trivariate PDF used in the equation set is a trivariate normal-lognormal-lognormal distribution, meaning that the individual marginal of x_1 is a normal distribution, the individual marginal of x_2 is a lognormal distribution, and the individual marginal of x_3 is a lognormal distribution. The functional form of this type of PDF is given by:

$$P_{NLL(i)}\left(x_1, x_2, x_3\right) = \frac{\exp\left\{-\frac{1}{2}\lambda_{NLL}\right\}}{(2\pi)^{\frac{3}{2}}\,\sigma_{x_1(i)}\tilde{\sigma}_{x_2(i)}\tilde{\sigma}_{x_3(i)}C_{t1}x_2x_3}; \tag{F3}$$

where:

$$\begin{aligned}\lambda_{NLL} = \frac{1}{C_{t1}^2}\Big[&C_{t2}\left(x_1 - \mu_{x_1(i)}\right)^2 + C_{t3}\left(\ln x_2 - \tilde{\mu}_{x_2(i)}\right)^2 + C_{t4}\left(\ln x_3 - \tilde{\mu}_{x_3(i)}\right)^2 \\ &+ C_{t5}\left(x_1 - \mu_{x_1(i)}\right)\left(\ln x_2 - \tilde{\mu}_{x_2(i)}\right) + C_{t6}\left(x_1 - \mu_{x_1(i)}\right)\left(\ln x_3 - \tilde{\mu}_{x_3(i)}\right) \\ &+ C_{t7}\left(\ln x_2 - \tilde{\mu}_{x_2(i)}\right)\left(\ln x_3 - \tilde{\mu}_{x_3(i)}\right)\Big];\end{aligned}$$

and where:

$$C_{t1} = \left[1 - \left(\tilde{\rho}^2_{x_1,x_2(i)} + \tilde{\rho}^2_{x_1,x_3(i)} + \tilde{\rho}^2_{x_2,x_3(i)}\right) + 2\tilde{\rho}_{x_1,x_2(i)}\tilde{\rho}_{x_1,x_3(i)}\tilde{\rho}_{x_2,x_3(i)}\right]^{\frac{1}{2}};$$

$$C_{t2} = \frac{1 - \tilde{\rho}^2_{x_2,x_3(i)}}{\sigma^2_{x_1(i)}}; \qquad C_{t3} = \frac{1 - \tilde{\rho}^2_{x_1,x_3(i)}}{\tilde{\sigma}^2_{x_2(i)}}; \qquad C_{t4} = \frac{1 - \tilde{\rho}^2_{x_1,x_2(i)}}{\tilde{\sigma}^2_{x_3(i)}};$$

$$C_{t5} = \frac{2\left(\tilde{\rho}_{x_1,x_3(i)}\tilde{\rho}_{x_2,x_3(i)} - \tilde{\rho}_{x_1,x_2(i)}\right)}{\sigma_{x_{1(i)}}\tilde{\sigma}_{x_{2(i)}}}; \quad C_{t6} = \frac{2\left(\tilde{\rho}_{x_1,x_2(i)}\tilde{\rho}_{x_2,x_3(i)} - \tilde{\rho}_{x_1,x_3(i)}\right)}{\sigma_{x_{1(i)}}\tilde{\sigma}_{x_{3(i)}}};$$

$$\text{and} \qquad C_{t7} = \frac{2\left(\tilde{\rho}_{x_1,x_2(i)}\tilde{\rho}_{x_1,x_3(i)} - \tilde{\rho}_{x_2,x_3(i)}\right)}{\tilde{\sigma}_{x_{2(i)}}\tilde{\sigma}_{x_{3(i)}}}.$$

In Eq. (F3), $\mu_{x_1(i)}$ is the mean of x_1 in the ith component, $\tilde{\mu}_{x_2(i)}$ is the mean of $\ln x_2$ in the ith component, and $\tilde{\mu}_{x_3(i)}$ is the mean of $\ln x_3$ in the ith component. The ith component standard deviation of x_1 is $\sigma_{x_1(i)}$, the ith component standard deviation of $\ln x_2$ is $\tilde{\sigma}_{x_2(i)}$, and the ith component standard deviation of $\ln x_3$ is $\tilde{\sigma}_{x_3(i)}$. The ith component correlation of x_1 and $\ln x_2$ is $\tilde{\rho}_{x_1,x_2(i)}$, the ith component correlation of x_1 and $\ln x_3$ is $\tilde{\rho}_{x_1,x_3(i)}$, and the ith component correlation of $\ln x_2$ and $\ln x_3$ is $\tilde{\rho}_{x_2,x_3(i)}$.

F.3 Functional Form of Bivariate PDFs

There are three types of bivariate PDFs used in the equation set. The first one is a bivariate normal distribution, meaning that the individual marginal for each of x_1 and x_2 is a normal distribution. The functional form of this type of PDF is given by:

$$P_{NN(i)}(x_1, x_2) = \frac{\exp\left\{-\frac{1}{2}\lambda_{NN}\right\}}{2\pi\sigma_{x_1(i)}\sigma_{x_2(i)}\left(1 - \rho^2_{x_1,x_2(i)}\right)^{\frac{1}{2}}}; \quad \text{where} \tag{F4}$$

$$\lambda_{NN} = \frac{1}{1 - \rho^2_{x_1,x_2(i)}}\left[\frac{1}{\sigma^2_{x_1(i)}}\left(x_1 - \mu_{x_1(i)}\right)^2 + \frac{1}{\sigma^2_{x_2(i)}}\left(x_2 - \mu_{x_2(i)}\right)^2 - \frac{2\rho_{x_1,x_2(i)}}{\sigma_{x_1(i)}\sigma_{x_2(i)}}\left(x_1 - \mu_{x_1(i)}\right)\left(x_2 - \mu_{x_2(i)}\right)\right];$$

where the ith component mean of x_1 is $\mu_{x_1(i)}$, the ith component mean of x_2 is $\mu_{x_2(i)}$, the ith component standard deviation of x_1 is $\sigma_{x_1(i)}$, the ith component standard deviation of x_2 is $\sigma_{x_2(i)}$, and the ith component correlation of x_1 and x_2 is $\rho_{x_1,x_2(i)}$.

The second type of bivariate PDF used in the equation set is a bivariate normal-lognormal distribution, meaning that the individual marginal of x_1 is a normal distribution and the individual marginal of x_2 is a lognormal distribution. The functional form of this type of PDF is given by:

$$P_{NL(i)}\left(x_1, x_2\right) = \frac{\exp\left\{-\frac{1}{2}\lambda_{NL}\right\}}{2\pi\sigma_{x_1(i)}\tilde{\sigma}_{x_2(i)}\left(1-\tilde{\rho}^2_{x_1,x_2(i)}\right)^{\frac{1}{2}} x_2}; \quad \text{where} \tag{F5}$$

$$\lambda_{NL} = \frac{1}{1-\tilde{\rho}^2_{x_1,x_2(i)}}\left[\frac{1}{\sigma^2_{x_1(i)}}\left(x_1-\mu_{x_1(i)}\right)^2 + \frac{1}{\tilde{\sigma}^2_{x_2(i)}}\left(\ln x_2-\tilde{\mu}_{x_2(i)}\right)^2 - \frac{2\tilde{\rho}_{x_1,x_2(i)}}{\sigma_{x_1(i)}\tilde{\sigma}_{x_2(i)}}\left(x_1-\mu_{x_1(i)}\right)\left(\ln x_2-\tilde{\mu}_{x_2(i)}\right)\right];$$

where the ith component mean of x_1 is $\mu_{x_1(i)}$, the ith component mean of $\ln x_2$ is $\tilde{\mu}_{x_2(i)}$, the ith component standard deviation of x_1 is $\sigma_{x_1(i)}$, the ith component standard deviation of $\ln x_2$ is $\tilde{\sigma}_{x_2(i)}$, and the ith component correlation of x_1 and $\ln x_2$ is $\tilde{\rho}_{x_1,x_2(i)}$.

The third type of bivariate PDF used in the equation set is a bivariate lognormal distribution, meaning that the individual marginal for each of x_1 and x_2 is a lognormal distribution. The functional form of this type of PDF is given by:

$$P_{LL(i)}\left(x_1, x_2\right) = \frac{\exp\left\{-\frac{1}{2}\lambda_{LL}\right\}}{2\pi\tilde{\sigma}_{x_1(i)}\tilde{\sigma}_{x_2(i)}\left(1-\tilde{\rho}^2_{x_1,x_2(i)}\right)^{\frac{1}{2}} x_1 x_2}; \quad \text{where} \tag{F6}$$

$$\lambda_{LL} = \frac{1}{1-\tilde{\rho}^2_{x_1,x_2(i)}}\left[\frac{1}{\tilde{\sigma}^2_{x_1(i)}}\left(\ln x_1-\tilde{\mu}_{x_1(i)}\right)^2 + \frac{1}{\tilde{\sigma}^2_{x_2(i)}}\left(\ln x_2-\tilde{\mu}_{x_2(i)}\right)^2 - \frac{2\tilde{\rho}_{x_1,x_2(i)}}{\tilde{\sigma}_{x_1(i)}\tilde{\sigma}_{x_2(i)}}\left(\ln x_1-\tilde{\mu}_{x_1(i)}\right)\left(\ln x_2-\tilde{\mu}_{x_2(i)}\right)\right];$$

where the ith component mean of $\ln x_1$ is $\tilde{\mu}_{x_1(i)}$, the ith component mean of $\ln x_2$ is $\tilde{\mu}_{x_2(i)}$, the

ith component standard deviation of $\ln x_1$ is $\tilde{\sigma}_{x_1(i)}$, the ith component standard deviation of $\ln x_2$ is $\tilde{\sigma}_{x_2(i)}$, and the ith component correlation of $\ln x_1$ and $\ln x_2$ is $\tilde{\rho}_{x_1,x_2(i)}$.

F.4 Functional Form of Single-Variable PDFs

There are two types of single-variable (univariate) PDFs used in the equation set. The first one is a normal distribution. The functional form of this type of PDF is given by:

$$P_{N(i)}(x) = \frac{1}{(2\pi)^{\frac{1}{2}}\,\sigma_{x(i)}} \exp\left\{\frac{-\left(x-\mu_{x(i)}\right)^2}{2\,\sigma_{x(i)}^2}\right\}; \tag{F7}$$

where the ith component mean of x is $\mu_{x(i)}$ and the ith component standard deviation of x is $\sigma_{x(i)}$. The second type of univariate PDF used in this equation set is a lognormal distribution. If the natural logarithm was taken for every point in a lognormal distribution, the resulting distribution would be a normal distribution. The functional form of this type of PDF is given by:

$$P_{L(i)}(x) = \frac{1}{(2\pi)^{\frac{1}{2}}\,\tilde{\sigma}_{x(i)}\,x} \exp\left\{\frac{-\left(\ln x-\tilde{\mu}_{x(i)}\right)^2}{2\,\tilde{\sigma}_{x(i)}^2}\right\}; \tag{F8}$$

where the ith component mean of $\ln x$ is $\tilde{\mu}_{x(i)}$ and the ith component standard deviation of $\ln x$ is $\tilde{\sigma}_{x(i)}$.

Appendix G: Integrals

G.1 Integrals of the form $\int_a^b x^p e^{-x^2}\ \mathrm{d}x$

In the following equations, p is an integer, where $p \geq 0$, a is the lower limit of integration, b is the upper limit of integration, $\mathrm{erf}\,(x)$ is the error function, and e^x is the exponential function.

$$\int_a^b x^p e^{-x^2}\ \mathrm{d}x = \begin{cases} \dfrac{1}{2}\left(\displaystyle\sum_{t=0}^{\frac{p-1}{2}} \frac{\left(\frac{p-1}{2}\right)!}{t!}\, a^{2t} e^{-a^2} \right. \\ \qquad \left. - \displaystyle\sum_{t=0}^{\frac{p-1}{2}} \frac{\left(\frac{p-1}{2}\right)!}{t!}\, b^{2t} e^{-b^2} \right);\ \text{where p is odd;} \\ \dfrac{1}{2}\left(\displaystyle\sum_{t=1}^{\frac{p}{2}} \frac{p!\ t!}{\left(\frac{p}{2}\right)!\ (2t)!\, 2^{p-2t}}\, a^{2t-1} e^{-a^2} \right. \\ \qquad \left. - \displaystyle\sum_{t=1}^{\frac{p}{2}} \frac{p!\ t!}{\left(\frac{p}{2}\right)!\ (2t)!\, 2^{p-2t}}\, b^{2t-1} e^{-b^2} \right) \\ + \dfrac{p!}{\left(\frac{p}{2}\right)!\, 2^p} \dfrac{\sqrt{\pi}}{2} \Big(\mathrm{erf}\,(b) - \mathrm{erf}\,(a) \Big);\ \text{where p is even.} \end{cases} \tag{G1}$$

$$\int_a^b x e^{-x^2}\ \mathrm{d}x = \frac{1}{2}\left(e^{-a^2} - e^{-b^2} \right) \tag{G2}$$

$$\int_a^b e^{-x^2}\ \mathrm{d}x = \frac{\sqrt{\pi}}{2} \Big(\mathrm{erf}\,(b) - \mathrm{erf}\,(a) \Big) \tag{G3}$$

$$\int_{-\infty}^{\infty} x^p e^{-x^2}\ \mathrm{d}x = \begin{cases} 0;\ \text{where p is odd;} \\ \dfrac{p!}{\left(\frac{p}{2}\right)!\, 2^p} \sqrt{\pi};\ \text{where p is even.} \end{cases} \tag{G4}$$

$$\int_{-\infty}^{\infty} xe^{-x^2}\,\mathrm{d}x = 0 \tag{G5}$$

$$\int_{-\infty}^{\infty} e^{-x^2}\,\mathrm{d}x = \sqrt{\pi} \tag{G6}$$

$$\int_{0}^{\infty} x^p e^{-x^2}\,\mathrm{d}x = \begin{cases} \dfrac{1}{2}\left(\dfrac{p-1}{2}\right)!\,; \text{ where p is odd;} \\ \dfrac{p!}{\left(\frac{p}{2}\right)!\,2^p}\dfrac{\sqrt{\pi}}{2}; \text{ where p is even.} \end{cases} \tag{G7}$$

$$\int_{0}^{\infty} xe^{-x^2}\,\mathrm{d}x = \frac{1}{2} \tag{G8}$$

$$\int_{0}^{\infty} e^{-x^2}\,\mathrm{d}x = \frac{\sqrt{\pi}}{2} \tag{G9}$$

$$\int_{-\infty}^{0} x^p e^{-x^2}\,\mathrm{d}x = \begin{cases} -\dfrac{1}{2}\left(\dfrac{p-1}{2}\right)!\,; \text{ where p is odd;} \\ \dfrac{p!}{\left(\frac{p}{2}\right)!\,2^p}\dfrac{\sqrt{\pi}}{2}; \text{ where p is even.} \end{cases} \tag{G10}$$

$$\int_{-\infty}^{0} xe^{-x^2}\,\mathrm{d}x = -\frac{1}{2} \tag{G11}$$

$$\int_{-\infty}^{0} e^{-x^2}\,\mathrm{d}x = \frac{\sqrt{\pi}}{2} \tag{G12}$$

$$\int_{a}^{\infty} x^p e^{-x^2}\,\mathrm{d}x = \begin{cases} \dfrac{1}{2}\displaystyle\sum_{t=0}^{\frac{p-1}{2}} \frac{\left(\frac{p-1}{2}\right)!}{t!}\,a^{2t}e^{-a^2}; \text{ where p is odd;} \\ \dfrac{1}{2}\displaystyle\sum_{t=1}^{\frac{p}{2}} \frac{p!\;t!}{\left(\frac{p}{2}\right)!\;(2t)!\,2^{p-2t}}\,a^{2t-1}e^{-a^2} \\ \quad + \dfrac{p!}{\left(\frac{p}{2}\right)!\,2^p}\dfrac{\sqrt{\pi}}{2}\Big(1-\operatorname{erf}(a)\Big); \text{ where p is even.} \end{cases} \tag{G13}$$

$$\int_{a}^{\infty} xe^{-x^2}\,\mathrm{d}x = \frac{1}{2}e^{-a^2} \tag{G14}$$

$$\int_{a}^{\infty} e^{-x^2}\,\mathrm{d}x = \frac{\sqrt{\pi}}{2}\Bigg(1-\operatorname{erf}(a)\Bigg) \tag{G15}$$

$$\int_{-\infty}^{b} x^p e^{-x^2}\,\mathrm{d}x = \begin{cases} -\dfrac{1}{2}\displaystyle\sum_{t=0}^{\frac{p-1}{2}} \frac{\left(\frac{p-1}{2}\right)!}{t!}\, b^{2t} e^{-b^2};\ \text{where p is odd;} \\ -\dfrac{1}{2}\displaystyle\sum_{t=1}^{\frac{p}{2}} \frac{p!\ t!}{\left(\frac{p}{2}\right)!\ (2t)!\, 2^{p-2t}}\, b^{2t-1} e^{-b^2} \\ +\dfrac{p!}{\left(\frac{p}{2}\right)!\, 2^p}\dfrac{\sqrt{\pi}}{2}\Bigg(1+\operatorname{erf}(b)\Bigg);\ \text{where p is even.} \end{cases} \tag{G16}$$

$$\int_{-\infty}^{b} x e^{-x^2}\,\mathrm{d}x = -\frac{1}{2}e^{-b^2} \tag{G17}$$

$$\int_{-\infty}^{b} e^{-x^2}\,\mathrm{d}x = \frac{\sqrt{\pi}}{2}\Bigg(1+\operatorname{erf}(b)\Bigg) \tag{G18}$$

$$\int_{0}^{b} x^p e^{-x^2}\,\mathrm{d}x = \begin{cases} \dfrac{1}{2}\left(\dfrac{p-1}{2}\right)! - \dfrac{1}{2}\displaystyle\sum_{t=0}^{\frac{p-1}{2}} \frac{\left(\frac{p-1}{2}\right)!}{t!}\, b^{2t} e^{-b^2};\ \text{where p is odd;} \\ -\dfrac{1}{2}\displaystyle\sum_{t=1}^{\frac{p}{2}} \frac{p!\ t!}{\left(\frac{p}{2}\right)!\ (2t)!\, 2^{p-2t}}\, b^{2t-1} e^{-b^2} \\ +\dfrac{p!}{\left(\frac{p}{2}\right)!\, 2^p}\dfrac{\sqrt{\pi}}{2}\operatorname{erf}(b)\,;\ \text{where p is even.} \end{cases} \tag{G19}$$

$$\int_{0}^{b} x e^{-x^2}\,\mathrm{d}x = \frac{1}{2}\left(1-e^{-b^2}\right) \tag{G20}$$

$$\int_{0}^{b} e^{-x^2}\,\mathrm{d}x = \frac{\sqrt{\pi}}{2}\operatorname{erf}(b) \tag{G21}$$

$$\int_a^0 x^p e^{-x^2}\,\mathrm{d}x = \begin{cases} \dfrac{1}{2}\displaystyle\sum_{t=0}^{\frac{p-1}{2}} \dfrac{\left(\frac{p-1}{2}\right)!}{t!}\, a^{2t} e^{-a^2} - \dfrac{1}{2}\left(\dfrac{p-1}{2}\right)!; \text{ where p is odd;} \\ \dfrac{1}{2}\displaystyle\sum_{t=1}^{\frac{p}{2}} \dfrac{p!\ t!}{\left(\frac{p}{2}\right)!\ (2t)!\, 2^{p-2t}}\, a^{2t-1} e^{-a^2} \\ -\dfrac{p!}{\left(\frac{p}{2}\right)!\, 2^p} \dfrac{\sqrt{\pi}}{2} \mathrm{erf}\,(a)\,; \text{ where p is even.} \end{cases} \tag{G22}$$

$$\int_a^0 x e^{-x^2}\,\mathrm{d}x = \frac{1}{2}\left(e^{-a^2} - 1\right) \tag{G23}$$

$$\int_a^0 e^{-x^2}\,\mathrm{d}x = -\frac{\sqrt{\pi}}{2}\,\mathrm{erf}\,(a) \tag{G24}$$

$$\int_{-b}^b x^p e^{-x^2}\,\mathrm{d}x = \begin{cases} 0; \text{ where p is odd;} \\ -\displaystyle\sum_{t=1}^{\frac{p}{2}} \dfrac{p!\ t!}{\left(\frac{p}{2}\right)!\ (2t)!\, 2^{p-2t}}\, b^{2t-1} e^{-b^2} \\ +\dfrac{p!}{\left(\frac{p}{2}\right)!\, 2^p} \sqrt{\pi}\,\mathrm{erf}\,(b)\,; \text{ where p is even.} \end{cases} \tag{G25}$$

$$\int_{-b}^b x e^{-x^2}\,\mathrm{d}x = 0 \tag{G26}$$

$$\int_{-b}^b e^{-x^2}\,\mathrm{d}x = \sqrt{\pi}\,\mathrm{erf}\,(b) \tag{G27}$$

G.2 Integrals of the form $\int_a^b e^{-Ax^2+Bx}\ \mathrm{d}x$

In the following equations, both A and B are coefficients, where $A > 0$, a is the lower limit of integration, b is the upper limit of integration, $\operatorname{erf}(x)$ is the error function, and the exponential function is written $\exp(x)$ or e^x.

$$\int_a^b e^{-Ax^2+Bx}\ \mathrm{d}x = \sqrt{\frac{\pi}{4A}}\ \exp\left\{\frac{B^2}{4A}\right\}\left(\operatorname{erf}\left(\sqrt{A}b - \frac{B}{2\sqrt{A}}\right) - \operatorname{erf}\left(\sqrt{A}a - \frac{B}{2\sqrt{A}}\right)\right) \tag{G28}$$

$$\int_{-\infty}^{\infty} e^{-Ax^2+Bx}\ \mathrm{d}x = \sqrt{\frac{\pi}{A}}\ \exp\left\{\frac{B^2}{4A}\right\} \tag{G29}$$

$$\int_0^{\infty} e^{-Ax^2+Bx}\ \mathrm{d}x = \sqrt{\frac{\pi}{4A}}\ \exp\left\{\frac{B^2}{4A}\right\}\left(1 + \operatorname{erf}\left(\frac{B}{2\sqrt{A}}\right)\right) \tag{G30}$$

$$\int_{-\infty}^{0} e^{-Ax^2+Bx}\ \mathrm{d}x = \sqrt{\frac{\pi}{4A}}\ \exp\left\{\frac{B^2}{4A}\right\}\left(1 - \operatorname{erf}\left(\frac{B}{2\sqrt{A}}\right)\right) \tag{G31}$$

$$\int_a^{\infty} e^{-Ax^2+Bx}\ \mathrm{d}x = \sqrt{\frac{\pi}{4A}}\ \exp\left\{\frac{B^2}{4A}\right\}\left(1 - \operatorname{erf}\left(\sqrt{A}a - \frac{B}{2\sqrt{A}}\right)\right) \tag{G32}$$

$$\int_{-\infty}^{b} e^{-Ax^2+Bx}\ \mathrm{d}x = \sqrt{\frac{\pi}{4A}}\ \exp\left\{\frac{B^2}{4A}\right\}\left(1 + \operatorname{erf}\left(\sqrt{A}b - \frac{B}{2\sqrt{A}}\right)\right) \tag{G33}$$

$$\int_0^{b} e^{-Ax^2+Bx}\ \mathrm{d}x = \sqrt{\frac{\pi}{4A}}\ \exp\left\{\frac{B^2}{4A}\right\}\left(\operatorname{erf}\left(\sqrt{A}b - \frac{B}{2\sqrt{A}}\right) + \operatorname{erf}\left(\frac{B}{2\sqrt{A}}\right)\right) \tag{G34}$$

$$\int_a^{0} e^{-Ax^2+Bx}\ \mathrm{d}x = \sqrt{\frac{\pi}{4A}}\ \exp\left\{\frac{B^2}{4A}\right\}\left(-\operatorname{erf}\left(\sqrt{A}a - \frac{B}{2\sqrt{A}}\right) - \operatorname{erf}\left(\frac{B}{2\sqrt{A}}\right)\right) \tag{G35}$$

$$\int_{-b}^{b} e^{-Ax^2+Bx}\ \mathrm{d}x = \sqrt{\frac{\pi}{4A}}\ \exp\left\{\frac{B^2}{4A}\right\}\left(\operatorname{erf}\left(\sqrt{A}b - \frac{B}{2\sqrt{A}}\right) + \operatorname{erf}\left(\sqrt{A}b + \frac{B}{2\sqrt{A}}\right)\right) \tag{G36}$$

G.3 Integrals of the form $\int_a^b x^p e^{-Ax^2+Bx}\ \mathrm{d}x$

In the following equations, p is an integer, where $p \geq 0$, both A and B are coefficients, where $A > 0$, a is the lower limit of integration, b is the upper limit of integration, $\operatorname{erf}(x)$ is the error function, and the exponential function is written $\exp(x)$ or e^x.

$$\int_a^b x^p e^{-Ax^2+Bx}\ \mathrm{d}x = \frac{1}{\sqrt{A}^{p+1}} \exp\left\{\frac{B^2}{4A}\right\} \sum_{r=0}^{p} \frac{p!}{(p-r)!\ r!} \left(\frac{B}{2\sqrt{A}}\right)^{p-r} \int_{\sqrt{A}a-\frac{B}{2\sqrt{A}}}^{\sqrt{A}b-\frac{B}{2\sqrt{A}}} y^r e^{-y^2} \mathrm{d}y \qquad \text{(G37)}$$

$$\begin{aligned}
&\int_a^b x^p e^{-Ax^2+Bx}\ \mathrm{d}x \\
&\quad = \frac{1}{\sqrt{A}^{p+1}} \exp\left\{\frac{B^2}{4A}\right\} \sum_{r=0}^{p} \frac{p!}{(p-r)!\ r!} \left(\frac{B}{2\sqrt{A}}\right)^{p-r} \\
&\qquad \times \begin{cases}
\dfrac{1}{2}\left(\displaystyle\sum_{t=0}^{\frac{r-1}{2}} \frac{\left(\frac{r-1}{2}\right)!}{t!} \left(\sqrt{A}a - \frac{B}{2\sqrt{A}}\right)^{2t} \exp\left\{-\left(\sqrt{A}a - \frac{B}{2\sqrt{A}}\right)^2\right\}\right. \\
\qquad \left. - \displaystyle\sum_{t=0}^{\frac{r-1}{2}} \frac{\left(\frac{r-1}{2}\right)!}{t!} \left(\sqrt{A}b - \frac{B}{2\sqrt{A}}\right)^{2t} \exp\left\{-\left(\sqrt{A}b - \frac{B}{2\sqrt{A}}\right)^2\right\}\right); \\
\text{when r is odd;} \\
\dfrac{1}{2}\left(\displaystyle\sum_{t=1}^{\frac{r}{2}} \frac{r!\ t!}{\left(\frac{r}{2}\right)!\ (2t)!\ 2^{r-2t}} \left(\sqrt{A}a - \frac{B}{2\sqrt{A}}\right)^{2t-1} \exp\left\{-\left(\sqrt{A}a - \frac{B}{2\sqrt{A}}\right)^2\right\}\right. \\
\qquad \left. - \displaystyle\sum_{t=1}^{\frac{r}{2}} \frac{r!\ t!}{\left(\frac{r}{2}\right)!\ (2t)!\ 2^{r-2t}} \left(\sqrt{A}b - \frac{B}{2\sqrt{A}}\right)^{2t-1} \exp\left\{-\left(\sqrt{A}b - \frac{B}{2\sqrt{A}}\right)^2\right\}\right) \\
\quad + \dfrac{r!}{\left(\frac{r}{2}\right)!\ 2^r} \dfrac{\sqrt{\pi}}{2} \left(\operatorname{erf}\left(\sqrt{A}b - \frac{B}{2\sqrt{A}}\right) - \operatorname{erf}\left(\sqrt{A}a - \frac{B}{2\sqrt{A}}\right)\right); \\
\text{when r is even.}
\end{cases}
\end{aligned} \qquad \text{(G38)}$$

$$\int_{-\infty}^{\infty} x^p e^{-Ax^2+Bx}\,\mathrm{d}x$$

$$= \frac{1}{\sqrt{A}^{p+1}} \exp\left\{\frac{B^2}{4A}\right\} \sum_{r=0}^{p} \frac{p!}{(p-r)!\; r!} \left(\frac{B}{2\sqrt{A}}\right)^{p-r} \begin{cases} 0; \text{ when r is odd;} \\ \dfrac{r!}{\left(\frac{r}{2}\right)!\, 2^r}\sqrt{\pi}; \text{ when r is even.} \end{cases} \tag{G39}$$

This can be rewritten as

$$\int_{-\infty}^{\infty} x^p e^{-Ax^2+Bx}\,\mathrm{d}x = \frac{\sqrt{\pi}}{\sqrt{A}^{p+1}} \exp\left\{\frac{B^2}{4A}\right\} \sum_{r=0}^{\lfloor \frac{p}{2} \rfloor} \frac{p!}{(p-2r)!\,(2r)!} \left(\frac{B}{2\sqrt{A}}\right)^{p-2r} \frac{(2r)!}{r!\, 2^{2r}}, \tag{G40}$$

and can be further rewritten as

$$\int_{-\infty}^{\infty} x^p e^{-Ax^2+Bx}\,\mathrm{d}x = \sqrt{\frac{\pi}{A}}\, \frac{1}{\left(2\sqrt{A}\right)^p} \exp\left\{\frac{B^2}{4A}\right\} \sum_{r=0}^{\lfloor \frac{p}{2} \rfloor} \frac{p!}{(p-2r)!\, r!} \left(\frac{B}{\sqrt{A}}\right)^{p-2r}. \tag{G41}$$

$$\int_{0}^{\infty} x^p e^{-Ax^2+Bx}\,\mathrm{d}x$$

$$= \frac{1}{\sqrt{A}^{p+1}} \exp\left\{\frac{B^2}{4A}\right\} \sum_{r=0}^{p} \frac{p!}{(p-r)!\; r!} \left(\frac{B}{2\sqrt{A}}\right)^{p-r}$$

$$\times \begin{cases} \dfrac{1}{2} \displaystyle\sum_{t=0}^{\frac{r-1}{2}} \frac{\left(\frac{r-1}{2}\right)!}{t!} \left(\frac{B^2}{4A}\right)^t \exp\left\{-\frac{B^2}{4A}\right\}; \text{ when r is odd;} \\ \dfrac{1}{2} \displaystyle\sum_{t=1}^{\frac{r}{2}} \frac{r!\; t!}{\left(\frac{r}{2}\right)!\; (2t)!\, 2^{r-2t}} \left(-\frac{B}{2\sqrt{A}}\right)^{2t-1} \exp\left\{-\frac{B^2}{4A}\right\} \\ \quad + \dfrac{r!}{\left(\frac{r}{2}\right)!\, 2^r} \dfrac{\sqrt{\pi}}{2} \left(1 - \operatorname{erf}\left(-\dfrac{B}{2\sqrt{A}}\right)\right); \text{ when r is even.} \end{cases} \tag{G42}$$

$$\int_{-\infty}^{0} x^p e^{-Ax^2+Bx}\,\mathrm{d}x$$

$$= \frac{1}{\sqrt{A}^{p+1}} \exp\left\{\frac{B^2}{4A}\right\} \sum_{r=0}^{p} \frac{p!}{(p-r)!\ r!} \left(\frac{B}{2\sqrt{A}}\right)^{p-r}$$

$$\times \begin{cases} -\frac{1}{2} \sum_{t=0}^{\frac{r-1}{2}} \frac{\left(\frac{r-1}{2}\right)!}{t!} \left(\frac{B^2}{4A}\right)^t \exp\left\{-\frac{B^2}{4A}\right\};\ \text{when r is odd;} \\ -\frac{1}{2} \sum_{t=1}^{\frac{r}{2}} \frac{r!\ t!}{\left(\frac{r}{2}\right)!\ (2t)!\, 2^{r-2t}} \left(-\frac{B}{2\sqrt{A}}\right)^{2t-1} \exp\left\{-\frac{B^2}{4A}\right\} \\ + \frac{r!}{\left(\frac{r}{2}\right)!\, 2^r} \frac{\sqrt{\pi}}{2} \left(1 + \operatorname{erf}\left(-\frac{B}{2\sqrt{A}}\right)\right);\ \text{when r is even.} \end{cases} \tag{G43}$$

$$\int_{a}^{\infty} x^p e^{-Ax^2+Bx}\,\mathrm{d}x$$

$$= \frac{1}{\sqrt{A}^{p+1}} \exp\left\{\frac{B^2}{4A}\right\} \sum_{r=0}^{p} \frac{p!}{(p-r)!\ r!} \left(\frac{B}{2\sqrt{A}}\right)^{p-r}$$

$$\times \begin{cases} \frac{1}{2} \sum_{t=0}^{\frac{r-1}{2}} \frac{\left(\frac{r-1}{2}\right)!}{t!} \left(\sqrt{A}a - \frac{B}{2\sqrt{A}}\right)^{2t} \exp\left\{-\left(\sqrt{A}a - \frac{B}{2\sqrt{A}}\right)^2\right\}; \\ \text{when r is odd;} \\ \frac{1}{2} \sum_{t=1}^{\frac{r}{2}} \frac{r!\ t!}{\left(\frac{r}{2}\right)!\ (2t)!\, 2^{r-2t}} \left(\sqrt{A}a - \frac{B}{2\sqrt{A}}\right)^{2t-1} \exp\left\{-\left(\sqrt{A}a - \frac{B}{2\sqrt{A}}\right)^2\right\} \\ + \frac{r!}{\left(\frac{r}{2}\right)!\, 2^r} \frac{\sqrt{\pi}}{2} \left(1 - \operatorname{erf}\left(\sqrt{A}a - \frac{B}{2\sqrt{A}}\right)\right); \\ \text{when r is even.} \end{cases} \tag{G44}$$

$$\int_{-\infty}^{b} x^p e^{-Ax^2+Bx}\,\mathrm{d}x$$

$$= \frac{1}{\sqrt{A}^{p+1}} \exp\left\{\frac{B^2}{4A}\right\} \sum_{r=0}^{p} \frac{p!}{(p-r)!\;r!} \left(\frac{B}{2\sqrt{A}}\right)^{p-r}$$

$$\times \begin{cases} -\frac{1}{2} \sum_{t=0}^{\frac{r-1}{2}} \frac{\left(\frac{r-1}{2}\right)!}{t!} \left(\sqrt{A}b - \frac{B}{2\sqrt{A}}\right)^{2t} \exp\left\{-\left(\sqrt{A}b - \frac{B}{2\sqrt{A}}\right)^2\right\}; \\ \text{when r is odd;} \\ -\frac{1}{2} \sum_{t=1}^{\frac{r}{2}} \frac{r!\;t!}{\left(\frac{r}{2}\right)!\;(2t)!\,2^{r-2t}} \left(\sqrt{A}b - \frac{B}{2\sqrt{A}}\right)^{2t-1} \exp\left\{-\left(\sqrt{A}b - \frac{B}{2\sqrt{A}}\right)^2\right\} \\ + \frac{r!}{\left(\frac{r}{2}\right)!\,2^r} \frac{\sqrt{\pi}}{2} \left(1 + \operatorname{erf}\left(\sqrt{A}b - \frac{B}{2\sqrt{A}}\right)\right); \\ \text{when r is even.} \end{cases} \tag{G45}$$

$$\int_0^b x^p e^{-Ax^2+Bx}\,\mathrm{d}x$$

$$= \frac{1}{\sqrt{A}^{p+1}} \exp\left\{\frac{B^2}{4A}\right\} \sum_{r=0}^{p} \frac{p!}{(p-r)!\ r!} \left(\frac{B}{2\sqrt{A}}\right)^{p-r}$$

$$\times \begin{cases} \dfrac{1}{2}\left(\displaystyle\sum_{t=0}^{\frac{r-1}{2}} \frac{\left(\frac{r-1}{2}\right)!}{t!} \left(\frac{B^2}{4A}\right)^t \exp\left\{-\frac{B^2}{4A}\right\} \right. \\ \qquad \left. - \displaystyle\sum_{t=0}^{\frac{r-1}{2}} \frac{\left(\frac{r-1}{2}\right)!}{t!} \left(\sqrt{A}b - \frac{B}{2\sqrt{A}}\right)^{2t} \exp\left\{-\left(\sqrt{A}b - \frac{B}{2\sqrt{A}}\right)^2\right\}\right); \\ \text{when r is odd;} \\ \dfrac{1}{2}\left(\displaystyle\sum_{t=1}^{\frac{r}{2}} \frac{r!\ t!}{\left(\frac{r}{2}\right)!\ (2t)!\ 2^{r-2t}} \left(-\frac{B}{2\sqrt{A}}\right)^{2t-1} \exp\left\{-\frac{B^2}{4A}\right\} \right. \\ \qquad \left. - \displaystyle\sum_{t=1}^{\frac{r}{2}} \frac{r!\ t!}{\left(\frac{r}{2}\right)!\ (2t)!\ 2^{r-2t}} \left(\sqrt{A}b - \frac{B}{2\sqrt{A}}\right)^{2t-1} \exp\left\{-\left(\sqrt{A}b - \frac{B}{2\sqrt{A}}\right)^2\right\}\right) \\ + \dfrac{r!}{\left(\frac{r}{2}\right)!\ 2^r} \dfrac{\sqrt{\pi}}{2}\left(\operatorname{erf}\left(\sqrt{A}b - \frac{B}{2\sqrt{A}}\right) + \operatorname{erf}\left(\frac{B}{2\sqrt{A}}\right)\right); \\ \text{when r is even.} \end{cases} \tag{G46}$$

$$\int_a^0 x^p e^{-Ax^2+Bx}\,\mathrm{d}x$$

$$= \frac{1}{\sqrt{A}^{p+1}} \exp\left\{\frac{B^2}{4A}\right\} \sum_{r=0}^{p} \frac{p!}{(p-r)!\ r!} \left(\frac{B}{2\sqrt{A}}\right)^{p-r}$$

$$\times \begin{cases} \dfrac{1}{2}\left(\displaystyle\sum_{t=0}^{\frac{r-1}{2}} \frac{\left(\frac{r-1}{2}\right)!}{t!} \left(\sqrt{A}a - \frac{B}{2\sqrt{A}}\right)^{2t} \exp\left\{-\left(\sqrt{A}a - \frac{B}{2\sqrt{A}}\right)^2\right\} \right. \\ \qquad \left. - \displaystyle\sum_{t=0}^{\frac{r-1}{2}} \frac{\left(\frac{r-1}{2}\right)!}{t!} \left(\frac{B^2}{4A}\right)^{t} \exp\left\{-\frac{B^2}{4A}\right\}\right); \\ \text{when r is odd;} \\ \dfrac{1}{2}\left(\displaystyle\sum_{t=1}^{\frac{r}{2}} \frac{r!\ t!}{\left(\frac{r}{2}\right)!\ (2t)!\, 2^{r-2t}} \left(\sqrt{A}a - \frac{B}{2\sqrt{A}}\right)^{2t-1} \exp\left\{-\left(\sqrt{A}a - \frac{B}{2\sqrt{A}}\right)^2\right\} \right. \\ \qquad \left. - \displaystyle\sum_{t=1}^{\frac{r}{2}} \frac{r!\ t!}{\left(\frac{r}{2}\right)!\ (2t)!\, 2^{r-2t}} \left(-\frac{B}{2\sqrt{A}}\right)^{2t-1} \exp\left\{-\frac{B^2}{4A}\right\}\right) \\ + \dfrac{r!}{\left(\frac{r}{2}\right)!\, 2^r} \dfrac{\sqrt{\pi}}{2} \left(\operatorname{erf}\left(-\frac{B}{2\sqrt{A}}\right) - \operatorname{erf}\left(\sqrt{A}a - \frac{B}{2\sqrt{A}}\right)\right); \\ \text{when r is even.} \end{cases} \tag{G47}$$

$$
\begin{aligned}
&\int_{-b}^{b} x^p e^{-Ax^2+Bx}\,\mathrm{d}x \\
&\quad= \frac{1}{\sqrt{A}^{p+1}} \exp\left\{\frac{B^2}{4A}\right\} \sum_{r=0}^{p} \frac{p!}{(p-r)!\;r!} \left(\frac{B}{2\sqrt{A}}\right)^{p-r} \\
&\qquad\times \begin{cases}
\dfrac{1}{2}\left(\displaystyle\sum_{t=0}^{\frac{r-1}{2}} \frac{\left(\frac{r-1}{2}\right)!}{t!} \left(\sqrt{A}b + \frac{B}{2\sqrt{A}}\right)^{2t} \exp\left\{-\left(\sqrt{A}b + \frac{B}{2\sqrt{A}}\right)^2\right\}\right. \\
\qquad\left. -\displaystyle\sum_{t=0}^{\frac{r-1}{2}} \frac{\left(\frac{r-1}{2}\right)!}{t!} \left(\sqrt{A}b - \frac{B}{2\sqrt{A}}\right)^{2t} \exp\left\{-\left(\sqrt{A}b - \frac{B}{2\sqrt{A}}\right)^2\right\}\right); \\
\text{when r is odd;} \\
\dfrac{1}{2}\left(\displaystyle\sum_{t=1}^{\frac{r}{2}} \frac{r!\;t!}{\left(\frac{r}{2}\right)!\;(2t)!\,2^{r-2t}} \left(-\sqrt{A}b - \frac{B}{2\sqrt{A}}\right)^{2t-1} \exp\left\{-\left(\sqrt{A}b + \frac{B}{2\sqrt{A}}\right)^2\right\}\right. \\
\qquad\left. -\displaystyle\sum_{t=1}^{\frac{r}{2}} \frac{r!\;t!}{\left(\frac{r}{2}\right)!\;(2t)!\,2^{r-2t}} \left(\sqrt{A}b - \frac{B}{2\sqrt{A}}\right)^{2t-1} \exp\left\{-\left(\sqrt{A}b - \frac{B}{2\sqrt{A}}\right)^2\right\}\right) \\
+\dfrac{r!}{\left(\frac{r}{2}\right)!\,2^r} \dfrac{\sqrt{\pi}}{2}\left(\operatorname{erf}\left(\sqrt{A}b - \frac{B}{2\sqrt{A}}\right) + \operatorname{erf}\left(\sqrt{A}b + \frac{B}{2\sqrt{A}}\right)\right); \\
\text{when r is even.}
\end{cases}
\end{aligned}
\tag{G48}
$$

G.4 Other related integrals

In the following equations, a is an integer, where $a \geq 0$, both A and B are coefficients, where $A > 0$, C is a coefficient, $\overline{x}$ is the overall mean of x, and the exponential function is written $\exp(x)$ or e^x.

$$\begin{aligned} &\int_{-\infty}^{\infty} (x-\overline{x})^a \, e^{-Ax^2+Bx} \, \mathrm{d}x \\ &\quad = \sqrt{\frac{\pi}{A}} \frac{1}{\left(2\sqrt{A}\right)^a} \exp\left\{\frac{B^2}{4A}\right\} \sum_{p=0}^{\lfloor \frac{a}{2} \rfloor} \frac{a!}{(a-2p)!\; p!} \left(\frac{B}{\sqrt{A}} - 2\sqrt{A}\,\overline{x}\right)^{a-2p} \end{aligned} \tag{G49}$$

$$\begin{aligned} &\int_{-\infty}^{\infty} (x+C)^a \, e^{-Ax^2+Bx} \, \mathrm{d}x \\ &\quad = \sqrt{\frac{\pi}{A}} \frac{1}{\left(2\sqrt{A}\right)^a} \exp\left\{\frac{B^2}{4A}\right\} \sum_{p=0}^{\lfloor \frac{a}{2} \rfloor} \frac{a!}{(a-2p)!\; p!} \left(\frac{B}{\sqrt{A}} + 2\sqrt{A}\,C\right)^{a-2p} \end{aligned} \tag{G50}$$

Appendix H: Integrals Related to the Parabolic Cylinder Function

In the following equations, A, B, and z are coefficients, where $A > 0$, $\Gamma(x)$ is the gamma function, $D_\nu(x)$ is the parabolic cylinder function of order ν, the exponential function is written $\exp(x)$ or e^x, and α is an exponent where $\alpha > 0$.

The integral form of the parabolic cylinder function is given by (multiple sources)

$$\int_0^\infty x^\alpha e^{-\frac{1}{2}x^2 - zx} \mathrm{d}x = \exp\left\{\frac{1}{4}z^2\right\} \Gamma(\alpha+1) D_{-(\alpha+1)}(z),$$

and can also be written as

$$\int_0^\infty x^\alpha e^{-Ax^2+Bx} \mathrm{d}x = \frac{1}{\sqrt{2A}^{\alpha+1}} \exp\left\{\frac{B^2}{8A}\right\} \Gamma(\alpha+1) D_{-(\alpha+1)}\left(\frac{-B}{\sqrt{2A}}\right). \tag{H1}$$

It can also be used to solve

$$\int_{-\infty}^0 x^\alpha e^{-Ax^2+Bx} \mathrm{d}x = \frac{(-1)^\alpha}{\sqrt{2A}^{\alpha+1}} \exp\left\{\frac{B^2}{8A}\right\} \Gamma(\alpha+1) D_{-(\alpha+1)}\left(\frac{B}{\sqrt{2A}}\right), \tag{H2}$$

where $(-1)^\alpha$ must not be a complex number.

Appendix I: Multivariate PDF Integrals of General Mixed Moment Form

I.1 Quadrivariate General Mixed Moment Integral

The quadrivariate integral of general mixed moment form is solved by splitting it into two integrals, such that

$$\begin{aligned}
&\int_{-\infty}^{\infty}\int_{-\infty}^{\infty}\int_{0}^{\infty}\int_{0}^{\infty}\left(x_1-C_1\right)^a\left(x_2^{\alpha}\left(H\left(-x_2\right)\right)^{\alpha}x_3^{\beta}x_4^{\gamma}-C_2\right)^b P_{NNLL}\left(x_1,x_2,x_3,x_4\right)\mathrm{d}x_4\,\mathrm{d}x_3\,\mathrm{d}x_2\,\mathrm{d}x_1 = \\
&\int_{-\infty}^{\infty}\int_{-\infty}^{0}\int_{0}^{\infty}\int_{0}^{\infty}\left(x_1-C_1\right)^a\left(x_2^{\alpha}\left(H\left(-x_2\right)\right)^{\alpha}x_3^{\beta}x_4^{\gamma}-C_2\right)^b P_{NNLL}\left(x_1,x_2,x_3,x_4\right)\mathrm{d}x_4\,\mathrm{d}x_3\,\mathrm{d}x_2\,\mathrm{d}x_1 \\
&+\int_{-\infty}^{\infty}\int_{0}^{\infty}\int_{0}^{\infty}\int_{0}^{\infty}\left(x_1-C_1\right)^a\left(x_2^{\alpha}\left(H\left(-x_2\right)\right)^{\alpha}x_3^{\beta}x_4^{\gamma}-C_2\right)^b P_{NNLL}\left(x_1,x_2,x_3,x_4\right)\mathrm{d}x_4\,\mathrm{d}x_3\,\mathrm{d}x_2\,\mathrm{d}x_1;
\end{aligned}$$

where both a and b are positive integers, both C_1 and C_2 are constants, and $\alpha > 0$. Additionally, $(-1)^{\alpha}$ must not be a complex number. The quadrivariate PDF, $P_{NNLL}\left(x_1,x_2,x_3,x_4\right)$, is a normal-normal-lognormal-lognormal PDF, meaning that the individual marginals of both x_1 and x_2 are normal distributions and the individual marginals of both x_3 and x_4 are lognormal distributions. The Heaviside step function is denoted $H\left(x\right)$. These two integrals can be reduced to

$$\begin{aligned}
&\int_{-\infty}^{\infty}\int_{-\infty}^{\infty}\int_{0}^{\infty}\int_{0}^{\infty}\left(x_1-C_1\right)^a\left(x_2^{\alpha}\left(H\left(-x_2\right)\right)^{\alpha}x_3^{\beta}x_4^{\gamma}-C_2\right)^b P_{NNLL}\left(x_1,x_2,x_3,x_4\right)\mathrm{d}x_4\,\mathrm{d}x_3\,\mathrm{d}x_2\,\mathrm{d}x_1 \\
&=\int_{-\infty}^{\infty}\int_{-\infty}^{0}\int_{0}^{\infty}\int_{0}^{\infty}\left(x_1-C_1\right)^a\left(x_2^{\alpha}x_3^{\beta}x_4^{\gamma}-C_2\right)^b P_{NNLL}\left(x_1,x_2,x_3,x_4\right)\mathrm{d}x_4\,\mathrm{d}x_3\,\mathrm{d}x_2\,\mathrm{d}x_1 \\
&\quad+\int_{-\infty}^{\infty}\int_{0}^{\infty}\left(x_1-C_1\right)^a\left(-C_2\right)^b P_{NN}\left(x_1,x_2\right)\mathrm{d}x_2\,\mathrm{d}x_1;
\end{aligned}$$

where the bivariate PDF, $P_{NN}\left(x_1, x_2\right)$, is a normal-normal PDF, since both x_1 and x_2 are normal distributions.

I.1.1 Quadrivariate Integral

The general form of the quadrivariate "lower" integral is

$$G_{QL} = \int_{-\infty}^{\infty}\int_{-\infty}^{0}\int_{0}^{\infty}\int_{0}^{\infty}\left(x_1 - C_1\right)^a\left(x_2^{\alpha}x_3^{\beta}x_4^{\gamma} - C_2\right)^b P_{NNLL}\left(x_1, x_2, x_3, x_4\right)\mathrm{d}x_4\,\mathrm{d}x_3\,\mathrm{d}x_2\,\mathrm{d}x_1.$$

When x_1, x_2, x_3, and x_4 all vary ($\sigma_{x_1} > 0$, $\sigma_{x_2} > 0$, $\sigma_{x_3} > 0$, and $\sigma_{x_4} > 0$), the integral is solved by first integrating over x_4 using Eq. (G29), then integrating over x_3 using Eq. (G29), then integrating over x_1 using Eq. (G50), and then integrating over x_2 using Eq. (H2). The solution to the integral, denoted G_{QL}, is

$$\begin{aligned}
G_{QL}=&\sum_{p=0}^{\lfloor\frac{a}{2}\rfloor}\sum_{r=0}^{a-2p}\sum_{q=0}^{b}\frac{1}{\sqrt{2\pi}}\frac{a!}{(a-2p)!\,p!}\frac{(a-2p)!}{(a-2p-r)!\,r!}\frac{b!}{(b-q)!\,q!}\left(-C_2\right)^{b-q}\\
&\times\left(-\sigma_{x_2}\right)^{\alpha q}\left[\frac{1}{2}\left(1-\rho_{x_1,x_2}^2\right)\sigma_{x_1}^2\right]^p\left(-\rho_{x_1,x_2}\sigma_{x_1}\right)^r\\
&\times\left(\mu_{x_1} - C_1 - \frac{\mu_{x_2}}{\sigma_{x_2}}\rho_{x_1,x_2}\sigma_{x_1} + \left(\tilde{\rho}_{x_1,x_3} - \rho_{x_1,x_2}\tilde{\rho}_{x_2,x_3}\right)\sigma_{x_1}\tilde{\sigma}_{x_3}\beta q\right.\\
&\qquad\left.+\left(\tilde{\rho}_{x_1,x_4} - \rho_{x_1,x_2}\tilde{\rho}_{x_2,x_4}\right)\sigma_{x_1}\tilde{\sigma}_{x_4}\gamma q\right)^{a-2p-r}\\
&\times\exp\left\{\tilde{\mu}_{x_3}\beta q + \tilde{\mu}_{x_4}\gamma q + \frac{1}{2}\left(1-\tilde{\rho}_{x_2,x_3}^2\right)\tilde{\sigma}_{x_3}^2\beta^2 q^2\right.\\
&\qquad\left.+\frac{1}{2}\left(1-\tilde{\rho}_{x_2,x_4}^2\right)\tilde{\sigma}_{x_4}^2\gamma^2 q^2 + \left(\tilde{\rho}_{x_3,x_4} - \tilde{\rho}_{x_2,x_3}\tilde{\rho}_{x_2,x_4}\right)\tilde{\sigma}_{x_3}\beta\tilde{\sigma}_{x_4}\gamma q^2\right\}\\
&\times\exp\left\{\frac{1}{4}\varsigma^2 - \frac{\mu_{x_2}}{\sigma_{x_2}}\varsigma + \frac{1}{2}\frac{\mu_{x_2}^2}{\sigma_{x_2}^2}\right\}\Gamma\left(\alpha q + r + 1\right)D_{-(\alpha q+r+1)}\left(\varsigma\right);
\end{aligned} \tag{I1}$$

where $\varsigma = \dfrac{\mu_{x_2}}{\sigma_{x_2}} + \tilde{\rho}_{x_2,x_3}\tilde{\sigma}_{x_3}\beta q + \tilde{\rho}_{x_2,x_4}\tilde{\sigma}_{x_4}\gamma q.$

The gamma function is denoted $\Gamma(x)$ and the parabolic cylinder function of order ν is denoted $D_\nu(x)$. Additionally, μ_{x_1} and σ_{x_1} denote the mean and standard deviation of x_1 in the quadrivariate PDF, μ_{x_2} and σ_{x_2} denote the mean and standard deviation of x_2 in the quadrivariate PDF, μ_{x_3} and σ_{x_3} denote the mean and standard deviation of x_3 in the quadrivariate PDF, and μ_{x_4} and σ_{x_4} denote the mean and standard deviation of x_4 in the quadrivariate PDF. For lognormal variates, $\tilde{\mu}_{x_3}$ and $\tilde{\sigma}_{x_3}$ denote the mean and standard deviation of $\ln x_3$ in the quadrivariate PDF, while $\tilde{\mu}_{x_4}$ and $\tilde{\sigma}_{x_4}$ denote the mean and standard deviation of $\ln x_4$ in the quadrivariate PDF. The correlation of x_1 and x_2 is denoted ρ_{x_1,x_2}, the correlation of x_1 and $\ln x_3$ is denoted $\tilde{\rho}_{x_1,x_3}$, the correlation of x_1 and $\ln x_4$ is denoted $\tilde{\rho}_{x_1,x_4}$, the correlation of x_2 and $\ln x_3$ is denoted $\tilde{\rho}_{x_2,x_3}$, the correlation of x_2 and $\ln x_4$ is denoted $\tilde{\rho}_{x_2,x_4}$, and the correlation of $\ln x_3$ and $\ln x_4$ is denoted $\tilde{\rho}_{x_3,x_4}$.

When one or more of the variables is constant (has a standard deviation of 0), the integral simplifies and reduces. The above integral has 16 sub-forms (including the fully-varying solution). There are four sub-forms that contain one constant variable. When x_1 is constant, but x_2, x_3, and x_4 vary, the solution is

$$\begin{aligned} G_{QL} = \sum_{q=0}^{b} & \frac{1}{\sqrt{2\pi}}\left(\mu_{x_1} - C_1\right)^a \frac{b!}{(b-q)!\,q!}\left(-C_2\right)^{b-q}\left(-\sigma_{x_2}\right)^{\alpha q} \\ & \times \exp\left\{\tilde{\mu}_{x_3}\beta q + \tilde{\mu}_{x_4}\gamma q + \frac{1}{2}\left(1-\tilde{\rho}_{x_2,x_3}^2\right)\tilde{\sigma}_{x_3}^2\beta^2 q^2 \right. \\ & \qquad \left. + \frac{1}{2}\left(1-\tilde{\rho}_{x_2,x_4}^2\right)\tilde{\sigma}_{x_4}^2\gamma^2 q^2 + \left(\tilde{\rho}_{x_3,x_4} - \tilde{\rho}_{x_2,x_3}\tilde{\rho}_{x_2,x_4}\right)\tilde{\sigma}_{x_3}\beta\tilde{\sigma}_{x_4}\gamma q^2\right\} \\ & \times \exp\left\{\frac{1}{4}\varsigma^2 - \frac{\mu_{x_2}}{\sigma_{x_2}}\varsigma + \frac{1}{2}\frac{\mu_{x_2}^2}{\sigma_{x_2}^2}\right\}\Gamma(\alpha q+1)\,D_{-(\alpha q+1)}(\varsigma)\,; \end{aligned} \tag{I2}$$

where $\varsigma = \dfrac{\mu_{x_2}}{\sigma_{x_2}} + \tilde{\rho}_{x_2,x_3}\tilde{\sigma}_{x_3}\beta q + \tilde{\rho}_{x_2,x_4}\tilde{\sigma}_{x_4}\gamma q.$

When x_2 is constant, but x_1, x_3, and x_4 vary, the solution is

$$\begin{aligned} G_{QL} = \sum_{p=0}^{\lfloor \frac{a}{2} \rfloor} \sum_{q=0}^{b} & \frac{a!}{(a-2p)!\,p!} \frac{b!}{(b-q)!\,q!} \big(-C_2\big)^{b-q} \mu_{x_2}^{\alpha q} \left(\frac{1}{2}\sigma_{x_1}^2\right)^p \\ & \times \left(\mu_{x_1} - C_1 + \tilde{\rho}_{x_1,x_3}\sigma_{x_1}\tilde{\sigma}_{x_3}\beta q + \tilde{\rho}_{x_1,x_4}\sigma_{x_1}\tilde{\sigma}_{x_4}\gamma q\right)^{a-2p} \\ & \times \exp\left\{\tilde{\mu}_{x_3}\beta q + \tilde{\mu}_{x_4}\gamma q + \frac{1}{2}\tilde{\sigma}_{x_3}^2\beta^2 q^2 + \frac{1}{2}\tilde{\sigma}_{x_4}^2\gamma^2 q^2 + \tilde{\rho}_{x_3,x_4}\tilde{\sigma}_{x_3}\beta\tilde{\sigma}_{x_4}\gamma q^2\right\}, \end{aligned} \tag{I3}$$

when $\mu_{x_2} \leq 0$; otherwise $G_{QL} = 0$ when $\mu_{x_2} > 0$ because the limits of integration for G_{QL} are outside the domain of the PDF in this special case. When x_3 is constant, but x_1, x_2, and x_4 vary, the solution is

$$\begin{aligned} G_{QL} = \sum_{p=0}^{\lfloor \frac{a}{2} \rfloor} \sum_{r=0}^{a-2p} \sum_{q=0}^{b} & \frac{1}{\sqrt{2\pi}} \frac{a!}{(a-2p)!\,p!} \frac{(a-2p)!}{(a-2p-r)!\,r!} \frac{b!}{(b-q)!\,q!} \big(-C_2\big)^{b-q} \\ & \times \big(-\sigma_{x_2}\big)^{\alpha q} \left[\frac{1}{2}\left(1-\rho_{x_1,x_2}^2\right)\sigma_{x_1}^2\right]^p \big(-\rho_{x_1,x_2}\sigma_{x_1}\big)^r \mu_{x_3}^{\beta q} \\ & \times \left(\mu_{x_1} - C_1 - \frac{\mu_{x_2}}{\sigma_{x_2}}\rho_{x_1,x_2}\sigma_{x_1} + \left(\tilde{\rho}_{x_1,x_4} - \rho_{x_1,x_2}\tilde{\rho}_{x_2,x_4}\right)\sigma_{x_1}\tilde{\sigma}_{x_4}\gamma q\right)^{a-2p-r} \\ & \times \exp\left\{\tilde{\mu}_{x_4}\gamma q + \frac{1}{2}\tilde{\sigma}_{x_4}^2\gamma^2 q^2 - \frac{1}{4}\varsigma^2\right\}\Gamma\left(\alpha q + r + 1\right) D_{-(\alpha q + r + 1)}\left(\varsigma\right); \end{aligned} \tag{I4}$$

where $\varsigma = \dfrac{\mu_{x_2}}{\sigma_{x_2}} + \tilde{\rho}_{x_2,x_4}\tilde{\sigma}_{x_4}\gamma q.$

When x_4 is constant, but x_1, x_2, and x_3 vary, the solution is

$$\begin{aligned} G_{QL} = \sum_{p=0}^{\lfloor \frac{a}{2} \rfloor} \sum_{r=0}^{a-2p} \sum_{q=0}^{b} & \frac{1}{\sqrt{2\pi}} \frac{a!}{(a-2p)!\,p!} \frac{(a-2p)!}{(a-2p-r)!\,r!} \frac{b!}{(b-q)!\,q!} \big(-C_2\big)^{b-q} \\ & \times \big(-\sigma_{x_2}\big)^{\alpha q} \left[\frac{1}{2}\left(1-\rho_{x_1,x_2}^2\right)\sigma_{x_1}^2\right]^p \big(-\rho_{x_1,x_2}\sigma_{x_1}\big)^r \mu_{x_4}^{\gamma q} \\ & \times \left(\mu_{x_1} - C_1 - \frac{\mu_{x_2}}{\sigma_{x_2}}\rho_{x_1,x_2}\sigma_{x_1} + \left(\tilde{\rho}_{x_1,x_3} - \rho_{x_1,x_2}\tilde{\rho}_{x_2,x_3}\right)\sigma_{x_1}\tilde{\sigma}_{x_3}\beta q\right)^{a-2p-r} \\ & \times \exp\left\{\tilde{\mu}_{x_3}\beta q + \frac{1}{2}\tilde{\sigma}_{x_3}^2\beta^2 q^2 - \frac{1}{4}\varsigma^2\right\}\Gamma\left(\alpha q + r + 1\right) D_{-(\alpha q + r + 1)}\left(\varsigma\right); \end{aligned} \tag{I5}$$

where $\quad \varsigma = \dfrac{\mu_{x_2}}{\sigma_{x_2}} + \tilde{\rho}_{x_2,x_3}\tilde{\sigma}_{x_3}\beta q.$

There are six sub-forms that contain two constant variables. When both x_1 and x_2 are constant, but both x_3 and x_4 vary, the solution is

$$\begin{aligned} G_{QL} = &\sum_{q=0}^{b} \left(\mu_{x_1} - C_1\right)^a \frac{b!}{(b-q)!\,q!}\left(-C_2\right)^{b-q}\mu_{x_2}^{\alpha q} \\ &\times \exp\left\{\tilde{\mu}_{x_3}\beta q + \tilde{\mu}_{x_4}\gamma q + \frac{1}{2}\tilde{\sigma}_{x_3}^2\beta^2 q^2 + \frac{1}{2}\tilde{\sigma}_{x_4}^2\gamma^2 q^2 + \tilde{\rho}_{x_3,x_4}\tilde{\sigma}_{x_3}\beta\tilde{\sigma}_{x_4}\gamma q^2\right\}, \end{aligned} \tag{I6}$$

when $\mu_{x_2} \leq 0$; otherwise $G_{QL} = 0$ when $\mu_{x_2} > 0$. When both x_1 and x_3 are constant, but both x_2 and x_4 vary, the solution is

$$\begin{aligned} G_{QL} = &\sum_{q=0}^{b} \frac{1}{\sqrt{2\pi}}\left(\mu_{x_1} - C_1\right)^a \frac{b!}{(b-q)!\,q!}\left(-C_2\right)^{b-q}\left(-\sigma_{x_2}\right)^{\alpha q}\mu_{x_3}^{\beta q} \\ &\times \exp\left\{\tilde{\mu}_{x_4}\gamma q + \frac{1}{2}\tilde{\sigma}_{x_4}^2\gamma^2 q^2 - \frac{1}{4}\varsigma^2\right\}\Gamma\left(\alpha q + 1\right) D_{-(\alpha q+1)}\left(\varsigma\right); \end{aligned} \tag{I7}$$

where $\quad \varsigma = \dfrac{\mu_{x_2}}{\sigma_{x_2}} + \tilde{\rho}_{x_2,x_4}\tilde{\sigma}_{x_4}\gamma q.$

When both x_1 and x_4 are constant, but both x_2 and x_3 vary, the solution is

$$\begin{aligned} G_{QL} = &\sum_{q=0}^{b} \frac{1}{\sqrt{2\pi}}\left(\mu_{x_1} - C_1\right)^a \frac{b!}{(b-q)!\,q!}\left(-C_2\right)^{b-q}\left(-\sigma_{x_2}\right)^{\alpha q}\mu_{x_4}^{\gamma q} \\ &\times \exp\left\{\tilde{\mu}_{x_3}\beta q + \frac{1}{2}\tilde{\sigma}_{x_3}^2\beta^2 q^2 - \frac{1}{4}\varsigma^2\right\}\Gamma\left(\alpha q + 1\right) D_{-(\alpha q+1)}\left(\varsigma\right); \end{aligned} \tag{I8}$$

where $\quad \varsigma = \dfrac{\mu_{x_2}}{\sigma_{x_2}} + \tilde{\rho}_{x_2,x_3}\tilde{\sigma}_{x_3}\beta q.$

When both x_2 and x_3 are constant, but both x_1 and x_4 vary, the solution is

$$G_{QL} = \sum_{p=0}^{\lfloor \frac{a}{2} \rfloor} \sum_{q=0}^{b} \frac{a!}{(a-2p)!\,p!} \frac{b!}{(b-q)!\,q!} \big(-C_2\big)^{b-q} \mu_{x_2}^{\alpha q} \mu_{x_3}^{\beta q} \left(\frac{1}{2}\sigma_{x_1}^2\right)^p \times \left(\mu_{x_1} - C_1 + \tilde{\rho}_{x_1,x_4}\sigma_{x_1}\tilde{\sigma}_{x_4}\gamma q\right)^{a-2p} \exp\left\{\tilde{\mu}_{x_4}\gamma q + \frac{1}{2}\tilde{\sigma}_{x_4}^2\gamma^2 q^2\right\}, \tag{I9}$$

when $\mu_{x_2} \leq 0$; otherwise $G_{QL} = 0$ when $\mu_{x_2} > 0$. When both x_2 and x_4 are constant, but both x_1 and x_3 vary, the solution is

$$G_{QL} = \sum_{p=0}^{\lfloor \frac{a}{2} \rfloor} \sum_{q=0}^{b} \frac{a!}{(a-2p)!\,p!} \frac{b!}{(b-q)!\,q!} \big(-C_2\big)^{b-q} \mu_{x_2}^{\alpha q} \mu_{x_4}^{\gamma q} \left(\frac{1}{2}\sigma_{x_1}^2\right)^p \times \left(\mu_{x_1} - C_1 + \tilde{\rho}_{x_1,x_3}\sigma_{x_1}\tilde{\sigma}_{x_3}\beta q\right)^{a-2p} \exp\left\{\tilde{\mu}_{x_3}\beta q + \frac{1}{2}\tilde{\sigma}_{x_3}^2\beta^2 q^2\right\}, \tag{I10}$$

when $\mu_{x_2} \leq 0$; otherwise $G_{QL} = 0$ when $\mu_{x_2} > 0$. When both x_3 and x_4 are constant, but both x_1 and x_2 vary, the solution is

$$\begin{aligned} G_{QL} = \sum_{p=0}^{\lfloor \frac{a}{2} \rfloor} \sum_{r=0}^{a-2p} \sum_{q=0}^{b} & \frac{1}{\sqrt{2\pi}} \frac{a!}{(a-2p)!\,p!} \frac{(a-2p)!}{(a-2p-r)!\,r!} \frac{b!}{(b-q)!\,q!} \big(-C_2\big)^{b-q} \\ & \times \big(-\sigma_{x_2}\big)^{\alpha q} \left[\frac{1}{2}\left(1-\rho_{x_1,x_2}^2\right)\sigma_{x_1}^2\right]^p \big(-\rho_{x_1,x_2}\sigma_{x_1}\big)^r \mu_{x_3}^{\beta q} \mu_{x_4}^{\gamma q} \\ & \times \left(\mu_{x_1} - C_1 - \frac{\mu_{x_2}}{\sigma_{x_2}}\rho_{x_1,x_2}\sigma_{x_1}\right)^{a-2p-r} \\ & \times \exp\left\{-\frac{1}{4}\frac{\mu_{x_2}^2}{\sigma_{x_2}^2}\right\} \Gamma\left(\alpha q + r + 1\right) D_{-(\alpha q + r + 1)}\left(\frac{\mu_{x_2}}{\sigma_{x_2}}\right). \end{aligned} \tag{I11}$$

There are four sub-forms that contain three constant variables. When x_1, x_2, and x_3 are constant, but x_4 varies, the solution is

$$G_{QL} = \sum_{q=0}^{b} \big(\mu_{x_1} - C_1\big)^a \frac{b!}{(b-q)!\,q!} \big(-C_2\big)^{b-q} \mu_{x_2}^{\alpha q} \mu_{x_3}^{\beta q} \exp\left\{\tilde{\mu}_{x_4}\gamma q + \frac{1}{2}\tilde{\sigma}_{x_4}^2\gamma^2 q^2\right\}, \tag{I12}$$

when $\mu_{x_2} \leq 0$; otherwise $G_{QL} = 0$ when $\mu_{x_2} > 0$. When x_1, x_2, and x_4 are constant, but x_3 varies, the solution is

$$G_{QL} = \sum_{q=0}^{b} \left(\mu_{x_1} - C_1\right)^a \frac{b!}{(b-q)!\,q!} \left(-C_2\right)^{b-q} \mu_{x_2}^{\alpha q}\, \mu_{x_4}^{\gamma q} \exp\left\{\tilde{\mu}_{x_3}\beta q + \frac{1}{2}\tilde{\sigma}_{x_3}^2 \beta^2 q^2\right\}, \tag{I13}$$

when $\mu_{x_2} \leq 0$; otherwise $G_{QL} = 0$ when $\mu_{x_2} > 0$. When x_1, x_3, and x_4 are constant, but x_2 varies, the solution is

$$\begin{aligned} G_{QL} = &\sum_{q=0}^{b} \frac{1}{\sqrt{2\pi}} \left(\mu_{x_1} - C_1\right)^a \frac{b!}{(b-q)!\,q!} \left(-C_2\right)^{b-q} \left(-\sigma_{x_2}\right)^{\alpha q} \mu_{x_3}^{\beta q}\, \mu_{x_4}^{\gamma q} \\ &\times \exp\left\{-\frac{1}{4}\frac{\mu_{x_2}^2}{\sigma_{x_2}^2}\right\} \Gamma\left(\alpha q + 1\right) D_{-(\alpha q+1)}\left(\frac{\mu_{x_2}}{\sigma_{x_2}}\right). \end{aligned} \tag{I14}$$

When x_2, x_3, and x_4 are constant, but x_1 varies, the solution is

$$G_{QL} = \sum_{p=0}^{\left\lfloor \frac{a}{2} \right\rfloor} \frac{a!}{(a-2p)!\,p!} \left(\frac{1}{2}\sigma_{x_1}^2\right)^p \left(\mu_{x_1} - C_1\right)^{a-2p} \left(\mu_{x_2}^{\alpha}\, \mu_{x_3}^{\beta}\, \mu_{x_4}^{\gamma} - C_2\right)^b, \tag{I15}$$

when $\mu_{x_2} \leq 0$; otherwise $G_{QL} = 0$ when $\mu_{x_2} > 0$. When x_1, x_2, x_3, and x_4 are all constant ($\sigma_{x_1} = 0$, $\sigma_{x_2} = 0$, $\sigma_{x_3} = 0$, and $\sigma_{x_4} = 0$), the solution is

$$G_{QL} = \left(\mu_{x_1} - C_1\right)^a \left(\mu_{x_2}^{\alpha}\, \mu_{x_3}^{\beta}\, \mu_{x_4}^{\gamma} - C_2\right)^b, \tag{I16}$$

when $\mu_{x_2} \leq 0$; otherwise $G_{QL} = 0$ when $\mu_{x_2} > 0$.

I.1.2 Bivariate Integral

The general form of the bivariate "upper" integral is

$$G_{BU} = \int_{-\infty}^{\infty} \int_{0}^{\infty} \left(x_1 - C_1\right)^a \left(-C_2\right)^b P_{NN}\left(x_1, x_2\right) \mathrm{d}x_2\, \mathrm{d}x_1.$$

When both x_1 and x_2 vary ($\sigma_{x_1} > 0$ and $\sigma_{x_2} > 0$), the solution to the main integral is

$$\begin{aligned}
&\int_{-\infty}^{\infty}\int_{0}^{\infty}\Big(x_1 - C_1\Big)^a P_{NN}\left(x_1, x_2\right)\mathrm{d}x_2\,\mathrm{d}x_1 \\
&= \sum_{p=0}^{\lfloor \frac{a}{2} \rfloor}\sum_{r=0}^{a-2p}\frac{1}{\sqrt{2\pi}}\frac{a!}{(a-2p)!\,p!}\frac{(a-2p)!}{(a-2p-r)!\,r!} \\
&\qquad \times \left[\frac{1}{2}\left(1-\rho_{x_1,x_2}^2\right)\sigma_{x_1}^2\right]^p\left(\rho_{x_1,x_2}\sigma_{x_1}\right)^r\left(\mu_{x_1} - C_1 - \frac{\mu_{x_2}}{\sigma_{x_2}}\rho_{x_1,x_2}\sigma_{x_1}\right)^{a-2p-r} \\
&\qquad \times \exp\left\{-\frac{1}{4}\frac{\mu_{x_2}^2}{\sigma_{x_2}^2}\right\}\Gamma\left(r+1\right)D_{-(r+1)}\left(-\frac{\mu_{x_2}}{\sigma_{x_2}}\right),
\end{aligned} \tag{I17}$$

and the solution to G_{BU} is

$$\begin{aligned}
G_{BU} = &\sum_{p=0}^{\lfloor \frac{a}{2} \rfloor}\sum_{r=0}^{a-2p}\frac{1}{\sqrt{2\pi}}\frac{a!}{(a-2p)!\,p!}\frac{(a-2p)!}{(a-2p-r)!\,r!}\Big(-C_2\Big)^b \\
&\times \left[\frac{1}{2}\left(1-\rho_{x_1,x_2}^2\right)\sigma_{x_1}^2\right]^p\left(\rho_{x_1,x_2}\sigma_{x_1}\right)^r\left(\mu_{x_1} - C_1 - \frac{\mu_{x_2}}{\sigma_{x_2}}\rho_{x_1,x_2}\sigma_{x_1}\right)^{a-2p-r} \\
&\times \exp\left\{-\frac{1}{4}\frac{\mu_{x_2}^2}{\sigma_{x_2}^2}\right\}\Gamma\left(r+1\right)D_{-(r+1)}\left(-\frac{\mu_{x_2}}{\sigma_{x_2}}\right).
\end{aligned} \tag{I18}$$

When x_1 is constant, but x_2 varies, the solution is

$$G_{BU} = \Big(\mu_{x_1} - C_1\Big)^a\Big(-C_2\Big)^b\frac{1}{2}\left(1+\mathrm{erf}\left(\frac{\mu_{x_2}}{\sqrt{2}\,\sigma_{x_2}}\right)\right). \tag{I19}$$

When x_2 is constant, but x_1 varies, the solution is

$$G_{BU} = \sum_{p=0}^{\lfloor \frac{a}{2} \rfloor}\frac{a!}{(a-2p)!\,p!}\Big(-C_2\Big)^b\left(\frac{1}{2}\sigma_{x_1}^2\right)^p\Big(\mu_{x_1} - C_1\Big)^{a-2p}, \tag{I20}$$

when $\mu_{x_2} > 0$; otherwise $G_{BU} = 0$ when $\mu_{x_2} \leq 0$ because the limits of integration for G_{BU} are outside the domain of the PDF in this special case. When both x_1 and x_2 are constant

($\sigma_{x_1} = 0$ and $\sigma_{x_2} = 0$), the solution is

$$G_{BU} = \Big(\mu_{x_1} - C_1\Big)^a \Big(-C_2\Big)^b, \tag{I21}$$

when $\mu_{x_2} > 0$; otherwise $G_{BU} = 0$ when $\mu_{x_2} \leq 0$.

I.2 Trivariate General Mixed Moment Integral

The trivariate integral of general mixed moment form is solved by splitting it into two integrals, such that

$$\begin{aligned}
&\int_{-\infty}^{\infty}\int_{-\infty}^{\infty}\int_{0}^{\infty} \Big(x_1 - C_1\Big)^a \Big(x_2^{\alpha}\left(H\left(x_2\right)\right)^{\alpha} x_3^{\beta} - C_2\Big)^b P_{NNL}\left(x_1, x_2, x_3\right) \mathrm{d}x_3 \, \mathrm{d}x_2 \, \mathrm{d}x_1 = \\
&\int_{-\infty}^{\infty}\int_{-\infty}^{0}\int_{0}^{\infty} \Big(x_1 - C_1\Big)^a \Big(x_2^{\alpha}\left(H\left(x_2\right)\right)^{\alpha} x_3^{\beta} - C_2\Big)^b P_{NNL}\left(x_1, x_2, x_3\right) \mathrm{d}x_3 \, \mathrm{d}x_2 \, \mathrm{d}x_1 \\
&+ \int_{-\infty}^{\infty}\int_{0}^{\infty}\int_{0}^{\infty} \Big(x_1 - C_1\Big)^a \Big(x_2^{\alpha}\left(H\left(x_2\right)\right)^{\alpha} x_3^{\beta} - C_2\Big)^b P_{NNL}\left(x_1, x_2, x_3\right) \mathrm{d}x_3 \, \mathrm{d}x_2 \, \mathrm{d}x_1;
\end{aligned}$$

where both a and b are positive integers, both C_1 and C_2 are constants, and $\alpha > 0$. The trivariate PDF, $P_{NNL}\left(x_1, x_2, x_3\right)$, is a normal-normal-lognormal PDF, meaning that the individual marginals of both x_1 and x_2 are normal distributions and the individual marginal of x_3 is a lognormal distribution. These two integrals can be reduced to

$$\begin{aligned}
&\int_{-\infty}^{\infty}\int_{-\infty}^{\infty}\int_{0}^{\infty} \Big(x_1 - C_1\Big)^a \Big(x_2^{\alpha}\left(H\left(x_2\right)\right)^{\alpha} x_3^{\beta} - C_2\Big)^b P_{NNL}\left(x_1, x_2, x_3\right) \mathrm{d}x_3 \, \mathrm{d}x_2 \, \mathrm{d}x_1 \\
&= \int_{-\infty}^{\infty}\int_{-\infty}^{0} \Big(x_1 - C_1\Big)^a \Big(-C_2\Big)^b P_{NN}\left(x_1, x_2\right) \mathrm{d}x_2 \, \mathrm{d}x_1 \\
&\quad + \int_{-\infty}^{\infty}\int_{0}^{\infty}\int_{0}^{\infty} \Big(x_1 - C_1\Big)^a \Big(x_2^{\alpha} x_3^{\beta} - C_2\Big)^b P_{NNL}\left(x_1, x_2, x_3\right) \mathrm{d}x_3 \, \mathrm{d}x_2 \, \mathrm{d}x_1;
\end{aligned}$$

where the bivariate PDF, $P_{NN}\left(x_1, x_2\right)$, is a normal-normal PDF, since both x_1 and x_2 are normal distributions.

I.2.1 Trivariate Integral

The general form of the trivariate "upper" integral is

$$G_{TU} = \int_{-\infty}^{\infty} \int_{0}^{\infty} \int_{0}^{\infty} \Big(x_1 - C_1\Big)^a \Big(x_2^\alpha x_3^\beta - C_2\Big)^b P_{NNL}\left(x_1, x_2, x_3\right) \mathrm{d}x_3 \, \mathrm{d}x_2 \, \mathrm{d}x_1.$$

When x_1, x_2, and x_3 all vary ($\sigma_{x_1} > 0$, $\sigma_{x_2} > 0$, and $\sigma_{x_3} > 0$), the integral is solved by first integrating over x_3 using Eq. (G29), then integrating over x_1 using Eq. (G50), and then integrating over x_2 using Eq. (H1). The solution to the integral, denoted G_{TU}, is

$$\begin{aligned} G_{TU} = \sum_{p=0}^{\lfloor \frac{a}{2} \rfloor} \sum_{r=0}^{a-2p} \sum_{q=0}^{b} & \frac{1}{\sqrt{2\pi}} \frac{a!}{(a-2p)!\, p!} \frac{(a-2p)!}{(a-2p-r)!\, r!} \frac{b!}{(b-q)!\, q!} \big(-C_2\big)^{b-q} \\ & \times \sigma_{x_2}^{\alpha q} \left[\frac{1}{2}\left(1 - \rho_{x_1,x_2}^2\right) \sigma_{x_1}^2\right]^p \left(\rho_{x_1,x_2} \sigma_{x_1}\right)^r \\ & \times \Bigg(\mu_{x_1} - C_1 - \frac{\mu_{x_2}}{\sigma_{x_2}} \rho_{x_1,x_2} \sigma_{x_1} \\ & \qquad + \left(\tilde{\rho}_{x_1,x_3} - \rho_{x_1,x_2} \tilde{\rho}_{x_2,x_3}\right) \sigma_{x_1} \tilde{\sigma}_{x_3} \beta q \Bigg)^{a-2p-r} \\ & \times \exp\left\{\tilde{\mu}_{x_3} \beta q + \frac{1}{2} \tilde{\sigma}_{x_3}^2 \beta^2 q^2 - \frac{1}{4} \varsigma^2\right\} \Gamma\left(\alpha q + r + 1\right) D_{-(\alpha q + r + 1)}\left(-\varsigma\right); \end{aligned} \tag{I22}$$

where $\quad \varsigma = \dfrac{\mu_{x_2}}{\sigma_{x_2}} + \tilde{\rho}_{x_2,x_3} \tilde{\sigma}_{x_3} \beta q.$

There are three sub-forms that contain one constant variable. When x_1 is constant, but x_2 and x_3 vary, the solution is

$$\begin{aligned} G_{TU} = &\sum_{q=0}^{b} \frac{1}{\sqrt{2\pi}} \big(\mu_{x_1} - C_1\big)^a \frac{b!}{(b-q)!\,q!} \big(-C_2\big)^{b-q} \sigma_{x_2}^{\alpha q} \\ &\times \exp\left\{\tilde{\mu}_{x_3}\beta q + \frac{1}{2}\tilde{\sigma}_{x_3}^2\beta^2 q^2 - \frac{1}{4}\varsigma^2\right\} \Gamma\left(\alpha q + 1\right) D_{-(\alpha q+1)}\left(-\varsigma\right); \end{aligned} \tag{I23}$$

where $\varsigma = \dfrac{\mu_{x_2}}{\sigma_{x_2}} + \tilde{\rho}_{x_2,x_3}\tilde{\sigma}_{x_3}\beta q.$

When x_2 is constant, but both x_1 and x_3 vary, the solution is

$$\begin{aligned} G_{TU} = &\sum_{p=0}^{\lfloor \frac{a}{2} \rfloor} \sum_{q=0}^{b} \frac{a!}{(a-2p)!\,p!} \frac{b!}{(b-q)!\,q!} \big(-C_2\big)^{b-q} \mu_{x_2}^{\alpha q} \left(\frac{1}{2}\sigma_{x_1}^2\right)^p \\ &\times \left(\mu_{x_1} - C_1 + \tilde{\rho}_{x_1,x_3}\sigma_{x_1}\tilde{\sigma}_{x_3}\beta q\right)^{a-2p} \exp\left\{\tilde{\mu}_{x_3}\beta q + \frac{1}{2}\tilde{\sigma}_{x_3}^2\beta^2 q^2\right\}, \end{aligned} \tag{I24}$$

when $\mu_{x_2} \geq 0$; otherwise $G_{TU} = 0$ when $\mu_{x_2} < 0$ because the limits of integration for G_{TU} are outside the domain of the PDF in this special case. When x_3 is constant, but both x_1 and x_2 vary, the solution is

$$\begin{aligned} G_{TU} = &\sum_{p=0}^{\lfloor \frac{a}{2} \rfloor} \sum_{r=0}^{a-2p} \sum_{q=0}^{b} \frac{1}{\sqrt{2\pi}} \frac{a!}{(a-2p)!\,p!} \frac{(a-2p)!}{(a-2p-r)!\,r!} \frac{b!}{(b-q)!\,q!} \big(-C_2\big)^{b-q} \\ &\times \sigma_{x_2}^{\alpha q} \left[\frac{1}{2}\left(1-\rho_{x_1,x_2}^2\right)\sigma_{x_1}^2\right]^p \left(\rho_{x_1,x_2}\sigma_{x_1}\right)^r \mu_{x_3}^{\beta q} \\ &\times \left(\mu_{x_1} - C_1 - \frac{\mu_{x_2}}{\sigma_{x_2}}\rho_{x_1,x_2}\sigma_{x_1}\right)^{a-2p-r} \\ &\times \exp\left\{-\frac{1}{4}\frac{\mu_{x_2}^2}{\sigma_{x_2}^2}\right\} \Gamma\left(\alpha q + r + 1\right) D_{-(\alpha q+r+1)}\left(-\frac{\mu_{x_2}}{\sigma_{x_2}}\right). \end{aligned} \tag{I25}$$

There are three sub-forms that contain two constant variables. When both x_1 and x_2 are

constant, but x_3 varies, the solution is

$$G_{TU} = \sum_{q=0}^{b} \big(\mu_{x_1} - C_1\big)^a \frac{b!}{(b-q)!\,q!}\big(-C_2\big)^{b-q} \mu_{x_2}^{\alpha q} \exp\left\{\tilde{\mu}_{x_3}\beta q + \frac{1}{2}\tilde{\sigma}_{x_3}^2\beta^2 q^2\right\}, \tag{I26}$$

when $\mu_{x_2} \geq 0$; otherwise $G_{TU} = 0$ when $\mu_{x_2} < 0$. When both x_1 and x_3 are constant, but x_2 varies, the solution is

$$\begin{aligned} G_{TU} = &\sum_{q=0}^{b} \frac{1}{\sqrt{2\pi}}\big(\mu_{x_1} - C_1\big)^a \frac{b!}{(b-q)!\,q!}\big(-C_2\big)^{b-q} \sigma_{x_2}^{\alpha q}\mu_{x_3}^{\beta q} \\ &\times \exp\left\{-\frac{1}{4}\frac{\mu_{x_2}^2}{\sigma_{x_2}^2}\right\}\Gamma\left(\alpha q + 1\right) D_{-(\alpha q+1)}\left(-\frac{\mu_{x_2}}{\sigma_{x_2}}\right). \end{aligned} \tag{I27}$$

When both x_2 and x_3 are constant, but x_1 varies, the solution is

$$G_{TU} = \sum_{p=0}^{\lfloor \frac{a}{2} \rfloor} \frac{a!}{(a-2p)!\,p!}\left(\frac{1}{2}\sigma_{x_1}^2\right)^p \big(\mu_{x_1} - C_1\big)^{a-2p}\big(\mu_{x_2}^{\alpha}\,\mu_{x_3}^{\beta} - C_2\big)^b, \tag{I28}$$

when $\mu_{x_2} \geq 0$; otherwise $G_{TU} = 0$ when $\mu_{x_2} < 0$. When x_1, x_2, and x_3 are all constant ($\sigma_{x_1} = 0$, $\sigma_{x_2} = 0$, and $\sigma_{x_3} = 0$), the solution is

$$G_{TU} = \big(\mu_{x_1} - C_1\big)^a\big(\mu_{x_2}^{\alpha}\mu_{x_3}^{\beta} - C_2\big)^b, \tag{I29}$$

when $\mu_{x_2} \geq 0$; otherwise $G_{TU} = 0$ when $\mu_{x_2} < 0$.

I.2.2 Bivariate Integral

The general form of the bivariate "lower" integral is

$$G_{BL} = \int_{-\infty}^{\infty}\int_{-\infty}^{0} \Big(x_1 - C_1\Big)^a \Big(-C_2\Big)^b P_{NN}\left(x_1, x_2\right) \mathrm{d}x_2\,\mathrm{d}x_1.$$

When both x_1 and x_2 vary ($\sigma_{x_1} > 0$ and $\sigma_{x_2} > 0$), the solution to the main integral is

$$\begin{aligned}
&\int_{-\infty}^{\infty}\int_{-\infty}^{0}\Big(x_1 - C_1\Big)^a P_{NN}\left(x_1, x_2\right)\mathrm{d}x_2\,\mathrm{d}x_1 \\
&= \sum_{p=0}^{\lfloor \frac{a}{2} \rfloor}\sum_{r=0}^{a-2p}\frac{1}{\sqrt{2\pi}}\frac{a!}{(a-2p)!\,p!}\frac{(a-2p)!}{(a-2p-r)!\,r!} \\
&\qquad \times \left[\frac{1}{2}\left(1-\rho_{x_1,x_2}^2\right)\sigma_{x_1}^2\right]^p\left(-\rho_{x_1,x_2}\sigma_{x_1}\right)^r\left(\mu_{x_1} - C_1 - \frac{\mu_{x_2}}{\sigma_{x_2}}\rho_{x_1,x_2}\sigma_{x_1}\right)^{a-2p-r} \\
&\qquad \times \exp\left\{-\frac{1}{4}\frac{\mu_{x_2}^2}{\sigma_{x_2}^2}\right\}\Gamma\left(r+1\right)D_{-(r+1)}\left(\frac{\mu_{x_2}}{\sigma_{x_2}}\right),
\end{aligned} \tag{I30}$$

and the solution to G_{BL} is

$$\begin{aligned}
G_{BL} = &\sum_{p=0}^{\lfloor \frac{a}{2} \rfloor}\sum_{r=0}^{a-2p}\frac{1}{\sqrt{2\pi}}\frac{a!}{(a-2p)!\,p!}\frac{(a-2p)!}{(a-2p-r)!\,r!}\big(-C_2\big)^b\left[\frac{1}{2}\left(1-\rho_{x_1,x_2}^2\right)\sigma_{x_1}^2\right]^p \\
&\times\left(-\rho_{x_1,x_2}\sigma_{x_1}\right)^r\left(\mu_{x_1} - C_1 - \frac{\mu_{x_2}}{\sigma_{x_2}}\rho_{x_1,x_2}\sigma_{x_1}\right)^{a-2p-r} \\
&\times\exp\left\{-\frac{1}{4}\frac{\mu_{x_2}^2}{\sigma_{x_2}^2}\right\}\Gamma\left(r+1\right)D_{-(r+1)}\left(\frac{\mu_{x_2}}{\sigma_{x_2}}\right).
\end{aligned} \tag{I31}$$

When x_1 is constant, but x_2 varies, the solution is

$$G_{BL} = \Big(\mu_{x_1} - C_1\Big)^a\Big(-C_2\Big)^b\frac{1}{2}\left(1 - \operatorname{erf}\left(\frac{\mu_{x_2}}{\sqrt{2}\,\sigma_{x_2}}\right)\right). \tag{I32}$$

When x_2 is constant, but x_1 varies, the solution is

$$G_{BL} = \sum_{p=0}^{\lfloor \frac{a}{2} \rfloor}\frac{a!}{(a-2p)!\,p!}\Big(-C_2\Big)^b\left(\frac{1}{2}\sigma_{x_1}^2\right)^p\Big(\mu_{x_1} - C_1\Big)^{a-2p}, \tag{I33}$$

when $\mu_{x_2} < 0$; otherwise $G_{BL} = 0$ when $\mu_{x_2} \geq 0$ because the limits of integration for G_{BL} are outside the domain of the PDF in this special case. When both x_1 and x_2 are constant

($\sigma_{x_1} = 0$ and $\sigma_{x_2} = 0$), the solution is

$$G_{BL} = \Big(\mu_{x_1} - C_1\Big)^a \Big(- C_2\Big)^b, \tag{I34}$$

when $\mu_{x_2} < 0$; otherwise $G_{BL} = 0$ when $\mu_{x_2} \geq 0$.

Appendix J: Multivariate PDF Integrals of Covariance and Mean Forms

J.1 Quadrivariate PDF Integrals of Covariance Form

The integrals of the general form

$$G_{QC} = \int_{-\infty}^{\infty}\int_{-\infty}^{\infty}\int_{0}^{\infty}\int_{0}^{\infty}\Big(x_1 - C_1\Big)\Big(x_2^{\alpha}\left(H\left(-x_2\right)\right)^{\alpha} x_3^{\beta} x_4^{\gamma} - C_2\Big) \times P_{NNLL}\left(x_1, x_2, x_3, x_4\right) \mathrm{d}x_4 \, \mathrm{d}x_3 \, \mathrm{d}x_2 \, \mathrm{d}x_1$$

are referred to as quadrivariate PDF integrals of covariance form. Both C_1 and C_2 are constants, and when they both represent the appropriate overall mean values, the resulting integral is a covariance. The quadrivariate PDF, $P_{NNLL}\left(x_1, x_2, x_3, x_4\right)$, is a normal-normal-lognormal-lognormal PDF, meaning that the individual marginals of both x_1 and x_2 are normal distributions and the individual marginals of both x_3 and x_4 are lognormal distributions. The Heaviside step function is denoted $H\left(x\right)$. The above integral has 16 sub-forms. When one or more of the variables is constant (has a standard deviation of 0), the integral simplifies and reduces.

In the solutions below, denoted G_{QC}, μ_{x_1} and σ_{x_1} denote the mean and standard deviation of x_1 in the quadrivariate PDF, μ_{x_2} and σ_{x_2} denote the mean and standard deviation of x_2 in the quadrivariate PDF, μ_{x_3} and σ_{x_3} denote the mean and standard deviation of x_3 in the quadrivariate PDF, and μ_{x_4} and σ_{x_4} denote the mean and standard deviation of x_4 in the quadrivariate PDF. For lognormal variates, $\tilde{\mu}_{x_3}$ and $\tilde{\sigma}_{x_3}$ denote the mean and standard deviation of $\ln x_3$ in the quadrivariate PDF, while $\tilde{\mu}_{x_4}$ and $\tilde{\sigma}_{x_4}$ denote the mean and standard deviation of $\ln x_4$ in the quadrivariate PDF. The correlation of x_1 and x_2 is denoted ρ_{x_1,x_2}, the correlation of x_1 and $\ln x_3$ is denoted $\tilde{\rho}_{x_1,x_3}$, the correlation of x_1 and $\ln x_4$ is denoted

$\tilde{\rho}_{x_1,x_4}$, the correlation of x_2 and $\ln x_3$ is denoted $\tilde{\rho}_{x_2,x_3}$, the correlation of x_2 and $\ln x_4$ is denoted $\tilde{\rho}_{x_2,x_4}$, and the correlation of $\ln x_3$ and $\ln x_4$ is denoted $\tilde{\rho}_{x_3,x_4}$. The gamma function is denoted $\Gamma(x)$ and the parabolic cylinder function of order ν is denoted $D_\nu(x)$.

When x_1, x_2, x_3, and x_4 all vary ($\sigma_{x_1} > 0$, $\sigma_{x_2} > 0$, $\sigma_{x_3} > 0$, and $\sigma_{x_4} > 0$), the solution is

$$
\begin{aligned}
G_{QC} = \frac{1}{\sqrt{2\pi}} (-\sigma_{x_2})^\alpha \exp\Bigg\{ & \tilde{\mu}_{x_3}\beta + \tilde{\mu}_{x_4}\gamma + \frac{1}{2}\left(1-\tilde{\rho}_{x_2,x_3}^2\right)\tilde{\sigma}_{x_3}^2\beta^2 \\
& + \frac{1}{2}\left(1-\tilde{\rho}_{x_2,x_4}^2\right)\tilde{\sigma}_{x_4}^2\gamma^2 + \left(\tilde{\rho}_{x_3,x_4} - \tilde{\rho}_{x_2,x_3}\tilde{\rho}_{x_2,x_4}\right)\tilde{\sigma}_{x_3}\beta\tilde{\sigma}_{x_4}\gamma \Bigg\} \\
& \times \exp\left\{ \frac{1}{4}\varsigma^2 - \frac{\mu_{x_2}}{\sigma_{x_2}}\varsigma + \frac{1}{2}\frac{\mu_{x_2}^2}{\sigma_{x_2}^2} \right\} \\
& \times \Bigg(- \rho_{x_1,x_2}\sigma_{x_1}\Gamma(\alpha+2) D_{-(\alpha+2)}(\varsigma) \\
& \quad + \Bigg(\mu_{x_1} - C_1 - \frac{\mu_{x_2}}{\sigma_{x_2}}\rho_{x_1,x_2}\sigma_{x_1} + \left(\tilde{\rho}_{x_1,x_3} - \rho_{x_1,x_2}\tilde{\rho}_{x_2,x_3}\right)\sigma_{x_1}\tilde{\sigma}_{x_3}\beta \\
& \qquad + \left(\tilde{\rho}_{x_1,x_4} - \rho_{x_1,x_2}\tilde{\rho}_{x_2,x_4}\right)\sigma_{x_1}\tilde{\sigma}_{x_4}\gamma \Bigg)\Gamma(\alpha+1) D_{-(\alpha+1)}(\varsigma) \Bigg) \\
& - C_2(\mu_{x_1} - C_1);
\end{aligned}
\tag{J1}
$$

where $\varsigma = \dfrac{\mu_{x_2}}{\sigma_{x_2}} + \tilde{\rho}_{x_2,x_3}\tilde{\sigma}_{x_3}\beta + \tilde{\rho}_{x_2,x_4}\tilde{\sigma}_{x_4}\gamma.$

There are four sub-forms that contain one constant variable. When x_1 is constant, but x_2,

x_3, and x_4 vary, the solution is

$$
\begin{aligned}
G_{QC} = & \frac{1}{\sqrt{2\pi}} \left(\mu_{x_1} - C_1\right) \left(-\sigma_{x_2}\right)^{\alpha} \\
& \times \exp\left\{ \tilde{\mu}_{x_3}\beta + \tilde{\mu}_{x_4}\gamma + \frac{1}{2}\left(1 - \tilde{\rho}^2_{x_2,x_3}\right)\tilde{\sigma}^2_{x_3}\beta^2 \right. \\
& \qquad \left. + \frac{1}{2}\left(1 - \tilde{\rho}^2_{x_2,x_4}\right)\tilde{\sigma}^2_{x_4}\gamma^2 + \left(\tilde{\rho}_{x_3,x_4} - \tilde{\rho}_{x_2,x_3}\tilde{\rho}_{x_2,x_4}\right)\tilde{\sigma}_{x_3}\beta\tilde{\sigma}_{x_4}\gamma \right\} \\
& \times \exp\left\{ \frac{1}{4}\varsigma^2 - \frac{\mu_{x_2}}{\sigma_{x_2}}\varsigma + \frac{1}{2}\frac{\mu^2_{x_2}}{\sigma^2_{x_2}} \right\} \Gamma\left(\alpha + 1\right) D_{-(\alpha+1)}\left(\varsigma\right) \\
& - C_2\left(\mu_{x_1} - C_1\right);
\end{aligned}
\tag{J2}
$$

where $\varsigma = \dfrac{\mu_{x_2}}{\sigma_{x_2}} + \tilde{\rho}_{x_2,x_3}\tilde{\sigma}_{x_3}\beta + \tilde{\rho}_{x_2,x_4}\tilde{\sigma}_{x_4}\gamma.$

When x_2 is constant, but x_1, x_3, and x_4 vary, the solution is

$$
G_{QC} = \begin{cases}
\mu^{\alpha}_{x_2}\Big(\mu_{x_1} - C_1 + \tilde{\rho}_{x_1,x_3}\sigma_{x_1}\tilde{\sigma}_{x_3}\beta + \tilde{\rho}_{x_1,x_4}\sigma_{x_1}\tilde{\sigma}_{x_4}\gamma\Big) & \\
\times \exp\left\{ \tilde{\mu}_{x_3}\beta + \tilde{\mu}_{x_4}\gamma + \dfrac{1}{2}\tilde{\sigma}^2_{x_3}\beta^2 + \dfrac{1}{2}\tilde{\sigma}^2_{x_4}\gamma^2 + \tilde{\rho}_{x_3,x_4}\tilde{\sigma}_{x_3}\beta\tilde{\sigma}_{x_4}\gamma \right\} & \\
-C_2\left(\mu_{x_1} - C_1\right), \qquad \text{when } \mu_{x_2} \leq 0; \text{ and} & \\
\\
-C_2\left(\mu_{x_1} - C_1\right), \qquad \text{when } \mu_{x_2} > 0.
\end{cases}
\tag{J3}
$$

When x_3 is constant, but x_1, x_2, and x_4 vary, the solution is

$$
\begin{aligned}
G_{QC} = & \frac{1}{\sqrt{2\pi}} \left(-\sigma_{x_2}\right)^{\alpha} \mu_{x_3}^{\beta} \exp\left\{\tilde{\mu}_{x_4}\gamma + \frac{1}{2}\tilde{\sigma}_{x_4}^2\gamma^2 - \frac{1}{4}\varsigma^2\right\} \\
& \times \Bigg(- \rho_{x_1,x_2}\sigma_{x_1}\Gamma\left(\alpha+2\right) D_{-(\alpha+2)}\left(\varsigma\right) \\
& \quad + \left(\mu_{x_1} - C_1 - \frac{\mu_{x_2}}{\sigma_{x_2}}\rho_{x_1,x_2}\sigma_{x_1} + \left(\tilde{\rho}_{x_1,x_4} - \rho_{x_1,x_2}\tilde{\rho}_{x_2,x_4}\right)\sigma_{x_1}\tilde{\sigma}_{x_4}\gamma\right) \\
& \quad\quad \times \Gamma\left(\alpha+1\right) D_{-(\alpha+1)}\left(\varsigma\right) \Bigg) \\
& - C_2\left(\mu_{x_1} - C_1\right);
\end{aligned}
\tag{J4}
$$

where $\varsigma = \dfrac{\mu_{x_2}}{\sigma_{x_2}} + \tilde{\rho}_{x_2,x_4}\tilde{\sigma}_{x_4}\gamma.$

When x_4 is constant, but x_1, x_2, and x_3 vary, the solution is

$$
\begin{aligned}
G_{QC} = & \frac{1}{\sqrt{2\pi}} \left(-\sigma_{x_2}\right)^{\alpha} \mu_{x_4}^{\gamma} \exp\left\{\tilde{\mu}_{x_3}\beta + \frac{1}{2}\tilde{\sigma}_{x_3}^2\beta^2 - \frac{1}{4}\varsigma^2\right\} \\
& \times \Bigg(- \rho_{x_1,x_2}\sigma_{x_1}\Gamma\left(\alpha+2\right) D_{-(\alpha+2)}\left(\varsigma\right) \\
& \quad + \left(\mu_{x_1} - C_1 - \frac{\mu_{x_2}}{\sigma_{x_2}}\rho_{x_1,x_2}\sigma_{x_1} + \left(\tilde{\rho}_{x_1,x_3} - \rho_{x_1,x_2}\tilde{\rho}_{x_2,x_3}\right)\sigma_{x_1}\tilde{\sigma}_{x_3}\beta\right) \\
& \quad\quad \times \Gamma\left(\alpha+1\right) D_{-(\alpha+1)}\left(\varsigma\right) \Bigg) \\
& - C_2\left(\mu_{x_1} - C_1\right);
\end{aligned}
\tag{J5}
$$

where $\varsigma = \dfrac{\mu_{x_2}}{\sigma_{x_2}} + \tilde{\rho}_{x_2,x_3}\tilde{\sigma}_{x_3}\beta.$

There are six sub-forms that contain two constant variables. When both x_1 and x_2 are

constant, but both x_3 and x_4 vary, the solution is

$$G_{QC} = \begin{cases} (\mu_{x_1} - C_1)\,\mu_{x_2}^{\alpha} \exp\left\{\tilde{\mu}_{x_3}\beta + \tilde{\mu}_{x_4}\gamma + \frac{1}{2}\tilde{\sigma}_{x_3}^2\beta^2 + \frac{1}{2}\tilde{\sigma}_{x_4}^2\gamma^2 + \tilde{\rho}_{x_3,x_4}\tilde{\sigma}_{x_3}\beta\tilde{\sigma}_{x_4}\gamma\right\} \\ -C_2\,(\mu_{x_1} - C_1)\,, \qquad \text{when } \mu_{x_2} \leq 0;\ \text{and} \\ \\ -C_2\,(\mu_{x_1} - C_1)\,, \qquad \text{when } \mu_{x_2} > 0. \end{cases} \tag{J6}$$

When both x_1 and x_3 are constant, but both x_2 and x_4 vary, the solution is

$$\begin{aligned} G_{QC} = {} & \frac{1}{\sqrt{2\pi}}\,(\mu_{x_1} - C_1)\,(-\sigma_{x_2})^{\alpha}\,\mu_{x_3}^{\beta} \exp\left\{\tilde{\mu}_{x_4}\gamma + \frac{1}{2}\tilde{\sigma}_{x_4}^2\gamma^2 - \frac{1}{4}\varsigma^2\right\}\Gamma\,(\alpha+1)\,D_{-(\alpha+1)}\,(\varsigma) \\ & - C_2\,(\mu_{x_1} - C_1)\,; \end{aligned} \tag{J7}$$

where $\quad \varsigma = \dfrac{\mu_{x_2}}{\sigma_{x_2}} + \tilde{\rho}_{x_2,x_4}\tilde{\sigma}_{x_4}\gamma.$

When both x_1 and x_4 are constant, but both x_2 and x_3 vary, the solution is

$$\begin{aligned} G_{QC} = {} & \frac{1}{\sqrt{2\pi}}\,(\mu_{x_1} - C_1)\,(-\sigma_{x_2})^{\alpha}\,\mu_{x_4}^{\gamma} \exp\left\{\tilde{\mu}_{x_3}\beta + \frac{1}{2}\tilde{\sigma}_{x_3}^2\beta^2 - \frac{1}{4}\varsigma^2\right\}\Gamma\,(\alpha+1)\,D_{-(\alpha+1)}\,(\varsigma) \\ & - C_2\,(\mu_{x_1} - C_1)\,; \end{aligned} \tag{J8}$$

where $\quad \varsigma = \dfrac{\mu_{x_2}}{\sigma_{x_2}} + \tilde{\rho}_{x_2,x_3}\tilde{\sigma}_{x_3}\beta.$

When both x_2 and x_3 are constant, but both x_1 and x_4 vary, the solution is

$$G_{QC} = \begin{cases} \mu_{x_2}^{\alpha}\mu_{x_3}^{\beta}\Big(\mu_{x_1} - C_1 + \tilde{\rho}_{x_1,x_4}\sigma_{x_1}\tilde{\sigma}_{x_4}\gamma\Big) \exp\left\{\tilde{\mu}_{x_4}\gamma + \frac{1}{2}\tilde{\sigma}_{x_4}^2\gamma^2\right\} \\ -C_2\,(\mu_{x_1} - C_1)\,, \qquad \text{when } \mu_{x_2} \leq 0;\ \text{and} \\ \\ -C_2\,(\mu_{x_1} - C_1)\,, \qquad \text{when } \mu_{x_2} > 0. \end{cases} \tag{J9}$$

When both x_2 and x_4 are constant, but both x_1 and x_3 vary, the solution is

$$G_{QC} = \begin{cases} \mu_{x_2}^{\alpha}\mu_{x_4}^{\gamma}\left(\mu_{x_1} - C_1 + \tilde{\rho}_{x_1,x_3}\sigma_{x_1}\tilde{\sigma}_{x_3}\beta\right)\exp\left\{\tilde{\mu}_{x_3}\beta + \frac{1}{2}\tilde{\sigma}_{x_3}^2\beta^2\right\} \\ -C_2\left(\mu_{x_1} - C_1\right), \qquad \text{when } \mu_{x_2} \leq 0; \text{ and} \\ \\ -C_2\left(\mu_{x_1} - C_1\right), \qquad \text{when } \mu_{x_2} > 0. \end{cases} \tag{J10}$$

When both x_3 and x_4 are constant, but both x_1 and x_2 vary, the solution is

$$\begin{aligned} G_{QC} = {} & \frac{1}{\sqrt{2\pi}}\left(-\sigma_{x_2}\right)^{\alpha}\mu_{x_3}^{\beta}\mu_{x_4}^{\gamma}\exp\left\{-\frac{1}{4}\frac{\mu_{x_2}^2}{\sigma_{x_2}^2}\right\} \\ & \times\left(-\rho_{x_1,x_2}\sigma_{x_1}\Gamma\left(\alpha+2\right)D_{-(\alpha+2)}\left(\frac{\mu_{x_2}}{\sigma_{x_2}}\right)\right. \\ & \quad \left.+\left(\mu_{x_1} - C_1 - \frac{\mu_{x_2}}{\sigma_{x_2}}\rho_{x_1,x_2}\sigma_{x_1}\right)\Gamma\left(\alpha+1\right)D_{-(\alpha+1)}\left(\frac{\mu_{x_2}}{\sigma_{x_2}}\right)\right) \\ & -C_2\left(\mu_{x_1} - C_1\right). \end{aligned} \tag{J11}$$

There are four sub-forms that contain three constant variables. When x_1, x_2, and x_3 are constant, but x_4 varies, the solution is

$$G_{QC} = \begin{cases} \left(\mu_{x_1} - C_1\right)\mu_{x_2}^{\alpha}\mu_{x_3}^{\beta}\exp\left\{\tilde{\mu}_{x_4}\gamma + \frac{1}{2}\tilde{\sigma}_{x_4}^2\gamma^2\right\} \\ -C_2\left(\mu_{x_1} - C_1\right), \qquad \text{when } \mu_{x_2} \leq 0; \text{ and} \\ -C_2\left(\mu_{x_1} - C_1\right), \qquad \text{when } \mu_{x_2} > 0. \end{cases} \tag{J12}$$

When x_1, x_2, and x_4 are constant, but x_2 varies, the solution is

$$G_{QC} = \begin{cases} \left(\mu_{x_1} - C_1\right) \mu_{x_2}^{\alpha} \mu_{x_4}^{\gamma} \exp\left\{\tilde{\mu}_{x_3}\beta + \frac{1}{2}\tilde{\sigma}_{x_3}^2\beta^2\right\} \\ -C_2\left(\mu_{x_1} - C_1\right), \qquad \text{when } \mu_{x_2} \leq 0; \text{ and} \\ -C_2\left(\mu_{x_1} - C_1\right), \qquad \text{when } \mu_{x_2} > 0. \end{cases} \tag{J13}$$

When x_1, x_3, and x_4 are constant, but x_2 varies, the solution is

$$\begin{aligned} G_{QC} = {} & \frac{1}{\sqrt{2\pi}}\left(\mu_{x_1} - C_1\right)\left(-\sigma_{x_2}\right)^{\alpha} \mu_{x_3}^{\beta} \mu_{x_4}^{\gamma} \exp\left\{ -\frac{1}{4}\frac{\mu_{x_2}^2}{\sigma_{x_2}^2}\right\} \Gamma\left(\alpha+1\right) D_{-(\alpha+1)}\left(\frac{\mu_{x_2}}{\sigma_{x_2}}\right) \\ & - C_2\left(\mu_{x_1} - C_1\right). \end{aligned} \tag{J14}$$

When x_2, x_3, and x_4 are constant, but x_1 varies, the solution is

$$G_{QC} = \begin{cases} \left(\mu_{x_1} - C_1\right)\left(\mu_{x_2}^{\alpha}\mu_{x_3}^{\beta}\mu_{x_4}^{\gamma} - C_2\right), \qquad \text{when } \mu_{x_2} \leq 0; \text{ and} \\ -C_2\left(\mu_{x_1} - C_1\right), \qquad \text{when } \mu_{x_2} > 0. \end{cases} \tag{J15}$$

When x_1, x_2, x_3, and x_4 are all constant ($\sigma_{x_1} = 0$, $\sigma_{x_2} = 0$, $\sigma_{x_3} = 0$, and $\sigma_{x_4} = 0$), the solution is

$$G_{QC} = \begin{cases} \left(\mu_{x_1} - C_1\right)\left(\mu_{x_2}^{\alpha}\mu_{x_3}^{\beta}\mu_{x_4}^{\gamma} - C_2\right), \qquad \text{when } \mu_{x_2} \leq 0; \text{ and} \\ -C_2\left(\mu_{x_1} - C_1\right), \qquad \text{when } \mu_{x_2} > 0. \end{cases} \tag{J16}$$

J.2 Trivariate PDF Integrals of Covariance Form

The integrals of the general form

$$G_{TC} = \int_{-\infty}^{\infty}\int_{-\infty}^{\infty}\int_{0}^{\infty}\Big(x_1 - C_1\Big)\Big(x_2^{\alpha}\left(H\left(x_2\right)\right)^{\alpha} x_3^{\beta} - C_2\Big) P_{NNL}\left(x_1, x_2, x_3\right) \mathrm{d}x_3\, \mathrm{d}x_2\, \mathrm{d}x_1$$

are referred to as trivariate PDF integrals of covariance form. Both C_1 and C_2 are constants, and when they both represent the appropriate overall mean values, the resulting integral is a covariance. The trivariate PDF, $P_{NNL}(x_1, x_2, x_3)$, is a normal-normal-lognormal PDF, meaning that the individual marginals of both x_1 and x_2 are normal distributions and the individual marginal of x_3 is a lognormal distribution. The above integral has eight sub-forms. When one or more of the variables is constant (has a standard deviation of 0), the integral simplifies and reduces.

When x_1, x_2, and x_3 all vary ($\sigma_{x_1} > 0$, $\sigma_{x_2} > 0$, and $\sigma_{x_3} > 0$), the solution, denoted G_{TC}, is

$$\begin{aligned} G_{TC} = {} & \frac{1}{\sqrt{2\pi}} \sigma_{x_2}^{\alpha} \exp\left\{ \tilde{\mu}_{x_3}\beta + \frac{1}{2}\tilde{\sigma}_{x_3}^2\beta^2 - \frac{1}{4}\varsigma^2 \right\} \\ & \times \Bigg(\rho_{x_1,x_2}\sigma_{x_1}\Gamma(\alpha+2) D_{-(\alpha+2)}(-\varsigma) \\ & \quad + \left(\mu_{x_1} - C_1 - \frac{\mu_{x_2}}{\sigma_{x_2}}\rho_{x_1,x_2}\sigma_{x_1} + (\tilde{\rho}_{x_1,x_3} - \rho_{x_1,x_2}\tilde{\rho}_{x_2,x_3})\sigma_{x_1}\tilde{\sigma}_{x_3}\beta \right) \\ & \quad\quad \times \Gamma(\alpha+1) D_{-(\alpha+1)}(-\varsigma) \Bigg) \\ & - C_2(\mu_{x_1} - C_1); \end{aligned} \tag{J17}$$

where $\varsigma = \dfrac{\mu_{x_2}}{\sigma_{x_2}} + \tilde{\rho}_{x_2,x_3}\tilde{\sigma}_{x_3}\beta.$

There are three sub-forms that contain one constant variable. When x_1 is constant, but x_2 and x_3 vary, the solution is

$$\begin{aligned} G_{TC} = {} & \frac{1}{\sqrt{2\pi}} (\mu_{x_1} - C_1) \sigma_{x_2}^{\alpha} \exp\left\{ \tilde{\mu}_{x_3}\beta + \frac{1}{2}\tilde{\sigma}_{x_3}^2\beta^2 - \frac{1}{4}\varsigma^2 \right\} \Gamma(\alpha+1) D_{-(\alpha+1)}(-\varsigma) \\ & - C_2(\mu_{x_1} - C_1); \end{aligned} \tag{J18}$$

where $\varsigma = \dfrac{\mu_{x_2}}{\sigma_{x_2}} + \tilde{\rho}_{x_2,x_3}\tilde{\sigma}_{x_3}\beta.$

When x_2 is constant, but x_1 and x_3 vary, the solution is

$$G_{TC} = \begin{cases} \mu_{x_2}^{\alpha}\left(\mu_{x_1} - C_1 + \tilde{\rho}_{x_1,x_3}\sigma_{x_1}\tilde{\sigma}_{x_3}\beta\right)\exp\left\{\tilde{\mu}_{x_3}\beta + \dfrac{1}{2}\tilde{\sigma}_{x_3}^2\beta^2\right\} \\ -C_2\left(\mu_{x_1} - C_1\right), \qquad \text{when } \mu_{x_2} \geq 0; \text{ and} \\ \\ -C_2\left(\mu_{x_1} - C_1\right), \qquad \text{when } \mu_{x_2} < 0. \end{cases} \tag{J19}$$

When x_3 is constant, but x_1 and x_2 vary, the solution is

$$\begin{aligned} G_{TC} = & \frac{1}{\sqrt{2\pi}}\sigma_{x_2}^{\alpha}\mu_{x_3}^{\beta}\exp\left\{-\frac{1}{4}\frac{\mu_{x_2}^2}{\sigma_{x_2}^2}\right\} \\ & \times\left(\rho_{x_1,x_2}\sigma_{x_1}\Gamma\left(\alpha+2\right)D_{-(\alpha+2)}\left(-\frac{\mu_{x_2}}{\sigma_{x_2}}\right)\right. \\ & \quad \left.+\left(\mu_{x_1} - C_1 - \frac{\mu_{x_2}}{\sigma_{x_2}}\rho_{x_1,x_2}\sigma_{x_1}\right)\Gamma\left(\alpha+1\right)D_{-(\alpha+1)}\left(-\frac{\mu_{x_2}}{\sigma_{x_2}}\right)\right) \\ & - C_2\left(\mu_{x_1} - C_1\right). \end{aligned} \tag{J20}$$

There are three sub-forms that contain two constant variables. When both x_1 and x_2 are constant, but x_3 varies, the solution is

$$G_{TC} = \begin{cases} \mu_{x_2}^{\alpha}\left(\mu_{x_1} - C_1\right)\exp\left\{\tilde{\mu}_{x_3}\beta + \dfrac{1}{2}\tilde{\sigma}_{x_3}^2\beta^2\right\} - C_2\left(\mu_{x_1} - C_1\right), \text{ when } \mu_{x_2} \geq 0; \text{ and} \\ -C_2\left(\mu_{x_1} - C_1\right), \qquad \text{when } \mu_{x_2} < 0. \end{cases} \tag{J21}$$

When both x_1 and x_3 are constant, but x_2 varies, the solution is

$$\begin{aligned} G_{TC} = & \frac{1}{\sqrt{2\pi}}\left(\mu_{x_1} - C_1\right)\sigma_{x_2}^{\alpha}\mu_{x_3}^{\beta}\exp\left\{-\frac{1}{4}\frac{\mu_{x_2}^2}{\sigma_{x_2}^2}\right\}\Gamma\left(\alpha+1\right)D_{-(\alpha+1)}\left(-\frac{\mu_{x_2}}{\sigma_{x_2}}\right) \\ & - C_2\left(\mu_{x_1} - C_1\right). \end{aligned} \tag{J22}$$

When both x_2 and x_3 are constant, but x_1 varies, the solution is

$$G_{TC} = \begin{cases} \left(\mu_{x_1} - C_1\right)\left(\mu_{x_2}^{\alpha}\mu_{x_3}^{\beta} - C_2\right), & \text{when } \mu_{x_2} \geq 0; \text{ and} \\ -C_2\left(\mu_{x_1} - C_1\right), & \text{when } \mu_{x_2} < 0. \end{cases} \tag{J23}$$

When x_1, x_2, and x_3 are all constant ($\sigma_{x_1} = 0$, $\sigma_{x_2} = 0$, and $\sigma_{x_3} = 0$), the solution is

$$G_{TC} = \begin{cases} \left(\mu_{x_1} - C_1\right)\left(\mu_{x_2}^{\alpha}\mu_{x_3}^{\beta} - C_2\right), & \text{when } \mu_{x_2} \geq 0; \text{ and} \\ -C_2\left(\mu_{x_1} - C_1\right), & \text{when } \mu_{x_2} < 0. \end{cases} \tag{J24}$$

J.3 Trivariate PDF Integrals of Mean Form

The integrals of the general form

$$\begin{aligned} G_{TM} &= \int_{-\infty}^{\infty}\int_{0}^{\infty}\int_{0}^{\infty} x_1^{\alpha}\left(H\left(-x_1\right)\right)^{\alpha} x_2^{\beta}x_3^{\gamma}P_{NLL}\left(x_1, x_2, x_3\right)\mathrm{d}x_3\,\mathrm{d}x_2\,\mathrm{d}x_1 \\ &= \int_{-\infty}^{0}\int_{0}^{\infty}\int_{0}^{\infty} x_1^{\alpha}x_2^{\beta}x_3^{\gamma}P_{NLL}\left(x_1, x_2, x_3\right)\mathrm{d}x_3\,\mathrm{d}x_2\,\mathrm{d}x_1 \end{aligned}$$

are referred to as trivariate PDF integrals of mean form. The trivariate PDF, $P_{NLL}\left(x_1, x_2, x_3\right)$, is a normal-lognormal-lognormal PDF, meaning that the individual marginal of x_1 is a normal distribution and the individual marginals of both x_2 and x_3 are lognormal distributions. The above integral has eight sub-forms. When one or more of the variables is constant (has a standard deviation of 0), the integral simplifies and reduces.

In the solutions below, denoted G_{TM}, μ_{x_1} and σ_{x_1} denote the mean and standard deviation of x_1 in the trivariate PDF, μ_{x_2} and σ_{x_2} denote the mean and standard deviation of x_2 in the trivariate PDF, and μ_{x_3} and σ_{x_3} denote the mean and standard deviation of x_3 in the trivariate PDF. For lognormal variates, $\tilde{\mu}_{x_2}$ and $\tilde{\sigma}_{x_2}$ denote the mean and standard deviation of $\ln x_2$ in the trivariate PDF, while $\tilde{\mu}_{x_3}$ and $\tilde{\sigma}_{x_3}$ denote the mean and standard deviation of

$\ln x_3$ in the trivariate PDF. The correlation of x_1 and $\ln x_2$ is denoted $\tilde{\rho}_{x_1,x_2}$, the correlation of x_1 and $\ln x_3$ is denoted $\tilde{\rho}_{x_1,x_3}$, and the correlation of $\ln x_2$ and $\ln x_3$ is denoted $\tilde{\rho}_{x_2,x_3}$. The gamma function is denoted $\Gamma(x)$ and the parabolic cylinder function of order ν is denoted $D_\nu(x)$.

When x_1, x_2, and x_3 all vary ($\sigma_{x_1} > 0$, $\sigma_{x_2} > 0$, and $\sigma_{x_3} > 0$), the solution is

$$G_{TM} = \frac{1}{\sqrt{2\pi}}(-\sigma_{x_1})^{\alpha} \exp\left\{\tilde{\mu}_{x_2}\beta + \tilde{\mu}_{x_3}\gamma + \frac{1}{2}\left(1-\tilde{\rho}_{x_1,x_2}^2\right)\tilde{\sigma}_{x_2}^2\beta^2 + \frac{1}{2}\left(1-\tilde{\rho}_{x_1,x_3}^2\right)\tilde{\sigma}_{x_3}^2\gamma^2 + \left(\tilde{\rho}_{x_2,x_3} - \tilde{\rho}_{x_1,x_2}\tilde{\rho}_{x_1,x_3}\right)\tilde{\sigma}_{x_2}\beta\tilde{\sigma}_{x_3}\gamma\right\} \times \exp\left\{\frac{1}{4}\varsigma^2 - \frac{\mu_{x_1}}{\sigma_{x_1}}\varsigma + \frac{1}{2}\frac{\mu_{x_1}^2}{\sigma_{x_1}^2}\right\}\Gamma(\alpha+1)\,D_{-(\alpha+1)}(\varsigma); \quad \text{(J25)}$$

where $\varsigma = \dfrac{\mu_{x_1}}{\sigma_{x_1}} + \tilde{\rho}_{x_1,x_2}\tilde{\sigma}_{x_2}\beta + \tilde{\rho}_{x_1,x_3}\tilde{\sigma}_{x_3}\gamma.$

There are three sub-forms that contain one constant variable. When x_1 is constant, but x_2 and x_3 vary, the solution is

$$G_{TM} = \begin{cases} \mu_{x_1}^{\alpha}\exp\left\{\tilde{\mu}_{x_2}\beta + \tilde{\mu}_{x_3}\gamma + \frac{1}{2}\tilde{\sigma}_{x_2}^2\beta^2 + \frac{1}{2}\tilde{\sigma}_{x_3}^2\gamma^2 + \tilde{\rho}_{x_2,x_3}\tilde{\sigma}_{x_2}\beta\tilde{\sigma}_{x_3}\gamma\right\}, \\ \quad \text{when } \mu_{x_1} \le 0; \text{ and} \\ 0, \text{ when } \mu_{x_1} > 0. \end{cases} \quad \text{(J26)}$$

When x_2 is constant, but x_1 and x_3 vary, the solution is

$$G_{TM} = \frac{1}{\sqrt{2\pi}}(-\sigma_{x_1})^{\alpha}\,\mu_{x_2}^{\beta}\exp\left\{\tilde{\mu}_{x_3}\gamma + \frac{1}{2}\tilde{\sigma}_{x_3}^2\gamma^2 - \frac{1}{4}\varsigma^2\right\}\Gamma(\alpha+1)\,D_{-(\alpha+1)}(\varsigma); \quad \text{(J27)}$$

where $\varsigma = \dfrac{\mu_{x_1}}{\sigma_{x_1}} + \tilde{\rho}_{x_1,x_3}\tilde{\sigma}_{x_3}\gamma.$

When x_3 is constant, but x_1 and x_2 vary, the solution is

$$G_{TM} = \frac{1}{\sqrt{2\pi}} \left(-\sigma_{x_1}\right)^{\alpha} \mu_{x_3}^{\gamma} \exp\left\{\tilde{\mu}_{x_2}\beta + \frac{1}{2}\tilde{\sigma}_{x_2}^2\beta^2 - \frac{1}{4}\varsigma^2\right\} \Gamma\left(\alpha+1\right) D_{-(\alpha+1)}\left(\varsigma\right); \tag{J28}$$

where $\varsigma = \dfrac{\mu_{x_1}}{\sigma_{x_1}} + \tilde{\rho}_{x_1,x_2}\tilde{\sigma}_{x_2}\beta.$

There are three sub-forms that contain two constant variables. When both x_1 and x_2 are constant, but x_3 varies, the solution is

$$G_{TM} = \begin{cases} \mu_{x_1}^{\alpha}\mu_{x_2}^{\beta} \exp\left\{\tilde{\mu}_{x_3}\gamma + \dfrac{1}{2}\tilde{\sigma}_{x_3}^2\gamma^2\right\}, \text{ when } \mu_{x_1} \leq 0; \text{ and} \\ \\ 0, \text{ when } \mu_{x_1} > 0. \end{cases} \tag{J29}$$

When both x_1 and x_3 are constant, but x_2 varies, the solution is

$$G_{TM} = \begin{cases} \mu_{x_1}^{\alpha}\mu_{x_3}^{\gamma} \exp\left\{\tilde{\mu}_{x_2}\beta + \dfrac{1}{2}\tilde{\sigma}_{x_2}^2\beta^2\right\}, \text{ when } \mu_{x_1} \leq 0; \text{ and} \\ \\ 0, \text{ when } \mu_{x_1} > 0. \end{cases} \tag{J30}$$

When both x_2 and x_3 are constant, but x_1 varies, the solution is

$$G_{TM} = \frac{1}{\sqrt{2\pi}} \left(-\sigma_{x_1}\right)^{\alpha} \mu_{x_2}^{\beta}\mu_{x_3}^{\gamma} \exp\left\{-\frac{1}{4}\frac{\mu_{x_1}^2}{\sigma_{x_1}^2}\right\} \Gamma\left(\alpha+1\right) D_{-(\alpha+1)}\left(\frac{\mu_{x_1}}{\sigma_{x_1}}\right). \tag{J31}$$

When x_1, x_2, and x_3 are all constant ($\sigma_{x_1} = 0$, $\sigma_{x_2} = 0$, and $\sigma_{x_3} = 0$), the solution is

$$G_{TM} = \begin{cases} \mu_{x_1}^{\alpha}\mu_{x_2}^{\beta}\mu_{x_3}^{\gamma}, \text{ when } \mu_{x_1} \leq 0; \text{ and} \\ \\ 0, \text{ when } \mu_{x_1} > 0. \end{cases} \tag{J32}$$

J.4 Bivariate PDF Integrals of Mean Form

The integrals of the general form

$$G_{BM} = \int_{-\infty}^{\infty}\int_{0}^{\infty} x_1^{\alpha}\left(H\left(x_1\right)\right)^{\alpha} x_2^{\beta} P_{NL}\left(x_1, x_2\right) \mathrm{d}x_2 \, \mathrm{d}x_1$$
$$= \int_{0}^{\infty}\int_{0}^{\infty} x_1^{\alpha} x_2^{\beta} P_{NL}\left(x_1, x_2\right) \mathrm{d}x_2 \, \mathrm{d}x_1$$

are referred to as bivariate PDF integrals of mean form. The bivariate PDF, $P_{NL}\left(x_1, x_2\right)$, is a normal-lognormal PDF, meaning that the individual marginal of x_1 is a normal distribution and the individual marginal of x_2 is a lognormal distribution. The above integral has four sub-forms. When one or more of the variables is constant (has a standard deviation of 0), the integral simplifies and reduces. In the solutions below, denoted G_{BM}, the notation is the same as in Section J.3.

When both x_1 and x_2 vary ($\sigma_{x_1} > 0$ and $\sigma_{x_2} > 0$), the solution is

$$G_{BM} = \frac{1}{\sqrt{2\pi}} \sigma_{x_1}^{\alpha} \exp\left\{\tilde{\mu}_{x_2}\beta + \frac{1}{2}\tilde{\sigma}_{x_2}^2\beta^2 - \frac{1}{4}\varsigma^2\right\}\Gamma\left(\alpha+1\right) D_{-(\alpha+1)}\left(-\varsigma\right); \tag{J33}$$

where $\varsigma = \dfrac{\mu_{x_1}}{\sigma_{x_1}} + \tilde{\rho}_{x_1,x_2}\tilde{\sigma}_{x_2}\beta.$

When x_1 is constant, but x_2 varies, the solution is

$$G_{BM} = \begin{cases} \mu_{x_1}^{\alpha} \exp\left\{\tilde{\mu}_{x_2}\beta + \dfrac{1}{2}\tilde{\sigma}_{x_2}^2\beta^2\right\}, \text{ when } \mu_{x_1} \geq 0; \text{ and} \\ 0, \text{ when } \mu_{x_1} < 0. \end{cases} \tag{J34}$$

When x_2 is constant, but x_1 varies, the solution is

$$G_{BM} = \frac{1}{\sqrt{2\pi}} \sigma_{x_1}^{\alpha} \mu_{x_2}^{\beta} \exp\left\{-\frac{1}{4}\frac{\mu_{x_1}^2}{\sigma_{x_1}^2}\right\}\Gamma\left(\alpha+1\right) D_{-(\alpha+1)}\left(-\frac{\mu_{x_1}}{\sigma_{x_1}}\right). \tag{J35}$$

When both x_1 and x_2 are constant ($\sigma_{x_1} = 0$ and $\sigma_{x_2} = 0$), the solution is

$$G_{BM} = \begin{cases} \mu_{x_1}^{\alpha} \mu_{x_2}^{\beta}, \text{ when } \mu_{x_1} \geq 0; \text{ and} \\ \\ 0, \text{ when } \mu_{x_1} < 0. \end{cases} \tag{J36}$$

Curriculum Vitae

Brian M. Griffin

Department of Mathematical Sciences
University of Wisconsin – Milwaukee
bmg2@uwm.edu

Education

University of Wisconsin – Milwaukee (UWM), Milwaukee, WI

- Graduate:
  Pursuing PhD, Mathematics (Atmospheric Science Concentration), 2011–present

  Dissertation Title: Improving the Subgrid-Scale Representation of Hydrometeors and Microphysical Feedback Effects Using a Multivariate PDF.

  Master of Science, Mathematics (Atmospheric Science Concentration), 2011

  Thesis Title: A PDF-Based Method for Parameterizing the Effects of Microphysics on Subgrid-Scale Variances and Covariances.

  Graduate GPA: 3.953

- Undergraduate:
  Bachelor of Science, Atmospheric Sciences, 2006 (Mathematics Minor)

Employment

- Graduate Research Assistant (Department of Mathematical Sciences) under Vincent E. Larson: August 2009 – present.
- Research Intern for Vincent E. Larson: May 2002 – August 2009.

Publications

- Griffin, B. M. and V. E. Larson, 2016: A new subgrid-scale representation of hydrometeor fields using a multivariate PDF. *Geosci. Model Dev. Discuss.*, doi:10.5194/gmd-2015-280, in review.
- Griffin, B. M. and V. E. Larson, 2013: Analytic upscaling of a local microphysics scheme. Part II: Simulations. *Quart. J. Roy. Meteor. Soc.*, **139**, 58–69, doi:10.1002/qj.1966.

- Larson, V. E. and B. M. Griffin, 2013: Analytic upscaling of a local microphysics scheme. Part I: Derivation. *Quart. J. Roy. Meteor. Soc.*, **139**, 46–57, doi:10.1002/qj.1967.

- Thayer-Calder, K., A. Gettelman, C. Craig, S. Goldhaber, P. A. Bogenschutz, C.-C. Chen, H. Morrison, J. Höft, E. Raut, B. M. Griffin, J. K. Weber, V. E. Larson, M. C. Wyant, M. Wang, Z. Guo, and S. J. Ghan, 2015: A unified parameterization of clouds and turbulence using CLUBB and subcolumns in the Community Atmosphere Model. *Geosci. Model Dev.*, **8**, 3801–3821, doi:10.5194/gmd-8-3801-2015.

- Storer, R. L., B. M. Griffin, J. Höft, J. K. Weber, E. Raut, V. E. Larson, M. Wang, and P. J. Rasch, 2015: Parameterizing deep convection using the assumed probability density function method. *Geosci. Model Dev.*, **8**, 1–19, doi:10.5194/gmd-8-1-2015.

- Guo, H., J.-C. Golaz, L. J. Donner, V. E. Larson, D. P. Schanen, and B. M. Griffin, 2010: Multivariate probability density functions with dynamics for cloud droplet activation in large-scale models: single column tests. *Geosci. Model Dev.*, **3**, 475–486, doi:10.5194/gmd-3-475-2010.

- Wyant, M. C., C. S. Bretherton, A. Chlond, B. M. Griffin, H. Kitagawa, C.-L. Lappen, V. E. Larson, A. Lock, S. Park, S. R. de Roode, J. Uchida, M. Zhao, and A. S. Ackerman, 2007: A single-column model intercomparison of a heavily drizzling stratocumulus-topped boundary layer. *J. Geophys. Res.*, **112**, D24204, doi:10.1029/2007JD008536.

- Golaz, J.-C., V. E. Larson, J. A. Hansen, D. P. Schanen, and B. M. Griffin, 2007: Elucidating model inadequacies in a cloud parameterization by use of an ensemble-based calibration framework. *Mon. Wea. Rev.*, **135**, 4077–4096, doi:10.1175/2007MWR2008.1.

Conference Papers

- Larson, V. E., J.-C. Golaz, J. A. Hansen, D. P. Schanen, and B. M. Griffin, 2008: Diagnosing structural errors in climate model parameterizations. Preprints, *Twentieth Conference on Climate Variability and Change*, New Orleans, Louisiana, American Meteorological Society.

- Larson, V. E. and B. M. Griffin, 2006: Coupling microphysics parameterizations to cloud parameterizations. Preprints, *Twelfth Conference on Cloud Physics*, Madison, Wisconsin, American Meteorological Society.

- Smith, A. J., B. M. Griffin, J.-C. Golaz, and V. E. Larson, 2006: Comparison of large-eddy simulations with a single-column model: Implications for mid-level cloud parameterization. Preprints, *Twelfth Conference on Cloud Physics*, Madison, Wisconsin, American Meteorological Society.

Awards and Honors

- Dhirenda Sikdar Memorial Scholarship: 2013. $500.
- UWM Graduate School Fellowship: 2011–2012. $12,332.
- UWMRF Research Fellow Award: 2010–2011. $10,000.